Post-transcriptional regulation and protein-protein interactions of the voltage-gated sodium channel $Na_v1.7$

Jennifer Koenig

A thesis submitted for the degree of Doctor of Philosophy to University College London

University College London
Wolfson Institute for Biomedical Research
2015

Declaration

I, Jennifer Koenig confirm that the work presented in this thesis is my own. Where information has been derived from other sources, I confirm that this has been indicated in the thesis.

Abstract

In mammals, ten isoforms of Na_v channels ($Na_v1.1$-1.9 and Na_x) are known that exhibit specific spatial and temporal expression patterns. Human genetics and transgenic mouse studies have revealed a pivotal role for voltage-gated sodium channel $Na_v1.7$ in both acute and chronic pain. Therefore $Na_v1.7$ is a promising analgesic drug target as individuals with loss of function mutations are normal except for a complete inability to perceive pain and having anosmia. As Na_v family members share high sequence homology, potential $Na_v1.7$ blockers need to be highly selective.

The aim of this thesis was to gain a greater understanding of $Na_v1.7$. Firstly, I examined the regulation of the *SCN9A* gene, which encodes $Na_v1.7$, through cloning and analysis of a natural antisense transcript *(NAT*). The complementary *NAT* overlaps tail-to-tail with the *SCN9A/Scn9a* sense transcript in both human and mouse genomes. Overexpression of the *NAT in vitro* specifically decreases the level of mRNA, protein and peak current of $Na_v1.7$. Therefore the *NAT* may play an important role in regulating human pain thresholds and is a potential candidate gene for individuals with chronic pain disorders that map to the *SCN9A* locus. Secondly, I investigated the protein-interaction network of $Na_v1.7$ through analysis of a newly developed $Na_v1.7$ TAP tagged mouse. Here, I aimed to identify subtype specific interaction partners of $Na_v1.7$ and found that $Na_v1.7$ is associated with β3 and β4 subunits ($Na_vβ$) as well as functional molecules that play a crucial role in protein synthesis, intracellular trafficking and pain processing. Finally, I studied a newly developed mouse model of inherited Primary Erythromelalgia (PE, $hNa_v1.7$ L858F), a human pain disorder caused by a mutation in *SCN9A*. This $hNa_v1.7$ L858F TAP tag mouse line recapitulated the human PE phenotype and will potentially be useful in preclinical screening of candidate $Na_v1.7$ blockers.

Acknowledgement

First and foremost I would like to express my gratitude to John Wood for giving me the opportunity to undertake a Ph.D. in his lab and supporting me throughout my Ph.D. It was a truly exciting experience.

I would also like to thank all the members of the Molecular Nociception group (past and present) for all their help and support along the way. With special thanks to Ana, Abdella, Ayako, Carine, Jane, Jeff, Joanne, Martine, Mike, Niels, Robert, Sam G, Sam S, Stephane, Sonia, Skip, Yury, Queeni and Vanessa. A special thanks to Jing for all his help, patience, encouragement and proofreading. I owe my deepest gratitude to James Cox for his encouragement, guidance and support from the outset all the way to the heroic proofreading of my thesis.

In addition I would like to thank my friends Charlotte & Gabry, Sarah, Maro & Bart, Grace, Michael, Robb & Celina, Rebecca & Aleks, Jason, Claire, Harry, Penelope, Cedric & Celine, Sophie, Barbara & Manuel, Brigit, Sherihane, Tina & Christian, Alexander and Istvan for their great support and patience listening to my science story.

A special thanks goes to Francois for his emotional support and his keen eye for detail.
Finally I would like to thank my family for their unconditional support and love.

Funding

I would like to thank the following:

Publications

Koenig J, Werdehausen R, Linley JE, Habib AM, Vernon J, Lolignier S, Eijkelkamp N, Zhao J, Okorokov AL, Woods CG, Wood JN, Cox JJ. (2015) *Regulation of Nav1.7:* ***A Conserved SCN9A Natural Antisense Transcript Expressed in Dorsal Root Ganglia***. PLoS One 2;10(6):e0128830.

Table of Contents

List of Figures

List of Tables

1 Introduction

Chronic pain is a major clinical problem. A Europe wide survey on the prevalence, severity, treatment and impact of pain found that 19 per cent of the participants suffered from chronic pain for more than 6 months, with one third describing their pain as so severe that it negatively impacted their life (Breivik, Collett et al. 2006). When asked about their pain treatment, 40 per cent of chronic pain sufferers reported that their pain medications were inadequate. This survey clearly depicts the magnitude of people affected but also highlights that analgesic drugs currently available are seemingly insufficient for the treatment of chronic pain. In order to develop new approaches to treat chronic pain, it is important to understand the key genes and mechanisms involved in pain processing.

The focus of this thesis is $Na_v1.7$, a voltage-gated sodium channel that is primarily found in peripheral sensory neurons and which has been highlighted as a promising new analgesic drug target through analysis of pain-free humans and transgenic mice (Nassar, Stirling et al. 2004, Cox, Reimann et al. 2006, Gingras, Smith et al. 2014). Blocking the function of this channel within damage-sensing neurons or by interfering with the transcription/translation of the *SCN9A* gene, which encodes $Na_v1.7$, may lead to the development of a new class of analgesic drugs (King and Vetter 2014).

Pain and Nociception

The international association for the study of pain (IASP) defines pain as “An unpleasant sensory and emotional experience associated with actual or potential tissue damage, or described in terms of such damage.” (http://www.iasp-pain.org). Pain in itself is essential for survival but in contrast to acute pain (which enables a fast response to a noxious stimulus) or inflammatory pain (which promotes the healing process), chronic pain fails to fulfill any useful physiological role. A further important distinction is made between pain and nociception. Pain is a perception, like vision or smell that is achieved by higher cortical processing. The sensation of pain not only leads to physical withdrawal and avoidance but also evokes an emotional response and

dramatic injury might change our perception of future pain experiences (Dar, Ariely et al. 1995). In contrast, nociception can be defined as the neural processes involved in detecting noxious stimuli and can occur in an unconscious individual. Hence, nociception can exist without pain.

Classification of Nociceptors

In 1906, Sherrington first suggested the existence of primary afferent neurons or nociceptors, which only respond to noxious stimuli but do not activate in the presence of innocuous stimuli such as light touch (Burgess and Perl 1967). Our current understanding confirms that nociceptors are a subset of sensory neurons that innervate the skin and deep tissue and convey noxious sensory information from the periphery to the central nervous system. Structurally, nociceptors are pseudo unipolar neurons with a small (<30 μm) to medium (30-40 μm) diameter somata that are located in dorsal root and trigeminal ganglia (Bessou and Perl 1969), and with a peripheral and central terminal. The peripheral terminals of primary afferents are typically free nerve endings, while the central branch projects its axon to second order neurons in the spinal cord (Figure 1-1). However, not all neurons in the dorsal root ganglia are nociceptors (e.g. proprioceptive neurons). An important goal of pain research is to further understand the subpopulations of nociceptive neurons and the types of noxious stimuli they detect.

One approach to categorize DRG neurons is based on anatomical features, such as diameter and myelination. For example, Aα- and Aβ-fibres are fast conducting (70-120m/s, and 40-70m/s, respectively) large (>40 μm) to medium size (30-40 μm) myelinated afferents, which have been historically associated with activation by innocuous stimuli (Julius and Basbaum 2001, Black, Frezel et al. 2012).

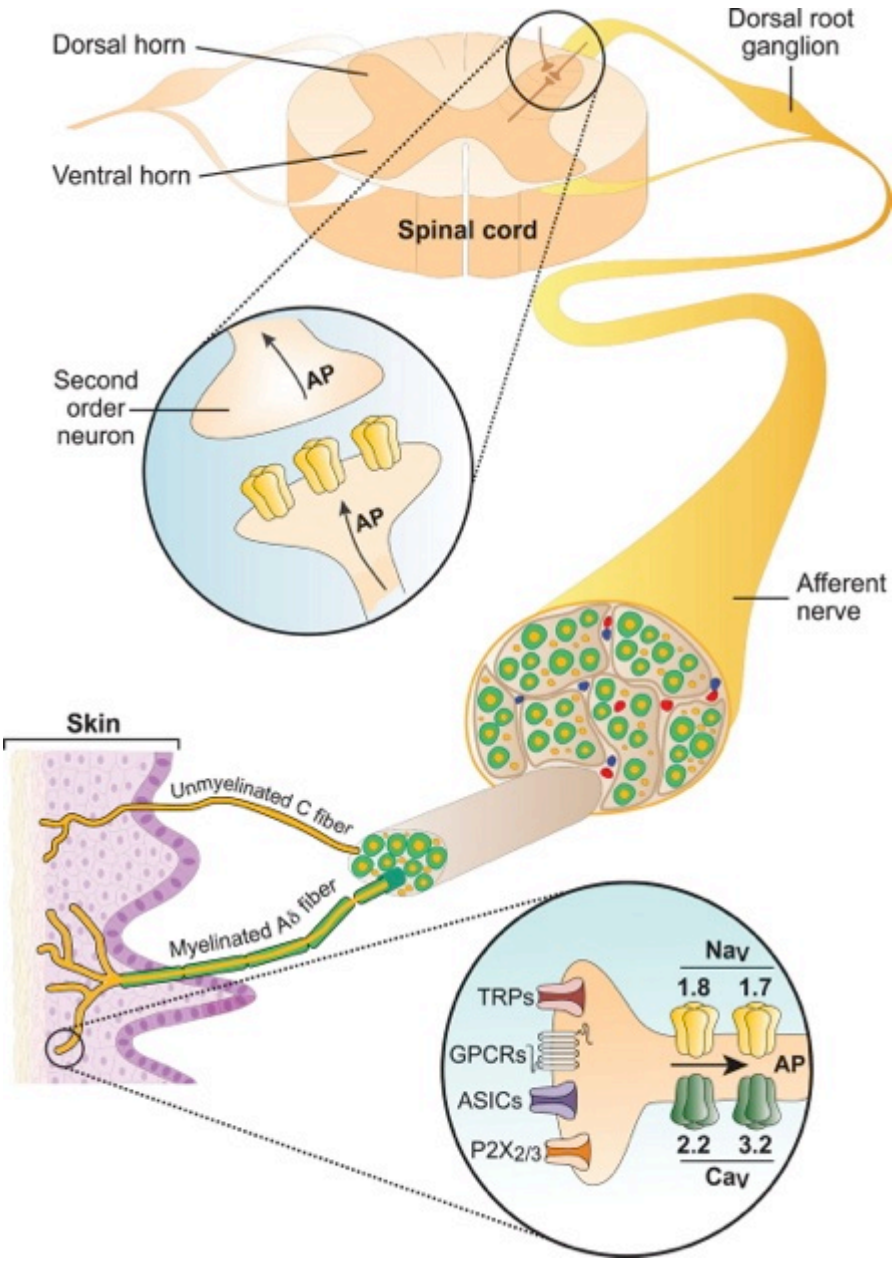

Figure 1-1: Pain signalling pathways

Unmyelinated C-fibres (orange) and thinly myelinated Aδ-fibres (green) innervate the skin (epidermis, light purple) with their free nerve endings that contain specialized channels and receptors (e.g. ASICs, G-protein-coupled receptors (GPCRs), and transient receptor potential (TRP) channels. In the presence of noxious stimuli, ion channels at the axon tip of primary afferents open and thereby create a generator potential that leads to further opening of voltage-gated sodium channels (VGSCs). VGSCs amplify the initial depolarization and enable action potentials to be generated. The generated action potential is transmitted from damage-sensing neurons in the periphery through the spinothalamic tract into the somatosensory cortex (not shown here) where finally the sensation of pain is created (Raouf, Quick et al. 2010). **Taken from King and Vetter (2014).**

Thinly myelinated Aδ-fibres or unmyelinated C-fibres differ in their conduction velocity (2-30 m/s and 1m/s respectively) (Figure 1-1). Functionally Aδ-fibres mediate first pain, which is well localized and fast. Aδ-fibers can be further divided into two classes according to their response to high threshold mechanical stimuli and responsiveness to noxious heat and tissue damage (Julius and Basbaum 2001).

C-fibres are unmyelinated small diameter primary afferents but in contrast to Aδ fibers, C-fibres mediate second or slow pain (Julius and Basbaum 2001). Functionally most C-fibres are polymodal (>70%) nociceptors that respond to mechanical, thermal and chemical stimuli (CMH) or are mechanoinsensitive (C-MIA) (Meyer, Davis et al. 1991, Cain, Khasabov et al. 2001). There is also a specific subset of C-fibres, known as silent or sleeping nociceptors. These 'silent' nociceptors are normally unresponsive to noxious stimuli but can become activated when sensitized by tissue injury (Schmidt, Schmelz et al. 1995).

Besides the broad classification of C-fibres by mechanosensitivity, C-fibre nociceptors are also biochemically distinguishable. Peptidergic and non-peptidergic nociceptors are two subpopulations of C-fibres that differ in expression of cell surface molecules and presence of neuropeptides. In peptidergic nociceptors, substance P and/or calcitonin gene-related peptide (CGRP) are present in the cytoplasm and trkA is expressed on the surface. Non-peptidergic damage sensing neurons are isolectin B4-positive ($IB4^+$) (Bennett, Michael et al. 1998) and express RET (receptor for the glia cell-line-derived family of neurotropic factors) and P2X3 receptors on their surface (Snider and McMahon 1998). A further refinement can be made via the expression of Mas-related G-protein coupled receptors (Mrgprs), a subfamily of G-protein coupled receptors (Dong, Han et al. 2001). Other markers include voltage-gated sodium channels ($Na_v1.7$ and $Na_v1.8$) and TRP channels (TRPA and TRPV1) (Tominaga, Caterina et al. 1998, Kobayashi, Fukuoka et al. 2005), VGlut, Tyrosine hydroxylase (TH) and delta opioid receptor (DOR) (Le Pichon and Chesler 2014) (Figure 1-2). The listed anatomical and functional attributes of nociceptors are useful but have limitations or overlap in defining certain

subpopulations of nociceptors. Therefore, no single criterion is a reliable indicator and often does not take into account the target of innervation (Le Pichon and Chesler 2014). Recent publications describe the differentiation of nociceptors based on their transcriptional profile. Thakur and Crow *et al.* (2014) identified nociceptor-enriched genes, most of which appear to be PNS specific (Thakur, Crow et al. 2014). A groundbreaking paper by Usoskin *et al.* (2015) examines the gene expression profile of DRG neurons and accordingly classified DRG neurons into 11 subtypes (Usoskin, Furlan et al. 2015).

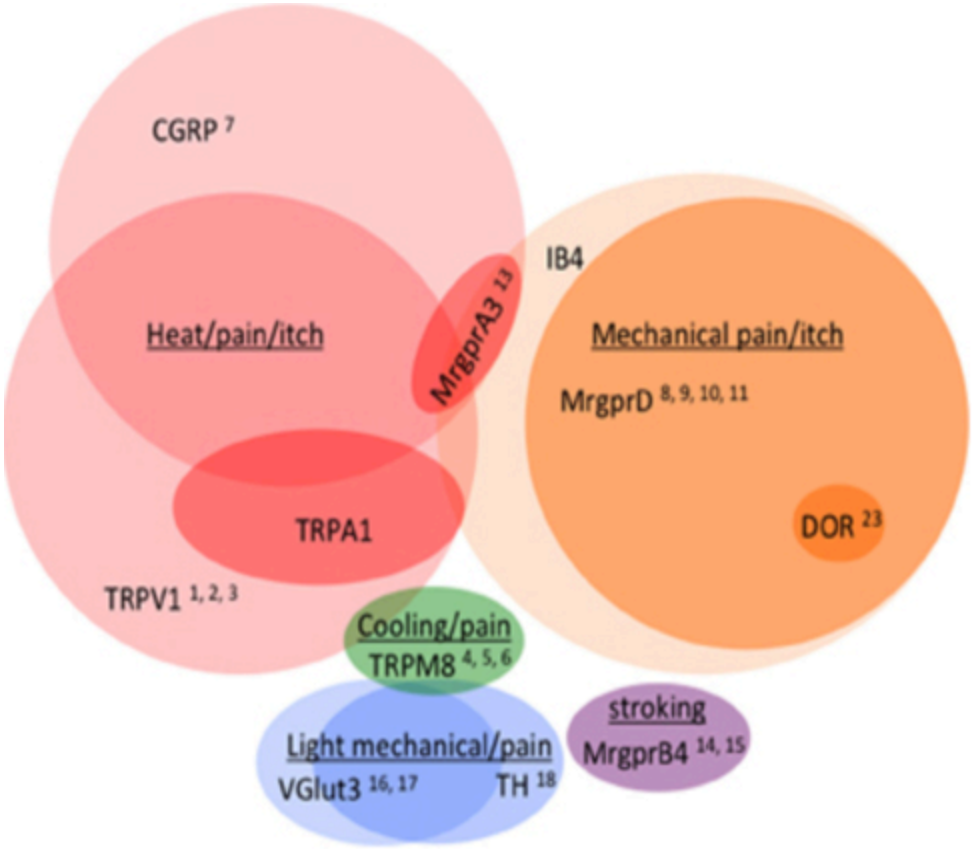

Figure 1-2: Venn diagram illustrating the distribution of markers across different classes of C-fibres (not to scale).

IB4 (isolectin B4-positive); TRPV1 (Transient receptor potential channel V1); TRPA1 (Transient receptor potential channel A1); TRPM8 (Transient receptor potential channel M8); CGRP (calcitonin gene-related peptide); DOR (delta opioid receptor); TH (Tyrosine hydroxylase); MrgprB4/D/A3 (Mas-related G-protein coupled receptor B4/D/A3); VGlut3 (vesicular glutamate transporter type 3). **Taken from Le Pichon and Chesler (2014).**

1.1 Molecular mechanisms of Nociception: Transduction

Sensory transduction is the process of converting information from the periphery into action potentials. In the presence of noxious stimuli, ion channels (e.g. TRP channels or acid-sensing ion channels) at the axon tip of primary afferents open and allow the influx of cations, thereby creating a generator potential that leads to further opening of voltage-gated sodium channels (VGSC) (Figure 1-3). VGSCs amplify the initial depolarization and enable action potentials to be generated. The generated action potential is transmitted from damage-sensing neurons in the periphery through the spinothalamic tract into the somatosensory cortex where finally the sensation of pain is created (Raouf, Quick et al. 2010). This section focuses on known key transduction channels expressed within DRG neurons and their role in transducing thermal, chemical and inflammatory pain.

Transient receptor potential channel (TRP)

Transient receptor potential (TRP) channels are highly conserved throughout the animal kingdom and expressed in sensory and non-sensory cells (Cheng, Sun et al. 2010). TRP channels act as polymodal cellular sensors that activate through a broad range of internal and external stimuli such as noxious and thermal heat, cold, chemicals, mechanical stimulation and osmolarity. In vertebrates, the TRP channel family is divided into two groups and seven subfamilies, based upon structure and sequence homologies (Montell 2005, Cheng, Sun et al. 2010). Structurally, TRP channels are integral membrane proteins with six transmembrane domains (S1-S6) and form a non-selective permeable cation pore (Ramsey, Delling et al. 2006). Mutations in TRP channels have been linked to human cardiovascular diseases, inflammation, sensory dysfunction and familial episodic pain syndrome (Nilius 2007). In particular, transient receptor potential vanilloid receptor 1 (TRPV1), member of the vanilloid subfamily of TRP channels, transient receptor potential melastatin 8 (TRPM8), member of the melastatin subfamily of TRP channels and transient receptor potential ankyrin 1 (TRPA1), member of the ankyrin TRP subfamily

have gained attention as possible new analgesic drug targets due to their role in nociception (Brederson, Kym et al. 2013).

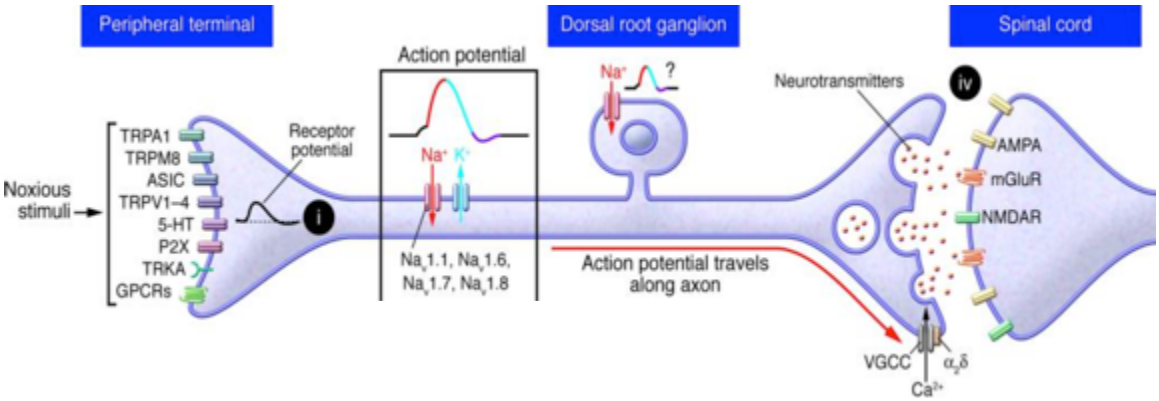

Figure 1-3: Schematic of ion channel distribution on nociceptors.

Taken from Raouf, Quick *et al.* (2010)

Transient receptor potential vanilloid receptor 1 (TRPV1)

TRPV1 is a thermo-sensitive TRP channel that marks a subpopulation of C-fibre nociceptors and is activated by noxious-heat (>43C) and tissue acidosis caused by inflammation (Caterina, Schumacher et al. 1997, Tominaga, Caterina et al. 1998, Kobayashi, Fukuoka et al. 2005, Leffler, Monter et al. 2006). Animal studies confirm that Trpv1 is an important target for various inflammatory agents. After traumatic injury, "the inflammatory soup" is released that render Trpv1 hypersensitive by lowering the channel's activation threshold (Huang, Zhang et al. 2006). Trpv1$^{-/-}$ mice exhibit a decreased response to acute thermal stimuli and develop milder thermal hyperalgesia due to inflammation (Caterina, Leffler et al. 2000, Kasama, Kawakubo et al. 2007).

Transient receptor potential ankyrin 1 (TRPA1)

TRPA1 is the only member of the ankyrin subfamily of TRP channels that is also found in humans, and is required for thermo-sensation and nociception. TRPA1 is mainly expressed in a subpopulation of primary sensory neurons (Story, Peier et al. 2003, Nagata, Duggan et al. 2005) but also in non-neuronal cell types (Nozawa, Kawabata-Shoda et al. 2009). Besides TRPA1's essential role in mediating acute inflammatory pain (Chen, Joshi et al. 2011, Moilanen,

Laavola et al. 2012), it is also activated by environmental irritants (Bautista, Jordt et al. 2006, Andrade, Meotti et al. 2012) and has been postulated to play a role in injury-evoked cold hypersensitivity (del Camino, Murphy et al. 2010) and hearing (Nagata, Duggan et al. 2005). Recently, a gain-of-function mutation in TRPA1 has also been implicated in inherited familial episodic pain syndrome type I (Kremeyer, Lopera et al. 2010).

Transient receptor potential melastatin 8 (TRPM8)

Inflammation, viral induced nerve injury and tissue damage can produce cold evoked hypersensitivity, which is primarily mediated by TRPM8 (Dhaka, Murray et al. 2007). Whereas TRPV1 is only activated by noxious stimuli, (Huang, Zhang et al. 2006), TRPM8 is also activated by innocuous cold temperatures (Bautista, Siemens et al. 2007). Genetic and pharmacological ablation provides the strongest evidence for this channel's non-redundant role in cold sensation. $TRPM8^{-/-}$ mice exhibit almost a complete loss of acute cold sensation (Knowlton, Bifolck-Fisher et al. 2010) and show attenuated injury-evoked hypersensitivity after inflammation and neuropathic nerve injury. However, knockout mice still remain responsive to noxious heat and mechanical stimuli (Proudfoot, Garry et al. 2006, Colburn, Lubin et al. 2007).

Acid-sensing ion channels (ASICs)

ASICs are voltage-independent, proton-gated ion channels (Waldmann, Champigny et al. 1997) that form homo- or heterotrimeric transmembrane complexes (Jasti, Furukawa et al. 2007, Gonzales, Kawate et al. 2009). ASICs are primarily expressed in the cell body, peripheral terminals of nociceptors (Price, McIlwrath et al. 2001) and central neurons (Alvarez de la Rosa, Krueger et al. 2003). At the peripheral terminals, ASICs are activated through changes in pH caused by inflammation and endo/exogenous irritants (Reeh and Steen 1996, Price, McIlwrath et al. 2001, Deval, Noel et al. 2008). In rodents, at least seven isoforms are known and implicated peripherally in nociception and possibly mechano-sensation (Gonzales, Kawate et al. 2009) Centrally, ASICs are believed to play a role in synaptic plasticity, learning, memory and pain processing (Zha, Wemmie et al. 2006, Cho and Askwith 2008). Furthermore,

several studies report a link between ASIC3 and anxiety and ASIC3 and insulin resistance (Huang, Yang et al. 2008, Wu, Lin et al. 2010).

1.2 Molecular mechanisms of Nociception: Transmission

Transduction sensors like TRP channels convey sensory information into an initial electrical signal, a generator potential. This leads to changes in the membrane potential and triggers the opening of voltage-gated sodium channels (VGSCs). VGSCs control cellular excitability and play a key role in action potential generation and propagation. However, dysregulated activity of voltage-gated sodium channels has been implicated in spontaneous and inherited human pain disorders. In the following section, the structure, function and distribution of voltage-gated sodium channels in the PNS and CNS will be discussed, with a special focus on $Na_v1.7$.

Voltage-gated sodium channel family

Sodium channels are members of the ion channel superfamily that also includes potassium and calcium channels. In contrast to sodium channels, potassium and calcium channels have lower amino acid sequence conservation among family members. In the mammalian VGSC superfamily, ten different members have been cloned ($Na_v1.1$-1.9 and Na_x), all of which have greater than 50 per cent conserved sequence homology in the transmembrane and extracellular domains (Catterall 2000, Yu and Catterall 2004, Catterall, Goldin et al. 2005). Voltage-gated sodium channels can be distinguished by their sensitivity to TTX, a tetrodotoxin from puffer fish that blocks the ion selective pore (Klugbauer, Lacinova et al. 1995). In both humans and mice, $Na_v1.1$, $Na_v1.2$, $Na_v1.3$ and $Na_v1.7$ are the most closely related and are encoded by a set of four genes clustered on chromosome 2 (George, Knittle et al. 1992). These channels exhibit high tetrodotoxin sensitivity (TTXs) and are blocked by the presence of nanomolar concentrations of TTX. $Na_v1.4$ and $Na_v1.6$ are also TTXs and share a greater than 80 per cent sequence homology with the gene cluster on chromosome 2. However, their locus of transcription in humans and mice is on chromosome 17 and 12 respectively (Catterall, Goldin et al. 2005). The voltage-

gated sodium channels, $Na_v1.5$, $Na_v1.8$ and $Na_v1.9$ share a greater than 64 per cent conservation with the four on chromosome 2q while in humans and mice their locus of transcription is on chromosome 3. In comparison, this group of channels is insensitive to TTX up to micromole concentrations. Mutagenesis studies show that responsiveness to TTX is determined by a single amino acid sequence at position 384 in domain I (Sivilotti, Okuse et al. 1997). In particular, a change from tyrosine or phenylalanine to serine at position 384 can transform a channel from TTX sensitive (TTXs) to almost TTX resistant (TTXr) (Herzog, Cummins et al. 2003). Given the high conservation and the clustering of genes in chromosomal loci, it was suggested that the family of voltage-gated sodium channels has arisen from gene duplication and chromosomal rearrangements relatively recently in evolution (Catterall, Goldin et al. 2005).

Structure and function of voltage-gated sodium channels

Voltage-gated sodium channels are essential for action potential generation and propagation and change conformation with changing membrane potential. Membrane depolarization induces the opening of the channel and influx of sodium, which is followed by inactivation, through intracellular binding of the cytoplasmic loop to the pore, which terminates the sodium flow. While the membrane potential is repolarizing to return to the resting membrane potential (-60mV) the channel is in a closed state: repriming (recovery from inactivation) (Klugbauer, Lacinova et al. 1995).

Structurally voltage-gated sodium channels are large multi-domain proteins composed of a 220-260 kDa large alpha subunit protein with associated beta subunits (Klugbauer, Lacinova et al. 1995). The alpha subunit of voltage-gated sodium channels is organized into four domains (DI-DIV), each of which consists of six transmembrane segments (S1-S6) that form the voltage sensors and the ion selective pore. The voltage sensors are found in the S4 alpha helix in each of the four alpha subunit domains (I-IV) (Figure 1-4). Residues in S4 are either lysine or arginine that are arranged in an interval of every third amino acid. The ion selective pore is formed by a re-entrant loop between helices S5 and S6 and is embedded into the transmembrane region of the channel to form

a narrow, ion selective filter at the extracellular end of the pore (Noda, Shimizu et al. 1984, Guy and Seetharamulu 1986). Due to membrane depolarization, the voltage-gated sensors that are surrounding the central part of the ion selective pore undergo rearrangements that lead to opening of the pore. When the pore is open the ion selective filter will allow positively charged Na^+ ions to enter through the pore. However, it is still unclear how ion selectivity and voltage-dependent pore gating is achieved in mammalian VGSCs. Our current understanding of channel structure is based on comparative sequence analysis (Noda, Shimizu et al. 1984), predictions of two-dimensional folding patterns (Guy and Seetharamulu 1986) and functional assays, as crystallization of a mammalian VGSC has not been successful yet (Figure 1-4,Top). Valuable insights have been gained from crystallization of Na_vAb, a bacterial voltage-gated sodium channel that shares around 20 percent sequence homology with mammalian Na_v channels (Charalambous and Wallace 2011). Na_vAb, originally derived from *Acrobacter butzleri*, is a homotetrameric VGSC with each of the homomers consisting of 6 transmembrane segments (Figure 1-4,Bottom). Its crystal structure revealed that the Na_vAb consists of two interconnected parts: the pore module and the voltage sensor domains. The pore is composed of four modules 1) an outer funnel-like vestibule 2) a selectivity filter 3) a central cavity and 4) an intracellular activation gate. These parts are enclosed and interact with four peripheral voltage sensor domains (VSD). Changes in membrane potential induce structural changes in the VSD that lead to the structural rearrangement of the pore module and subsequently its opening. The selectivity filter in the pore module is short and water filled with four glutamate residues at its narrowest part that generate an electronegative high-field strength side where Na^+ is captured and partial dehydrated via interaction with the acidic side chains. In this way, Na^+ is conducted though the pore (Payandeh, Scheuer et al. 2011)(Figure1-4, Bottom).

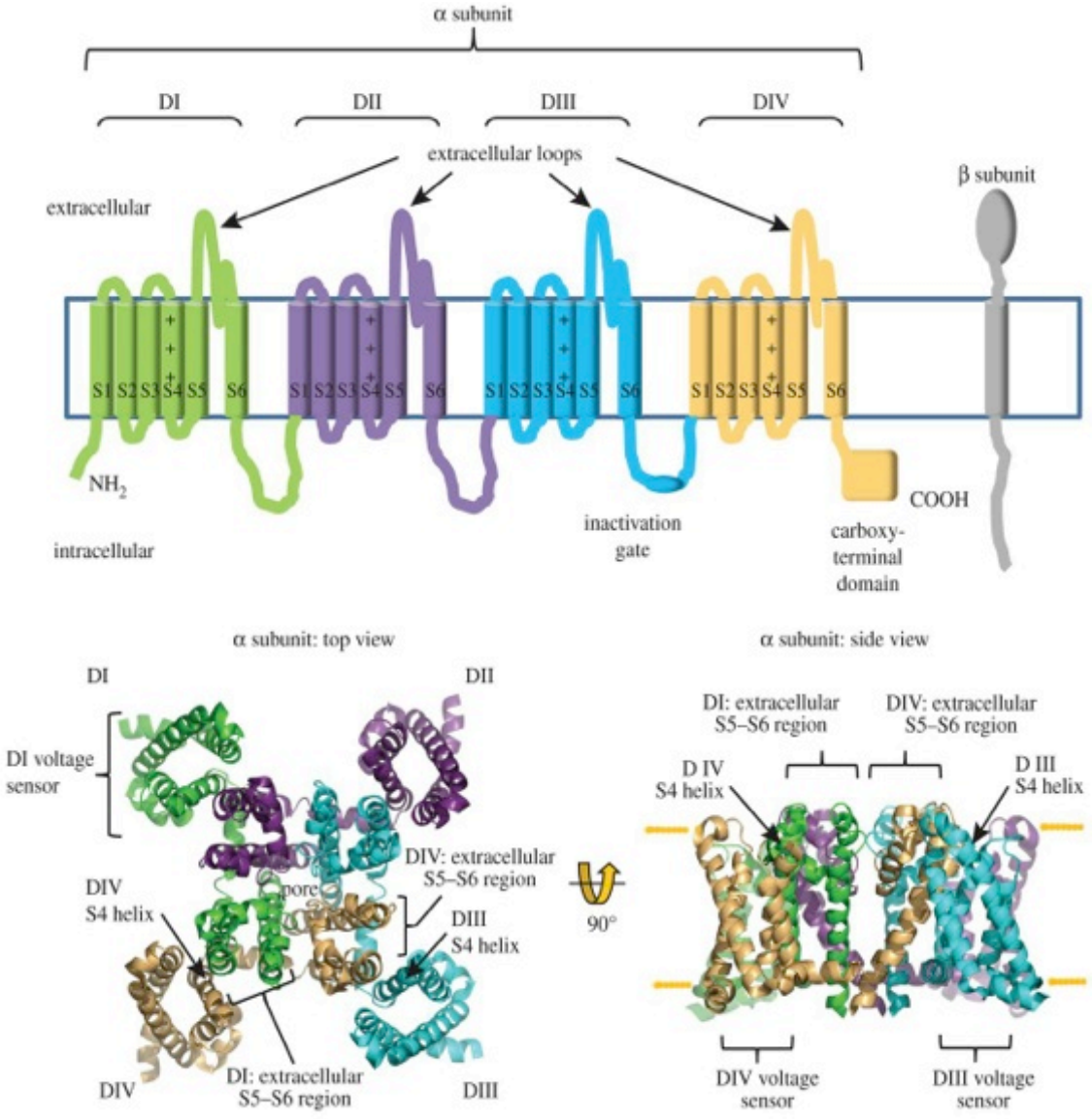

Figure 1-4: The subunit organization of the voltage-gated Na_v channel.

Top I Alpha subunits of voltage-gated sodium channels (VGSCs) are integral membrane proteins organized in four homologous domains (DI-DIV). Each domain consists of 6 transmembrane segments (S1-S6) that form voltage sensors and ion selective pores. The voltage sensor is found in the S4 alpha helix in each of the four alpha subunit domains (I-IV) residues in S4. The ion selective pore is formed by a re-entrant loop between helices S5 and S6 and is embedded into the transmembrane region of the channel to form a narrow, ion selective filter at the extracellular end of the pore (Noda, Shimizu et al. 1984, Guy and Seetharamulu 1986). **Bottom I** Crystallization of Na_vAb. Top and side view of the Na_vAb channel from the bacterium *Acrobacter butzleri*. **Taken from Namadurai, Yereddi *et al.* (2015).**

The high resolution crystal structure of Na_vAb in a closed conformation but with an activated voltage sensor domain (Payandeh, Scheuer et al. 2011) and in two potentially inactivated states (Payandeh, Gamal El-Din et al. 2012) has shed light on a possible mechanism of voltage-dependent pore gating and ion selectivity in mammalian VGSCs. However, it is important to note that mammalian VGSCs are likely to be structured differently as they are multi-domain proteins. Only a high-resolution crystal structure of a mammalian VGSC will bring clarity on how precisely pore gating is achieved (Dib-Hajj, Yang et al. 2013).

Beta subunits

Alpha subunits are associated with beta subunits and can function to modulate their gating properties. Four β-subunit genes (*SCN1B*-*SCN4B*) (Isom, De Jongh et al. 1992, Isom, Scheuer et al. 1995, Kazen-Gillespie, Ragsdale et al. 2000, Morgan, Stevens et al. 2000, Qin, D'Andrea et al. 2003, Yu, Westenbroek et al. 2003, Cheng, Sun et al. 2010) have been identified in the human genome, which encode for β1, β2, β3, β4 subunit. These subunits have a molecular weight of around 30-40 kDa. In addition, β1-subunit is alternatively spliced into β1a and β1b (Kazen-Gillespie, Ragsdale et al. 2000). Aside from β1b, which is soluble, all β-subunits share a common structure: an extracellular N-terminal immunoglobulin loop (Ig), a transmembrane domain and a small intracellular C-terminal domain. Na_v alpha subunits and β-subunits are linked together through the extracellular Ig domain with disulfide bonds in β2 and β4 and non-covalently with β1 and β3 (Hartshorne, Messner et al. 1982, Messner and Catterall 1985, Chen, Calhoun et al. 2012). Although all β-subunits were thought to be single transmembrane proteins, this seems to hold true for most but not all subunits i.e. β1b is soluble (Kazen-Gillespie, Ragsdale et al. 2000) and a high-resolution crystal structure has revealed that β3 assembles into a trimer (Namadurai, Balasuriya et al. 2014). Trimeric formation of β3 increases the number of possible binding sites to Na_v channels and might be important in connecting the Na_v alpha subunits to each other and to other functional components. Higher order clusters of Na_v channels may also influence the electrophysiological properties of the channel individually as well as the whole cluster (Namadurai,

Balasuriya et al. 2014). A comparison of primary structures indicates that β3 and β1 are closely related, with most of the amino acids critical for trimerization found at identical positions with the exception of Pro-6 that is changed to Asp-6 in β1. Although β1 trimers may also form, they will most likely differ from β3 trimers as the change from proline to aspartic acid will interfere with trimer formation due to electrostatic repulsion (Namadurai, Balasuriya et al. 2014). β4 and β2 also share high sequence homology. In contrast to β3, crystallization showed that β4 does not form oligomers (Gilchrist, Das et al. 2013). Association of a Na_v α-subunit with a specific β-subunit can directly modulate the sodium channel gating properties (Isom, Ragsdale et al. 1995, Zimmer and Benndorf 2002, Meadows and Isom 2005).

Animal studies confirm that electrophysiological properties of sodium channels are changed in β-subunit null mice. For instance, *Scn1b* null mice have severe neurological deficiencies and exhibit hyperexcitable DRG neurons (Lopez-Santiago, Brackenbury et al. 2011). In contrast, DRG neurons in *Scn2b* knockout mice exhibit a fifty per cent decrease in activation and inactivation of TTX-S sodium currents due to decreased $Na_v1.7$ expression in the plasma membrane (Lopez-Santiago, Pertin et al. 2006). Although *Scn2b* null mice are more susceptible to seizures, they exhibit no severe neurological deficits (Chen, Bharucha et al. 2002, Chen, Westenbroek et al. 2004, Patino, Brackenbury et al. 2011). *Scn3b* mice suffer from arrhythmia, likely due to *Scn3b* being normally expressed in the heart (Hakim, Gurung et al. 2008, Hu, Barajas-Martinez et al. 2009, Hakim, Brice et al. 2010). A recent publication by Laedermann *et al.* (2013) suggests that the co-expression of $Na_v1.7$ with β1- or β3-subunits in HEK293 cells not only changes gating properties of the channel in the cell membrane but also modulates the $Na_v1.7$ glycosylation state and in this way regulates its trafficking and stabilization in the plasma membrane (Laedermann, Syam et al. 2013).

Distribution of voltage-gated sodium channels (VGSCs)

VGSCs are structurally and functionally related to each other but cellular and subcellular location varies among family members. $Na_v1.1$, $Na_v1.2$, $Na_v1.3$ and $Na_v1.6$ are predominantly located in the CNS, whereas $Na_v1.7$, $Na_v1.8$ and $Na_v1.9$ are primarily found in the peripheral nervous system, $Na_v1.4$ mainly in the skeletal muscles and $Na_v1.5$ in heart (King and Vetter 2014). The following section gives examples of the diverse location and function of voltage-gated sodium channel family members.

$Na_v1.1$ (*SCN1A*)

$Na_v1.1$ is found in the soma and dendrites of neuronal cells, the spinal cord (Westenbroek, Merrick et al. 1989) and in cardiac myocytes where it plays a significant role in excitation-contraction coupling (Maier, Westenbroek et al. 2003). Missense and nonsense mutations in *SCN1A* have been linked to generalized-epilepsy with febrile seizures plus type 2 or GEFS+2 (Escayg, Heils et al. 2001), familial hemiplegic migraine (Dichgans, Freilinger et al. 2005) and various other forms of epilepsy (Nabbout, Gennaro et al. 2003, Meisler and Kearney 2005).

$Na_v1.3$ (*SCN3A*)

In DRG, $Na_v1.3$ is predominantly expressed during embryonic and prenatal stages and is transcriptionally silent during adulthood (Beckh, Noda et al. 1989, Shah, Stevens et al. 2001). In rats, peripheral nerve and CNS injuries re-induces and upregulates the expression of $Na_v1.3$ mRNA and protein in spinal cord and DRG neurons (Waxman, Kocsis et al. 1994, Dib-Hajj, Tyrrell et al. 1998), which possibly contributes to neuronal hyperexcitability in neuropathic pain states. However, the role of $Na_v1.3$ in neuropathic pain is still unclear and a species-specific effect could be present. Global and DRG specific $Na_v1.3^{-/-}$ mice do not exhibit alleviated pain behaviour after nerve injury (Lindia, Kohler et al. 2005, Nassar, Baker et al. 2006). In contrast, neuropathic rats show decreased pain-related behavior after intrathecal AS-ODN treatment and virus-mediated siRNA knock down of $Na_v1.3$ (Hains, Saab et al. 2006, Samad, Tan et al. 2013).

$Na_v1.8$ *(SCN10A)*

$Na_v1.8$ is exclusively found in peripheral sensory neurons (Akopian, Sivilotti et al. 1996) with 85 per cent of $Na_v1.8$-positive cells identified as nociceptors (Djouhri, Fang et al. 2003). In contrast to $Na_v1.7$, $Na_v1.8$ activates at a higher threshold and exhibits slow-inactivating characteristics. Therefore, it is the most significant contributor in the depolarization phase of action potentials in DRG neurons. Animal studies report a specialized role for $Na_v1.8$ in mediating noxious cold pain. While very low temperatures affect responsiveness of TTXs channels, $Na_v1.8$ still remains responsive (Zimmermann, Leffler et al. 2007). Knockout studies on $Na_v1.8$ emphasize its crucial role in cold but also inflammatory and mechanical pain. However, development of neuropathic pain and the response to acute heat stimuli are seemingly unaffected by the ablation of $Na_v1.8$ (Nassar, Levato et al. 2005, Abrahamsen, Zhao et al. 2008). A recent study by Faber *et al.* (2012) concludes that certain gain-of-function mutations in $Na_v1.8$ (*SCN10A*) underlie painful peripheral neuropathy (Faber, Lauria et al. 2012). Furthermore, in rats with bone cancer the expression of $Na_v1.8$ is linked to the development of pain in this model (Qiu, Jiang et al. 2012).

$Na_v1.9$ (*SCN11A*)

$Na_v1.9$ is mostly found in small diameter nociceptive DRG neurons (Dib-Hajj, Tyrrell et al. 1998, Fang, Djouhri et al. 2002) and expresses a permanent TTX resistant current that is around the resting membrane potential (Cummins, Dib-Hajj et al. 1999, Priest, Murphy et al. 2005). Therefore $Na_v1.9$ mainly contributes to the setting of DRG excitability by modulation of the resting potential (Baker, Chandra et al. 2003, Ostman, Nassar et al. 2008). $Na_v1.9$ knockout mice exhibit attenuated inflammatory pain responses whereas acute and neuropathic pain thresholds are unchanged (Priest, Murphy et al. 2005, Amaya, Wang et al. 2006). A recent study by Leipold *et al.* (2013) showed that a recurrent gain-of-function missense mutation in $Na_v1.9$ can lead to congenital inability to experience pain (Leipold, Liebmann et al. 2013).

1.3 Distribution of $Na_v1.7$ and *SCN9A/Scn9a*

SCN9A/Scn9a

$Na_v1.7$ plays an important role in initiation and propagation of action potentials (Cummins, Howe et al. 1998) and acts as a threshold channel. Spontaneous and inherited mutations in *SCN9A* ($Na_v1.7$) are associated with the human pain disorders Primary erythromelalgia (PE) (Yang, Wang et al. 2004, Drenth, te Morsche et al. 2005), Paroxysmal extreme pain disorder (PEPD) (Fertleman, Baker et al. 2006, Dib-Hajj, Estacion et al. 2008) and Channelopathy-associated insensitivity to pain (CAIP) (Cox, Reimann et al. 2006).

Cellular distribution of $Na_v1.7$

$Na_v1.7$ is mainly expressed in small and medium diameter nociceptive DRG neurons, sympathetic ganglia (Sangameswaran, Fish et al. 1997, Toledo-Aral, Moss et al. 1997) and olfactory sensory neurons (Weiss, Pyrski et al. 2011). Nociception and olfaction are both linked to $Na_v1.7$ function: CIP patients are anosmic and individuals carrying specific SNPs in *SCN9A* (R1150W allelic frequency of 14%, and P610T allelic frequency of 4%) that are associated with altered pain perception (Samuels, te Morsche et al. 2008, Reimann, Cox et al. 2010) also have altered olfactory thresholds. These findings highlight that $Na_v1.7$ blockers will likely block nociception and olfaction (Heimann, Lotsch et al. 2013).

Additionally, $Na_v1.7$ is expressed in adrenal chromaffin cells (Toledo-Aral, Moss et al. 1997), visceral sensory neurons, nodose ganglion neurons (Muroi, Ru et al. 2011), smooth myocytes (Holm, Rich et al. 2002, Jo, Nagata et al. 2004), myenteric neurons (Sage, Salin et al. 2007) and non-excitable cells such as immune cells (Kis-Toth, Hajdu et al. 2011), human erythroid progenitor cells (Hoffman, Dodson et al. 2004) and β-cells in the pancreatic islets where $Na_v1.7$ might trigger glucose-stimulated insulin secretion (Ernst, Aguilar-Bryan et al. 2009, Zhang, Chibalina et al. 2014). Furthermore, human cells derived from prostate cancer (Diss, Stewart et al. 2005) and breast cancer patients (Fraser, Diss et al. 2005) show increased expression of $Na_v1.7$.

Subcellular location of $Na_v1.7$

Immuno-staining of DRG neurons shows that $Na_v1.7$ is highly expressed in unmyelinated small diameter C-fibre neurons. Co-immunostaining of $Na_v1.7$ with the C-fibre marker peripherin (Einheber, Zanazzi et al. 1997) shows that around sixty-three per cent of peripherin-positive neurons exhibit $Na_v1.7$ expression whereas only a small minority of peripherin-negative cells is immunolabelled for $Na_v1.7$. Co-immunostaining of Neurofilament 200 (N200), an A-fiber marker (Goldstein, House et al. 1991) and $Na_v1.7$ exhibits a fifteen per cent overlap in expression of $Na_v1.7$ in medium diameter neurons. However, large diameter DRG neurons only rarely exhibit $Na_v1.7$ expression (Figure 1-5,Top).

C-fibres can be divided into peptidergic and non-peptidergic nociceptors that differ in expression of cell surface molecules and presence of neuropeptides (Bennett, Michael et al. 1998, Snider and McMahon 1998). Black, Frezel *et al.* (2012) report that a similar percentage of peptidergic (CGRP) and non-peptidergic (IB4) neurons express $Na_v1.7$ (Figure 1-5,Top) (Black, Frezel et al. 2012)(Figure 1-5,Top). A recent paper by Usoskin, Furlan *et al.* (2015) identified 11 subtypes of DRG neurons based on comprehensive RNA-seq. Controversly, they showed that *Scn9a* is highly expressed in small unmyelinated low threshold mechano C-fibre neurons, unmyelinated peptidergic and non-peptidergic neurons as well as myelinated neurons with the exception of only one subtype of large propioceptor neurons ('NF5') (Usoskin, Furlan et al. 2015).

Co-immunostaining of $Na_v1.7$, peripherin (unmyelinated fibres) and caspr (paranodal regions of myelinated fibers) in the sciatic nerve shows that $Na_v1.7$ is also strongly expressed along the peripheral branch of approximately 27 per cent of unmyelinated C-fibres. Additionally, in a subset of small diameter myelinated Aδ-fibers, $Na_v1.7$ is expressed in the nodes of Ranvier. $Na_v1.7$ is usually not expressed in the nodal or paranodal segment of nodes of Ranvier (Figure 1-5,Bottom). This expression pattern correlates with the expression of $Na_v1.6$ and might underlie a regulatory function in pain signaling (Black, Frezel et al. 2012).

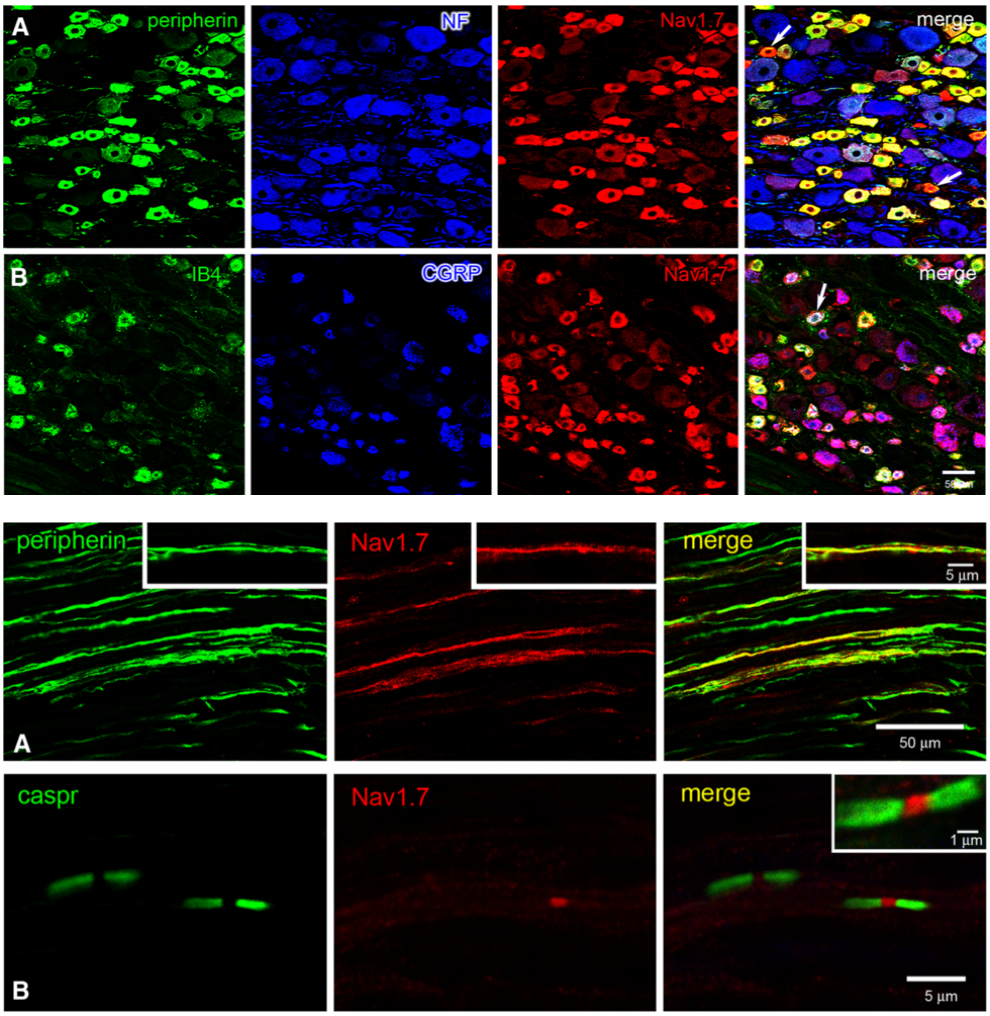

Figure 1-5: Expression of $Na_v1.7$ in DRG neurons and sciatic nerve.

Top I Expression of $Na_v1.7$ in DRG neurons (A) Expression of $Na_v1.7$ in DRG neurons, immunostaining against peripherin (green), neurofilament 200 (NF, blue) and $Na_v1.7$ (red). Peripherin co-localization with $Na_v1.7$ (yellow). A few small peripherin-negative neurons display robust $Na_v1.7$ immunolabeling (arrows) and NF co-localization with $Na_v1.7$ (magenta). **(B)** $IB4^+$(green) CGRP (blue) and $Na_v1.7$ (red). $IB4^+$ co-localization with $Na_v1.7$ (yellow) and CGRP co-localization with $Na_v1.7$ (magenta). Few DRG neurons display co-localization of IB4, CGRP and $Na_v1.7$ (arrow). **Bottom I Expression of $Na_v1.7$ in sciatic nerve (A)** Immunostaining against peripherin (green), $Na_v1.7$ (red) and co-localization with $Na_v1.7$ (yellow) (B) Nodal regions in sciatic, paranodal marker caspr (green) and $Na_v1.7$ (red). **Taken from Black, Frezel *et al.* (2012).**

The central branch of nociceptors projects its axon to second order neurons in the superficial lamina of the spinal cord dorsal horn. Co-immunostaining of $Na_v1.7$ with peripherin and Neurofilament 200 in the dorsal and ventral roots reveals that $Na_v1.7$ is present along unmyelinated and myelinated fibres in the dorsal but not the ventral roots. Similar to sciatic nerve, a small subset of small diameter myelinated A-fibres express $Na_v1.7$ in the nodal region of the dorsal but not the ventral root (Black, Frezel et al. 2012). Peripherally, peptidergic and non-peptidergic C-fibers terminate in different layers in the epidermis. In skin, intraepidermal nerve fibres (IENF) are the peripheral terminals of C-fibre and A-fibres (Zylka, Rice et al. 2005). Co-immunostaining of $Na_v1.7$ with Protein Gene Product 9.5 (PGP9.5), an IENF marker, shows that $Na_v1.7$ is robustly expressed in IENFs, from the point of branching to the axon tip (Figure 1-6,Top).

Centrally, peptidergic fibres (CGRP) terminate in lamina I and IIo and non-peptidergic ($IB4^+$) fibers terminate in lamina IIi of the spinal cord dorsal horn (Snider and McMahon 1998). Co-immunostaining of $Na_v1.7$ with CGRP and $IB4^+$ as well as synaptophysin, a pre-synaptic marker, demonstrated that $Na_v1.7$ is robustly expressed within pre-synaptic terminals in lamina I, Iio and IIi (Figure 1-6,Bottom). However, $Na_v1.7$ is not expressed in post-synaptic neurons (Black, Frezel et al. 2012).

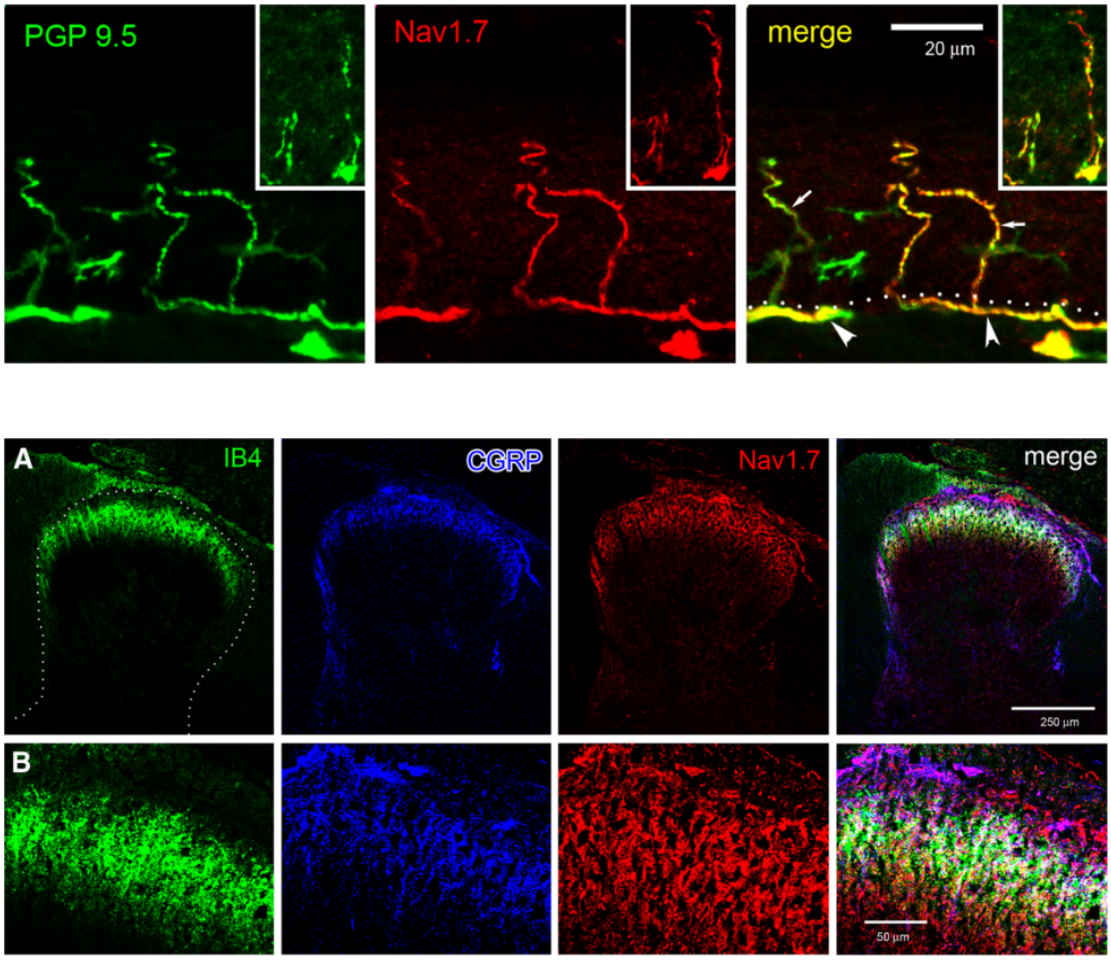

Figure 1-6: Expression of $Na_v1.7$ in glabrous skin and spinal cord dorsal horn.

Top I Expression of $Na_v1.7$ in glabrous skin PGP9.5 (green) intraepidermal fibres (IENF) branch from nerve bundles (arrowheads) at dermis/epidermis boundary (dotted line) and ascend in the epidermis. PGP9.5-positive IENFs exhibit $Na_v1.7$ (red) immunolabeling. **Bottom I $Na_v1.7$ expression in spinal cord dorsal horn. (A)** Immunostaining against IB4 (green), CGRP (blue) and $Na_v1.7$ (red). Robust $Na_v1.7$ immunolabelling is present within lamina I and II. $Na_v1.7$ co-localization with $IB4^+$ (yellow) and with CGRP (magenta). **(B)** Increased magnification of IB4, CGRP and $Na_v1.7$ labeling in superficial lamina of dorsal horn**. Taken from Black, Frezel *et al.* (2012).**

Alternative splicing of *SCN9A* in human DRG

Sanger sequencing of *SCN9A* PCR products amplified from human DRG cDNA showed that *SCN9A* ($Na_v1.7$) is alternatively spliced in exon 5 and exon 11 (Raymond, Castle et al. 2004). Further qPCR analysis of *SCN9A* splice variant distribution in human DRG also showed that splicing of exon 5 and exon 11 is uncoupled (Figure 1-7). Exon 5 encodes for the extracellular linker and voltage sensor in DI and exists as two similar mutually exclusive exons that are denoted as exon 5N and 5A. The second site, exon 11, encodes for an intracellular linker between DI and II and is spliced into 11S (short) and exon 11L (long) (Figure 1-7). The exon 5N-containing transcript is reported to be a developmental and DRG restricted variant only, whereas the alternatively spliced exon 5A transcript is found in the adult PNS and CNS (Raymond, Castle et al. 2004). Also, 11S shows increased expression in neonatal DRG neurons whereas the longer isoform 11L is predominantly found in adult tissues. The 11S-containing *Scn9A* transcripts are enriched in rats after neuropathic surgery (Raymond, Castle et al. 2004). Functionally, alternative splicing changes the channel's ability to interact with the beta1-subunit and thereby modulates its voltage dependent activation and steady state inactivation (Farmer, Cox et al. 2012).

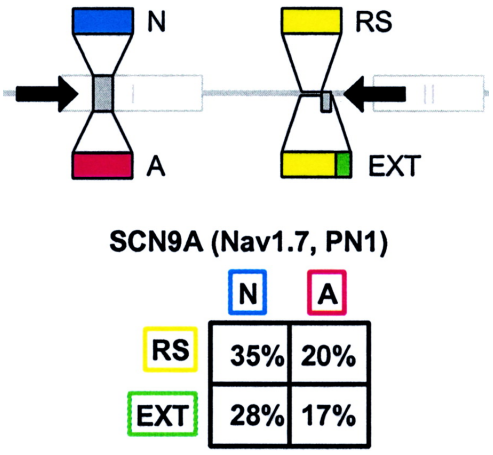

Figure 1-7: Alternative splicing patterns of *SCN9A* are not coupled.

Top I Sanger sequencing of *SCN9A* PCR products amplified from human DRG cDNA showed that *SCN9A* is alternatively sliced in exon 5 and exon 11. Exon 5 has a neonatal (N) and adult (A) and exon 11 has an extended coding exon 11 (EXT or 11L), shorter coding exon 11 (RS or 11S) variant. Bottom I *SCN9A* isoform specific qPCR analysis from human DRG cDNA showed that splicing of exon 5 and exon 11 is not linked. **Taken from Raymond, Castle *et al.* (2004).**

1.4 Post-translational modification of $Na_v1.7$

Akin to other proteins, voltage-gated sodium channels undergo post-translational modification and intracellular trafficking, yet our understanding of possible mechanisms and protein-protein interaction partners that mediate these processes is very limited, in particular in regards to specific voltage-gated sodium channel subtypes such as $Na_v1.7$. This section discusses post-translational modification and protein-interactions of VGSCs that have been identified through Yeast-2-hybrid, Co-immunoprecipitation, pull-down assays and phosphorylation studies.

Post-translational glycosylation

A protein's journey starts with its synthesis in the rough endoplasmic reticulum (RER) followed by transportation into the ER lumen where it is folded. Proteins are then moved toward the smooth ER, where the newly synthesized protein is packed into vesicles that bud off to the Golgi apparatus. In the ER and Golgi apparatus proteins undergo extensive glycosylation, which can make up 30 per cent of a protein's molecular weight (MW) (Schmidt and Catterall 1987). As the mature protein arrives at the trans-end (the site of the release) of the Golgi apparatus, it is packed into vesicles and sent off to its final destination i.e. the plasma membrane in the case of VGSCs (Alberts, Bray et al. 1995, Alberts 2010, Moremen, Tiemeyer et al. 2012).

Protein glycosylation is functionally important in a variety of biological processes, from protein folding, cell signaling, cell-cell adhesion to regulation of development and immunity (Moremen, Tiemeyer et al. 2012). Voltage-gated sodium channels are subject to glycosylation that directly impacts their gating properties and trafficking (Waechter, Schmidt et al. 1983, Schmidt and Catterall 1987, Bennett, Urcan et al. 1997, Zhang, Hartmann et al. 1999, Tyrrell, Renganathan et al. 2001, Cronin, O'Reilly et al. 2005). As for $Na_v1.7$, active alpha subunits are present on the cell surface. However, the majority of $Na_v1.7$ might be localized intracellularly, either going through the secretory pathway or stored in intracellular pools (Schmidt, Rossie et al. 1985). In the ER/Golgi where glycosylation takes place, alpha subunits and $\beta1/\beta3$ assemble, which enhances

trafficking of the Na_v alpha subunit to the plasma membrane (Fahmi, Patel et al. 2001, Zimmer, Biskup et al. 2002). In the case of $Na_v1.8$, this is achieved by binding of β3, which mask an ER retention signal and leads to increased transport of the channel to the plasma membrane (Zhang, Li et al. 2008). The impact of glycosylation on $Na_v1.7$ electrophysiological properties is well documented and so is the direct influence on alpha subunit gating properties and expression by β-subunits (O'Malley and Isom 2015). Leaderman *et al*. (2013) addressed the question of whether these two regulator mechanisms are linked, hence if β-subunits directly influence alpha subunit glycosylation. Under experimental conditions, when $Na_v1.7$ is expressed on its own, the channel is present in two mutually exclusive glycosylated forms 1) a core-glycosylation with a MW of 250 kDA and 2) a full-glycosylation state with a MW of 280 kDA. However, $Na_v1.7$ glycosylation state shifts (i.e. from core-glycosylation to fully-glycosylation) and current density increases when co-transfected with β1- or β3-subunit while the activation and inactivation kinetics are only modestly altered. This argues for an increased number of $Na_v1.7$ molecules in the plasma membrane (Laedermann, Syam et al. 2013). The proposed model is that β1- and β3-subunits assemble with the alpha subunits in the ER/Golgi and mediate from there a specifically glycosylated form of cell surface expressed $Na_v1.7$. Co-expression of β1/$Na_v1.7$ enhances the plasma membrane expression of a fully glycosylated $Na_v1.7$ but strikingly also of a third alternatively glycosylated form. β3 mediates the membrane expression of the core-glycosylated form (Figure 1-8). In contrast co-expression of $Na_v1.7$ and β2 or β4 does not shift the glycosylation pattern towards a particular form, neither is the current density changed (Figure 1-8). These findings correlate with the kinetics model proposed by Schmidt and Catterall *et al.* (1987) and findings from Ho *et al.* (2012). Here, interaction of β2 or β4 with the alpha subunit occurs just before anchoring in the membrane, thus after the Golgi apparatus where the glycans are added (Schmidt and Catterall 1987, Ho, Zhao et al. 2012, Laedermann, Syam et al. 2013). The physiological relevance of different glycosylation states is still elusive, however it may be important in membrane stabilization and relevant in pathological pain conditions that are linked to altered $Na_v1.7$ excitability.

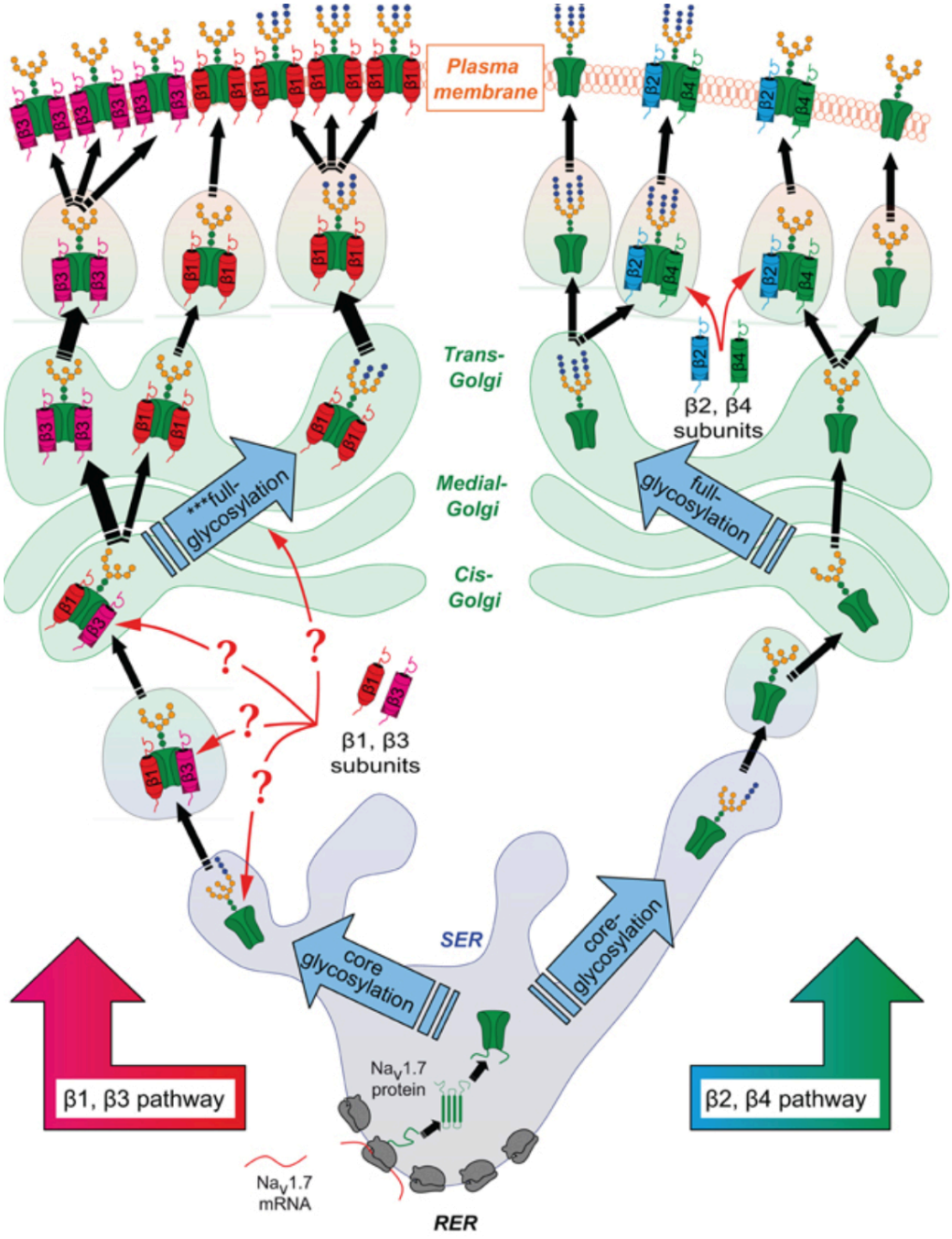

Figure 1-8: Proposed model of the different intracellular pathways of α-subunits depending on the presence of different β-subunits.

The proposed model is that β1- and β3-subunits assemble with the alpha subunits in the ER/Golgi and mediate from there a specifically glycosylated form of cell surface expressed $Na_v1.7$. In contrast, co-expression of $Na_v1.7$ and β2 or β4 does not shift the glycosylation state of $Na_v1.7$. Here interaction of β2 or β4 with the alpha subunit occurs just before anchoring in the membrane, thus after the Golgi apparatus where the glycans are added. **Taken from Laedermann, Syam *et al.* (2013).**

Post-translational phosphorylation

MAPK – ERK1/2

Phosphorylation is a reversible post-translational mechanism that mediates a broad range of functions from membrane transport to gene transcription. During development and in pathological pain states, neurotrophic factors are released that activate mitogen-activated protein kinases (MAPKs), which in turn recruit transcription factors and turn on gene expression (Averill, Delcroix et al. 2001, Woodall, Richards et al. 2008). Extracellular signal-regulated protein kinase 1/2 (ERK1/2) a member of the MAPK family, is found in DRG neurons where pERK1/2, the kinase's active, phosphorylated form is implicated in injury-induced hyperalgesia. Hyperalgesia is a common symptom of acute and chronic pain and is caused by altered neuronal excitability (Ji, Baba et al. 1999, Ji, Samad et al. 2002, Obata, Yamanaka et al. 2004). Stamboulian *et al.* (2010) reported a link of hyperalgesia with altered $Na_v1.7$ activity on the level of ERK1/2. During hyperalgesia, neurotrophic factors are released that activate ERK1/2, which in turn phosphorylates $Na_v1.7$ in the intracellular loop (L1) between domains I and II. This leads to structural changes and altered gating properties of the channel, which subsequently influence the excitability of DRG neurons. In comparison to glycosylation, phosphorylation does not change $Na_v1.7$ current density but its ion conductance (Stamboulian, Choi et al. 2010). Furthermore phosphorylation also regulates *SCN9A* mRNA stability. Constitutive phosphorylation of ERK1/2 leads to increased degradation of *SCN9A* ($Na_v1.7$) mRNA and in this way alters the amount of functional $Na_v1.7$ protein in the plasma membrane (Yanagita, Kobayashi et al. 2003).

Protein Kinase A

Protein kinase A (PKA) and C (PKC) are important cellular modulators of ion channel activity under normal and pathological conditions. Activation and regulation of PKA are dependent on activation via cAMP and interaction with AKAP15 (Cantrell, Tibbs et al. 1999, Cantrell, Tibbs et al. 2002).

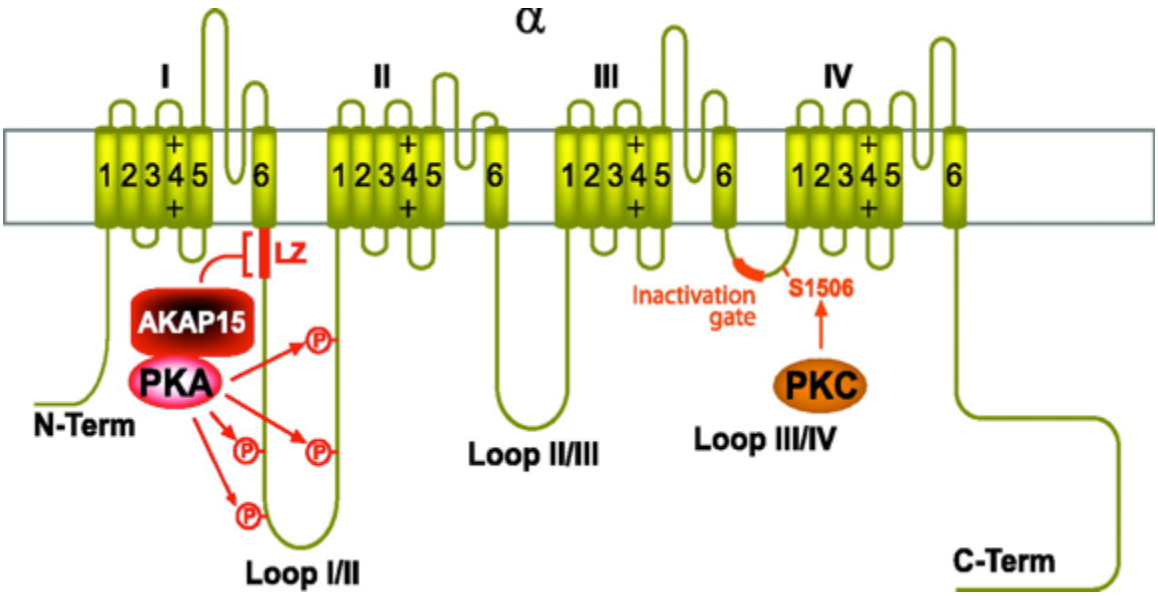

Figure 1-9: Sodium channel alpha subunit-AKAP15-PKA complex and PKC.

Sodium channel alpha subunit (yellow, $Na_v1.2$); AKAP15 binding site (dark red;LZ, bracket and segment); PKA (light red); four phosphorylation sites for PKA within loop I/II (arrows); PKC (orange) PKC phosphorylation site serine-1506, and the inactivation gate sequence within loop III/IV (arrow). **Taken from Dai, Hall *et al.* (2009).**

Additionally, the PKA isoform RIIβ, which is primarily expressed in peripheral nociceptive DRG neurons, is activated through inflammatory agents (Isensee, Diskar et al. 2014). Multiple VGSCs are reported to have PKA phosphorylation sites in their DI-II loop while the AKAP15 binding site is present in all channel subtypes (Dai, Hall et al. 2009). AKAP15 is a small cAMP-dependent protein kinase-anchoring protein that binds to a cytoplasmic motif (LZ-binding site) in loop I/II (L1) of Na_v channels (Figure 1-9) (Cantrell, Tibbs et al. 2002, Few, Scheuer et al. 2007). Although the regulatory and phosphorylation sites are highly conserved, PKA mediated effects on Na_v alpha subunits may be subtype-specific. In $Na_v1.2$, PKA phosphorylates the alpha subunit at four conserved residues in the DI-II linker domain (Smith and Goldin 1996, Smith and Goldin 2000)(Figure1-9). This in turn reduces the channel's opening probability in response to depolarization (Rossie and Catterall 1987, Li, West et al. 1992, Murphy, Rossie et al. 1993, Cantrell, Tibbs et al. 2002). In $Na_v1.5$, PKA phosphorylation sites coincide with a retention signal and phosphorylation of

these sites increasing the trafficking of the channel to the plasma membrane (Zhou, Shin et al. 2002).

As for $Na_v1.7$, a study in *Xenopus* oocytes reports that PKA activation causes a reduction of $Na_v1.7$ sodium peak current while the gating kinetics and voltage sensitivity of $Na_v1.7$ were not affected (Vijayaragavan, Boutjdir et al. 2004). However, PKA regulation of $Na_v1.7$ could be dependent on the expression system and on the channel isoform. For instance exon 11 that encodes for the cytoplasmic loop in DI-DII is spliced into long (11L) or short (11S) splice variants, which affect the loop I-II length that contains an important regulatory site for AKAP15/PKA. While *Scn9a* splice variant 11L has no impact on $Na_v1.7$ kinetics, expression of the exon 11S isoforms and the presence of the PKA activator cAMP lowers the $Na_v1.7$ activation threshold (Chatelier, Dahllund et al. 2008) and could be an explanation for the observed hyperexcitablity of DRG neurons during pathological pain states. This is consistent with observations from Raymond *et al.* (2004) that surgery induced neuropathic pain leads to upregulation of cAMP and 11S-containing *Scn9a* transcripts (Raymond, Castle et al. 2004).

Protein Kinase C

PKC, similar to PKA, phosphorylates alpha subunit $Na_v1.2$ at specific residues in two sites in L1, DI-DII domain of VGSCs and at an additional site in the DIII-DV region, the inactivation loop (Figure 1-9). Both regions are highly conserved among all voltage-gated sodium channels and may be also required for the regulation of $Na_v1.7$ (Numann, Catterall et al. 1991, Cantrell, Tibbs et al. 2002). Various studies suggest that PKC isoforms modulate specific alpha subunits in an isoform and tissue-dependent manner. For instance activation of PKCα isoform in adrenal chromaffin cells, promotes $Na_v1.7$ internalization while PKCε activation negatively influences the stability of *SCN9A* mRNA (Wada, Yanagita et al. 2004). Vijayaragavan *et al.* (2004) also reports that two isoforms of PKC (ε and βII) are responsible for reduction of $Na_v1.7$ and $Na_v1.8$ current amplitudes in *Xenopus* oocytes (Vasilets, Schmalzing et al. 1990, Vijayaragavan, Boutjdir et al. 2004).

PKC isoforms are also involved in modulation of inflammatory and neuropathic pain responses (Malmberg, Chen et al. 1997, Aley, Messing et al. 2000, Igwe and Chronwall 2001). Inhibition of PKC in DRG neurons of diabetic rats attenuates hyperalgesia (Ahlgren and Levine 1994, Kim, Sasaki et al. 2003). Moreover inhibition of specific PKC isoforms in mice diminishes thermal hyperalgesia and opioid-mediated anti-nociceptive behavior (Ohsawa and Kamei 1997, Ohsawa and Kamei 1999). This is consistent with findings in rodents where increased PKC activity correlates with enhanced MAPK p38 activity and upregulation of $Na_v1.7$ (Hong, Morrow et al. 2004, Jin and Gereau 2006, Chattopadhyay, Mata et al. 2008). PKC activation reportedly induces upregulation of $Na_v1.7$ in DRG neurons via activation of p38. Additionally a synergetic effect of PKC activation on PKA was reported. Here, PKC binding to the DI-DII loop of $Na_v1.2$ through AKAP-15/18 mediates PKA activation and targeting to its phosphorylation sites on $Na_v1.2$ (Cantrell, Tibbs et al. 2002).

Calmodulin (CaM) and Ca^{2+}-dependent CaM-kinase II (CaM-KII)

Calmodulin (CaM) is a Ca^{2+}-sensing protein that is ubiquitously expressed. Increase in cytoplasmic Ca^{2+} activates CaM and induces intracellular signaling cascades. CaM binds and modulates voltage-gated sodium channels (Figure 1-10). $Na_v1.4$ in the skeletal muscle associates with CaM via a C-terminal motif, also known as an IQ motif (Mori, Konno et al. 2000, Deschenes, Neyroud et al. 2002). Although the IQ motif appears to be highly conserved among voltage-gated sodium channels, CaM regulation may be subtype-specific and for some ion channels, CaM binding is calcium-independent (Deschenes, Neyroud et al. 2002, Herzog, Liu et al. 2003, Adams, Ben-Johny et al. 2014). $Na_v1.2$, $Na_v1.4$, and $Na_v1.6$ are prime targets of CaM while $Na_v1.1$ and $Na_v1.3$ show lower affinity to CaM in the presence or absence of calcium. Herzog *et al.* (2003) reported that CaM regulates the current density of both $Na_v1.4$ and $Na_v1.6$. However, binding of calcium/CaM to $Na_v1.4$ is critical and mutations in the IQ motif reduce the number of $Na_v1.4$ channels in the plasma membrane but only mildly impact its gating properties (Biswas, Deschenes et al. 2008).

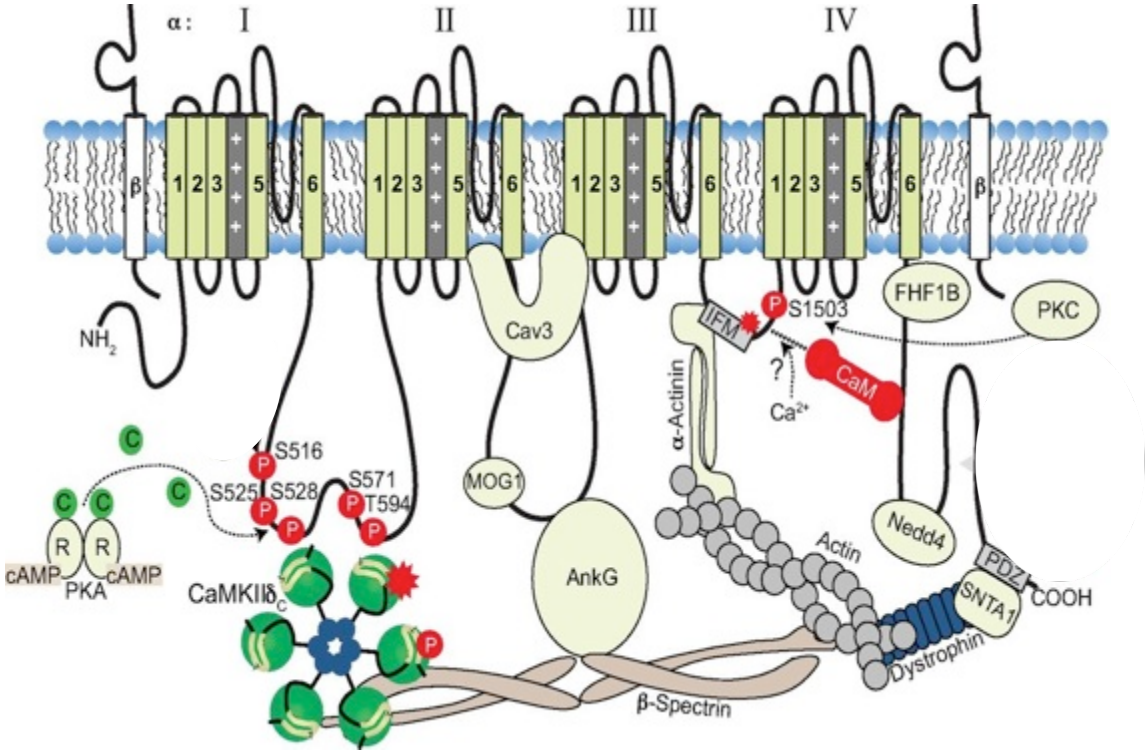

Figure 1-10: Na_v channel as a macromolecular signalling complex.

AnkG, ankyrin-G; Nedd4, neural precursor cell expressed developmentally downregulated protein 4; C, catalytic; R, regulatory; P, phosphorylation; Cav3, caveolin-3; PDZ, postsynaptic density protein/Drosophila disk large tumor suppressor/zonula occludens-1; SNTA1, α_1-syntrophin. PKA, Protein kinase A; PKC protein kinase C; CaM, Calmodulin**;** CaM-KII, Ca^{2+}/CaM-dependent kinases II**; Taken from Herren, Bers *et al.* (2013).**

In comparison, IQ motif mutations in $Na_v1.6$ impact the channel's gating properties (Herzog, Liu et al. 2003). Also mutations of this motif in $Na_v1.5$ have little effect on CaM binding but reduce calcium affinity in another regulatory domain. It was suggested that $Na_v1.5$ is indirectly regulated by CaM through activation of CaM-KII (Deschenes, Neyroud et al. 2002, Shah, Wingo et al. 2006). Calmodulin activates a group of Ca^{2+}/CaM-dependent kinases (CaM-K) that phosphorylate membrane proteins including ion channels. CaM-kinase II is a multifunctional Ser/Thr kinase that mediates a broad range of cellular functions i.e. membrane excitability, ion channel biophysical properties and synaptic plasticity (Frankland, O'Brien et al. 2001). It targets specific isoforms to the AIS (Axon initial segment) by βIV-spectrin–targeted calcium/calmodulin-

dependent kinase II (CaM-KII) interaction (Uemoto, Suzuki et al. 2007). This complex is an important regulatory unit for voltage-gated sodium clustering in the membrane (Hund, Koval et al. 2010) (Figure 1-10). In cardiac myocytes, $Na_v1.5$ is directly phosphorylated via a βIV-spectrin–targeted calcium/calmodulin-dependent kinase II complex in loop I (DI-II, L1) (Wagner, Dybkova et al. 2006, Ashpole, Herren et al. 2012). This in turn regulates the membrane excitability in the mouse heart. During heart failure, CaM-KII expression is significantly increased and CaM-KII overexpression in myocytes recapitulates the human Brugada and long QT syndrome phenotype. Both diseases are linked to dysregulated expression of $Na_v1.5$ that lead to cardiac arrhythmia (Veldkamp, Viswanathan et al. 2000, Wagner, Dybkova et al. 2006, Herren, Bers et al. 2013). As for $Na_v1.7$, increased intracellular Ca^{2+} in adrenal chromaffin cells decreases the level of surface expressed protein. This effect might be mediated by the interaction of a PKC isoform with calneurin and calpains (Wada, Yanagita et al. 2004).

Post-translational SUMOtylation

Collapsin response mediator protein 2 (CRMP2), a protein linked to axonal growth, axonal and dendritic fate (Inagaki, Chihara et al. 2001) and trafficking of voltage-gated ion channels (Brittain, Piekarz et al. 2009, Chi, Schmutzler et al. 2009), undergoes reversible SUMOtylation (small ubiquitin-like modifier, 11 kDA SUMO proteins are added) at 1 to 3 lysine residues (Wilkinson and Henley 2010, Ju, Li et al. 2013). Mutations in CRMP2 SUMOtylation sites decrease the level of surface expressed $Na_v1.7$. The effect is specific to $Na_v1.7$, which by itself, unlike other VGSCs, does not have a SUMOtylation motif. However, CRMP2 does not directly interact with $Na_v1.7$ but rather CRMP2 SUMOtylation recruits isoform-specific binding proteins that promote the trafficking of the channel to the plasma membrane. Hence, CRMP2 SUMOtylation provides a novel mechanism for the modulation of $Na_v1.7$ trafficking (Dustrude, Wilson et al. 2013).

Post-translational ubiquitylation

Newly synthesized proteins undergo various quality controls in the ER to prevent partially or incorrectly folded proteins from leaving the endoplasmic reticulum (Alberts, Bray et al. 1995). Voltage-gated sodium channels $Na_v1.5$ and $Na_v1.8$ are held back through arginine-based intracellular retention motives of the type RXR that are found in the DI-DII loop. $Na_v1.8$ is released, for instance, when β3 associates with the channel and thereby masks the C-terminal RXR signal in the DI-DII loop, which leads to increased membrane expression of the channel (Zhang, Li et al. 2008). Although not highly conserved, RXR motifs are also present and functionally important in other voltage-gated sodium channels (Figure 1-12) (Allouis, Le Bouffant et al. 2006, Zhang, Li et al. 2008). However, the majority of $Na_v1.7$ might be stored in intracellular pools. This may permit the cell to quickly change the number of surface expressed channels (Schmidt, Rossie et al. 1985).

Another quality and regulatory mechanism is ubiquitylation. Ubiquitylation is a reversible post-translational modification that regulates the internalization and degradation of proteins through covalent, C-terminal attachment of ubiquitin. Ubiquitylation was first discovered as a mechanism to mark cytosolic proteins for proteomic degradation (Abriel and Staub 2005) and can be reversed by deubiquitylating enzymes (DUBs)(Amerik and Hochstrasser 2004) (Figure 1-11, right). Cell surface proteins, such as voltage-gated sodium channels, are tagged for internalization or degradation by the lysosome or proteasome to control the number of channels present in the plasma membrane (van Bemmelen, Rougier et al. 2004, Xu, Duong et al. 2009). The ubiquitylation pattern determines the fate of a protein and can be mono-, multi-, or polyubiquitylated. The latter is often a marker for degradation by cytoplasmic, nuclear or endoplasmic proteasomes (Xu, Duong et al. 2009). Ubiquitylation requires three consecutive enzymatic steps 1) E1 (ubiquitin activation enzyme) activates ubiquitin, 2) activated ubiquitin is transferred to E2, an ubiquitin carrier enzyme that allows the interaction with 3) E3 (ubiquitin protein ligase) that in the final step

covalently ubiquitylates lysine residues in the target protein (Huang, Kinnucan et al. 1999) (Figure 1-11).

There are two main classes of E3 ligases, Ring finger E3 (Joazeiro and Weissman 2000) and HECT E3 ligases with more than 1000 isoforms in humans to ensure the specificity of the ubiquitylation (Varshavsky 2012). HECT E3 ligases, which include Nedd4 and Nedd4-like proteins (Rotin, Staub et al. 2000), contain a catalytic HECT domain (Huibregtse, Scheffner et al. 1995), a C2 domain (Nalefski and Falke 1996) and various WW domains (Staub, Dho et al. 1996). These domains are responsible for ubiquitylation, target localization, phospholipid binding and protein-protein interaction (Plant, Lafont et al. 2000, Rotin and Kumar 2009). WW domains of E3 ligases recognize highly conserved proline-rich sequences, also known as PPxY motifs, in the C-terminal region of the substrate (Macias, Hyvonen et al. 1996) (Figure 1-11).

Most voltage-gated sodium channels contain a PPxY motif except for $Na_v1.4$, $Na_v1.9$ and Na_x (Decosterd and Woolf 2000, Fotia, Ekberg et al. 2004, Rougier, van Bemmelen et al. 2005). *In vitro* and *in vivo* studies of voltage-gated sodium channel PPxY motifs and Nedd4/Nedd4-like proteins have shed light on the importance of these proteins in the regulation of Na_v trafficking.

Nedd4-2 expression is decreased after surgery-induced neuropathic pain (SNI) (Decosterd and Woolf 2000,Cachemaille, Laedermann et al. 2012), which coincides with an increased expression of $Na_v1.7$ and $Na_v1.8$ in damage-sensing neurons after SNI. The strongest evidence comes from nociceptor specific Nedd4-$2^{-/-}$ mice that exhibit changes in pain thresholds and dysregulated trafficking of $Na_v1.7$ and $Na_v1.8$ (Cachemaille, Laedermann et al. 2012, Laedermann, Cachemaille et al. 2013). *In vitro,* neuronal isoforms like $Na_v1.5$ and $Na_v1.7$ are polyubiquitylated suggesting that they are degraded by the proteasome (Rougier, van Bemmelen et al. 2005, Xu, Duong et al. 2009).

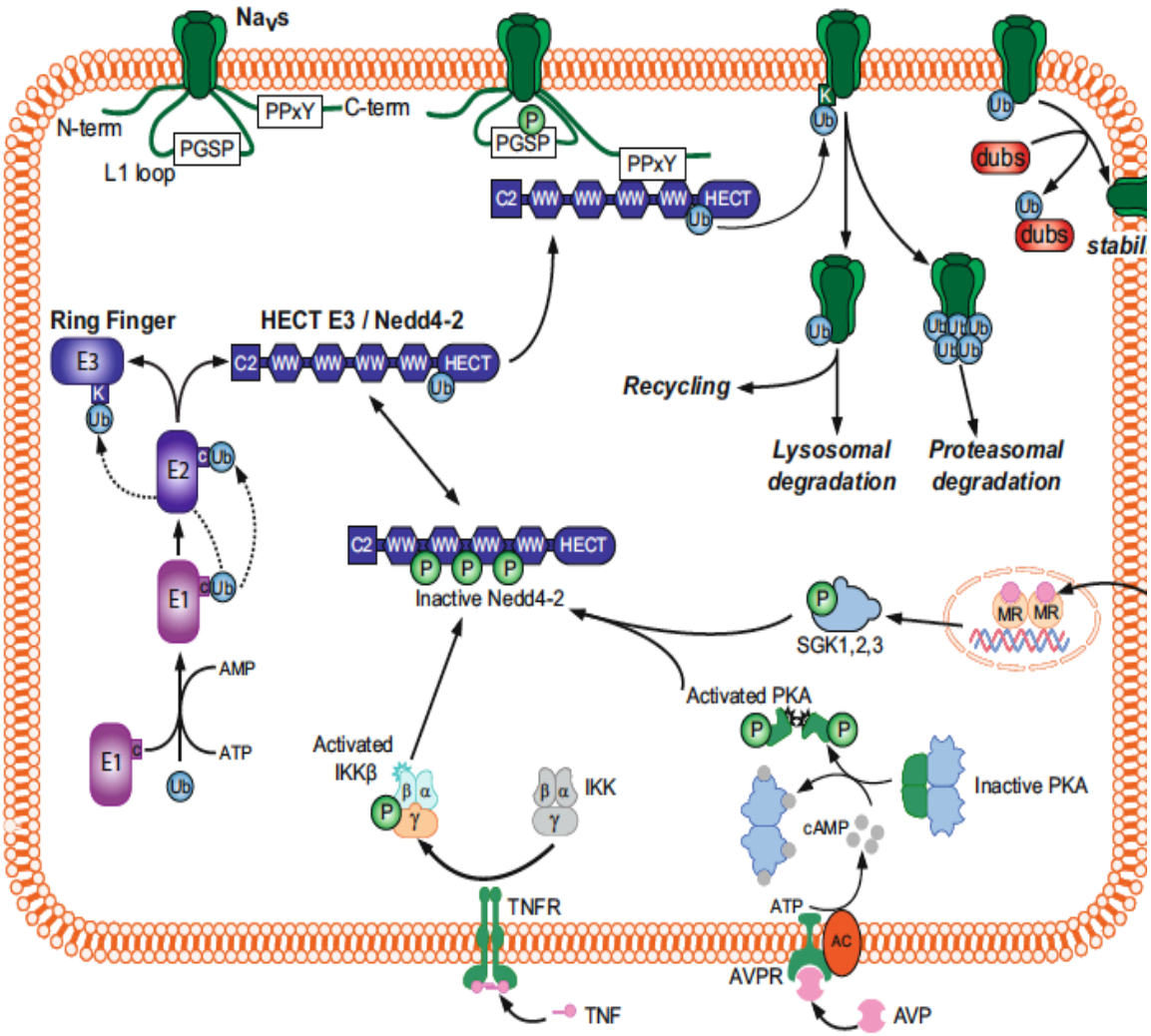

Figure 1-11: Schematic representation of the roles of Na_v channel ubiquitylation and its regulatory pathways.

Ub, ubiquitin; E1, Ubiquitin-activating enzyme; E2, Ubiquitin-conjugating enzyme; E3, Ubiquitin ligase; C, cysteine residue; L, lysine residue; RING, really interesting new gene ubiquitin ligases family; HECT, Homologous to E6-AP carboxyl-terminus ubiquitin ligases family; C2, calcium-dependent lipid binding domain; dubs, deubiquitylating enzymes; P, phosphate group; MPKA, protein kinase A; IKK, IκB [inhibitor of nuclear factor κB (NF-κB) kinase; IKKβ, IκB kinase β-subunit; **Taken from Laedermann, Decosterd *et al.* (2014).**

However, $Na_v1.7$ expression in Nedd4-$2^{-/-}$ shows no change in total channel number but increased amount of $Na_v1.7$ in the plasma membrane, suggesting that channel ubiquitylation mediates internalization and recycling of channels rather than degradation (Cachemaille, Laedermann et al. 2012, Laedermann, Cachemaille et al. 2013, Laedermann, Decosterd et al. 2014). Similar observations were made for $Na_v1.5$ *in vivo* (Fotia, Ekberg et al. 2004, van Bemmelen, Rougier et al. 2004). In contrast, $Na_v1.8$ is internalized and degraded as the amount of total protein changes in Nedd4-$2^{-/-}$ mice compared to wild-type (Cachemaille, Laedermann et al. 2012). Alteration in Nedd4-2 expression in primary sensory neurons leading to changes in voltage-gated sodium channel trafficking might be the underlying cause for hyperexcitablity of sensory neurons in pathological states (Laedermann, Cachemaille et al. 2013).

Lipid rafts and post-translational palmitylation

Lipid rafts are highly dynamic micro-membrane domains, rich in glycosphingolipids, cholesterol, gangliosides and other functional components including cytoskeletal regulators. Voltage-gated sodium channel $Na_v1.5$ is clustered in caveols, a type of lipid raft that is rich in the cholesterol-binding protein caveolin (Yarbrough, Lu et al. 2002, Head, Hu et al. 2011) (Figure 1-10). Various reports suggest a regulatory role of lipid rafts in the dynamic rearrangement of the cytoskeleton and modulation of signaling molecules (Echarri, Muriel et al. 2007, Gowrishankar, Ghosh et al. 2012). Pristera *et al.* (2012) reports that $Na_v1.8$ is clustered in lipid rafts along the sciatic nerve and DRG neurons. Chemically-induced dissociation of the channel from the rafts negatively impacts neuronal excitability (Pristera, Baker et al. 2012). Palmitylation of cysteine residues is a reversible lipid modification on newly synthesized protein in the ER/Golgi (Schmidt and Catterall 1987) that plays a role in cellular signaling, protein trafficking and functionality of membrane proteins (Iwanaga, Tsutsumi et al. 2009) by targeting proteins to lipid rafts in the plasma membrane. Dysregulation of this process is suspected to underlie various neurodegenerative diseases and psychiatric disorders (Huang, Kang et al. 2010). Na_v channel palmitylation provides an important step in channel

biosynthesis but also influences Na_v gating properties and toxin sensitivity. C1182A in the intracellular loop of $Na_v1.2$ is an important palmitylation site. Mutation in this site and another independent mutation to cysteine (G1079C) also within the loop region of DII-DIII render $Na_v1.2$ more sensitive to the PaurTx3 toxin and influence the channel's gating properties. As the mutations are in the intracellular loop and in no direct contact with the toxin, it is believed that they influence palmitylation. Normally palmitylation helps to traffic membrane proteins to specific lipid micro domains and changes in the palmitylation state may lead to altered trafficking (Bosmans, Milescu et al. 2011).

1.5 Voltage-gated sodium channel protein-protein interactions

Ankyrin

The scaffolding protein ankyrin is important in clustering and localization of membrane and cytosolic proteins to specific domains. Three isoforms of the protein are known (Ankyrin-R, -B, -G) which mediate voltage-gated sodium channel clustering and supra-molecular complex formation at the axon initial segment, somata and node of Ranvier (Hedstrom and Rasband 2006). This is likely achieved through an N-terminally membrane-binding domain in ankyrin that recognizes a highly conserved 9 residue long segment in the DII-III loop of VGSCs (Figure 1-10 and Figure 1-12) (Lemaillet, Walker et al. 2003). The domain is essential for channel expression in the plasma membrane. Brugada Syndrome, a cardiac arrhythmic disorder, is caused by a mutation in this binding site in $Na_v1.5$ and leads to loss of channel function by preventing its clustering in the cardiomyocyte plasma membrane (Mohler, Rivolta et al. 2004). This is further supported by siRNA-induced knockdown of ankyrin-G that causes loss of function in $Na_v1.5$ in cardiomyocytes (Lowe, Palygin et al. 2008). The exact molecular mechanism through which ankyrin achieves trafficking and clusters voltage-gated sodium channels still remains elusive. However a possible mechanism might involve the interaction with the cytoskeletal protein spectrin. Here spectrin and ankyrin might act as a scaffold for newly synthesized VGSCs and facilitate trafficking after the ER/Golgi (Jenkins and

Bennett 2001, Garrido, Fernandes et al. 2003, Shao, Okuse et al. 2009). Makara *et al.* (2014) showed that ankyrin-G functionally guides $Na_v1.5$ and calcium/calmodulin-dependent kinase-II to their destined site via interaction with βIV-spectrin (Makara, Curran et al. 2014).

P11 or annexin A2 light chain

P11 or annexin A2 light chain is a Ca^{2+}-insensitive protein that forms heterotetrameric complexes with the calcium-sensitive membrane-binding protein annexin 2 that targets the complex to specific sites i.e. to the plasma membrane. p11 also interacts with Ca^{2+}-independent partners including ASIC (Donier, Rugiero et al. 2005), Serotonin 1B receptor (Svenningsson, Chergui et al. 2006) and the voltage-gated sodium channel $Na_v1.8$ (Okuse, Malik-Hall et al. 2002). Okuse *et al.* (2002) reports that p11 binds to the cytosolic N-terminus of $Na_v1.8$ and when co-overexpressed *in vitro* leads to an increased functional expression and activity of the channel in the plasma membrane (Okuse, Malik-Hall et al. 2002). Further evidence for the role of p11 in protein trafficking comes from the finding that a tissue-specific knockout of p11 in small nociceptive neurons leads to decreased levels of functional $Na_v1.8$.

Furthermore, $Na_v1.8$ null mice and p11 null mice have a similar acute pain response. Surprisingly, the absence of p11 in nociceptive neurons does not change inflammatory pain thresholds but ameliorates neuropathic pain behavior (Okuse, Malik-Hall et al. 2002, Foulkes, Nassar et al. 2006). Also, annexin 2 levels in p11 knockout mice are unchanged suggesting that p11 appears to be important but not essential for the intracellular trafficking of $Na_v1.8$ to the plasma membrane (Foulkes, Nassar et al. 2006).

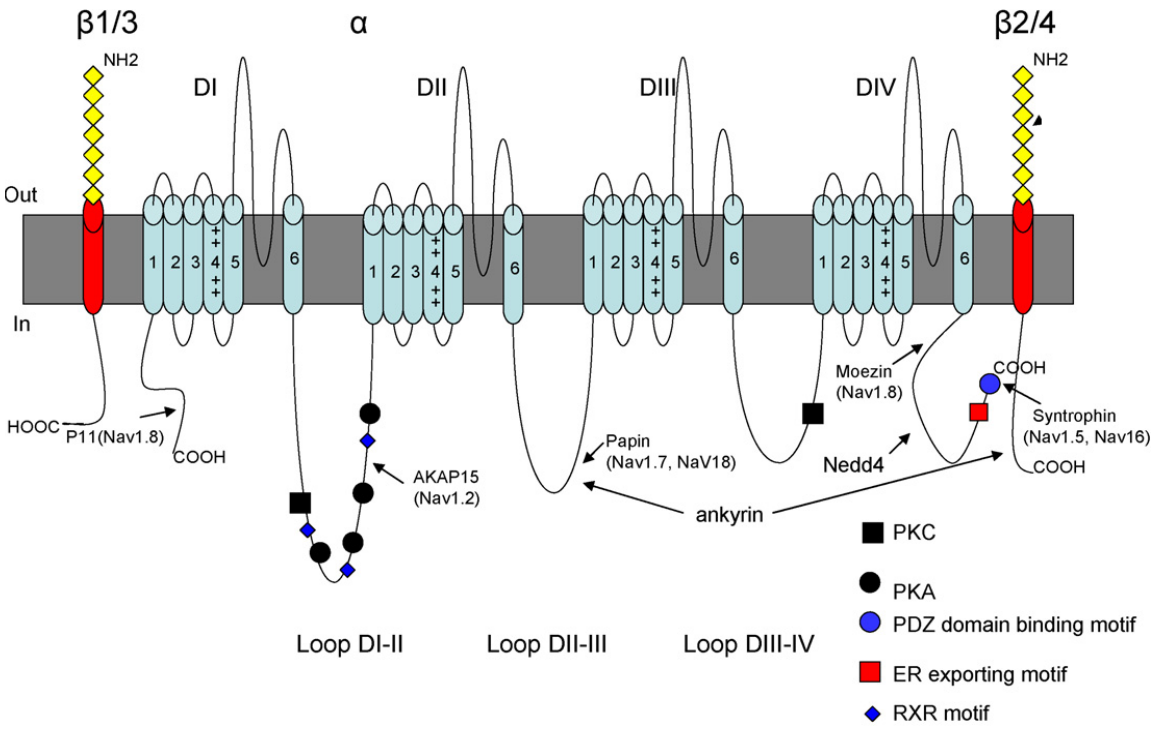

Figure 1-12: Schematic overview of Na_v protein interactions.

AKAP15 (cAMP-dependent protein kinase-anchoring protein); PKC (Protein Kinase C); PKA (Protein Kinase A); RXR motif (ER retention signal); p11 (Annexin A2 light chain); Papin (Plakophilin-related armadillo-repeat protein-interacting protein); Nedd4 (neural precursor cell expressed developmentally down-regulated protein 4); Moesin (Ezrin/radixin/moesin (ERM) cytoskeletal linker proteins). **Taken from Shao, Baker *et al.* (2009).**

Papin

Plakophilin-related armadillo-repeat protein-interacting protein or papin, was first discovered in rat brain and prostate cancer cells and later in small and large diameter sensory neurons (Deguchi, Iizuka et al. 2000, Chaib, Rubin et al. 2001, Shao, Baker et al. 2009). Structurally, papin has four N- and two C-terminally located PDZ domains that interact with a highly conserved binding motif in the DII-III loop of VGSCs (Shao, Baker et al. 2009) (Figure1-12). The PDZ binding motif is found in most VGSCs with the exception of $Na_v1.4$. Papin has been shown to directly interact with $Na_v1.8$ and $Na_v1.7$ via this DII-DIII binding domain (Malik-Hall, Poon et al. 2003).

However unlike p11, papin is not required for the translocation of $Na_v1.8$ but rather acts as scaffolding protein that stabilizes the channel in the membrane.

siRNA-mediated knockdown of papin *in vitro* reduces $Na_v1.8$ current density possibly due to decreased numbers of channels in the plasma membrane. In comparison to Nav1.8$^{-/-}$, papin$^{-/-}$ mice show no change in pain thresholds but exhibit increased levels of p11 mRNA through a yet unknown mechanism (Shao, Baker et al. 2009, Shao, Okuse et al. 2009). Papin is believed to act as an intermediate between plasma membrane localized VGSCs and the E-cadherin-catenin system that plays a crucial role in cell motility. For instance, Chaib *et al.,* (2001) reported that in non-cancerous prostate cells papin expression is only found in the basal cell layer. However during early stages of prostate cancer its expression extents to other areas and correlates with the upregulated expression of known papin binding proteins such as $Na_v1.7$ (Diss, Stewart et al. 2005) and δ-catenin (Lu, Dobbs et al. 2005) that have also been be implicated in human prostate cancer (Shan, Dong et al. 2014).

Syntrophin/Dystrophin Complex

The adapter protein syntrophin consists of two-pleckstrin homology domains, a PDZ domain and a unique, highly conserved syntrophin domain that enables simultaneous association with a variety of proteins. All known isoforms of syntrophin (alpha, beta and gamma) directly interact with members of the dystrophin family through binding to the pleckstrin and the unique syntrophin domain. The PDZ domain is important in binding signaling proteins and interacts with the C-terminal residues in $Na_v1.4$ and $Na_v1.5$ (Schultz, Hoffmuller et al. 1998). VGSC $Na_v1.5$ is in complex with syntrophin and dystrophin: tissue specific knockout of dystrophin in cardiomyocytes decreases the level of functional $Na_v1.5$ while mRNA levels are unchanged (Gavillet, Rougier et al. 2006). Functionally the syntrophin/dystrophin complex is important in capturing and anchoring signaling proteins and voltage-gated sodium channels in the plasma membrane and prohibiting internalization by stabilizing $Na_v1.5$ in the plasma membrane (Schultz, Hoffmuller et al. 1998) (Figure 1-12).

ERM proteins

Ezrin/radixin/moesin (ERM) are cytoskeletal linker proteins that share a high level of homology. Functionally, ERM proteins have been implicated in cellular

adhesion, changes of motility, polarity and membrane protein trafficking. These processes are achieved through interaction and modulation of the actin cytoskeleton underneath the plasma membrane. Indeed ERM proteins and Rho GTPase provide the dynamic link between plasma membrane proteins and the actin cytoskeleton (McClatchey 2014). $Na_v1.8$ pull-down assays provide evidence for direct interaction between a highly conserved C-terminal region in $Na_v1.8$ and moesin (Malik-Hall, Poon et al. 2003). Although no functional mechanism has been established yet, it is possible that ERM proteins are important in clustering voltage-gated sodium channels in specialized membrane segments (i.e. nodes of Ranvier) (Shao, Baker et al. 2009, Shao, Okuse et al. 2009). Furthermore actin and moesin interaction and subsequent reorganization of the cytoskeleton may influence $Na_v1.8$ gating properties through actin (de) polymerization (Shumilina, Negulyaev et al. 2003). In *D. Melanogaster* eye*,* ERM protein Dmoesin is essential in light-induced reorganization of the actin cytoskeleton and translocation of a light sensitive TRP channel, the main contributor to light induced currents in eye (Hardie and Minke 1992). In illuminated conditions, Dmoesin is not bound to the TRP channel and is trafficked to the cytosol. Ablation of Dmoesin decreases the viability of retinal cells suggesting that the dynamic association of Dmoesin and TRP are important in regulation and maintenance of the Drosophila eye (Chorna-Ornan, Tzarfaty et al. 2005). A hallmark of cancer is increased motility and invasiveness of cells supported by rapid changes of the cytoskeleton. Dysregulation of ERM and Rho GTPase protein activity is implicated in various invasive forms of cancer including breast cancer (Fritz, Brachetti et al. 2002, Halon, Donizy et al. 2013). $Na_v1.7$ expression can also impact cytoskeletal-mediated cellular activity and lead to increased invasiveness in cancer. For instance $Na_v1.7$ is upregulated in human prostate, breast and non-small cell lung cancer (Fraser, Diss et al. 2005, Brackenbury, Chioni et al. 2007, Roger, Rollin et al. 2007). Uysal-Onganer and Djamgoz (2007) found that upregulation of epidermal growth factor (EGF) in the human prostate cancer cell line PCa PC-3M stimulates the expression of $Na_v1.7$, which in turn enhances migration, endocytosis and invasiveness of these cells. Additional evidence for an

important role of $Na_v1.7$ in these cancer cells comes from the finding that metastatic invasion in these cells can be blocked by TTX. (Uysal-Onganer and Djamgoz 2007). A recent paper by Campbell, Main *et al.* (2013) showed that epidermal growth factor (EGF) induces $Na_v1.7$ expression in cultured non-small cell lung cancer (NSCLC) which is crucial for proliferation, migration and invasiveness of these cancer cells. However, human non-invasive NSCLC cells, which lack expression of $Na_v1.7$, can be transformed into invasive cells by expression of the channel (Campbell, Main et al. 2013).

1.6 Natural antisense transcript

Natural antisense transcripts have long been described as 'junk DNA' or transcriptional noise (Alberts, Bray et al. 1995). However, in recent years, long non-coding RNAs (LncRNA) including natural antisense transcripts have emerged as a new class of RNA-based regulation (Wang, Yang et al. 2011, Rinn and Chang 2012, Yang and Deng 2014). A clear advantage for RNA mediated transcriptional regulation is RNA's quick production and degradation, its local storage, conformational flexibility, distribution, and its ability to interact with both nucleic acids and proteins (Lapidot and Pilpel 2006). Natural antisense transcripts (NATs) are endogenous, protein or non-protein coding transcripts that work through a broad range of mechanisms from interfering with transcription (Prescott and Proudfoot 2002), translation (Centonze, Rossi et al. 2007), or masking binding sites on DNA, RNA and proteins (Lapidot and Pilpel 2006). NATs can act on their targets in *cis* through perfect sequence complementary or in *trans* through imperfect sequence complementary (Li, Qin et al. 2006, Faghihi and Wahlestedt 2009) (Figure 1-13). The most comprehensive studies predict that in humans 35% and in mice 72% of the transcriptome is transcribed bidirectionally (Grinchuk, Jenjaroenpun et al. 2010, Katayama, Tomaru et al. 2005), most of which give rise to partially or fully overlapping non-coding RNAs (Yelin, Dahary et al. 2003). Given NAT abundance throughout the genome, then this implies an evolutionary benefit of such a genomic arrangement (Werner and Berdal 2005, Ling, Ban et al. 2013).

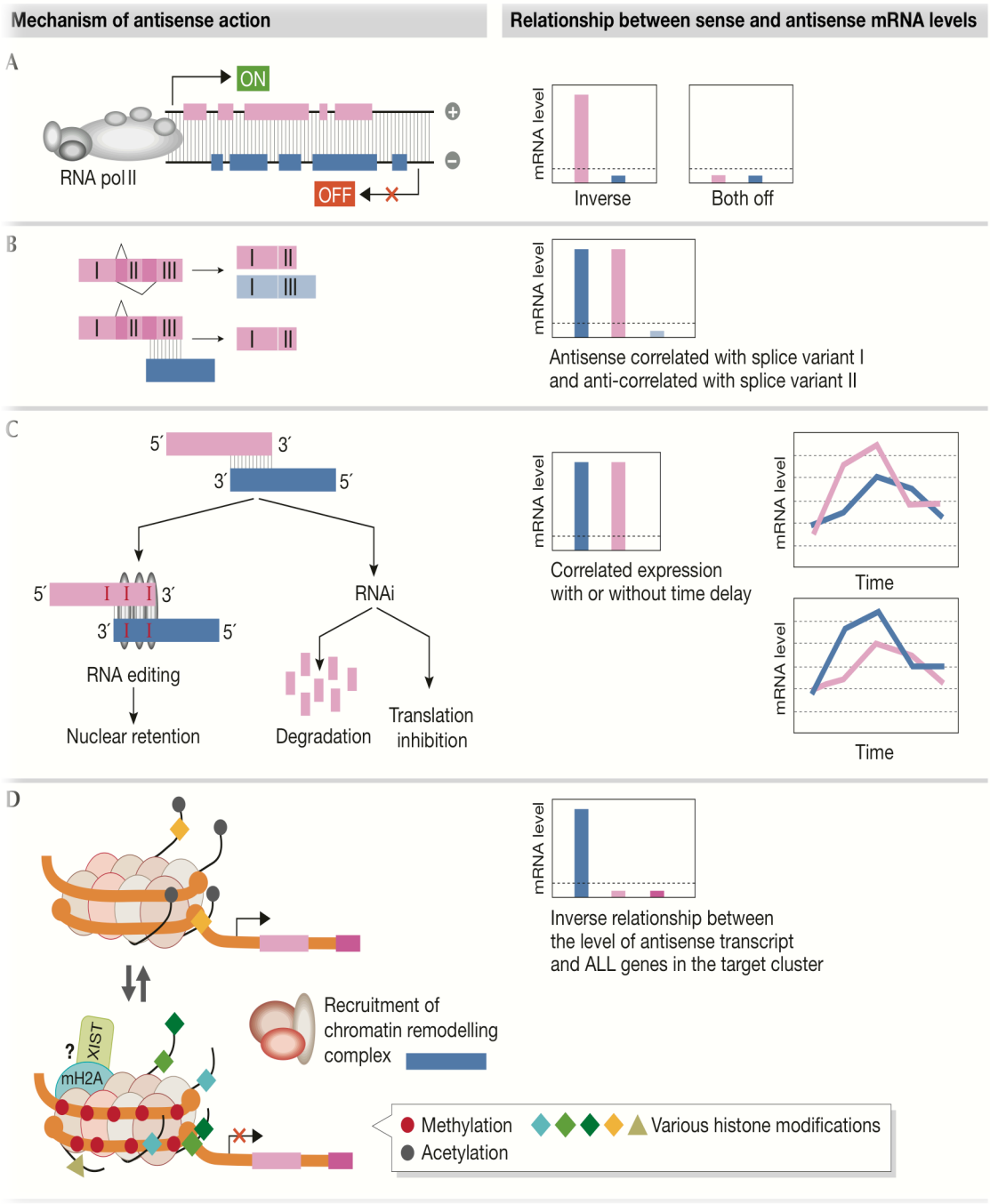

Figure 1-13: Regulatory mechanisms of natural antisense transcripts.

Possible regulatory mechanisms by which NATs can influence expression levels of corresponding sense transcripts. Left: Mechanism of antisense action: **(A)** Transcriptional interference **(B)** Alternative splicing **(C)** RNA editing and RNAi **(D)** Chromatin remodeling. Right: Relationship between sense and antisense mRNA levels. **Taken from Lapidot and Pilpel (2006).**

However, evolutionary conservation of NATs may not be primarily at the sequence level, as non-protein coding NATs genes have quite a low sequence conservation (Beiter, Reich et al. 2009), but common characteristics of NATs suggest that conservation occurs on a structural level either through splicing patterns or secondary or tertiary structures (Khaitovich, Kelso et al. 2006, Werner, Carlile et al. 2009). Furthermore natural antisense transcripts are unequally distributed on the autosomes and X chromosomes with underrepresentation of exonic overlapping NATs on the X chromosome (Kiyosawa, Yamanaka et al. 2003).

Natural antisense transcripts as therapeutic targets

Prominent examples of NATs regulating their corresponding sense transcripts include BACE-1 antisense that regulates beta secretase levels in Alzheimer's disease through RNA masking (Faghihi, Modarresi et al. 2008), HTT antisense at the Huntington gene locus which regulates HTT expression levels through RNA interference (Chung, Rudnicki et al. 2011) and Wrap53 NAT of p53 that stabilizes p53 mRNA upon damage and leads to an increase in both mRNA and protein levels of p53 (Mahmoudi, Henriksson et al. 2009). The *CDKN1A* antisense transcript regulates the expression of cell cycle regulator and tumor suppressor gene *CDKN1A* (p21) through chromatin remodeling. The expression of the *CDKN1A* antisense RNA recruits histone-modifying enzymes and mediates trimethylation at the sense promoter region, which induces heterochromatin formation and subsequently suppresses transcription of the sense gene (Morris, Santoso et al. 2008). Another example of a NAT that regulates its corresponding sense transcript is *HIF1-α* antisense transcript. The *HIF1-α* sense gene encodes for a transcription factor that is linked to tumour growth and progression. Binding of the *HIF1-α* antisense transcript to *HIF1-α* decreases the sense mRNA stability dramatically by exposing an Alu rich element in *HIF1-α,* which induces its decay (Uchida, Rossignol et al. 2004).

Evidence for the regulatory role of antisense transcripts and its involvement in pain comes from Zhao *et al.* (2013). *Kcna2* encoding for a voltage-dependent potassium channel and predominately found in DRG neurons has a conserved

natural antisense transcript. Nerve injury induces the binding of transcription factor myeloid zinc finger protein 1 to the *Kcna2* antisense promoter and upregulates expression of the transcript in DRG. Although the exact mechanism by which the *Kcna2* antisense transcript acts on the *Kcna2* is still elusive, the authors found that increased expression of the *Kcna2* antisense downregulates *Kcna2* and leads to a reduction of total voltage-gated potassium current. This in turn increases the excitability in DRG neurons and leads to neuropathic pain symptoms (Zhao, Tang et al. 2013). Interestingly, *SCN9A* ($Na_v1.7$) has a corresponding natural antisense transcript encoded on the opposite strand that overlaps tail-to-tail (3' end overlap of the sense and *NAT*) with the sense transcript in both human and mouse and has a putative role in $Na_v1.7$ regulation (Koenig, Werdehausen et al. 2015).

1.7 $Na_v1.7$ in inherited human pain syndromes

Channelopathy-associated inability to experience pain (CIP)

CIP is a rare autosomal recessive disorder with only a handful of reported cases. Individuals suffering from CIP do not exhibit cognitive or inherited physical impairments and have normal responses to light touch, warm and cold stimuli, and proprioception but their sense of pain and smell is completely abolished (Cox, Reimann et al. 2006, Weiss, Pyrski et al. 2011). CIP is caused by nonsense mutations in *SCN9A* that leads to a loss of function in $Na_v1.7$. Genome-wide linkage analysis of three consanguineous Pakistani families led to the identification of nonsense amino acid changes in exon 10 (S459X), 13 (I767X) and exon 15 (W897X) to be responsible for the pain-free phenotype (Cox, Reimann et al. 2006). While loss of function mutations in $Na_v1.7$ in humans are associated with a congenital inability to experience pain in otherwise healthy individuals, global $Na_v1.7$ knockout mice die shortly after birth. One explanation for the perinatal lethality in $Na_v1.7$ knockout mice draws on the finding that no milk content was found in their stomach suggesting they were not able to find their mother's mammary gland and die due to malnutrition (Nassar, Stirling et al. 2004).

Primary erythromelalgia (PE)

Primary erythromelalgia is a rare inherited autosomal dominant neuropathy characterized by an early onset phenotype with painful reddened feet and hands due to moderate physical exercise, long periods of standing and exposure to warm temperatures. In the later stages of inherited PE, the individual experiences reoccurring episodes of persistent pain, redness and elevated temperatures of the lower extremities which can extend to the upper legs, feet, and also often the hands (Finley, Lindsey et al. 1992, van Genderen, Michiels et al. 1993). *SCN9A* mutations were first reported to cause PE following genome-wide linkage analysis in a three-generation Chinese family (Yang, Wang et al. 2004). To date, all known PE mutations are gain-of-function (Figure 1-14) that lead to increased $Na_v1.7$ activity by lowering the channel's activation threshold and also slowing deactivation (Cummins, Dib-Hajj et al.

2004). Additionally, some reported mutations including I136V, L858F, A863P and F1449V boost $Na_v1.7$'s recovery from inactivation (Dib-Hajj, Rush et al. 2005, Harty, Dib-Hajj et al. 2006, Cheng, Dib-Hajj et al. 2008). This in turn increases the frequency of action potential firing and prolongs the opening of the channel, which subsequently renders DRG neurons hyperexcitable. Furthermore, a correlation with clinical severity, age of PE onset and mutation has been reported with the greater the hyperpolarization shift due to the mutation, the earlier the PE age of onset (Han, Rush et al. 2006, Cregg, Cox et al. 2014).

Paroxysmal extreme pain disorder (PEPD)

PEPD is a rare inherited autosomal dominant disease characterized by sudden onset of reoccurring pain in the rectal, submandibular and ocular regions. Generally, affected individuals experience their first painful episodes during infancy (Hayden and Grossman 1959, Fertleman, Baker et al. 2006, Fertleman, Ferrie et al. 2007). Painful episodes are triggered by drinking hot or cold liquids, eating spicy, acidic or hot food and also by strong wind and sunlight. During the course of PEPD, the intensity of episodes steadily increases and are often accompanied by non-epileptic seizures and cardiac symptoms (Fertleman, Ferrie et al. 2007). Similar to PE, genome-wide linkage analysis identified gain-of-function mutations in *SCN9A*/$Na_v1.7$ as the underlying cause for PEPD (Figure 1-14). $Na_v1.7$ gain-of-function mutations render DRG neurons hyperexcitable by increasing the frequency of action potential firing (Fertleman, Baker et al. 2006). In contrast to PE, *SCN9A* mutations in PEPD do not lower the $Na_v1.7$ voltage-dependent activation threshold but shift the voltage-dependent steady-state fast inactivation towards more depolarizing potentials and, depending on the mutation, cause incomplete inactivation of $Na_v1.7$ which leads to a persistent current (Fertleman, Baker et al. 2006, Dib-Hajj, Estacion et al. 2008). Although both inherited pain disorders have been linked to gain-of-function mutations in *SCN9A*, it is still not clear why affected areas and clinical symptoms vary significantly between PE and PEPD

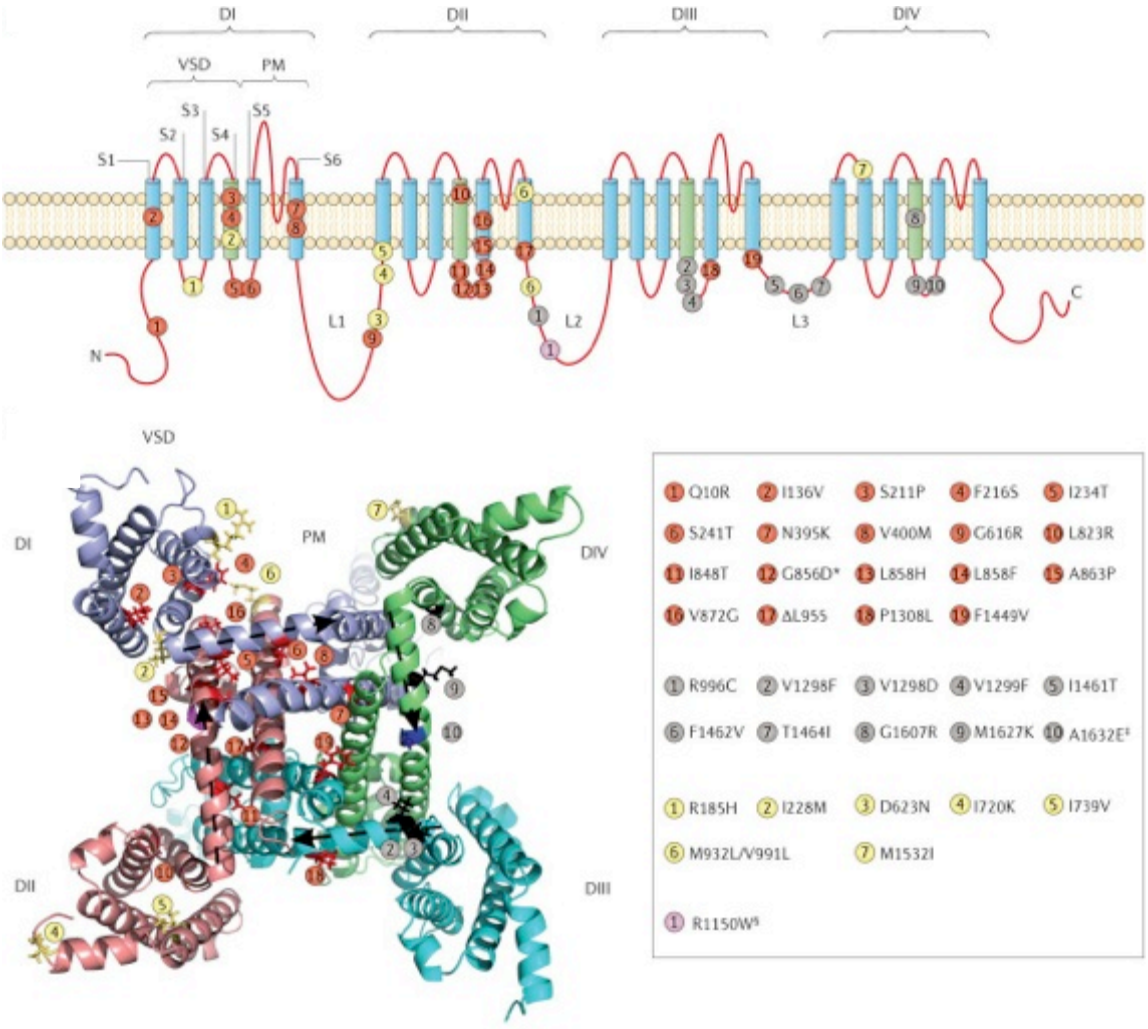

Figure 1-14: Structure of $Na_v1.7$ and mutations in inherited pain syndromes.

Alpha subunits of voltage-gated sodium channels (VGSC) are integral membrane proteins that are organized in four homologous domains (DI-DIV). Each domain consists of 6 transmembrane segments (S1-S6) that form voltage sensors and ion selective pores. (Guy and Seetharamulu, 1986; Noda et al 1984). *SCN9A* mutations that are linked to primary erythromelalgia (red symbols), PEPD (grey symbols), small fibre neuropathy (yellow symbols). (Bottom, left) Nav1.7 crystal structure based on recently determined crystal structure of a bacterial sodium channel (right). **Taken from Dib-Hajj, Yang *et al.* (2013).**

1.8 $Na_v1.7$ in chronic pain disorders

Neuropathic pain

The international association for the study of pain (IASP) defines neuropathic pain as ‘‘pain caused by a lesion or disease of the somatosensory system’’ (Jensen, Baron et al. 2011). In contrast to nociceptive pain, neuropathic pain is spontaneous, provoked and long-lasting and not per se a physiological reaction to potential or actual tissue damage (Serra, Bostock et al. 2012). Neuropathic pain is classified as central (caused by brain damage i.e. stroke, Multiple sclerosis, spinal cord injury) or peripheral (referring to damage to PNS nerve pathway) or a combination of both. Some of the most common causes are post-traumatic, post surgery induced nerve injury, post herpetic neuralgia and diabetes with prevalence steadily increasing (Wild, Roglic et al. 2004).

$Na_v1.7$ and neuropathic pain

Neuropathic pain is one of the most common but yet least understood forms of pain mostly due to its multi-mechanistic nature. Symptoms may include spontaneous burning pain, allodynia and dysesthesias (Attal, Fermanian et al. 2008). Electrophysiological recording on DRGs shows that these neurons exhibit ectopic TTXs discharge after insult, concluding that TTXs voltage-gated sodium channels might underlie neuropathic pain (Matzner and Devor 1994, Omana-Zapata, Khabbaz et al. 1997). Damage-sensing DRG neurons express different subsets of VGSCs thus expression and electrophysiological properties are subject to change due to inflammation and nerve injury. In particular, the role of $Na_v1.7$ in various animal models of neuropathic and inflammatory pain has been closely examined. Global ablation of $Na_v1.7$ is postnatal lethal in mice but deletion of $Na_v1.7$ in $Na_v1.8$ positive neurons abolishes inflammatory symptoms and sensitivity to high-threshold noxious mechanical stimuli (Nassar, Stirling et al. 2004). However, SNL induced neuropathic pain develops normally in $Na_v1.7^{Nav1.8}$ and $Na_v1.7^{-/-}$ $Na_v1.8^{-/-}$ double knockout mice (Nassar, Stirling et al. 2004, Nassar, Levato et al. 2005). Interestingly, in humans some neuropathies can be successfully treated with sympathetic blockers suggesting an involvement of the sympathetic nervous system in the development of

neuropathic pain (Yoo, Nahm et al. 2011, de Oliveira Rocha, Teixeira et al. 2014). $Na_v1.7$ is expressed in peripheral sensory neurons and sympathetic neurons (Toledo-Aral, Moss et al. 1997). Minett *et al.,* (2012) compared three different tissue specific $Na_v1.7^{-/-}$ mouse lines and reported that some forms of neuropathic pain are mediated by $Na_v1.7$ in sensory neurons while others require the $Na_v1.7$ expression in both sensory and sympathetic neurons. Ablation of $Na_v1.7$ in all sensory neurons attenuates mechanical, inflammatory pain and spinal withdrawal reflexes to heat but not surgically induced neuropathic pain. Deletion of *SCN9A* in sensory and sympathetic neurons abolishes surgically-induced neuropathic pain and recapitulates the human loss-of-function phenotype. In contrast, other neuropathies as bone cancer-induced pain and oxaliplatin-induced pain operate under a $Na_v1.7$-independent mechanism (Minett, Falk et al. 2014). It has been suggested that oxaliplatin-induced pain is mediated by $Na_v1.6$ (Sittl, Lampert et al. 2012, Deuis, Zimmermann et al. 2013). However in the course of bone cancer induced pain in rats, $Na_v1.8$ and $Na_v1.9$ are upregulated (Qiu, Jiang et al. 2012). In recent studies, antisense knockdown of $Na_v1.8$ in this model reversed pain-related behaviour suggesting development and maintenance of bone cancer pain relies on $Na_v1.8$ (Miao, Gao et al. 2010, Liu, Yang et al. 2014). The role of other VGSCs, such as $Na_v1.3$, in neuropathic pain is still not clear: a species-specific effect and mechanistic differences could be the reason for the contradicting results obtained from mouse and rat and in different models of neuropathic pain. Global and DRG specific $Na_v1.3^{-/-}$ mice did not exhibit alleviated pain behaviour after nerve injury (SNL) (Lindia, Kohler et al. 2005, Nassar, Baker et al. 2006). CCI induced but not SNT in $Na_v1.3^{-/-}$ reduced mechanical and cold allodynia (Minett, Falk et al. 2014). In contrast, intrathecal AS-ODN treatment and virus-mediated shRNA knockdown of $Na_v1.3$ in rats attenuates mechanical allodynia in neuropathic pain (Hains, Saab et al. 2004, Samad, Tan et al. 2013).

Inflammatory pain

Acute inflammatory pain is a crucial physiological response to infection and tissue damage that promotes healing. Peripheral damage recruits immune cells to the site of injury and induces the release of inflammatory mediators ATP, H+, NGF, pro-inflammatory cytokines and others, which are collectively referred to as “the inflammatory soup”. This in turn stimulates and modulates peripheral primary sensory neurons and renders them hyperexcitable. Peripheral sensitization of nociceptors is a hallmark of inflammation and increases neurotransmitter (Glutamate) and neuromodulator (Substance P, CGRP, BDNF) release from their peripheral and central terminals. Neurogenic inflammation is a result of peripheral release of neuromodulator agents as it induces the production and release of inflammatory agents from cells in the vicinity and the vascular tissue and the release from neurotransmitters and neuromodulators at central terminals into the spinal cord (Julius and Basbaum 2001, Tan, Piekarz et al. 2014).

$Na_v1.7$ in inflammatory pain

During acute inflammation, a cocktail of inflammatory mediators are released leading to increased sensitivity in and around the injured site (Julius and Basbaum 2001). The general consensus is that chronic pain states arise from altered neuronal activity due to peripheral and central sensitization of nociceptive neurons. $Na_v1.7$ has been shown to mediate inflammatory pain states. In inflammatory pain rat and mouse models, the TTXs sodium current is increased and $Na_v1.7$ is upregulated (Toledo-Aral, Moss et al. 1997, Black, Liu et al. 2004, Gould, England et al. 2004, Strickland, Martindale et al. 2008). Sensory neuron specific knockdown of $Na_v1.7$ and $Na_v1.7$/$Na_v1.8$ attenuates pain related behaviour in inflammatory pain models (Nassar, Stirling et al. 2004, Nassar, Levato et al. 2005). Components of the ‘inflammatory soup’ directly interact with $Na_v1.7$ and modulate the magnitude of $Na_v1.7$ sodium currents and shift the threshold of activation to more hyperpolarized potentials (Black, Liu et al. 2004). This increases the rates of activation and inactivation dramatically and in a second instance leads to increased sensitization of the nociceptors and the inflamed tissue (Julius and Basbaum et al. 2001).

1. 9 Aim of thesis

The principal aim of this thesis was to investigate the post-transcriptional regulation of *SCN9A* and to identify novel protein-protein interactions that influence trafficking and regulation of voltage-gated sodium channel $Na_v1.7$.

In chapter 2, I cloned a previously unreported *SCN9A* natural antisense transcript (*NAT*) that overlaps tail-to-tail with *Scn9a/SCN9A* in human and mouse DRG. The aim of this project was to evaluate the regulatory role of this *NAT* on *Scn9a*/$Na_v1.7$ expression. I demonstrated that the *NAT* is a non-protein coding RNA (lnRNA) that is alternatively spliced in DRG neurons and when overexpressed *in vitro*, specifically reduces mRNA, protein and sodium peak current of $Na_v1.7$ by around 30 percent. Given these results, it is possible that the *NAT* plays an important role in regulating pain thresholds *in vivo* and is therefore a potential new analgesic drug target.

In chapter 3, I examined the protein – protein interactome of $Na_v1.7$ through an in-depth analysis of a newly developed epitope-tagged $Na_v1.7$ ($Na_v1.7^{TAP}$) mouse. The goal was to get a comprehensive picture of all direct and indirect interaction partners of $Na_v1.7$. The TAP-tag method described in this chapter allowed me to isolate $Na_v1.7$ under native conditions, and coupled with mass spectrometry, it revealed a list of protein interaction partners. These proteins might be the key to understanding the basic nature of $Na_v1.7$ trafficking and regulation.

In the final chapter, I investigated a new mouse model of Primary Erythromelalgia (PE) that recapitulates the human phenotype. In humans, Primary Erythromelalgia is caused by autosomal dominant mutations in $Na_v1.7$ and is characterized by recurring episodes of excruciating pain that are induced by moderate heat and exercise. The aim of this project was to establish and characterize the first transgenic mouse model of PE that carries the human $Na_v1.7$L858F PE mutation. Therefore, I examined the transgene integration of the human gene in mouse and assessed the behavioral phenotype. I found that

this mouse model mimics the to human PE phenotype whereby warm temperatures or an irritant trigger painful episodes. In the future this mouse model will not only enable us to further study this disease but potentially also help in the screening of new analgesic drugs.

2 *Scn9a / SCN9A* natural antisense transcripts

2.1 Summary

The voltage-gated sodium channel $Na_v1.7$, encoded by *SCN9A*, is critical for human pain perception yet the transcriptional and post-transcriptional mechanisms that regulate this gene are still incompletely understood. In this chapter I examine a novel natural antisense transcript (*NAT*) for *SCN9A*, which is conserved in humans and mice. The *NAT* has a corresponding tissue expression pattern to the sense gene and is alternatively spliced within dorsal root ganglia. The human and mouse *NAT*s exist in *cis* with the sense gene in a tail-to-tail orientation and both share sequences that are complementary to the terminal exon of *SCN9A/Scn9a*. Overexpression analyses of the human *NAT* in human embryonic kidney (HEK293A) and human neuroblastoma (SH-SY5Y) cell lines show that it can function to downregulate $Na_v1.7$ mRNA, protein levels and currents by at least thirty per cent. Therefore the *NAT* may play an important role in regulating human pain thresholds and is a potential candidate gene for individuals with chronic pain disorders that map to the *SCN9A* locus, such as Inherited Primary Erythromelalgia, Paroxysmal Extreme Pain Disorder and Painful Small Fibre Neuropathy, but who do not contain mutations in the sense gene. My results strongly suggest the *SCN9A NAT* as a prime candidate for new chronic pain therapies based upon augmentation of existing antisense RNAs in the treatment of chronic pain conditions in man.

2.2 Introduction

Natural antisense transcripts

In recent years, it has become apparent that there are probably more genes in the human genome that encode regulatory RNAs than those that encode proteins (Morris and Mattick 2014). One major class of regulatory RNAs is the long non-coding RNAs (lncRNAs), of which natural antisense transcripts (NATs) are an important subset. NATs can be defined as processed transcripts that are complementary to the corresponding processed sense transcript in exonic regions (Werner and Sayer 2009). NATs can exist in *cis* or *trans* and are relatively common, with approximately 70% of all genomic loci showing

evidence of transcription from both sense and antisense strands (Katayama, Tomaru et al. 2005). Prominent examples of NATs include *Tsix* (the NAT for *Xist*), *Wrap53* (the NAT for p53) and *BACE1-AS* (the NAT for beta-secretase-1) (Lee, Davidow et al. 1999, Faghihi, Modarresi et al. 2008, Mahmoudi, Henriksson et al. 2009). In the pain field, a NAT was recently reported for the voltage-dependent potassium channel *Kcna2* (Zhao, Tang et al. 2013). This NAT is expressed in rat dorsal root ganglia (DRG) neurons and is upregulated in response to peripheral nerve injury. The increase in NAT levels downregulates *Kcn2a*, reducing total voltage-gated potassium currents, increasing excitability in DRG neurons and producing neuropathic pain symptoms.

In this chapter, I show that the *SCN9A* gene also has a corresponding natural antisense transcript that is encoded on the opposite strand and overlaps tail-to-tail with the sense transcript. The *SCN9A NAT* is present in both human and mouse genomes and has a putative role in $Na_v1.7$ regulation.

2.3 Results

Genomic arrangement of *SCN9A/Scn9a* natural antisense transcripts

In silico analysis of the human *SCN9A* gene footprint using the UCSC genome browser identified several expressed sequence tags (ESTs) (BC051759, BC029452, BM905527, BE566126, BG215777, AA383040) that were partially complementary to exonic regions of the sense gene. Alignment of the longest human EST, BC051759, to the genomic sequence indicated a cDNA comprised of 12 exons four of which were complementary and overlapped exons from *SCN9A* and with five exons containing Short Interspersed Nuclear Elements (SINEs) and/or Long Interspersed Nuclear Elements (LINEs) repeat sequences. Exons were flanked with the canonical AG-GT splice acceptor and donor sites and the final exon contained an AAUAAA polyadenylation signal. In Genbank the assembly of ESTs has subsequently been annotated as LOC101929680

(NR_110260), an uncharacterized long non-coding RNA of 2305 bp that spans 220 kb on chromosome 2 (Figure 2-1,B).

Analysis of the mouse genome also led to the identification of several ESTs that were antisense to *Scn9a*. For the mouse antisense gene, I identified the following antisense ESTs: AK039017 (hypothalamus cDNA), AK045660 (corpora quadrigemina cDNA), AK020721 (hypothalamus cDNA), AK138511 (spinal cord) and AK138532 (spinal cord). EST AK138532 indicated a cDNA comprised of four exons, one of which splices into a LINE repeat and two of which overlap *Scn9a* sense gene exons (NR_033495; Figure 2-1,A). Similar to the human *SCN9A NAT*, exons were flanked with canonical AG-GT splice acceptor and donor sites and the final exon contained an AAUAAA polyadenylation signal. Both the human and mouse NATs contain sequences that overlap the final sense *SCN9A*/*Scn9a* exon, potentially indicating a conserved regulatory function of these *NAT*s in man and mouse. Using mouse dorsal root ganglia cDNA as template I amplified the identical sequence to NR_033495 (KM096552, Figure 2-1,A) as well as a splice variant (KM096553), which uses an alternative splice donor site in exon 3.

The human and mouse *SCN9A/Scn9a* sense genes are organized in a tail-to-tail arrangement on chromosome 2. A tail-to-tail arrangement of *NAT* and sense gene is given when both genes overlap at their 3' ends while the transcription start sites (TSS) are not within the overlapping region. By way of comparison, in a head-to-head arrangement, *NAT* and sense gene overlap at the 5' ends which includes the TSS (Lapidot and Pilpel 2006). The genomic footprints of both the human and mouse *NATs* overlap with their corresponding sense *SCN9A* genes. Additionally in human, *SCN1A* and *NAT* are arranged in a head-to-head orientation with the transcription start sites at the 5' ends of both *NAT and SCN1A* overlapping (Figure 2-1,B). In mouse the TSS of the *Scn9a NAT* and *SCN1A* are in close proximity but not overlaping (Figure 2-1,A).

Cloning of the mouse and human antisense transcripts: splice variants detected

The mouse *Scn9a* natural antisense transcript was amplified from freshly prepared mouse DRG cDNA with primers flanking the 3´and 5´ of the longest EST, AK138532 (see Methods 6.1.1). Primers were designed using the mouse genomic sequence (UCSC genome browser) and online primer design tool Primer3. Amplification of the potential full-length transcript gave two different sized fragments. The longer isoform has a 993 bp overlap with the *Scn9a* sense gene over exons 2 to 4 (Figure 2-1,A). The shorter isoform misses parts of the penultimate exon 3 due to an internal exonic splice donor site. Consequently, the overlap with the sense gene is around 797 bp long hence, 200 bp shorter in comparison to the longer isoform.

Using human dorsal root ganglia cDNA as template I amplified two alternative splice variants, which were submitted to Genbank. Compared to NR_110260, the first splice variant (KM096550) excludes exon 2 and uses an alternative splice acceptor site within exon 7. The second splice variant (KM096551) excludes both exon 2 and exon 8 (Figure 2-1,B).

In silico translation of the cloned human and mouse *NAT* sequences in three frames shows that the longest potential open reading frames are 67 (Figure 2-2) in human and 114 amino acids in mouse (Figure 2-3). The lack of a long open reading frame and the poor codon conservation is consistent with the definition of a long non-coding RNA (Morris and Mattick 2014).

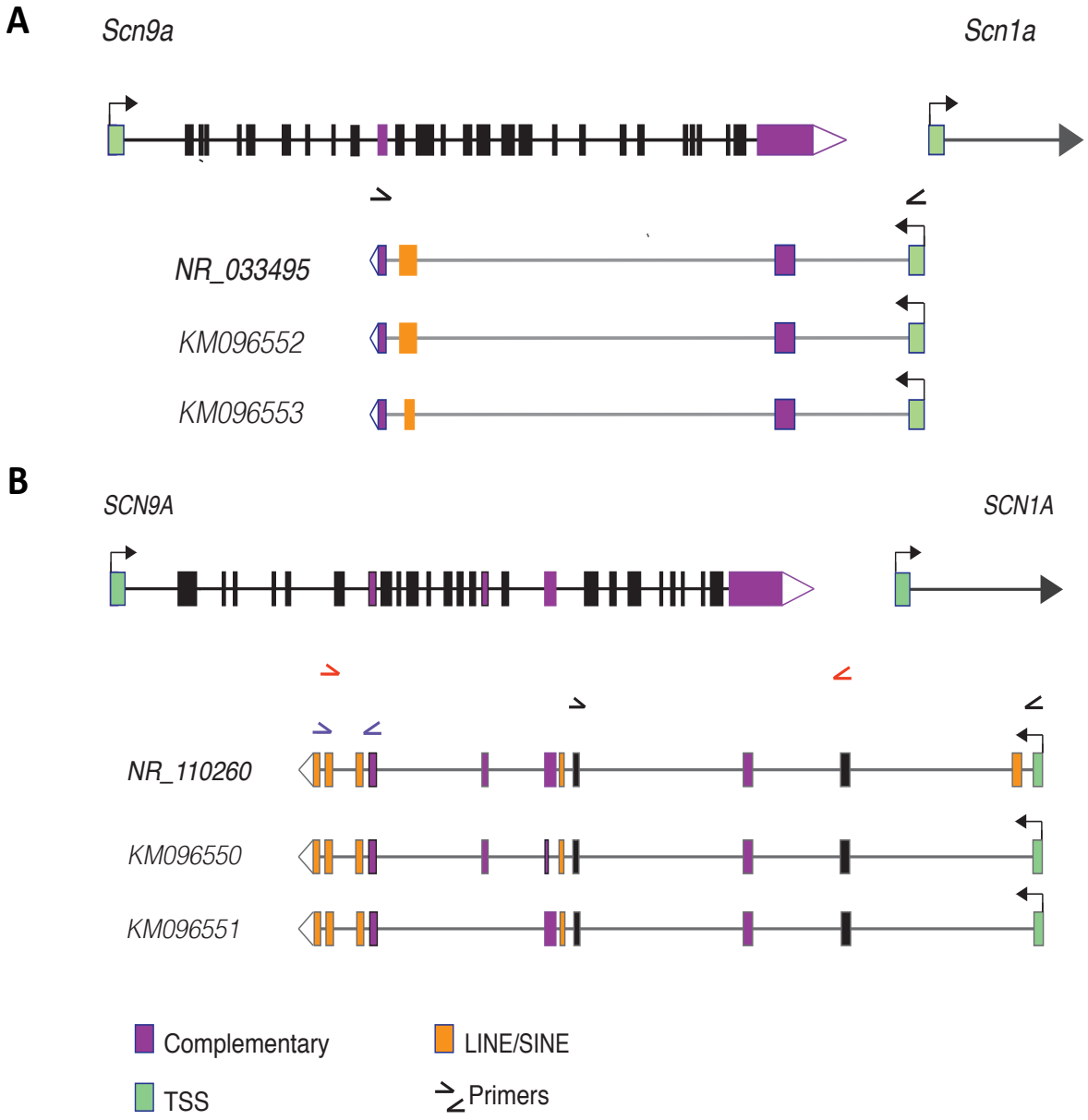

Figure 2-1: Genomic organization of the mouse (A) and human (B) *SCN9A/Scn9a* natural antisense transcripts (*NAT*s).

The sense genes are shown at the top of each panel with the *NAT* splice variants shown below. *Scn9a/SCN9A* and *NAT*s are arranged in a tail-to-tail orientation in human and mouse (3' ends overlapping), while human *SCN1A* and *NATs* are arranged in a head-to-head orientation (5' ends overlapping). In mouse the transcriptional start sites of the *NAT* and *Scn1a* are in close proximity but not overlaping. Transcriptional start sites (TSS) and direction of transcription are denoted by green exons and arrows respectively; overlapping regions between sense and *NAT* sequences are shown by purple exons; LINE and SINE repeat sequences are shown as orange exons; and the primer pairs used to amplify the respective *NAT* sequences are also highlighted.

Translation of KM096550 (human NAT splice variant 1):

Frame 1:

PRDTQHPQLHTLMPLCIYARNTITKELDIIRQ-IKRY-QLRLSDGPCLGFGIFA-NRDSS
HQRQRSQGDCGL-EALPGNRNSGKVGHSKDGVDEHDQEEQEADVKQRRKGHHQSKEQRAD
PLCSFD-T-DSANPGKTDHSEQGNRDLWR-NIALNWH-F-PSSCRPITNLSISLQCLELD
LAHRQRVINCAAL-GA-PV-SLERNSPPHQHAEHNQEGVEEVVHVPPWERTVIIDLADTF
FVALTKELHADHSKNEDDDGQH-AFRLKRKQILHTLNLC-NHKGEHLWILPSNKNILLKK
NLNSYNITDFNL-L--RRSN-KI-LLGDFWSNHGRKTMKSDILGFECCFYPFLT-IHGHS
LSSVPNLAEPQSTHNLASVFSMLATKWLNVGGETLTTK-MVIF-FRSCCPGWSAMARSRL
TATSASRVQAILLPQPPE-LELQAPTTMPG-FFVFL

Frame 2:

RETPSIHNFTL-CHCVFMQEIP-LRNLTSSDSKSRGTDN-D-VMVPA-DLESLHEIGTLA
TSDKEVRETAVSRKHFQETGIQAKLDIPKMA-MNMTRKSRRPMLNNAGRDIIKAKSSVRI
PFAPLTRRRIRPILARRITRNRVTEISGGETLL-TGIDSSPALVDQLPTCPSPSSAWNWT
WHTGKGLSTVLHSEELDRFNL-KGIHHPTSTRNTIRKEWKKSFMCHRGSVQSSLILQTHS
L-LLPKSCMPTTAKMKTMMANTKPLD-KENKYYIP-ICAETTKESIFGSFQVIKIFC-RR
I-TVITSQTLICDCDKGGQIKKSDYWETFGVIMEERL-NQIFLDLNVASIPS-LKSMGIH
YHQCLTWQNHSLHIIWHLSFPCWLPNG-MLVEKLSQPSEWLYFNFALVAQAGVQWHDLGS
PQPLPPEFKRFSCLSLLSSWNYRRPPPCPANFLYF

Frame 3:

ERHPASTTSHSDAIVYLCKKYHN-GT-HHQTVNQEVLTTETE-WSLPRIWNLCMK-GL-P
PATKKSGRLRSLGSTSRKQEFRQSWTFQRWRR-T-PGRAGGRC-TTQEGTSSKQRAACGS
PLLL-LDVGFGQSWQDGSLGTG-QRSLEVKHCSELALILAQLL-TNYQLVHLPPVPGTGP
GTQAKGYQLCCTLRSLTGLISRKEFTTPPARGTQSGRSGRSRSCATVGAYSHH-SCRHIL
CSSYQRAACRPQQK-RR-WPTLSL-TKKKTNITYPESVLKPQRRASLDPSK--KYSVEEE
FEQL-HHRL-SVIVIKEVKLKNLIIGRLLE-SWKKDYEIRYSWI-MLLLSLLNLNPWAFI
IISA-PGRTTVYT-SGICLFHAGYQMAECWWRNSHNQVNGYILISLLLPRLECNGTISAH
RNLCLPSSSDSPASAS-VAGITGAHHHARLIFCIF

Translation of KM096551 (human NAT splice variant 2):

Frame 1:

PRDTQHPQLHTLMPLCIYARNTITKELDIIRQ-IKRY-QLRLSDGPCLGFGIFA-NRDSS
HQRQRSQGDCGL-EALPGNRNSGKVGHSKDGVDEHDQEEQEADVKQRRKGHHQSKEQRAD
PLCSFD-T-DSANPGKTDHSEQGNRDLWR-NIALNWH-F-PSSCRPITNLSISLQCLELD
LAHRPLAHRNS-VQPLLLLLLQAKGYQLCCTLRSLTGLISRKEFTTPPAFRLKRKQILHT
LNLC-NHKGEHLWILPSNKNILLKKNLNSYNITDFNL-L--RRSN-KI-LLGDFWSNHGR
KTMKSDILGFECCFYPFLT-IHGHSLSSVPNLAEPQSTHNLASVFSMLATKWLNVGGETL
TTK-MVIF-FRSCCPGWSAMARSRLTATSASRVQAILLPQPPE-LELQAPTTMPG-FFVF
L

Frame 2:

RETPSIHNFTL-CHCVFMQEIP-LRNLTSSDSKSRGTDN-D-VMVPA-DLESLHEIGTLA
TSDKEVRETAVSRKHFQETGIQAKLDIPKMA-MNMTRKSRRPMLNNAGRDIIKAKSSVRI
PFAPLTRRRIRPILARRITRNRVTEISGGETLL-TGIDSSPALVDQLPTCPSPSSAWNWT
WHTGLWLIGIHRFSLCFFSFSRQRVINCAAL-GA-PV-SLERNSPPHQPLD-KENKYYIP
-ICAETTKESIFGSFQVIKIFC-RRI-TVITSQTLICDCDKGGQIKKSDYWETFGVIMEE
RL-NQIFLDLNVASIPS-LKSMGIHYHQCLTWQNHSLHIIWHLSFPCWLPNG-MLVEKLS
QPSEWLYFNFALVAQAGVQWHDLGSPQPLPPEFKRFSCLSLLSSWNYRRPPPCPANFLYF

Frame 3:

ERHPASTTSHSDAIVYLCKKYHN-GT-HHQTVNQEVLTTETE-WSLPRIWNLCMK-GL-P
PATKKSGRLRSLGSTSRKQEFRQSWTFQRWRR-T-PGRAGGRC-TTQEGTSSKQRAACGS
PLLL-LDVGFGQSWQDGSLGTG-QRSLEVKHCSELALILAQLL-TNYQLVHLPPVPGTGP
GTQASGSSEFIGSASASSPSPGKGLSTVLHSEELDRFNL-KGIHHPTSL-TKKKTNITYP
ESVLKPQRRASLDPSK--KYSVEEEFEQL-HHRL-SVIVIKEVKLKNLIIGRLLE-SWKK
DYEIRYSWI-MLLLSLLNLNPWAFIIISA-PGRTTVYT-SGICLFHAGYQMAECWWRNSH
NQVNGYILISLLLPRLECNGTISAHRNLCLPSSSDSPASAS-VAGITGAHHHARLIFCIF

Figure 2-2: In-silico translation of human *NAT* splice variants KM096550 and KM096551 cloned from DRG.

Open reading frames, as shown in red, begin with a methionine residue and stop codons are denoted by a hyphen. The longest potential open reading frames are 67 amino acids long (Frame 2 of KM096550/51**),** which suggests the transcript is not translated into a protein.

Translation of KM096552 (mouse NAT splice variant 1):

Frame 1:

SSKQAGRLRSCMEIMNQVLLFVFETFWKESYE-PRNRSHFVGRKNDQKHES-ISWQVQGT
SLGVCSKPEGTTSPAVNS-TITSGVKEGAGEAL--MQRMLLRALVCL-LIVAKLDIPKMA
-MNMTRKSRRPMLNSAGRDIIRAKSSVRIPLAPLIRRRIRPILARRMTRNRMLLPVFTEK
LL-PVNDSE-RNAWLLETPRVTAACSAQEDVHILLQGSRNKAW--QEDSKSPGHRDGSYE
ALCCTKDTINVIAAP-QRSAVGSCNTERVSIHSFIYREGPCSHIFSAEL-ATDGLWEKQT
FSSALGPLLSSLG-TSSMLAWFCSSYAMATTARIKFIR-KDPRNITTTKKIM-VLPAARS
VYGEQKRDMIILVIQKFH-GFYCS-YIMNVQTRYFCIILL-KDK-R-YL-GKSVLNKLFN
IKDTALLYVH-GLIL

Frame 2:

AASRRAG-DLAWKS-TRSCFSFLKRFGRRVMNSPEIGLILWVGRMTRSMKAKSPGKCRGP
LLECAVNPRGRLLLLSTPEPSHLE-RKGLVKPCNKCKGCC-ELWSAFNSLWQSWTSQRWR
R-T-RGKAGGRC-TAQEGTSSEQRAACGSPWRL-SGVGFVQSWPGE-LGTGCYSQSSLRN
CSSQ-TTVNEEMPGCSRHRE-QLRAQLRRTFISFFKALGTKRGDDRKTVRAQDIGMGAMK
LCAVPRTQSM-SRHHNRGQQWVRAILSGSAFIHSYTERAHAATSSLLNYELPMDCGRNKH
SLQPWAHF-VH-VKLLRCWPGSVPRTPWLPQPGSSLSGKRIPEISPRQRKSCRFCQQHAV
SMGSKKET-LF--YKNFTKVFIAASI--MCKPDIFV-FCCRKINKDNIFEENQY-TNFLI
-KIQHCYMYIKA-F

Frame 3:

QQAGGQAEILHGNHEPGLAFRF-NVLEGEL-IAQK-VSFCG-EE-PEA-KLNLLASAGDL
SWSVQ-TRGDDFSCCQLLNHHIWSEGRGW-SLVINAKDAAESFGLPLTHCGKVGHPKDGV
DEHDEEKQEADVEQRRKGHHQSKEQRADPLGAFDQA-DSSNPGQANDSEQDATPSLH-ET
ALASERQ-MKKCLAARDTESDSCVLSSGGRSYPSSRL-EQSVVMTGRQ-EPRT-GWEL-S
SVLYQGHNQCNRGTITEVSSGFVQY-AGQHSFIHIQRGPMQPHLLC-IMSYRWIVGETNI
LFSLGPTSEFTRLNFFDVGLVLFLVRHGYHSQDQVYQVKGSQKYHHDKENHVGFASSTQC
LWGAKKRHDYFSNTKISLRFLLQLVYNECANQIFLYNFVVER-IKIISLRKISIKQTF-Y
KRYSIVICTLRLDS

Translation of KM096553 (mouse NAT splice variant 2):

Frame 1:

SSKQAGRLRSCMEIMNQVLLFVFETFWKESYE-PRNRSHFVGRKNDQKHES-ISWQVQGT
SLGVCSKPEGTTSPAVNS-TITSGVKEGAGEAL--MQRMLLRALVCL-LIVAKLDIPKMA
-MNMTRKSRRPMLNSAGRDIIRAKSSVRIPLAPLIRRRIRPILARRMTRNRMLLPVFTEK
LL-PVNDSE-RNAWLLETPRVTAACSAQEDVHILLQGSRNKAW--QEDSKSPGHRDGSYE
ALCCTKDTINVIAAP-QSFFDVGLVLFLVRHGYHSQDQVYQVKGSQKYHHDKENHVGFAS
STQCLWGAKKRHDYFSNTKISLRFLLQLVYNECANQIFLYNFVVER-IKIISLRKISIKQ
TF-YKRYSIVICTLRLDS

Frame 2:

AASRRAG-DLAWKS-TRSCFSFLKRFGRRVMNSPEIGLILWVGRMTRSMKAKSPGKCRGP
LLECAVNPRGRLLLLSTPEPSHLE-RKGLVKPCNKCKGCC-ELWSAFNSLWQSWTSQRWR
R-T-RGKAGGRC-TAQEGTSSEQRAACGSPWRL-SGVGFVQSWPGE-LGTGCYSQSSLRN
CSSQ-TTVNEEMPGCSRHRE-QLRAQLRRTFISFFKALGTKRGDDRKTVRAQDIGMGAMK
LCAVPRTQSM-SRHHNRASSMLAWFCSSYAMATTARIKFIR-KDPRNITTTKKIM-VLPA
ARSVYGEQKRDMIILVIQKFH-GFYCS-YIMNVQTRYFCIILL-KDK-R-YL-GKSVLNK
LFNIKDTALLYVH-GLIL

Frame 3:

QQAGGQAEILHGNHEPGLAFRF-NVLEGEL-IAQK-VSFCG-EE-PEA-KLNLLASAGDL
SWSVQ-TRGDDFSCCQLLNHHIWSEGRGW-SLVINAKDAAESFGLPLTHCGKVGHPKDGV
DEHDEEKQEADVEQRRKGHHQSKEQRADPLGAFDQA-DSSNPGQANDSEQDATPSLH-ET
ALASERQ-MKKCLAARDTESDSCVLSSGGRSYPSSRL-EQSVVMTGRQ-EPRT-GWEL-S
SVLYQGHNQCNRGTITELLRCWPGSVPRTPWLPQPGSSLSGKRIPEISPRQRKSCRFCQQ
HAVSMGSKKET-LF--YKNFTKVFIAASI--MCKPDIFV-FCCRKINKDNIFEENQY-TN
FLI-KIQHCYMYIKA-F

Figure 2-3: In-silico translation of mouse *NAT* splice variants KM096552 and KM096553 cloned from DRG

Open reading frames, as shown in red, begin with a methionine residue and stop codons are denoted by a hyphen. The longest potential open reading frame is 114 amino acids long (Frame 3 of KM096552), which suggests the transcripts are not translated into a protein.

Expression patterns of mouse natural antisense transcript

Mouse tissue panel

To investigate the tissue expression profile of the *Scn9a NAT* compared with the sense gene *(Scn9a),* I ran qPCR assays across a range of mouse tissue cDNA samples (Figure 2-4) (see Methods 6.1.3.1). The *Scn9a* sense and *NAT* genes have a relatively restricted expression pattern and are co-expressed in adult brain, DRG and spinal cord tissues. In addition, the *NAT* also shows expression within adult eye. The co-expression of the sense and *NATs* in corresponding tissues suggests that the *NAT* could have a direct regulatory effect on *Scn9a* gene functions.

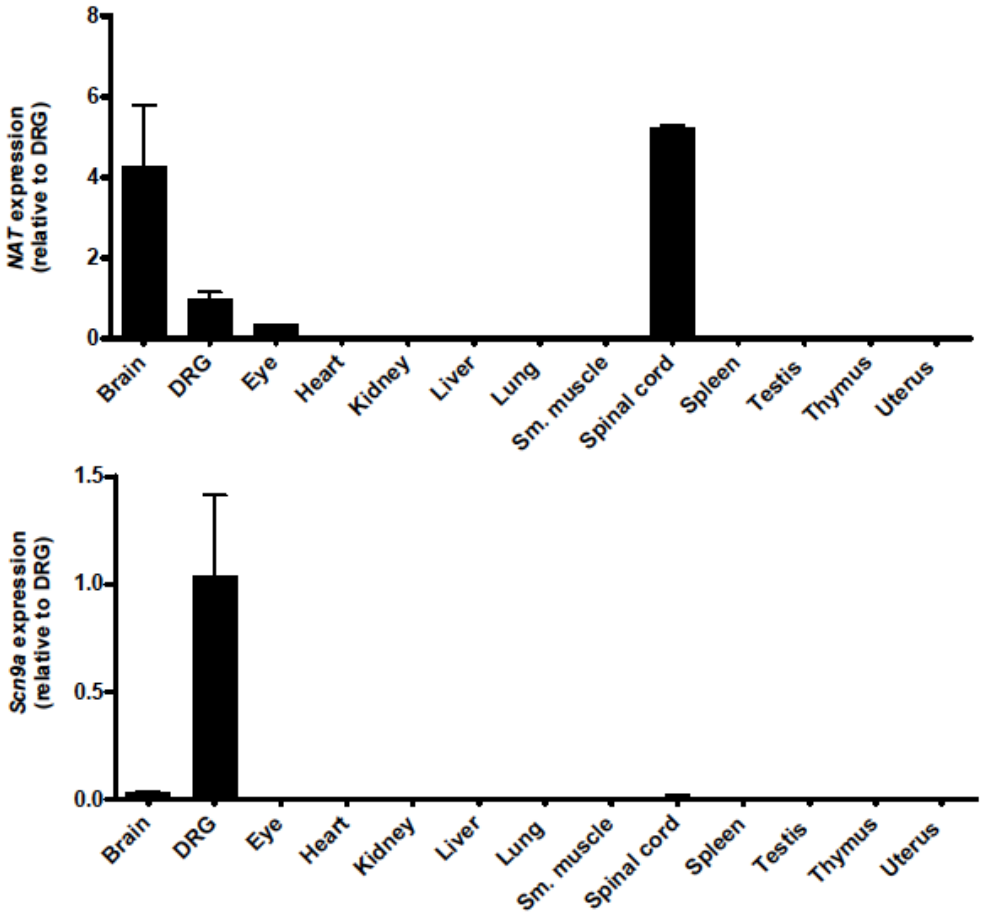

Figure 2-4: *Scn9a* and *NAT* expression pattern.

Mouse tissue panel real-time qPCR assays measuring the expression level relative to DRG of the mouse *NAT* (upper panel) and the *Scn9a* sense gene (lower panel). Both the sense and *NAT* genes are expressed in corresponding tissues.

To further understand the relative expression of the *NAT* and *Scn9a* within DRG neurons, I analysed a recent paper in which DRG neurons have been categorized into 11 subtypes based on single-cell RNA-seq expression data (Usoskin, Furlan et al. 2015). This shows that the *NAT* is expressed in six of the eleven DRG neuronal subtypes. Interestingly, in the remaining five DRG subtypes with no *NAT* expression detected, there is robust *Scn9a* expression Conversely, in the only neuronal subtype without *Scn9a* expression ('NF5'), there is relatively high expression of the *NAT*, indicating that within particular neuronal cell populations there is contrasting expression profiles of the *NAT* and *Scn9a* (Figure 2-5).

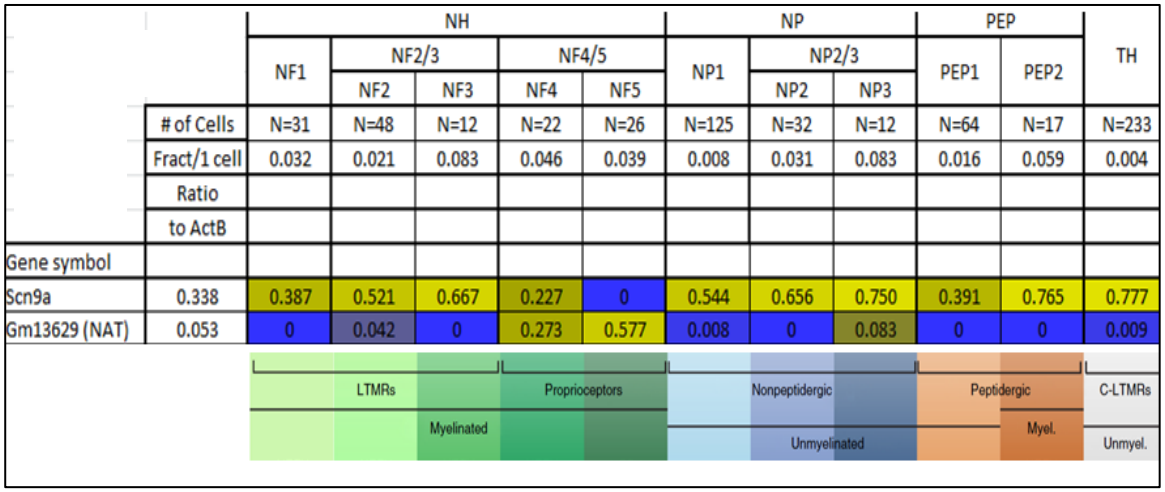

		NH					NP			PEP		TH
		NF1	NF2/3		NF4/5		NP1	NP2/3		PEP1	PEP2	
			NF2	NF3	NF4	NF5		NP2	NP3			
	# of Cells	N=31	N=48	N=12	N=22	N=26	N=125	N=32	N=12	N=64	N=17	N=233
	Fract/1 cell	0.032	0.021	0.083	0.046	0.039	0.008	0.031	0.083	0.016	0.059	0.004
	Ratio											
	to ActB											
Gene symbol												
Scn9a	0.338	0.387	0.521	0.667	0.227	0	0.544	0.656	0.750	0.391	0.765	0.777
Gm13629 (NAT)	0.053	0	0.042	0	0.273	0.577	0.008	0	0.083	0	0	0.009
			LTMRs		Proprioceptors		Nonpeptidergic			Peptidergic		C-LTMRs
				Myelinated			Unmyelinated				Myel.	Unmyel.

Figure 2-5: Unbiased classification of sensory neuron types by large-scale single-cell RNA sequencing.

Comprehensive RNA-seq analysis identified 11 genetically definied subtypes of DRG neurons. The population size and the fraction of the population that would correspond to one cell are shown at the top. Neuronal subclasses corresponding to the 11 subtypes are shown on the bottom. The *NAT(Gm13629)* is expressed in six neuronal subtypes with the highest expression in large propioceptor neurons ('NF5'), the only subtype of DRG neurons that does not express *Scn9a*. In the remaining DRG subtypes that do not exhibit *NAT* expression, *Scn9a* is robustly expressed.**Taken from Usoskin, Furlan *et al.* 2015.**

Next, I examined if the human *NAT* carries known single nucleotide polymorphisms (SNP) that are linked to *SCN9A* related pain disorders (Figure 2-6,A-C). Indeed NAT and *SCN9A* overlapping sequences in exon 15 and exon 26 of *SCN9A* carry point mutations that have been associated with an altered function of $Na_v1.7$, resulting in a painful or painless human phenotype. In the *NAT:SCN9A* overlapping region of exon 15, three mutations linked to primary erythromelalgia (PE) (A863P, V872G, Q875E)(Harty,Dib-hajj et al. 2006,Choi, Zhang et al. 2009, Stadler, O'Reilly et al. 2015, Skeik, Rooke et al. 2012) and two SNP's linked to congenital insensitivity to pain (CIP) (R896Q, W897X) (Cox, Sheynin et al. 2010, Cox, Reimann et al. 2006) have been reported (Figure 2-6,A). Additionally the overlapping exonic region of exon 26 in *SCN9A* contains five mutations linked to CIP (R1599X) (Mansouri, Chafai Elalaoui et al. 2014), PE (A1632T) (Eberhardt, Nakajima et al. 2014) cold-sensitive paroxysmal extreme pain disorder (PEPD) (L1612P) (Suter, Bhuiyan et al. 2015), PEPD (M1627K)(Dib-Hajj, Estacion et al. 2008) and to an overlapping phenotype of erythromelalgia and PEPD (A1632E)(Estacion, Dib-Hajj et al. 2008)(Figure 2-6,B). However, the *NAT:SCN9A* overlapping regions in exon 7 and exon 17 carry no reported disease-associated SNPs (Figure 2-6,C). Taken together, this shows that *SCN9A* point mutations previously shown to cause the human monogenic pain disorders CIP, IEM and PEPD also change the sequence of the *NAT*.

Overexpression of the human *NAT* specifically reduces $Na_v1.7$ peak sodium currents

To functionally test the effects of overexpressing the human *NAT* (h*NAT*) on sodium currents, HEK293 cells stably expressing either $Na_v1.7$ or $Na_v1.6$ were transfected with (1) *NAT* in pcDNA3 plus a GFP-expressing vector (pEGFP-N1) or (2) empty pcDNA3 plus pEGFP-N1 (see Methods 6.2.2) Two days after transfection the green fluorescing cells were patch clamped by Dr John Linley, Molecular Nociception Group (see Methods 6.1.4 and 6.3).

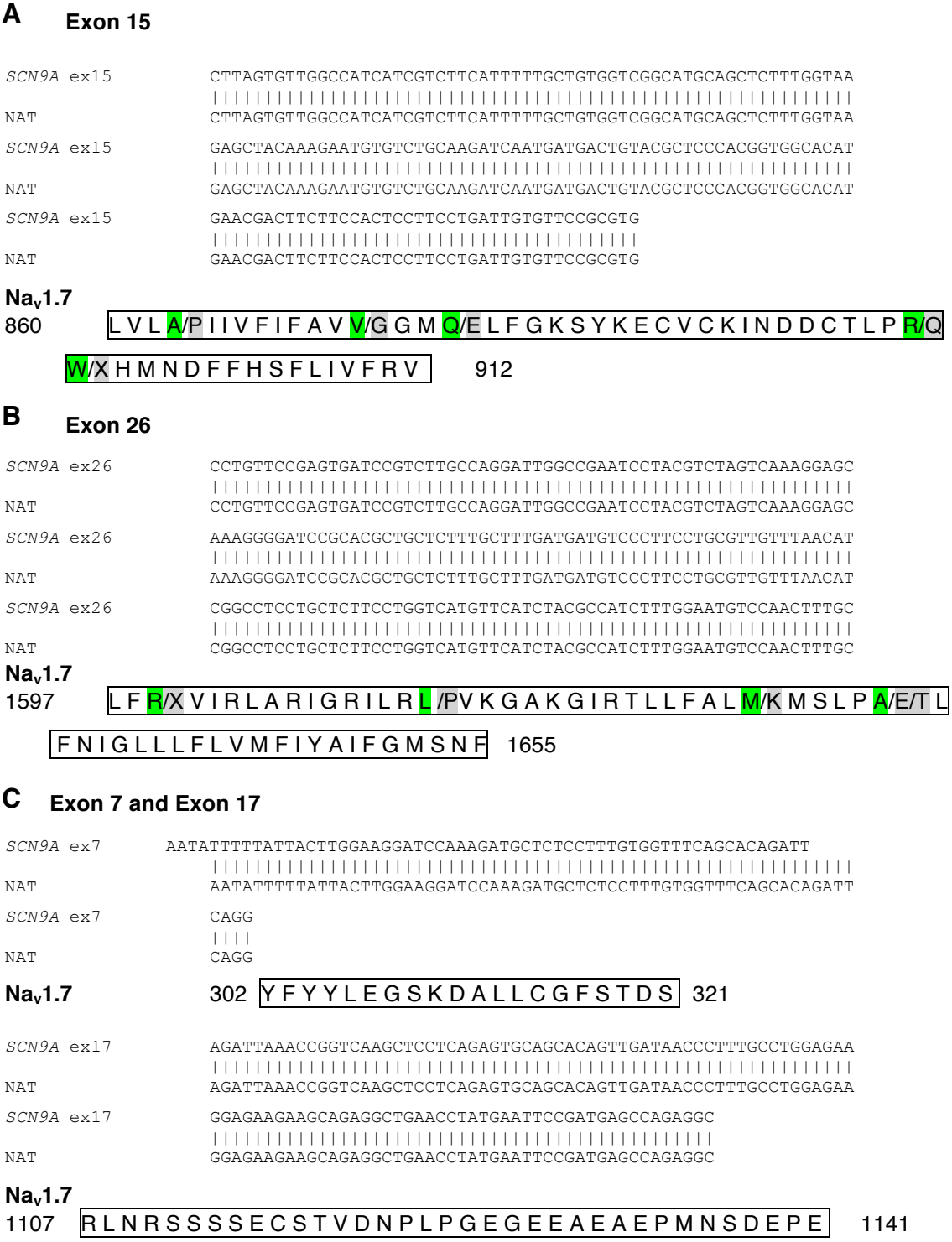

Figure 2-6: Alignment of *NAT:SCN9A* overlapping regions and reported disease-associated SNPs in these regions

(A) Alignment of *NAT:SCN9A* overlapping regions in exon 15 (A863P, V872G, Q875E, R896Q, W897X) and **(B)** exon 26 (R1599X, L1612P, M1627K, A1632E, A1632T), linked to painful and painless *SCN9A*-Channelopathies in humans, are found in overlapping regions with the *NAT* (green highlight, original sequence; gray highlight, SNP) **(C)** *NAT:SCN9A* overlapping regions in exon 7 and exon 17 carry no reported disease-associated SNPs.

Overexpression of the human *SCN9A NAT* in the $Na_v1.7$ stable cell line resulted in a statistically significant reduction in the peak sodium current (Figure 2-7,C).
In $Na_v1.6$ stably expressing cells, overexpression of the *NAT* had no effect on the sodium current, indicating that the *NAT* specifically affects the activity of $Na_v1.7$. To test whether the decrease in sodium current observed is related to a reduction in *SCN9A* mRNA expression, I ran a qPCR. $hNa_v1.7$ HEK293 cells were transfected with either h*NAT* or empty vector. RNA was collected 24 and 48 hours after transfection. cDNA of non-transfected hNav1.7 stable HEK cells was used as a basal control (sham)(see Methods 6.1.4 and 6.3). The results suggest that the *SCN9A* mRNA levels are not altered as a result of overexpression of the *NAT*, indicating that sense mRNA is not downregulated or degraded (Figure 2-7 A,B). Furthermore I compared the protein expression levels of $Na_v1.7$ in untransfected HEK293 $hNa_v1.7$ stable cells (Nav1.7), transiently *NAT* transfected HEK293 $hNa_v1.7$ cells (NAT) and naive HEK293 cells (sham) (see Methods 6.2.2) 24 hours after transfection (Figure 2-7,D). Cells were collected and protein was isolated in RIPA buffer (see Methods 6.5.3). Crude protein lysate was immunoblotted using an anti-$Na_v1.7$ antibody (Neuromab). There was no significant change in protein expression between *NAT* transfected and untransfected HEK293 $hNa_v1.7$ stable cells 24 hours after transfection. However, the human HEK293 $hNa_v1.7$ stable cell line has the clear disadvantage that $Na_v1.7$ is ectopically expressed from a CMV promoter. Therefore small changes in mRNA or protein expression can go undetected. Additionally, transfection efficacy might also affect the results as non-transfected cells can also cause a false-negative qPCR and western blot result.
To address these problems I generated a SH-SY5Y-*NAT* stable cell line that endogenously expresses $Na_v1.7$ in order to further test the effect of *NAT* overexpression on *SCN9A* mRNA. However, as SH-SY5Y cells not only express $Na_v1.7$ but also other voltage-gated sodium channels, I decided to also design a $Na_v1.7$ TAP-tag stable cell line that allows for the detection of $Na_v1.7$ with commercially available antibodies. This enabled me to specifically examine the protein expression of $Na_v1.7$.

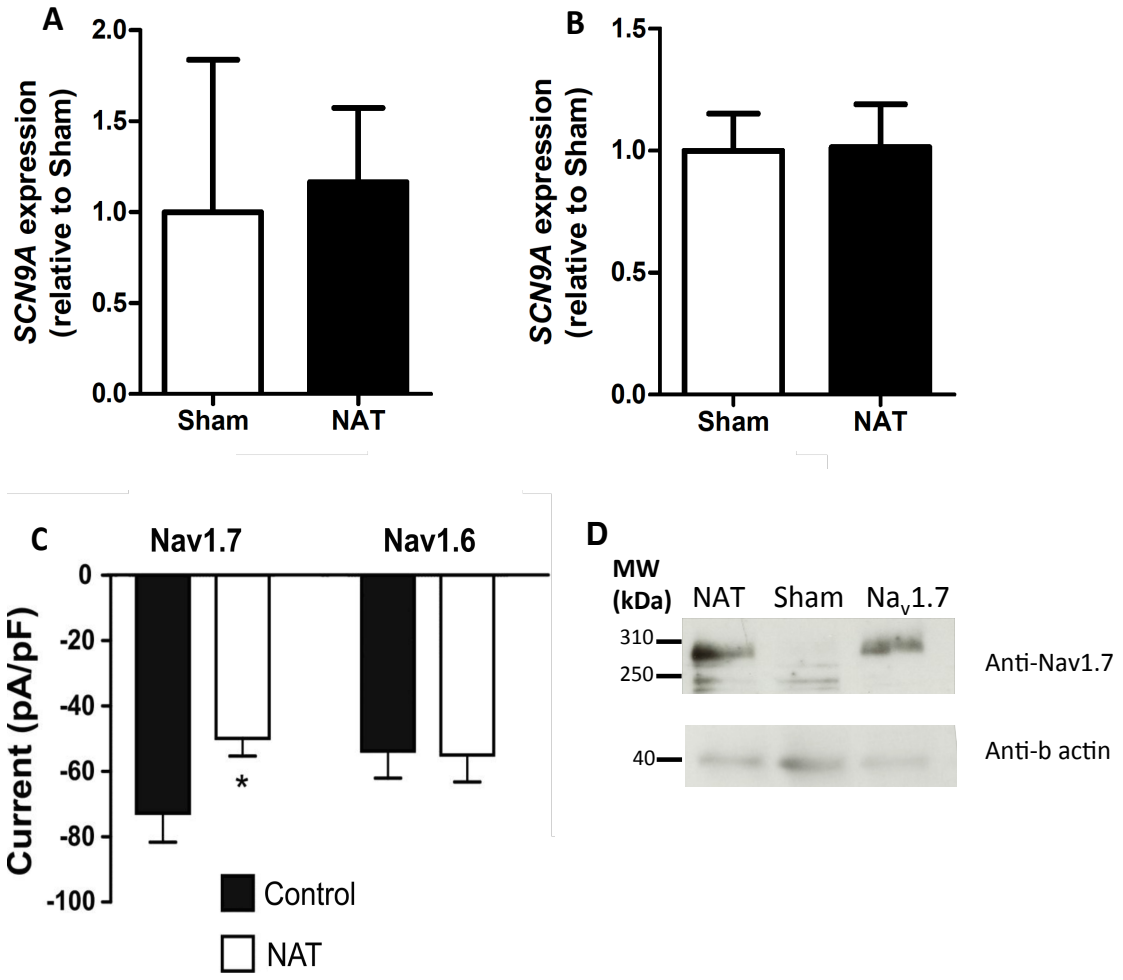

Figure 2-7: qPCR, immunoblotting and electrophysiology recordings on hNa$_v$1.7 stable HEK293 cells transiently transfected with *NAT.*

(A) Real-time qPCR showing that the *NAT* overexpression after 24 hours (n=3) or **(B)** 48hrs does not impact the *SCN9A* mRNA level in hNa$_v$1.7 stable HEK293 cells relative to untransfected hNav1.7 stable HEK293 cells (sham)(n=3). **(C)** Overexpression of the human *NAT* inhibits Na$_v$1.7 but not Na$_v$1.6 currents. Whole cell voltage clamp recording from HEK cells stably expressing human Na$_v$1.7 or human Na$_v$1.6. Cells were transiently transfected with either pcDNA3 vector (black bars) or Na$_v$1.7 *NAT* (white bars) along with a GFP-expressing vector and recorded from 48 hrs. later. Peak whole cell current (pA) was measured in response to a 10 ms voltage step from the holding potential of -120 mV to 0 mV and normalized to cell size (pF). N = 17-20; * indicates $p<0.05$ when compared to control (unpaired t-test). Patch clamping performed by Dr John Linley. **(D)** Immunoblotting of crude lysate using an anti-Na$_v$1.7 antibody (Neuromab) showed no significant difference between *NAT* transfected (NAT) and untransfeccted HEK293 hNa$_v$1.7 stable cells (Nav1.7). Naïve HEK293 cells (Sham) were used as control. β-actin was used as a loading control.

Generation of a *NAT*-SH-SY5Y stable human neuroblastoma cell line

The human neuroblastoma SH-SY5Y cell line endogenously expresses a range of voltage-gated sodium channels ($Na_v1.2$, $Na_v1.3$, $Na_v1.4$, $Na_v1.5$, $Na_v1.7$), among which $Na_v1.7$ is the one of the most abundantly expressed isoforms. Furthermore, beta subunit genes, *SCN2B* and *SCN3B*, are also endogenously expressed (Vetter, Mozar et al. 2012). However, SH-SY5Y cells show no endogenous expression of the h*NAT* (Figure 2-8,A). Here, I generated a SH-SY5Y *NAT*-cell line that stably expresses the human *NAT* cDNA under a CMV promoter to further study the overexpression of h*NAT* on endogenously expressed $Na_v1.7$ (see Methods 6.2.3). The *SCN9A* mRNA level in the *NAT*-stable cell line was significantly downregulated compared to naïve SH-SY5Y cells (sham) (Figure 2-8,B). Patch clamping showed a statistically significant reduction in the peak sodium current compared to control SH-SY5Y cells (sham) that did not express the h*NAT* (Figure 2-8,C-D)(see Methods 6.1.3.1 and 6.3). Voltage-current relationships appeared unaltered between the two cell lines.

Next, the stable cell line was tested for the expression of *SCN1A* ($Na_v1.1$), *SCN2A* ($Na_v1.2$) and *SCN3A* ($Na_v1.3$)(see Methods 6.1.3.2). Although *SCN1A*, *SCN2A* and *SCN3A* do not overlap with the *NAT,* they share conserved exon sequences (exon 15 and 26) with the antisense transcript (Figure 2-9,A). However *SCN4A, SCN5A*, *SCN7A*, *SCN8A*, *SCN10A* and *SCN11A SCN9A* NAT (NR_110260) do not share sequences with *SCN9A* NAT (NR_110260). As the *NAT* shows high expression in the brain, it is possible that the *NAT* may also regulate the $Na_v1.1$-$Na_v1.3$ brain-expressed sodium channels encoded by *SCN1A*-*SCN3A*. I was therefore interested to determine whether overexpression of the *NAT* downregulated endogenously expressed $Na_v1.1$, $Na_v1.2$ or $Na_v1.3$ in the *NAT*-stable SH-SY5Y cell line. Real-time qPCR showed the expression level of *SCN2A* and *SCN3A* was not significantly different between the naïve SH-SY5Y cells (sham) and the stable-*NAT* SH-SY5Y cells (*SCN1A* expression could not be detected in the SH-SY5Y cell lines) (Figure 2-9, B-C), further indicating that the functional effects of the *NAT* are *SCN9A*-specific.

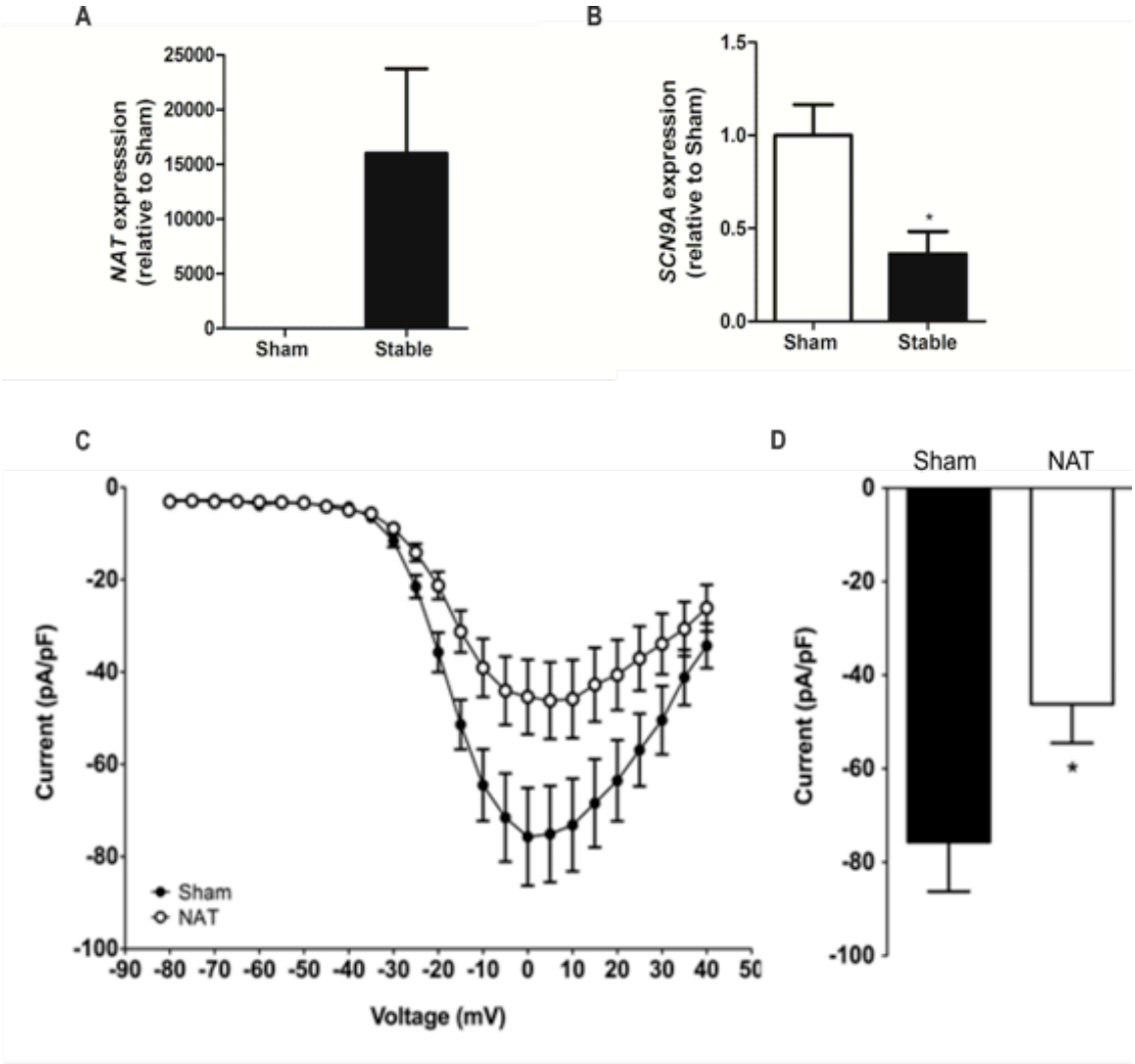

Figure 2-8: Overexpression of the *NAT* reduces $Na_v1.7$-mRNA and currents in SH-SY5Y *NAT* stable cells.

(A) Real-time qPCR showing that the *NAT* is not expressed in naïve SH-SY5Y cells (sham) but is expressed in the stable-*NAT* SH-SY5Y cell line (n=3). **(B)** Real-time qPCR showing that the endogenous *SCN9A* mRNA level is significantly reduced in the stable-*NAT* SH-SY5Y cell line compared to in naïve SH-SY5Y cells (sham) (n=3). (C-D) Whole cell voltage clamp recordings of naïve (sham) and stable-*NAT* SH-SYSY ($Na_v1.7$ *NAT*) cells showed a significant reduction of the peak sodium current **(D),** with voltage current relationships unaltered **(C)** (n=16-21). * indicates $p<0.05$ when compared to control (unpaired t-test). Data shown in mean ± S.E.M Patch clamping by Dr Robert Werdehausen.

A

SCN1A **(NM_001165963)**

Exon 15

SCN1A ex15 TTGGCCATCATCGTCTTCATTTTTGCCGTGGTCGGCATGCAGCTCTTTGGTAAAAGCTAC
NAT TTGGCCATCATCGTCTTCATTTTTGCTGTGGTCGGCATGCAGCTCTTTGGTAAGAGCTAC

SCN1A ex15 AAAGATTGTGTCTGCAAGATCGCCAG-TGATTGTCAACTCCCACGCTGGCACATGAATGA
NAT AAAGAATGTGTCTGCAAGATC-AATGATGACTGTACGCTCCCACGGTGGCACATGAACGA

SCN1A ex15 CTTCTTCCACTCCTTCCTGATTGTGTTCCGCGTGCTGTGTGGGG
NAT CTTCTTCCACTCCTTCCTGATTGTGTTCCGCGTGCTG-GTGGGG

Exon 26:

SCN1A ex26 CTACCCTGTTCCGAGTGATCCGTCTTGCTAGGATTGGCCGAATCCTACGTCTGATCAAAG
NAT CTACCCTGTTCCGAGTGATCCGTCTTGCCAGGATTGGCCGAATCCTACGTCTAGTCAAAG

SCN1A ex26 GAGCAAAGGGGATCCGCACGCTGCTCTTTGCTTTGATGATGTCCCTTCCTGCGTTGTTTA
NAT GAGCAAAGGGGATCCGCACGCTGCTCTTTGCTTTGATGATGTCCCTTCCTGCGTTGTTTA

SCN1A ex26 ACATCGGCCTCCTACTCTTCCTAGTCATGTTCATCTACGCCATCTTTGGGATGTCCAACT
NAT ACATCGGCCTCCTGCTCTTCCTGGTCATGTTCATCTACGCCATCTTTGGAATGTCCAACT

SCN1A ex26 TTGCCT
NAT TTGCCT

SCN2A **(NM_021007)**

Exon 15

SCN2A ex15 CTTGGTATTGGCCATCATCGTCTTCATTTTTGCTGTGGTCGGCATGCAGCTCTTTGGTAA
NAT CTTAGTGTTGGCCATCATCGTCTTCATTTTTGCTGTGGTCGGCATGCAGCTCTTTGGTAA

SCN2A ex15 GAGCTACAAAGAATGTGTCTGCAAGATTTCCAATGATTG-TGAA--CTCCCACGCTGGCA
NAT GAGCTACAAAGAATGTGTCTGCAAGAT--C-AATGATGACTGTACGCTCCCACGGTGGCA

SCN2A ex15 CATGCATGACTTTTTCCACTCCTTCCTGATCGTGTTCCGCGTGCTGTGTGG
NAT CATGAACGACTTCTTCCACTCCTTCCTGATTGTGTTCCGCGTGCTG-GTGG

Exon 26:

SCN2A ex26 CTACCCTGTTCCGAGTGATCCGTCTTGCCAGGATTGGCCGAATCCTACGTCTGATCAAAG
NAT CTACCCTGTTCCGAGTGATCCGTCTTGCCAGGATTGGCCGAATCCTACGTCTAGTCAAAG

SCN2A ex26 GAGCAAAGGGGATCCGCACGCTGCTCTTTGCTTTGATGATGTCCCTTCCTGCGTTGTTTA
NAT GAGCAAAGGGGATCCGCACGCTGCTCTTTGCTTTGATGATGTCCCTTCCTGCGTTGTTTA

SCN2A ex26 ACATCGGCCTCCTTCTTTTCCTGGTCATGTTCATCTACGCCATCTTTGGGATGTCCAATT
NAT ACATCGGCCTCCTGCTCTTCCTGGTCATGTTCATCTACGCCATCTTTGGAATGTCCAACT

SCN2A ex26 TTGCCT
NAT TTGCCT

SCN3A **(NM_006922)**

Exon 15

SCN3A ex15 CTTGGTGTTGGCCATCATCGTCTTCATTTTTGCTGTGGTCGGCATGCAGCTCTTTGGTAA
NAT CTTAGTGTTGGCCATCATCGTCTTCATTTTTGCTGTGGTCGGCATGCAGCTCTTTGGTAA

SCN3A ex15 GAGCTACAAAGAATGTGTCTGCAAGATCAATGATGACTGTACGCTCCCACGGTGGCACAT
NAT GAGCTACAAAGAATGTGTCTGCAAGATCAATGATGACTGTACGCTCCCACGGTGGCACAT

```
SCN3A ex15      GAACGACTTCTTCCACTCCTTCCTGATTGTGTTCCGCGTGCTGTGTGG
                |||||||||||||||||||||||||||||||||||||||||||| ||||
NAT             GAACGACTTCTTCCACTCCTTCCTGATTGTGTTCCGCGTGCTG-GTGG
```

Exon 26:

```
SCN3A ex26      CTACCTTGTTCCGAGTGATCCGTCTTGCCAGGATTGGCCGAATCCTACGTCTGATCAAAG
                ||||| ||||||||||||||||||||||||||||||||||||||||||  ||||||
NAT             CTACCCTGTTCCGAGTGATCCGTCTTGCCAGGATTGGCCGAATCCTACGTCTAGTCAAAG

SCN3A ex26      GAGCAAAGGGGATCCGCACGCTGCTCTTTGCTTTGATGATGTCCCTTCCTGCGTTGTTTA
                ||||||||||||||||||||||||||||||||||||||||||||||||||||||||||||
NAT             GAGCAAAGGGGATCCGCACGCTGCTCTTTGCTTTGATGATGTCCCTTCCTGCGTTGTTTA

SCN3A ex26      ACATCGGCCTCCTGCTCTTCCTGGTCATGTTTATCTATGCCATCTTTGGGATGTCCAACT
                |||||||||||||||||||||||||||||| ||||| |||||||||||| ||||||||||
NAT             ACATCGGCCTCCTGCTCTTCCTGGTCATGTTCATCTACGCCATCTTTGGAATGTCCAACT

SCN3A ex26      TTGCCT
                ||||||
NAT             TTGCCT
```

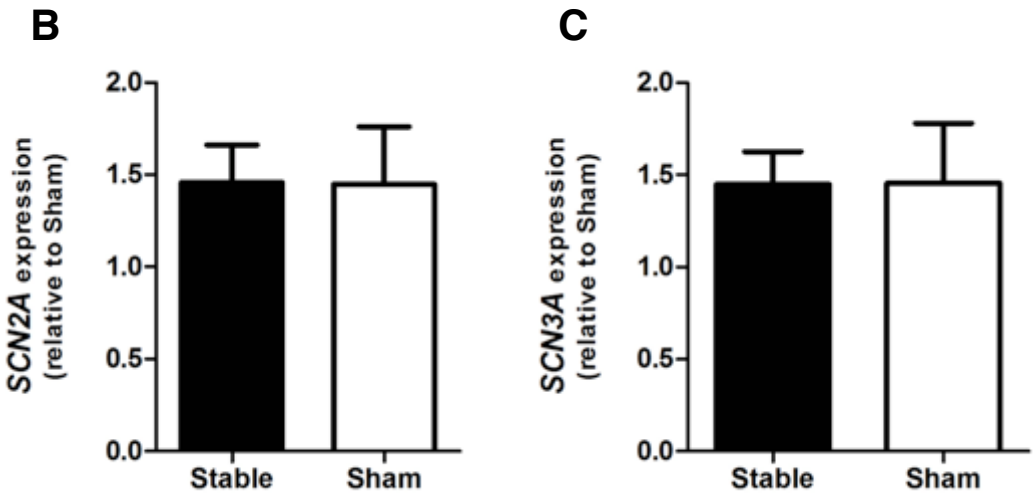

Figure 2-9: Alignment of *SCN1A*, *SCN2A* and *SCN3A* exons with complementary *SCN9A* NAT sequence (NR_110260) and *SCN1A, SCN2A* and *SCN3A* expression in SH-SY5Y *NAT*-stable cells.

(A) *SCN1A*, *SCN2A* and *SCN3A* share conserved sequences with *SCN9A* NAT (NR_110260) in exon 15 and 26 while *SCN4A, SCN5A*, *SCN7A*, *SCN8A*, *SCN10A* and *SCN11A* have no significant similarity to the *SCN9A* NAT. Real-time qPCR showed that *SCN1A* is not expressed in naïve SH-SY5Y cells (sham) or stable-*NA*T SH-SY5Y cell line. **(B)** While *SCN2A* is expressed but not unchanged between SH-SY5Y (sham) and stable-*NAT* SH-SY5Y cell line **(C)** Real-time qPCR showing that the endogenous *SCN3A* mRNA level is unchanged in the stable-*NAT* SH-SY5Y cell line compared to in naïve SH-SY5Y cells (sham) (n=4). Data shown in mean ± S.E.M.

HEK293 hNa$_v$1.7 TAP-tag stable cell line

Members of the voltage-gated sodium channel family share high sequence homology, which makes it generally hard to purify and access the protein expression level of a specific subtype. In order to test for the effect of *NAT* overexpression on the protein levels of Na$_v$1.7, I designed a Na$_v$1.7 tandem affinity purification (TAP)-tagged stable HEK293 cell line that enables me to specifically purify and detect Na$_v$1.7. Here, the TAP-tag construct contains a Tobacco Etch Virus (TEV) cleavage site flanked by two epitope tags, namely FLAG and histidine affinity tag (HAT), which can be detected by commercially available antibodies. The HEK293 cell line stably expresses this epitope-tagged TAP-Na$_v$1.7 under a CMV promoter (See Methods 6.2.3). The advantages of naive HEK293 cell line over a SH-SY5Y cell line are that HEK293 cells do not endogenously express any members of the voltage-gated sodium channel family and CMV promoter, unlike endogenous expression levels in SH-SY5Y, ensures high expression of the channel.

HEK293 hNa$_v$1.7 TAP cells were tested for expression of the hNav1.7-TAP with co-immunostaining with anti-FLAG (green) and DAPI (blue)(see Methods 6.5.1). hNa$_v$1.7-TAP appears to be expressed almost exclusively in the cell membrane (Figure 2-10,A-B). Immunoblotting of naïve HEK293 and HEK293 hNa$_v$1.7-TAP showed that the Na$_v$1.7-TAP is robustly expressed in the stable cell line (Figure 2-10,C). Next, the effect of *NAT* overexpression on Na$_v$1.7 protein levels was investigated. The stable cell line was transiently transfected with the human *NAT* and TAP-tagged Na$_v$1.7 was co-immunoprecipitated with anti-FLAG coupled Dynabeads and immunoblotted using an anti-HAT antibody (see Methods 6.5.1 and 6.5.7) Comparison of *NAT* transfected and sham transfected cells showed the *NAT* resulted in a significant reduction in TAP-tagged Na$_v$1.7 protein levels in two of the western blot sets shown in Figure 2-10, D. However in the third set of western blot data, the housekeeping gene tubulin was not fully transferred onto the membrane, which prevented the quantification of Na$_v$.17 protein levels in this data set (Figure 2-10,D).

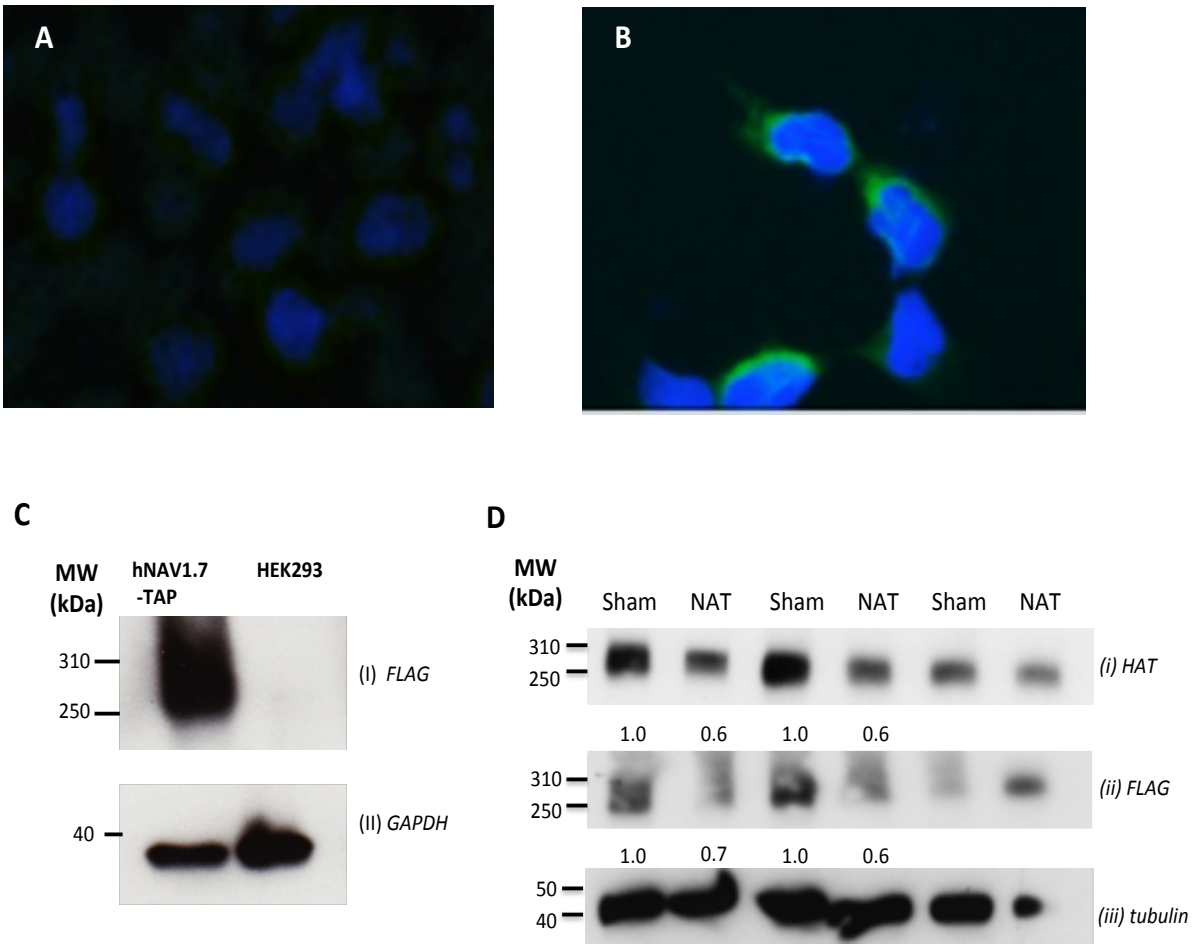

Figure 2-10: Overexpression of the *NAT* reduces $Na_v1.7$ protein levels.

Immunohistochemistry of HEK293 $hNa_v1.7$ TAP-tag stable cell line. Immunostaining of $hNa_v1.7$-TAP (green) in **(A)** naïve HEK293 **(B)** and HEK293 $hNa_v1.7$-TAP stable cells, blue DAPI staining of the nucleus. **(C)** Western blot of HEK293 $hNa_v1.7$-TAP and control HEK293 against anti-FLAG and anti-GAPDH **(D)** Reduction in $Na_v1.7$-TAP tag protein levels due to overexpression of the *NAT* for 48 hrs in a $Na_v1.7$-TAP stable HEK293 cell line. Densitometry readings comparing alpha-tubulin to either HAT or FLAG bands were normalized to the sham controls and shown below each band. Transfection of the *NAT* results in a 30-40% reduction in $Na_v1.7$ protein. (i) $Na_v1.7$-TAP protein detected by immunoblotting using an anti-HAT antibody following pull-down of $Na_v1.7$-TAP with an anti-FLAG antibody (sham corresponds to mock transfected cells). (ii) Immunoblot of crude lysate using an anti-FLAG antibody confirms a reduction in $Na_v1.7$ protein levels following *NAT* transfection. (iii) Immunoblot of crude lysate using an antibody to a housekeeping protein, confirming equal loading. The third western blot data set shown was not quantified due to incomplete tubulin transfer to the membrane.

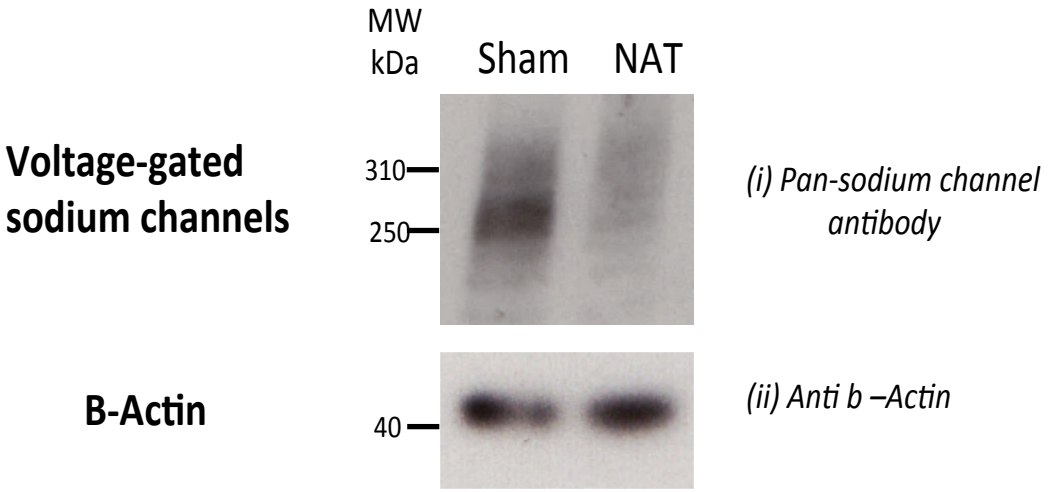

Figure 2-11: Reduction in $Na_v1.7$-TAP tag protein levels due to overexpression of the *NAT* for 48 hrs in a $Na_v1.7$-TAP stable HEK293 cell line.

Upper panel: (i) Immunoblot of crude lysate using an anti-pan sodium channel antibody confirms a reduction in $Na_v1.7$ protein levels following NAT transfection. Lower panel: (ii) Immunoblot of crude lysate using an antibody to the beta actin housekeeping protein, confirming equal loading.

Next, I verified these results on immunoblotting $Na_v1.7$-TAP stable HEK293 and $Na_v1.7$-TAP-*NAT* transfected cells with a pan-sodium channel antibody that recognizes all voltage-gated sodium channel subtypes (see Methods 6.5.4). HEK293 cells show no endogenous expression of voltage-gated sodium channels. Here, the stable cell line shows clear expression of the TAP-tagged $Na_v1.7$. However, overexpression of h*NAT* shows reduced expression of the channel (Figure 2-11). These results confirm previous findings and suggest that the *NAT* reduces the protein levels of $Na_v1.7$.

Scn9a and *NAT* expression in inflammatory and neuropathic pain models

Electrophysiological recordings and RT-PCR analyses performed on stable cell lines (HEK293 $Na_v1.7$, SH-SY5Y) strongly suggest an impact of *SCN9A* natural antisense transcript on its corresponding sense transcript. These results indicate that the *SCN9A* antisense transcript is modulating $Na_v1.7$ sodium currents, leading to a decrease of sodium influx into the cells as a result of decreased mRNA and protein expression. A possible reason for this change in $Na_v1.7$ mRNA, protein and sodium current could be that the antisense transcript down-regulates the expression of $Na_v1.7$ by binding to *SCN9A* mRNA and causing it to be degraded, thus leading to a decreased amount of $Na_v1.7$ in the membrane. Next, I tested whether the *NAT* plays a role in different pain states.

Animal models of inflammatory pain and neuropathic pain

Two different inflammatory pain models (carrageenan and complete Freund's adjuvant (CFA) as well as two neuropathic pain models (chronic constriction injury and sciatic nerve transection) were examined. Injection of carrageenan into the hindpaw induces an acute and highly reproducible inflammatory response resulting in edema, hyperalgesia and erythema that can persist for 6 days. Likewise, injection of CFA results in acute thermal and mechanical hyperalgesia that can persist for more than 2 weeks. In the chronic constriction injury model, sutures are tied around the sciatic nerve, which leads to thermal and mechanical hyperalgesia presenting within the first week and persisting for several weeks. In the sciatic nerve transection model (SNT) the sciatic nerve is completely transected (Minett, Quick et al. 2011) (See Methods 6.4.1 and 6.4.2). I ran a qPCR to test whether the relative expression of *NAT* and *Scn9a* in DRG changes during inflammatory and neuropathic pain states (see Methods 6.1.3.2). I found no significant change in relative expression of these two genes in DRG at different time points (2 and 24 hrs) after Carrageenan or CFA injection (Figure 2-12). I also found no change of expression in *NAT* or *Scn9a* in CCI (2 and 3 weeks) and SNT (2 weeks) at different time points (Figure 2-13).

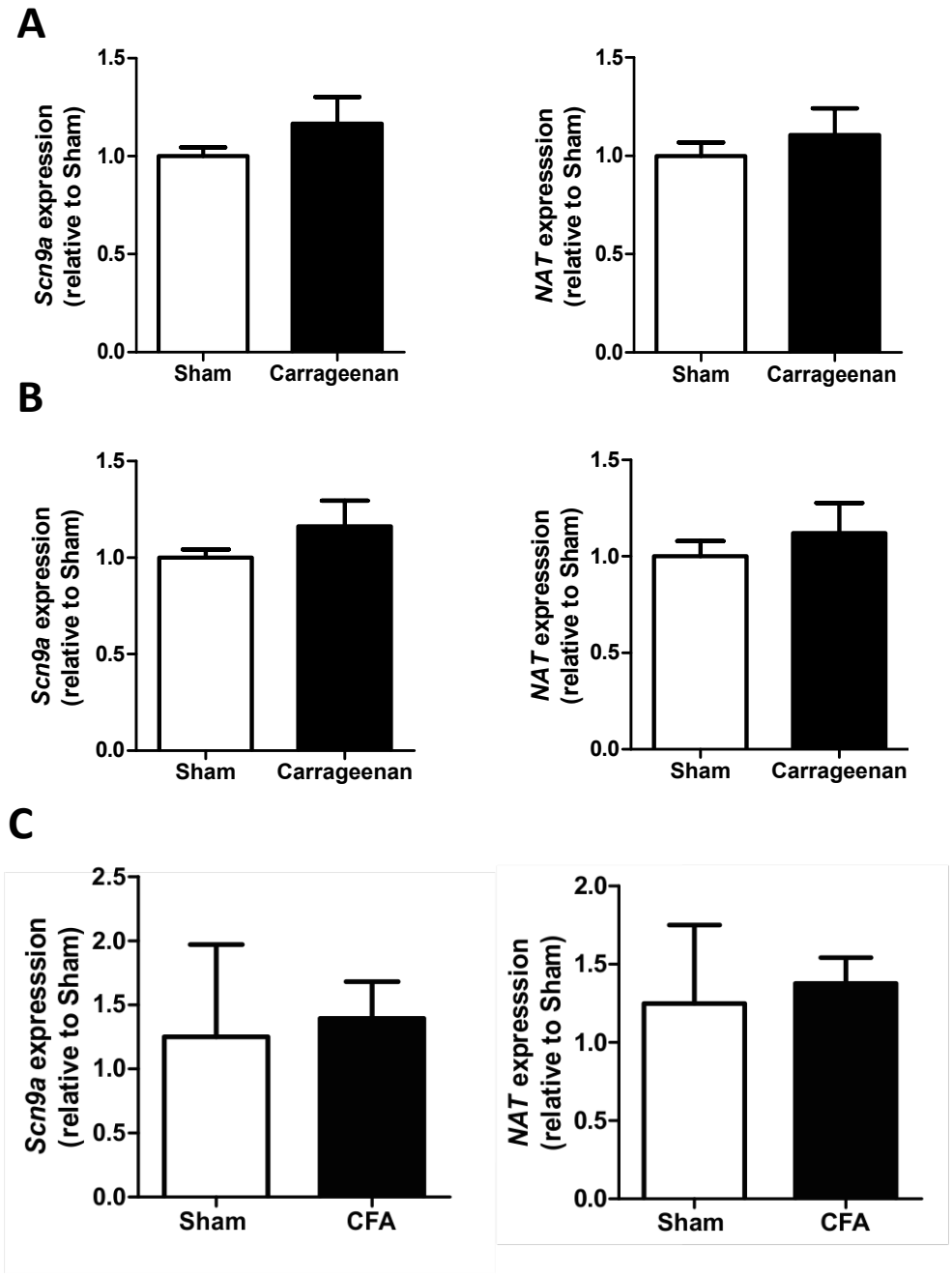

Figure 2-12: *Scn9a* and antisense expression in Saline (Sham), Carrageenan and CFA injected mice.

L2-L5 DRG ipsilateral, and spinal cord lumbar were isolated from BL6 mice injected with saline or Carrageenan **(A)** 2hrs **(B)** 24 hrs. and **(C)** CFA 3 days after injection. mRNA expression was measured by qPCR, Eppendorf realplex, Cybergreen; Relative expression normalized to *GAPDH* and shown relative to saline. Data shown in mean ± S.E.M.

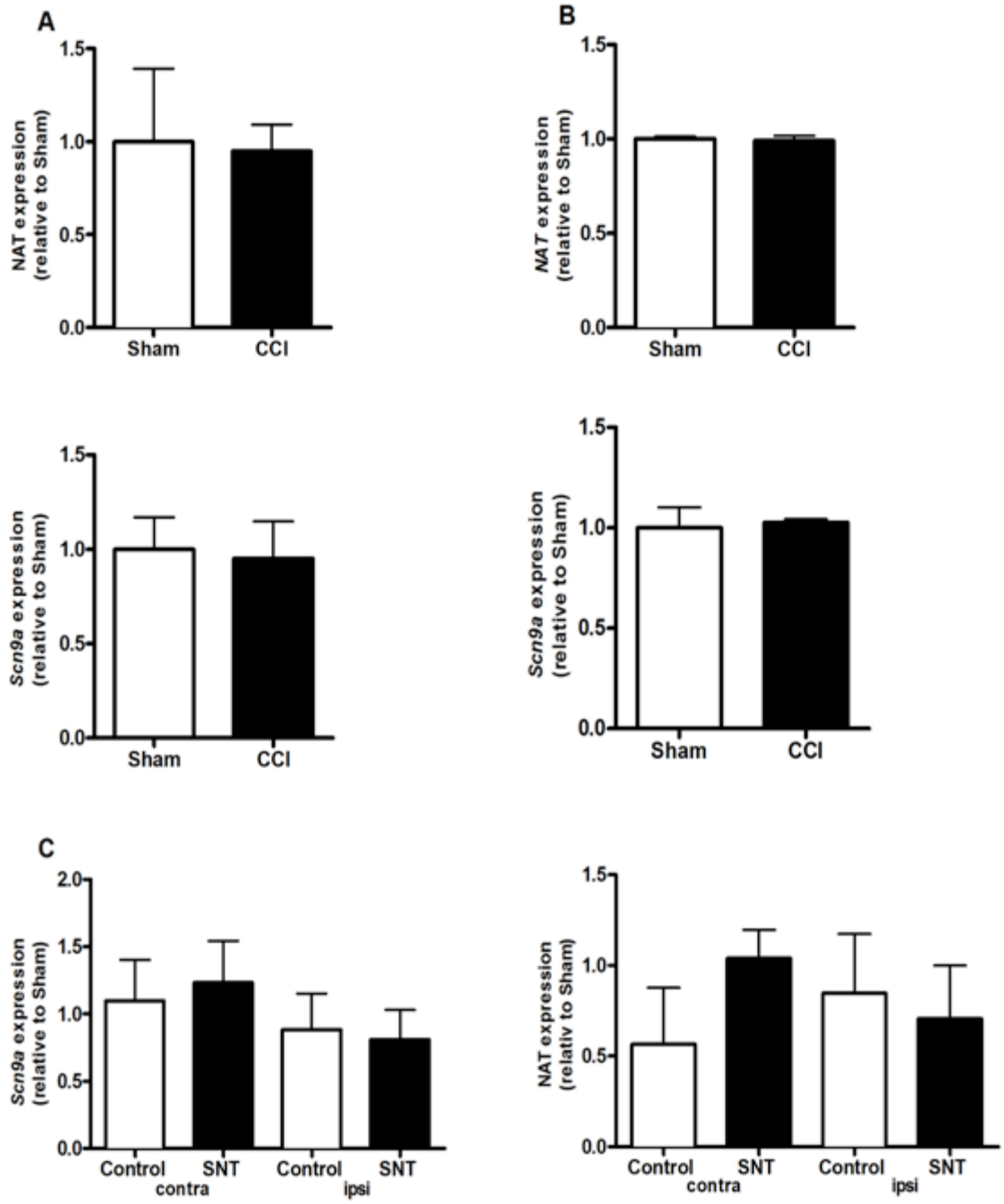

Figure 2-13: *Scn9a* sense and antisense expression after neuropathic surgery (CCI and SNL).

Scn9a and antisense expression levels were assessed by qPCR **(A)** CCI after 2 weeks and **(B)** 3 weeks after surgery. DRGs L4-L6 were taken out ipsilateral of operated mice (N=5) and non-operated mice (Black 6, n=5). **(C)** SNL DRGs L5-L6 ipsilateral were taken out and RNA isolated. Expression changes were measured via qPCR. There was no significant change in expression levels of sense or antisense transcript in any of the tested neuropathic pain models. Data shown in mean ± S.E.M.

2.4 Discussion

I have identified, cloned and characterized a human and mouse natural antisense transcript for the *SCN9A* gene. Both human and mouse *NAT*s are organised in a tail-to-tail configuration with the sense gene and both show evidence of alternative splicing, which is consistent with other reported NATs (Morris and Mattick 2014). Although the mouse *Scn9a NAT* has fewer exons than the human *NAT*, both share conserved sequences with the final sense *SCN9A*/*Scn9a* exon. Given this conserved gene structure and the corresponding tissue expression profile of the sense and *NAT* genes, it can be hypothesized that the *NAT* may somehow regulate the function of *SCN9A*. To this end, I overexpressed the *NAT* in cell lines, which endogenously expressed $Na_v1.7$, and also in cells which stably expressed from a CMV promoter either $Na_v1.7$ or epitope-tagged $Na_v1.7$. Real-time qPCR, immunoblotting and electrophysiological assays showed a significant reduction in $Na_v1.7$ mRNA, protein levels and currents.

How do *NAT*s regulate the function of their sense gene counterparts? Characterization of other NATs have ascribed several diverse cellular functions including transcriptional collision, RNA interference, regulation of alternative splicing, RNA editing, epigenetic regulation, RNA masking, translation inhibition and mRNA destabilisation (Lapidot and Pilpel 2006). In this experimental set-up I overexpressed the processed *NAT* RNA from a CMV promoter in cell lines. This led to a reduction in sense mRNA and consequently a reduction in functional $Na_v1.7$ protein. It could be speculated therefore that perhaps the *NAT* functions by downregulating *SCN9A* transcription, perhaps by guiding chromatin-modifying enzymes to the *SCN9A* promoter region. Alternatively, overexpression of the *NAT* could be leading to the generation of endogenous short RNAs (endo-siRNAs) thus leading to promotion of the RNA interference pathway. A third mechanism could be that the *NAT*: sense mRNA duplexes are promoting destabilisation and degradation of the sense mRNA and/or inhibiting translation. A greater insight into the function of the *NAT in vivo* could be gleaned from the creation of a *NAT* knockout mouse. In a comparable

experiment, Komine *et al.* (2006) generated a *Zfhx2-AS* knockout mouse through deletion of the transcriptional start site region for the *NAT* (Komine, Nakamura et al. 2006). Normally, the *Zfhx2* expression pattern in the developing brain is complementary to the expression of the *NAT*. However in the *Zfhx2-AS* knockout mouse, the expression of the Zfhx2 homeobox-containing transcription factor becomes dysregulated. It would be interesting to determine whether the expression pattern of *Scn9a* is altered in a *Scn9a NAT* knockout mouse.

Detailed analyses of *Scn9a* knockout mice have shown that acute, inflammatory and some forms of neuropathic pain require the expression of $Na_v1.7$ (Nassar, Stirling et al. 2004, Minett, Nassar et al. 2012, Minett, Falk et al. 2014). I hypothesized that the *NAT* may be downregulated in pain states, hence leading to upregulation of *SCN9A*. To test this, I assessed mRNA levels of the sense and *NAT* genes in CFA and carrageenan-induced models of inflammatory pain and in the chronic constriction injury neuropathic pain model. This showed that the mRNA level of neither the sense nor the *NAT* gene was significantly altered. The lack of change in the sense gene mRNA was a surprising finding given that, for example, $Na_v1.7$ protein levels have previously been shown to increase following carrageenan injections (Black, Liu et al. 2004). Further work using the epitope-tagged $Na_v1.7$ knock-in mice and anti-FLAG/HAT antibodies should help to confirm whether protein levels change in different pain models. Furthermore, intrathecal viral *NAT* overexpression experiments could help to determine whether the *NAT* is able to confer analgesia and reduce the pain experienced in different inflammatory and neuropathic pain states.

In summary, this DRG-expressed natural antisense transcript has the potential to regulate pain thresholds via transcriptional and post-transcriptional regulation of *SCN9A*. Given that the presence of the *NAT* reduces $Na_v1.7$ currents, then intuitively the lack of the NAT may increase sodium currents. This could lead to increased excitability of damage-sensing neurons, enabling a fine-control of responses to painful stimuli. It will be interesting to determine whether loss of

function mutations in the *NAT* are responsible for inherited painful disorders that map to human chromosome 2, and whether SNPs within the *NAT* alter pain thresholds in the general population.

[See Appendix A for related PlosOne article]

3 TAP-tagged sodium channel $Na_v1.7$

3.1 Summary

Voltage-gated sodium channels (VGSCs) are large integral membrane proteins that are composed of a pore-forming alpha subunit ($Na_v1.1$-$Na_v1.9$ and Na_x) and auxiliary beta subunits. The voltage-gated sodium channel $Na_v1.7$ is important in the initiation and propagation of action potentials in excitable cells and spontaneous and inherited mutations in $Na_v1.7$ are linked to human pain disorders. Here, I investigate the expression profile and protein-protein interaction network of $Na_v1.7$ through an in-depth analysis of a newly generated TAP-tagged $Na_v1.7$ knock-in mouse. The tandem affinity purification (TAP) tag, consisting of a 3XFLAG, a Tobacco Etch Virus (TEV) protease cleavage site and a histidine affinity tag (HAT), was fused to the C-terminus of *Scn9a* ($Na_v1.7$). I found no altered behavior or abnormal expression of $Na_v1.7$ protein *in vitro* and *in vivo* due to the expression of the TAP-tag. Furthermore the TAP method allowed me to isolate TAP-tagged $Na_v1.7$ under native conditions in three independent single-step purifications and coupled with Liquid chromatography–mass spectrometry (MS/LC-MS), it revealed a list of proteins in complex with $Na_v1.7$.

3.2 Introduction

Voltage-gated sodium channels $Na_v1.7$, $Na_v1.8$ and $Na_v1.9$ (VGSC) are primarily found in peripheral sensory neurons and are important in the initiation ($Na_v1.7$) (Klugbauer, Lacinova et al. 1995), upstroke ($Na_v1.8$) of action potentials (Renganathan, Cummins et al. 2001) and setting of the resting membrane potential ($Na_v1.9$) of electrically excitable cells (Dib-Hajj, Black et al. 2002). However neuronal transmission rests not only upon the expression of voltage-gated sodium channels but also on their correct transport and anchoring in the cell membrane of highly specialized domains such as the axon initial segment (AIS) and nodes of Ranvier. Assemblies of multi-molecular complexes are required to transport, anchor and enrich VGSCs in these highly specialized axonal segments (Salzer 2003, Leterrier, Brachet et al. 2010, Leterrier, Brachet et al. 2011). It is estimated that greater than eighty per cent of all proteins are

part of multi-protein complexes (Berggard, Linse et al. 2007) which are composed of adhesion, cytoskeletal adaptor, transport proteins and many more (Okuse, Malik-Hall et al. 2002, Leterrier, Brachet et al. 2010). However, very little is known about voltage-gated sodium channel multi-protein complex composition and the individual role of molecules in regulation and trafficking of voltage-gated sodium channels to the plasma membrane. What is known is that VGSC beta-subunits are involved in these processes and expression of a certain β-subunit with a Na_v alpha subunit can promote trafficking and glycosylation (Laedermann, Syam et al. 2013). Other proteins that are implicated in the regulation and trafficking of voltage-gated sodium channels are Nedd4/Nedd4-like proteins (Cachemaille, Laedermann et al. 2012, Laedermann, Decosterd et al. 2014) ankyrins (Hedstrom and Rasband 2006), papin (Shao, Baker et al. 2009), ERM proteins (Malik-Hall, Poon et al. 2003), p11 (Okuse, Malik-Hall et al. 2002), syntrophin (Schultz, Hoffmuller et al. 1998) and CRMP2 (Dustrude, Wilson et al. 2013). Interestingly, CRMP2 indirectly regulates $Na_v1.7$ trafficking through post-translational SUMOtylation of CRMP2. Dustrude *et al*. (2013) found that CRMP2 SUMOtylation recruits isoform specific voltage-gated sodium channel binding proteins that promote the trafficking of $Na_v1.7$ to the plasma membrane and provides a novel mechanism for the modulation of $Na_v1.7$ trafficking (Dustrude et al. 2013).

In recent years the field of proteomics has rapidly advanced through the development of high-throughput methods like tandem affinity purification that allow large-scale protein-interaction studies. Initially TAP was developed for the use in Yeast proteomics (Rigaut, Shevchenko et al. 1999, Gavin, Bosche et al. 2002) and has since been successfully adapted to other organisms including mammals (Angrand, Segura et al. 2006, Fernandez, Collins et al. 2009). Targeted tandem affinity purification combined with mass spectrometry (TAP-MS) is a tool for mapping the organization of multi-protein complexes under native conditions (Berggard, Arrigoni et al. 2006, Fernandez, Collins et al. 2009). One of the advantages of the TAP assay is that small peptide affinity tags do not alter function or impact the three-dimensional folding of the protein

and therefore do not need to be removed. The purification method itself is simple yet applicable to a wide range of proteins and enables identification of all direct and indirect interaction partners in a single experiment. Furthermore, the tandem affinity purification method requires no further consideration of abundance, composition or function of the isolated protein complex and only depends upon high reproducibility and accurate protein purification (Rigaut, Shevchenko et al. 1999, Puig, Caspary et al. 2001). Variations of the TAP-tag are used but the basic TAP construct consists of a TEV protease cleavage site that is flanked by affinity tags.

Since there isn't a good commercially available anti-$Na_V1.7$ antibody for use in pull-down assays I instead used the TAP-MS method to characterize protein complexes from $Na_v1.7$ TAP-tagged knock-in mice to allow me to isolate $Na_v1.7$ interaction partners in their physiological environment. I found no evidence that TAP-tag insertion into $Na_v1.7$ results in an abnormal phenotype. mRNA and protein expression levels and electrophysiological properties of the channel were comparable to wildtype. Mass spectrometry analysis identified 42 proteins in complex with $Na_v1.7^{TAP/TAP}$ from DRG and olfactory bulb, some of which (Tmed10, Aqp-1, Scn3b and mTor) have already been implicated in cellular trafficking, pain processing or shown to associate with other VGSCs.

3.3 Results

Generation and testing of TAP-tagged $Na_v1.7$ mouse line

To investigate the protein-protein interaction and distribution of $Na_v1.7$, Jing Zhao (Molecular Nociception group) generated a TAP-tagged $Na_v1.7$ mouse line. Here, a tandem affinity purification (TAP)-tagged $Na_v1.7$ targeting vector, which contains a HAT domain, 3x FLAG tags and a neomycin selection cassette (neoR) was inserted before the stop codon of exon 28 in the $Na_v1.7$ wild-type (WT) allele using *Escherichia coli* recombineering-based methods (Lee, Yu et al. 2001). Figure 3-1a demonstrates the structure of the $Na_V1.7$ wild-type (WT) allele, the TAP-tagged $Na_V1.7$ targeting construct and the TAP-tagged $Na_V1.7$ targeted allele with and without the neomycin selection cassette (neoR).

The final targeting construct containing a 5'-end homology arm of 3.4 kb and a 3'-end homology arm of 5.8 kb, was transfected into 129/Sv embryonic stem cells (ES) (Figure 3-1a). After electroporation of the construct into embryonic stem cells, 346 colonies that survived selection with G418 were screened with 3' external probe using Southern blotting, and 12 correctly targeted colonies were confirmed with correct integration using 5' external probe (targeting efficiency was 3.5%). Three positive ES cell lines were used to generate chimeras through microinjection of the cells into blastocysts. Electroporation and blastocysts microinjection of ES cells was performed by Dr Massimo Signore in JP Martinez-Barbera's research group (UCL). Four chimeras were obtained and crossed with C57BL/6 mice. Germ line transmission from the chimeras was confirmed with 3' external and 5' external probes using Southern blotting (Figure 3-1,b). Furthermore F1 animals were crossed with global Cre mice to remove the neomycin (neoR) cassette. Southern blot analysis of genomic DNA from TAP-tagged $Na_v1.7$ mice after removal of the neo cassette compared to wildtype is presented in Figure 3-1c. Both Southern blotting (Figure 3-1,c) and PCR (Figure 3-3,a) results indicate that the TAP-tag was integrated as a whole, without deletions, into the intended location. This line of mice is referred to herein as $Na_v1.7^{TAP}$.

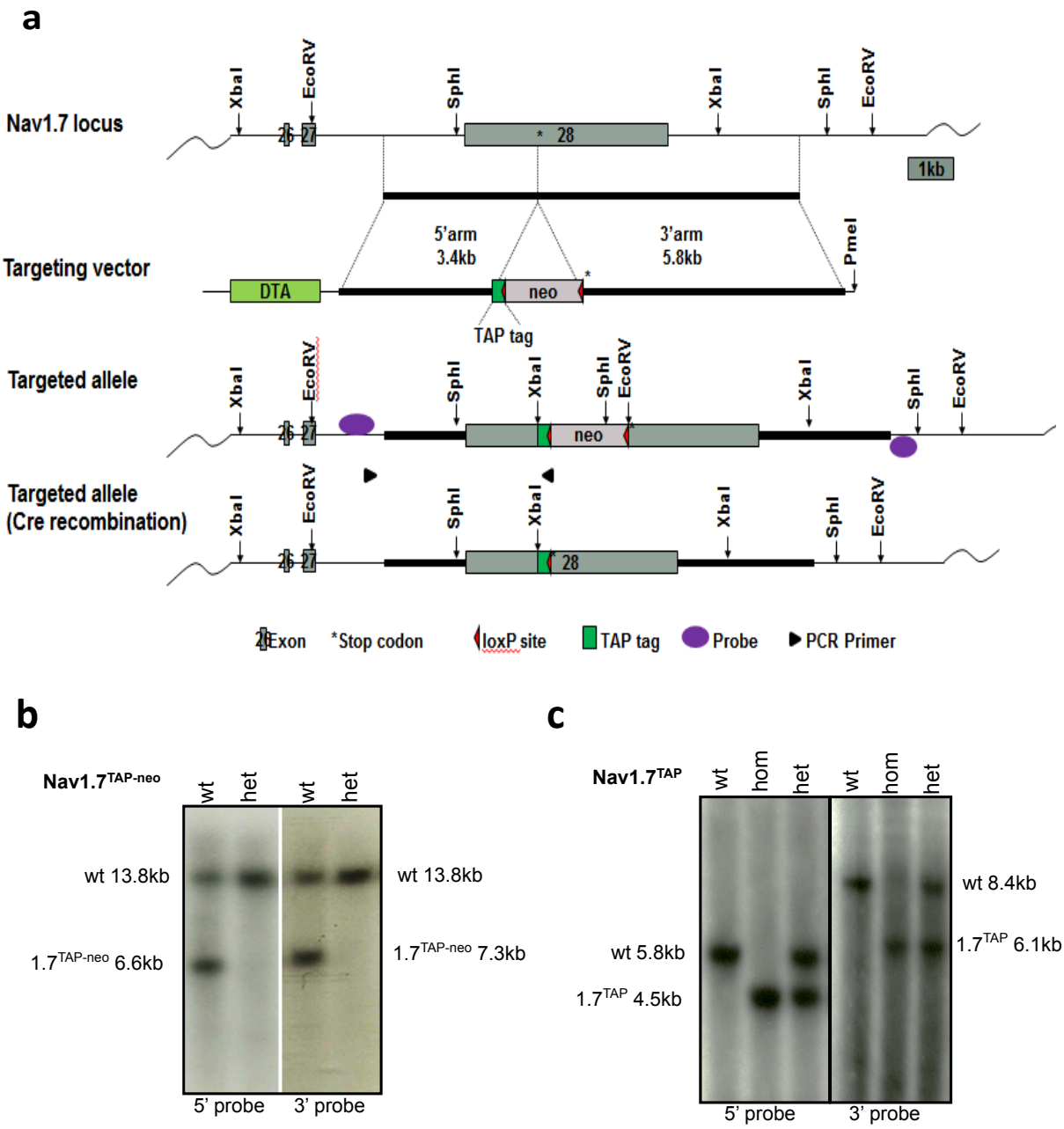

Figure 3-1: Generation of $Na_v1.7$ TAP-tagged mouse line.

(a) The TAP-tagged $Na_V1.7$ targeting construct was inserted into the open reading frame in the 3'-end before the stop codon of exon 28 of $Na_v1.7$ using *Escherichia coli* recombineering-based methods. The figure shows the structure of the $Na_V1.7$ wild-type (WT) allele, the TAP-tagged $Na_V1.7$ targeting construct and the TAP-tagged $Na_V1.7$ targeted allele with and without the neomycin selection cassette (neoR). **(b)** Germ line transmission from the chimeras was confirmed with 3' external and 5' external probes using Southern blotting **(c)** Southern blot analysis of genomic DNA from homozygote (homo) and heterozygote (het) TAP-tagged $Na_v1.7$ mice compared to wildtype after the removal of neo cassette (performed by Jing Zhao).

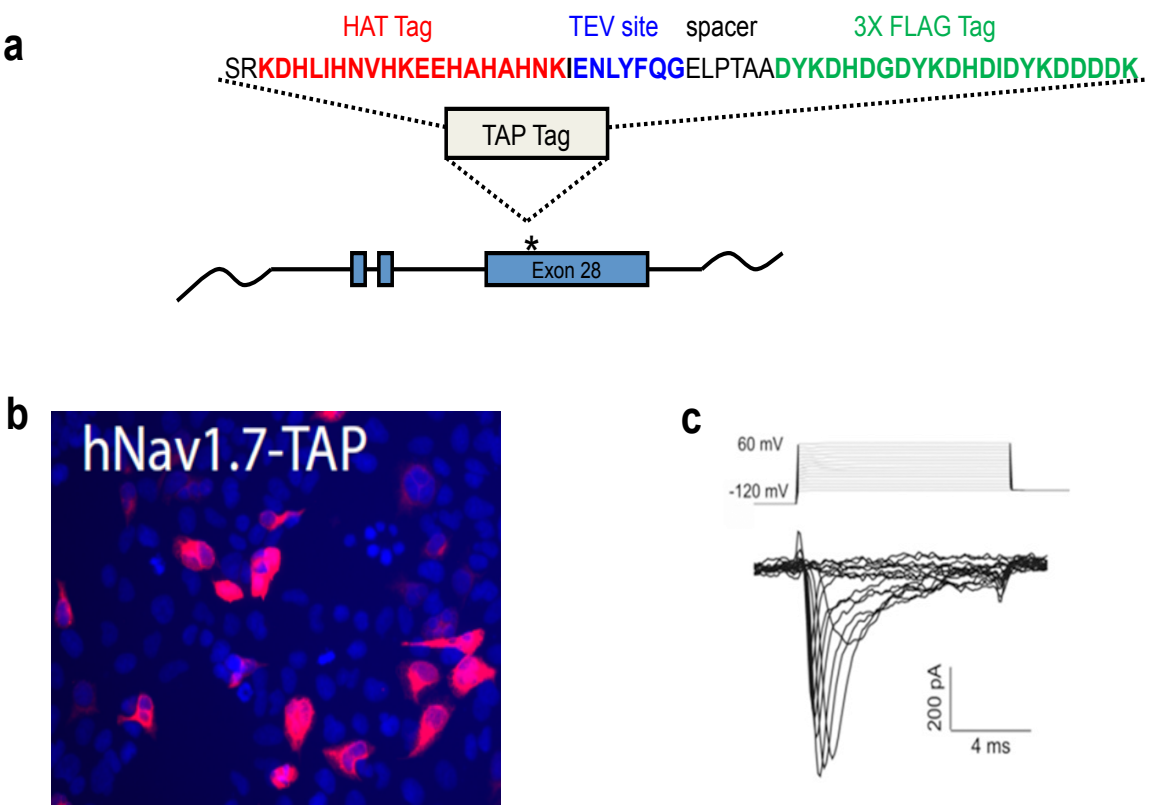

Figure 3-2: Transient transfection of HEK293 cells with $Na_v1.7$ TAP-tag

(a) $Na_v1.7$ TAP-tag consisting of a 3XFLAG, a TEV protease cleavage site and a HAT domain. The construct was inserted at the C-terminus, just prior to the stop codon in *SCN9A* **(b)** Immunohistochemistry of HEK293 cells that were transiently transfected with $Na_v1.7$ TAP-tag and detected with an anti-FLAG antibody (red) (blue: DAPI) **(c)** and functional integrity of the sodium channel via electrophysiology analysis.

Expression of human $Na_v1.7$ TAP-tag in HEK293 cells

To test the channel function of this TAP-tagged $Na_v1.7$ *in vitro*, HEK293 cells were transiently transfected with the TAP-tagged $Na_v1.7$ construct (Figure 3-2,a) (3XFLAG tag, a TEV protease cleavage site and a HAT-domain) and immunostained 24 hours after transfection (Figure 3-2,b) (see Methods 6.2.2 and 6.5.1). $Na_v1.7$ appears to be primarily expressed in the plasma membrane of transfected HEK293 cells (red) and electrophysiological recordings confirmed

the functionality of the channel (Figure 3-2,c). To verify the protein expression of $Na_v1.7$ and test for the specificity of commercially available FLAG and HAT antibodies, TAP-tagged $Na_v1.7$ was immunoprecipitated from HEK293 cells and immunoblotted with anti-HAT antibody (see Methods 6.5.3 and 6.5.7). Western blot of $Na_v1.7$ confirmed the expression of $Na_v1.7$ TAP-tagged protein and the specificity of the antibodies (Figure 3-3,b-c)

$Na_v1.7^{TAP/TAP}$ tag knock-in mouse

Next, I examined a newly developed $Na_v1.7^{TAP/TAP}$ tag knock-in mouse. First $Na_v1.7^{TAP/+}$ heterozygous mice were intercrossed and I found no abnormalities of transmission frequency in the offspring of $Na_v1.7^{TAP/+}$ intercrosses (not shown). I then went on to PCR genotype $Na_v1.7^{TAP}$ tag knock-in mice by extracting genomic DNA from littermates (control), $Na_v1.7^{TAP/+}$ (heterozygous) and $Na_v1.7^{TAP/TAP}$ (homozygous) (see Methods 6.1.2). The samples were PCR genotyped using a common forward and reverse primer in $Na_v1.7$ (see Methods 6.1.2) that amplify the wildtype ($Na_v1.7^{+/+}$, 170bp, lower band) and targeted allele ($Na_v1.7^{TAP/TAP}$, 411 bp, top band) (Figure 3-3,a). Next, I looked at the expression of $Na_v1.7^{TAP/TAP}$ (homozygous*) in vivo* to confirm protein expression as well as localization of the TAP-tagged protein. DRG from $Na_v1.7^{TAP/TAP}$ and littermate controls were collected, immunoprecipitated in CHAPS buffer and immunoblotted with anti-HAT and anti-FLAG (see Methods 6.5.4 and 6.5.7). The band size was comparable to $hNa_v1.7$-TAP transfected HEK293 immunoblots against these two antibodies (Figure 3-3,b-c), confirming that TAP-tagged protein is expressed.

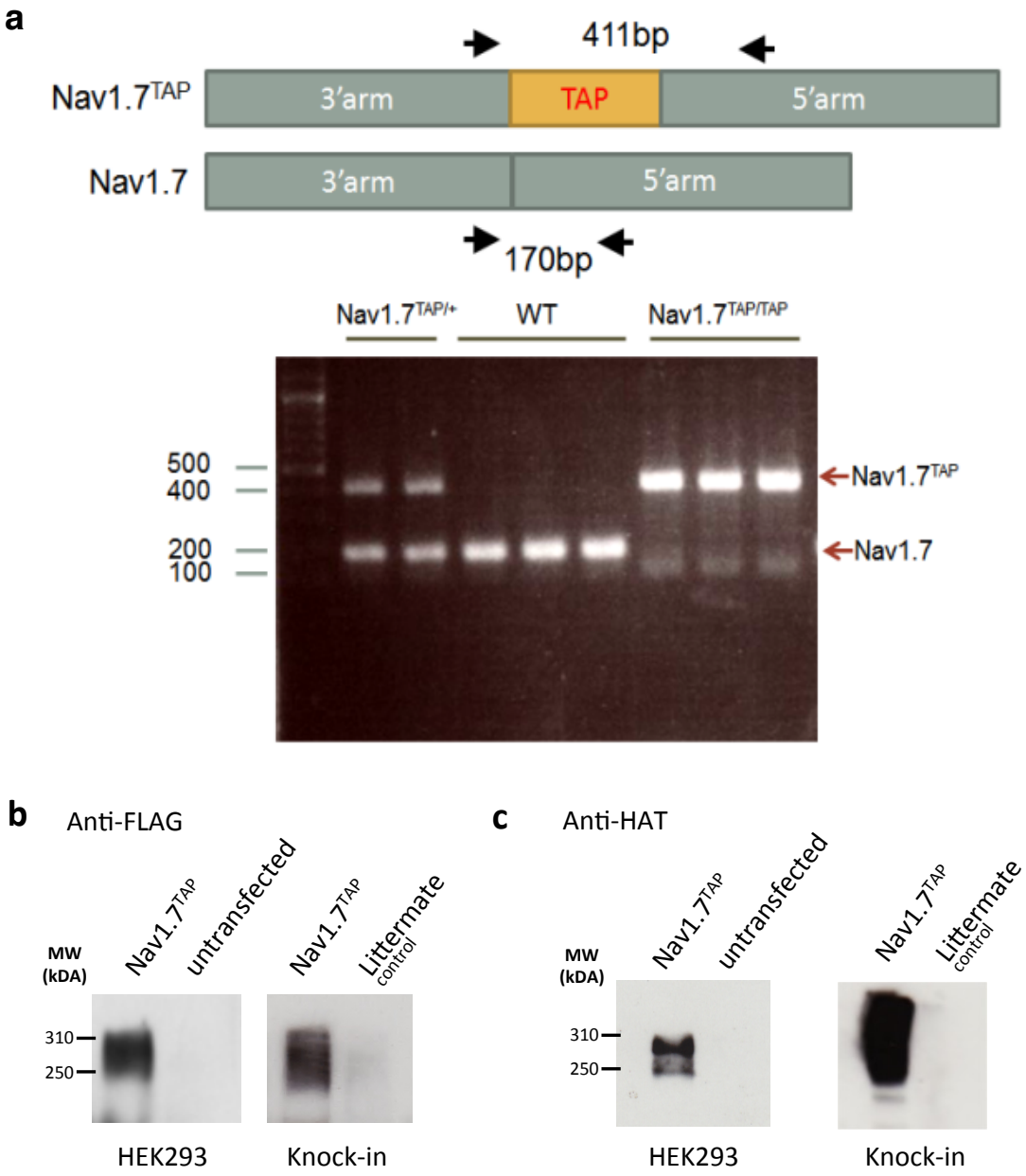

Figure 3-3: $Na_v1.7^{TAP/TAP}$ genotyping and protein expression

(a) PCR genotyping of $Na_v1.7$ TAP-tagged mice using a common forward and reverse primer in $Na_v1.7$ (top) that amplify the wild type (170 bp, lower band) and targeted allele (411 bp, top band) from gDNA**. (b)** Western blot detection of $Na_v1.7$ TAP-tag with anti-FLAG antibody on crude lysate shows that $Na_v1.7$ is expressed and antibodies can detect $Na_v1.7^{TAP/TAP}$ tagged protein in both transgenic mice and transiently transfected HEK293 cells **(c)** Western blot detection of $Na_v1.7$ TAP-tag with anti-HAT antibody on crude lysate shows that $Na_v1.7$ is expressed and antibodies can detect $Na_v1.7^{TAP/TAP}$ tagged in both transgenic mice and transiently transfected HEK cells.

$Na_v1.7^{TAP/TAP}$ is highly expressed in DRG, olfactory bulb and hypothalamus/thalamus

In mammals, ten channel isoforms ($Na_v1.1$-1.9 and Na_x) are known that share a greater than 50 per cent sequence homology (Catterall 2000, Goldin et al. 2005). However this makes it challenging to only examine the distribution of one specific isoform. Antibodies currently in use to detect $Na_v1.7$ are often not specific and therefore detect other sodium channels as well. Here, a C-terminal insertion of TAP-tag epitope into exon 28 of $Na_v1.7$, allows me to purify only $Na_v1.7$ and enables me to investigate its cellular and subcellular distribution. I have shown that transient transfection of $hNa_v1.7$ TAP-tag vector into HEK293 cells does not alter the function and expression of the sodium channel (Figure 3-1,b-c).

In rodents and humans, $Na_v1.7$ is primarily expressed in DRG neurons and the olfactory bulb (Toledo-Aral, Moss et al. 1997, Weiss, Pyrski et al. 2011). Therefore protein lysates from DRG neurons of TAP-tagged $Na_v1.7$ knock-in mice were immunoprecipitated with anti-FLAG and blotted with an anti-HAT antibody. Western blot confirmed the expression of $Na_v1.7^{TAP/TAP}$ tag *in vivo* (Figure 3-3,b-c). Next, I compared the levels of expression of TAP-tagged $Na_v1.7$ from DRG neurons in homozygote ($Na_v1.7^{TAP/TAP}$) and heterozygote ($Na_v1.7^{TAP/+}$) mice and found that the band height is similar but intensity varies (Figure 3-4,a). To investigate the tissue specific distribution of $Na_v1.7$, 14 different tissues from a $Na_v1.7^{TAP/TAP}$ mouse were collected and protein lysates prepared then co-immunoprecipitated with anti-FLAG and immunoblotted with anti-HAT antibody (see Methods 6.5.5 and 6.5.7). I found that $Na_v1.7$ is highly expressed in DRG neurons and the hypothalamus/thalamus but the highest expression was detected in the olfactory bulb (Figure 3-4,b). Besides these three tissues, $Na_v1.7$ expression was also detected in spinal cord, sciatic nerve and testis but was absent in tissues such as lung, liver, spleen, eye, kidney, brain* and cerebellum. Next, the expression of $Na_v1.7$ in the pancreas was examined. Zhang *et al.* (2014) reported that $Na_v1.7$ is expressed in pancreatic islets where it is suspected to trigger glucose-stimulated insulin secretion (Zhang, Chibalina et al. 2014). However under two experimental conditions,

$Na_v1.7$ protein in mouse pancreas tissue was not detected (Figure 3-4, c). As shown in Figure 3-5, Jing Zhao performed immunohistochemistry against TAP-tagged $Na_v1.7$ with anti-FLAG antibody (green) in spinal cord, olfactory bulb and DRG sections (see Methods 6.5.2), which showed that $Na_v1.7^{TAP/TAP}$ was expressed only in the knock-in mice and not in the control ($Na_v1.7^{+/+}$) mice.

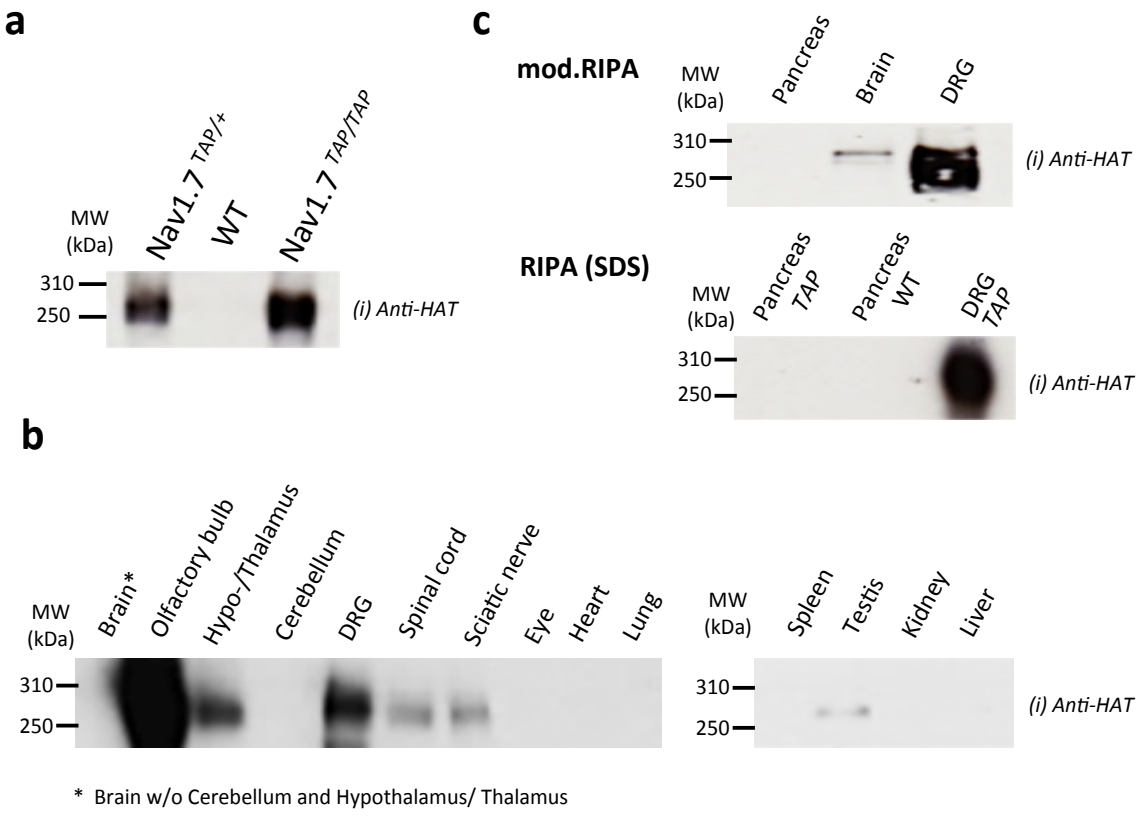

Figure 3-4: $Na_v1.7^{TAP/TAP}$ is highly expressed in olfactory bulb, DRG and hypothalamus/thalamus.

(a) Co-immunoprecipitation of $Na_v1.7^{TAP/TAP}$, $Na_v1.7^{TAP/+}$ and control (wildtype) from DRG neurons with anti-FLAG antibody covalently coupled to Dynabeads and immunoblotted with anti-HAT antibody **(b)** $Na_v1.7^{TAP/TAP}$ tissue panel. $Na_v1.7$ TAP-tagged protein is highly expressed in olfactory bulb, DRG and hypothalamus/thalamus, with expression also detected in spinal cord, testis and sciatic nerve **(c)** Co-immunoprecipitation of $Na_v1.7^{TAP/TAP}$ in pancreas, DRG, brain and wildtype pancreas in modified Ripa (w/o SDS) and Ripa buffer (SDS). $Na_v1.7^{TAP/TAP}$, and control (wildtype) were co-immunoprecipitated with anti-FLAG antibody covalently coupled to Dynabeads and immunoblotted with anti-HAT antibody.

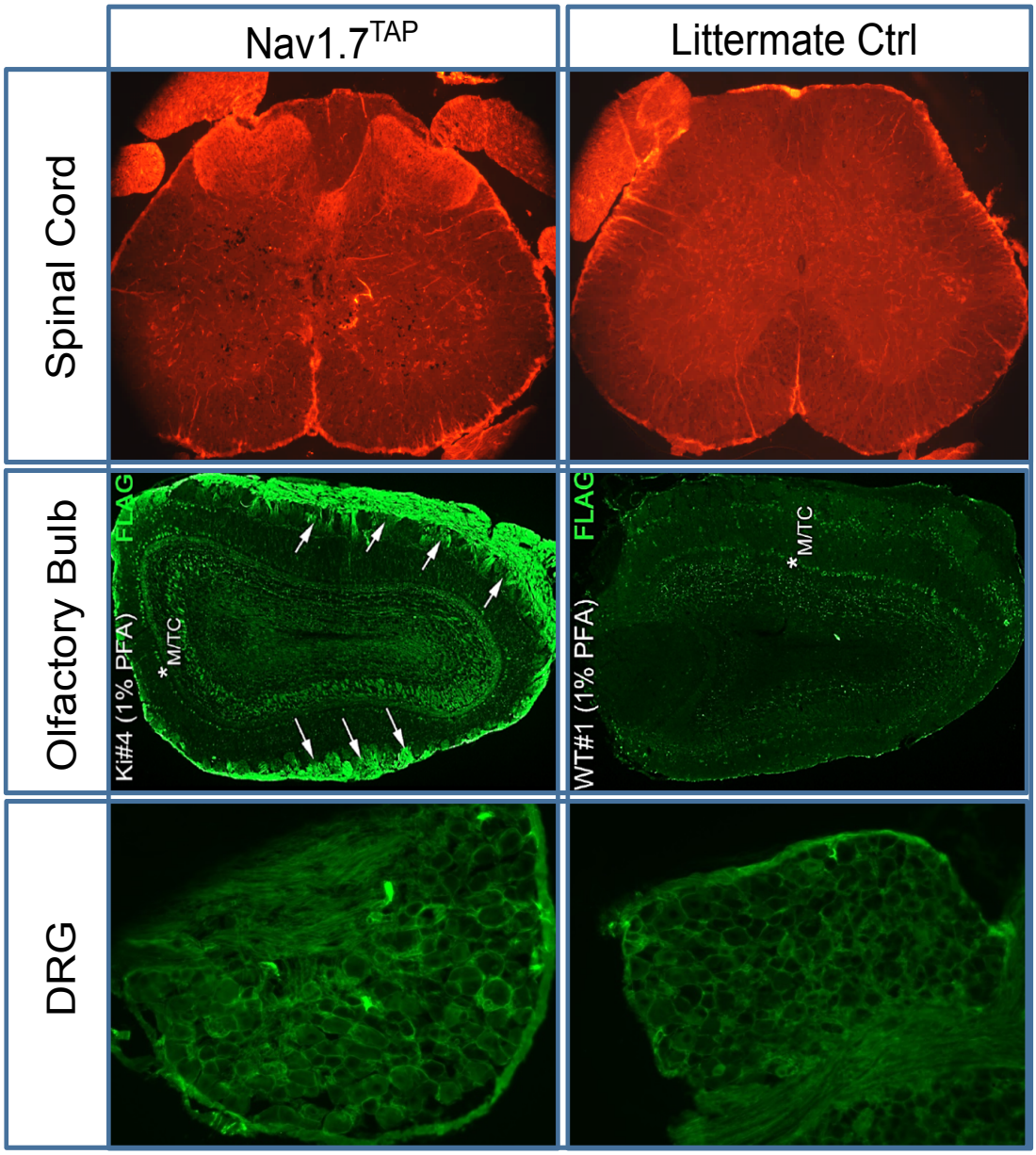

Figure 3-5: $Na_v1.7$ expression in the spinal cord, olfactory bulb and DRG.

Analysis of $Na_v1.7^{TAP/TAP}$ expression via immunohistochemistry in spinal cord, olfactory bulb and DRG section from $Na_v1.7^{TAP/TAP}$ and wildtype mice (Wt). Sections of $Na_v1.7^{TAP/TAP}$ and Wt from olfactory bulb and DRG were stained with anti-FLAG and visualized with Alexa Fluor-488 and in spinal cord with Alexa Fluor-594 (performed by Jing Zhao).

Optimization of single step and tandem affinity purification of $Na_v1.7^{TAP/TAP}$

Tandem affinity purification is a four-step process to purify a TAP-tagged protein from crude lysate through two consecutive affinity purifications. Here, the TAP-tag epitope inserted into $Na_v1.7$ contains a TEV site flanked by a 3XFLAG tag and a HAT domain (Figure 3-6,a). In the first steps, the specificity of the 3XFLAG binding sites and a unique TEV protease cleavage site are exploited. For the solubilisation of $Na_v1.7^{TAP/TAP}$ tag protein from DRG and olfactory neurons, 1% CHAPS buffer was experimentally evaluated to be the most suitable detergent. CHAPS is a non-denaturating zwitterionic detergent, commonly used to extract membrane proteins in their native conformation. In comparison to strong anionic detergents like SDS, CHAPS preserves protein-protein interactions and is compatible with downstream applications such as mass spectrometry. Protein was extracted from DRG and olfactory bulb neurons and $Na_v1.7^{TAP/TAP}$ captured from crude DRG/olfactory bulb lysates with magnetic M290 Epoxy-Dynabeads covalently bound to anti-FLAG antibody. This step allows the rapid first purification of $Na_v1.7$ TAP-tag complex from the crude lysate while preserving its native conformation. In the second step, the expression of a unique *Tobacco Etch Virus* (TEV) protease cleavage site within the TAP-tag is exploited to elute the $Na_v1.7^{TAP/TAP}$ tagged complex from the beads (Figure 3-6,b). A modified TEV protease with enhanced temperature stability (AcTEV) is incubated with the $Na_v1.7$ TAP-anti-FLAG complex. Addition of TEV releases the $Na_v1.7^{TAP/TAP}$ complex from the beads through site-specific cleavage and completes the single purification. In the third step, magnetic Ni-NTA beads capture the recovered $Na_v1.7$ TAP-tag complex, which also contains a poly-histidine affinity tag (HAT). Ni-NTA beads contain immobilized Nickel ions on their surface that have a high selectivity and affinity for polyhistidine residues independent of the three dimensional confirmation. In the last step $Na_v1.7^{TAP/TAP}$ complex is eluted from the beads with SDS and DTT, completing the tandem affinity purification process (see Methods 6.5.6). All steps where monitored with immunoblotting with anti-HAT (Figure 3-6,b).

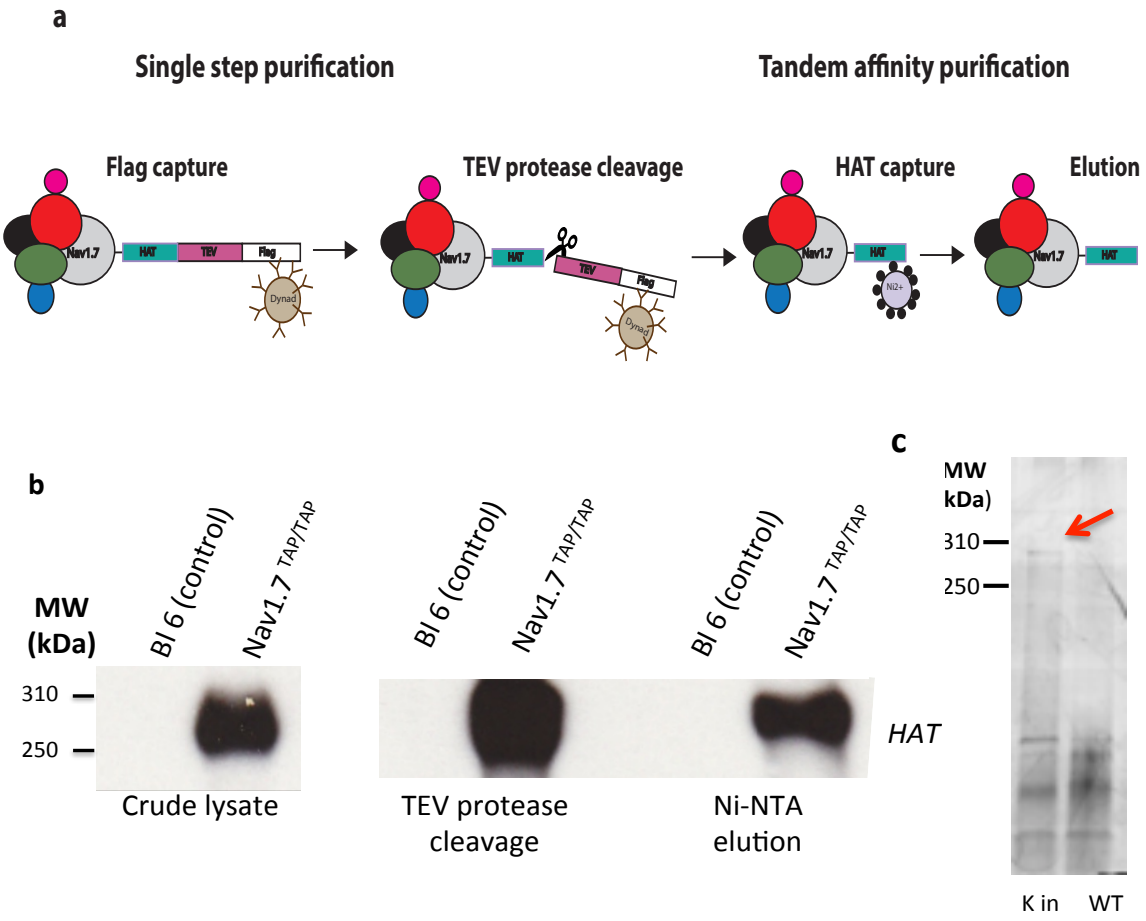

Figure 3-6: Single and tandem affinity purification.

(a) Schematic overview of the four-step tandem affinity purification protocol. In the first step, $Na_v1.7$ TAP-tag protein is captured with anti-FLAG coupled Dynabeads and released by the addition of AcTEV protease, completing the single step purification. In the third and fourth steps of the tandem affinity purification, the HAT domain is exploited and $Na_v1.7$-TAP protein is captured by Ni^{2+} beads and released by boiling in SDS and DTT **(b)** Tandem affinity purification of $Na_v1.7^{TAP/TAP}$ steps were monitored using Western blot and immunoblotted with anti-HAT antibody (1:500) **(c)** Silver staining of protein isolated from $Na_v1.7^{TAP/TAP}$ mice (red arrow) and littermate controls after a single purification from DRG/olfactory bulb pooled sample.

Next, single affinity purified $Na_v1.7^{TAP/TAP}$ complexes were silver stained (see Methods 6.5.8) (Figure 3-6c, red arrow). Three independent single (n=3) and tandem purifications (n=3) from pooled DRG/olfactory bulb samples were performed and sent for Liquid chromatography–mass spectrometry (LC-MS) analyses.

Mass spectrometry analysis of single-step purified $Na_v1.7$ TAP-tag protein

LS-MS/MS of single-step purified $Na_v1.7$-tap tag complexes was performed by Honglei Huang (University of Oxford) (see Methods 6.6). All raw MS data were processed to generate MGF files (200 most intense peaks) using the Proteowizard v.2.1.2476 software. The identification of proteins was performed using MGF files with the central proteomics facilities pipeline. A homo sapiens database containing entries from UniProtKB was used in the CPF Proteomics pipeline for data analysis. This pipeline combines data from three search engines (Mascot, OMSSA and X! tandem k-score). The search was carried out using the following parameters. Trypsin was the enzyme used for the digestion of the proteins and only one missed cleavage was allowed. The accepted tolerance for the precursor was 50 ppm and 0.1 Da for the fragment. The search encompassed 1+, 2+ and 3+ charge states, fixed modification for cysteine carbamidomethyl and variable modification for asparagine and glutamine deamidation, and methionine oxidation. All trypsin fragments were added to an exclusion list. False discovery rate was calculated by peptide/proteinprophet or estimated empirically from decoy hits, identified proteins were filtered to an estimated 1% FDR. The label-free analysis was carried out using the normalized spectral index (SINQ).

Functional protein-interaction partners of $Na_v1.7$

Proteins were manually clustered through use of PHANTER (http://www.pantherdb.org/), IPA (Quiagen) and UniProt. PHANTER and UniProt are online protein annotation tools that analyse high throughput, genome wide data from proteomic and expression studies (Mi, Muruganujan et al. 2013). Group data analysis of DRG/olfactory bulb proteins isolated from wildtype (n=3) mice compared to $Na_v1.7^{TAP}$ homozygous knock-in mice (n=3, single purification) determined that in total 201 proteins were two-fold increased in the knock-in mice, 77 of which were specific for $Na_v1.7^{TAP/TAP}$ tag samples after a single-step purification (Table 1). 164 proteins out of 201 proteins were 2-fold increased and came up in at least 2 out of 3 of the single purification runs for $Na_v1.7^{TAP/TAP}$ (Table 2,white). In three separate LS-MS/MS runs of $Na_v1.7^{TAP/TAP}$,

42 proteins come up only in the $Na_v1.7^{TAP/TAP}$ group but not in wildtype controls (Table 2, light green). Proteins that were not only enriched in $Na_v1.7^{TAP/TAP}$ mice but were more than 8-fold increased in $Na_v1.7^{TAP/TAP}$ compared to the wildtype group are shown in light blue in Table 2.

Additionally, proteins were grouped into *Channels/receptors/transporters, Enzymes, Vesicular/trafficking/transport, Cytoskeletal/structural/cell-adhesion, Nuclei acid binding protein/transcription factor and unclassified*. Unclassified proteins include uncharacterized proteins and proteins with unknown GO function/Protein class annotation in any annotation tools (Table 2). Furthermore, Table 2 shows the spectral index, hence the relationship between peptide lengths, spectral counts and fragment-ion intensity.

Proteins specific for $Na_v1.7^{TAP/TAP}$ were also grouped by GO Components (UniProt) (Table 3). Table 3 gives an overview of all proteins only enriched in $Na_v1.7^{TAP/TAP}$ (2 out of 3 runs, > 2-fold increase) and proteins that were at least 8-fold increased in $Na_v1.7^{TAP/TAP}$ group compared to the wildtype group, and their location in subcellular compartments/cellular component.

Table 1: Full list of mass spectrometry data: 201 proteins at least 2 fold increase

Protein	Description	Abbreviate	KI/WT or FI [1]
Q5SX40	Myosin-1	Myh1	KI Only
A6H8H5	Potassium voltage-gated channel subfamily B member 2	Kcnb2	KI Only
E9Q8I9-2I	Isoform 2 of Protein furry homolog	Fry	KI Only
O09111	NADH dehydrogenase [ubiquinone] 1 beta subcomplex subunit 11, mitochondrial	Ndufb11	KI Only
O35668-2	Isoform A of Huntingtin-associated protein 1	Hap1	KI Only
O88384	Vesicle transport through interaction with t-SNAREs homolog 1B	Vti1b	KI Only
O88951	Protein lin-7 homolog B	Lin7b	KI Only
O89112	LanC-like protein 1	Lancl1	KI Only
P02088	Hemoglobin subunit beta-1	Hbb-b1	KI Only
P02089	Hemoglobin subunit beta-2	Hbb-b2	KI Only
P39054-2	Isoform 2 of Dynamin-2	Dnm2	KI Only
P40240	CD9 antigen	Cd9	KI Only
P48320	Glutamate decarboxylase 2	Gad2	KI Only
P62192	26S protease regulatory subunit 4	Psmc1	KI Only
P62821	Ras-related protein Rab-1A	Rab1A	KI Only
P70452	Syntaxin-4	Stx4	KI Only
Q3U1J4	DNA damage-binding protein 1	Ddb1	KI Only
Q3UJU9	Regulator of microtubule dynamics protein 3	Rmdn3	KI Only
Q3ULD5	Methylcrotonoyl-CoA carboxylase beta chain, mitochondrial	Mccc2	KI Only
Q3V3R1	Monofunctional C1-tetrahydrofolate synthase, mitochondrial	Mthfd1l	KI Only
Q5DTL9-2	Isoform 2 of Sodium-driven chloride bicarbonate exchanger	Slc4a10	KI Only
Q60631-2	Isoform 2 of Growth factor receptor-bound protein 2	Grb2	KI Only
Q61029-2	Isoform Delta of Lamina-associated polypeptide 2, isoforms beta/delta/epsilon/gamma	Tmpo	KI Only
Q61234	Alpha-1-syntrophin	Snta1	KI Only
Q62205	Sodium channel protein type 9 subunit alpha	Scn9a	KI Only
Q62383	Transcription elongation factor SPT6	Supt6h	KI Only
Q64133	Amine oxidase [flavin-containing] A	Maoa	KI Only
Q6IRU2	Tropomyosin alpha-4 chain	Tpm4	KI Only
Q6P5F6	Zinc transporter ZIP10	Slc39a10	KI Only
Q6ZPS2-2	Isoform 2 of Carnosine synthase 1	Carns1	KI Only
Q7M729	Sodium channel subunit beta-4	Scn4b	KI Only
Q7TME0	Lipid phosphate phosphatase-related protein type 4	Lppr4	KI Only
Q7TPD3-2	Isoform 2 of Roundabout homolog 2	Robo2	KI Only
Q7TQH0-2	Isoform 2 of Ataxin-2-like protein	Atxn2l	KI Only
Q80VC9-2	Isoform 2 of Calmodulin-regulated spectrin-	Camsap3	KI Only

	associated protein 3		
Q80WM4	Hyaluronan and proteoglycan link protein 4	Hapln4	KI Only
Q80WM5	Hyaluronan and proteoglycan link protein 3	Hapln3	KI Only
Q811P8-2	Isoform 2 of Rho GTPase-activating protein 32	Arhgap32	KI Only
Q8BGH2	Sorting and assembly machinery component 50 homolog	Samm50	KI Only
Q8BHK2	Sodium channel subunit beta-3	Scn3b	KI Only
Q8BK64	Activator of 90 kDa heat shock protein ATPase homolog 1	Ahsa1	KI Only
Q8BYR1-2	Isoform 2 of tRNA wybutosine-synthesizing protein 4	Lcmt2	KI Only
Q8C419	Probable G-protein coupled receptor 158	Gpr158	KI Only
Q8CGY8-2	Isoform 2 of UDP-N-acetylglucosamine--peptide N-acetylglucosaminyltransferase 110 kDa subunit	Ogt	KI Only
Q8K019-2	Isoform 2 of Bcl-2-associated transcription factor 1	Bclaf1	KI Only
Q99KG3-2	Isoform 2 of RNA-binding protein 10	Rbm10	KI Only
Q99MI1-2	Isoform 2 of ELKS/Rab6-interacting/CAST family member 1	Erc1	KI Only
Q99PJ0	Neurotrimin	Ntm	KI Only
Q9CQ75	NADH dehydrogenase [ubiquinone] 1 alpha subcomplex subunit 2	Ndufa2	KI Only
Q9CQJ8	NADH dehydrogenase [ubiquinone] 1 beta subcomplex subunit 9	Ndufb9	KI Only
Q9CQZ5	NADH dehydrogenase [ubiquinone] 1 alpha subcomplex subunit 6	Ndufa6	KI Only
Q9CR51	V-type proton ATPase subunit G 1	Atp6v1g1	KI Only
Q9CZT8	Ras-related protein Rab-3B	Rab3b	KI Only
Q9D0R8	Protein LSM12 homolog	Lsm12	KI Only
Q9D1D4I	Transmembrane emp24 domain-containing protein 10	Tmed10	KI Only
Q9D517	1-acyl-sn-glycerol-3-phosphate acyltransferase gamma	Agpat3	KI Only
Q9D855	Cytochrome b-c1 complex subunit 7	Uqcrb	KI Only
Q9D8W5	26S proteasome non-ATPase regulatory subunit 12	Psmd12	KI Only
Q9DCJ1	Target of rapamycin complex subunit LST8	Mlst8	KI Only
Q9DCZ4	Apolipoprotein O	Apoo	KI Only
Q9EPK2-2	Isoform 2 of Protein XRP2	Rp2	KI Only
Q9JJ28I	Protein flightless-1 homolog	Flii	KI Only
Q9JLI8I	Squamous cell carcinoma antigen recognized by T-cells 3	Sart3	KI Only
Q9JLN9	Serine/threonine-protein kinase mTOR	Mtor	KI Only
Q9QWK4	CD5 antigen-like	Cd5l	KI Only
Q9QWW1-2	Isoform 2 of Homer protein homolog 2	Homer2	KI Only
Q9WTS6-2	Isoform 2 of Teneurin-3	Tenm3	KI Only
Q9WV34-2	Isoform 2 of MAGUK p55 subfamily member 2	Mpp2	KI Only
Q9WV85	Nucleoside diphosphate kinase 3	Nme3	KI Only
Q9Z0P4	Paralemmin-1	Palm	KI Only

Q9Z0V2	Potassium voltage-gated channel subfamily D member 2	Kcnd2	KI Only
B1APX2	Protein 5031439G07Rik	5031439G07Rik	KI Only
ID3YWG1	Uncharacterized protein	Gm7964	KI Only
G3UZJ2	Microtubule-associated protein (Fragment)	Map2	KI Only
H3BJD0	Protein Ppp1r9a	Ppp1r9a	KI Only
Q0VGU4	MCG18019	Vgf	KI Only
Q3U422	NADH dehydrogenase [ubiquinone] flavoprotein 3, mitochondrial	Ndufv3	KI Only
Q8CF89	TGF-beta-activated kinase 1 and MAP3K7-binding protein 1	Tab1	43.63
Q9DBZ5	Eukaryotic translation initiation factor 3 subunit K	Eif3k	32.97
Q9WTT4	V-type proton ATPase subunit G 2	Atp6v1g2	19.16
O70439l	Syntaxin-7	Stx7	18.61
Q9JME5	AP-3 complex subunit beta-2	Ap3b2	15.09
Q99MR8	Methylcrotonoyl-CoA carboxylase subunit alpha, mitochondrial	Mccc1	13.76
P97450	ATP synthase-coupling factor 6, mitochondrial	Atp5j	11.15
Q9JJY3	Sphingomyelin phosphodiesterase 3	Smpd3	11.15
Q80Y17	Lethal (2) giant larvae protein homolog 1	Llgl1	10.64
P48193-2	Isoform 2 of Protein 4.1	Epb41	8.86
Q9ER00	Syntaxin-12	Stx12	7.31
Q91ZU6-2	Isoform 1 of Dystonin	Dst	7.05
Q3UGC7	Eukaryotic translation initiation factor 3 subunit J-A	Eif3j1	7.02
P12787	Cytochrome c oxidase subunit 5A, mitochondrial	Cox5a	6.83
Q9ESN9-2	Isoform 1a of C-Jun-amino-terminal kinase-interacting protein 3	Mapk8ip3	6.37
Q9JKK7	Tropomodulin-2	Tmod2	6.30
Q14BI2	Metabotropic glutamate receptor 2	Grm2	5.98
Q921I1	Serotransferrin	Tf	5.80
P62334	26S protease regulatory subunit 10B	Psmc6	5.67
Q80TL0	Protein phosphatase 1E	Ppm1e	5.65
Q9Z127	Large neutral amino acids transporter small subunit 1	Slc7a5	5.53
Q8QZY1	Eukaryotic translation initiation factor 3 subunit L	Eif3l	5.19
Q9R0N7	Synaptotagmin-7	Syt7	5.07
Q9D6J6	NADH dehydrogenase [ubiquinone] flavoprotein 2, mitochondrial	Ndufv2	5.06
Q5DTY9	BTB/POZ domain-containing protein KCTD16	Kctd16	5.01
Q61335	B-cell receptor-associated protein 31	Bcap31	5.01
Q91XD7	Cysteine-rich with EGF-like domain protein 1	Creld1	4.62
Q3UH68-3	Isoform 3 of LIM and calponin homology domains-containing protein 1	Limch1	4.60
Q9QXV0	ProSAAS	Pcsk1n	4.60
Q9DBR7-2	Isoform 2 of Protein phosphatase 1 regulatory subunit 12A	Ppp1r12a	4.50

Q61330	Contactin-2	Cntn2	4.42
P70414	Sodium/calcium exchanger 1	Slc8a1	4.41
Q8JZR6-2	Isoform 2 of Electroneutral sodium bicarbonate exchanger 1	Slc4a8	4.35
Q7TMF3	NADH dehydrogenase [ubiquinone] 1 alpha subcomplex subunit 12	Ndufa12	4.32
O70194	Eukaryotic translation initiation factor 3 subunit D	Eif3d	4.30
Q7TQ95	Protein lunapark	Lnp	4.22
S4R2K9	Ankyrin-3 (Fragment)	Ank3	4.12
Q0VE82	Copine-7	Cpne7	4.03
Q9DBG6	Dolichyl-diphosphooligosaccharide--protein glycosyltransferase subunit 2	Rpn2	4.00
Q8R5H1-2	Isoform 2 of Ubiquitin carboxyl-terminal hydrolase 15	Usp15	3.88
Q9QUR8	Semaphorin-7A	Sema7a	3.74
Q9Z1P6	NADH dehydrogenase [ubiquinone] 1 alpha subcomplex subunit 7	Ndufa7	3.71
Q80TS3-3	Isoform 3 of Latrophilin-3	Lphn3	3.69
O35526l	Syntaxin-1A	Stx1a	3.64
A2ALS5-2	Isoform 2 of Rap1 GTPase-activating protein 1	Rap1gap	3.60
P55012	Solute carrier family 12 member 2	Slc12a2	3.58
Q8R5C5	Beta-centractin	Actr1b	3.58
E9PVU0	Unconventional myosin-VI	Myo6	3.48
Q7TPR4	Alpha-actinin-1	Actn1	3.47
Q78IK2	Up-regulated during skeletal muscle growth protein 5	Usmg5	3.45
P48771	Cytochrome c oxidase subunit 7A2, mitochondrial	Cox7a2	3.44
E9Q3L2	Protein Pi4ka	Pi4ka	3.40
P62812	Gamma-aminobutyric acid receptor subunit alpha-1	Gabra1	3.30
B8QI35	Liprin-alpha 3	Ppfia3	3.28
P63137-2	Isoform 2 of Gamma-aminobutyric acid receptor subunit beta-2	Gabrb2	3.25
Q9WTR5	Cadherin-13	Cdh13	3.18
Q8BW75	Amine oxidase [flavin-containing] B	Maob	3.16
Q8C522	Endonuclease domain-containing 1 protein	Endod1	3.13
Q9DC69	NADH dehydrogenase [ubiquinone] 1 alpha subcomplex subunit 9, mitochondrial	Ndufa9	3.10
P01631	Ig kappa chain V-II region 26-10	Ig kappa chain V-II region 26-10 OS=Mus musculus	3.07
P28738	Kinesin heavy chain isoform 5C	Kif5c	3.06
Q9DB77	Cytochrome b-c1 complex subunit 2, mitochondrial	Uqcrc2	3.03
Q61768	Kinesin-1 heavy chain	Kif5b	3.01
Q8R366	Immunoglobulin superfamily member 8	Igsf8	2.98
Q9WTS5	Teneurin-2	Tenm2	2.94
P23116l	Eukaryotic translation initiation factor 3 subunit A	Eif3a	2.91

Q9JI91	Alpha-actinin-2	Actn2	2.91
P32037I	Solute carrier family 2, facilitated glucose transporter member 3	Slc2a3	2.88
Q6PDL0	Cytoplasmic dynein 1 light intermediate chain 2	Dync1li2	2.88
B2RUJ5-3	Isoform 3 of Amyloid beta A4 precursor protein-binding family A member 1	Apba1	2.81
Q99LC3	NADH dehydrogenase [ubiquinone] 1 alpha subcomplex subunit 10, mitochondrial	Ndufa10	2.79
P18242	Cathepsin D	Ctsd	2.78
Q6WVG3	BTB/POZ domain-containing protein KCTD12	Kctd12	2.78
Q60931	Voltage-dependent anion-selective channel protein 3	Vdac3	2.77
Q9ERG2	Striatin-3	Strn3	2.73
Q8R1B4	Eukaryotic translation initiation factor 3 subunit C	Eif3c	2.72
Q80SW1	Putative adenosylhomocysteinase 2	Ahcyl1	2.70
Q9WTM5	RuvB-like 2	Ruvbl2	2.68
P01837I	Ig kappa chain C region	Ig kappa chain C region OS=Mus musculus	2.67
E9Q7C9	Kinesin light chain 1	Klc1	2.66
O70252	Heme oxygenase 2	Hmox2	2.58
Q8BG32	26S proteasome non-ATPase regulatory subunit 11	Psmd11	2.58
Q8BGN3	Ectonucleotide pyrophosphatase/phosphodiesterase family member 6	Enpp6	2.57
P14685	26S proteasome non-ATPase regulatory subunit 3	Psmd3	2.54
Q61735-2	Isoform 2 of Leukocyte surface antigen CD47	Cd47	2.51
O88737-2	Isoform 2 of Protein bassoon	Bsn	2.39
O88741	Ganglioside-induced differentiation-associated protein 1	Gdap1	2.39
Q60598	Src substrate cortactin	Cttn	2.38
Q9QY76	Vesicle-associated membrane protein-associated protein B	Vapb	2.37
Q8K3J1	NADH dehydrogenase [ubiquinone] iron-sulfur protein 8, mitochondrial	Ndufs8	2.34
Q8K400	Syntaxin-binding protein 5	Stxbp5	2.34
Q8CAQ8-2	Isoform 2 of Mitochondrial inner membrane protein	Immt	2.33
P23927	Alpha-crystallin B chain	Cryab	2.33
Q9JHU4	Cytoplasmic dynein 1 heavy chain 1	Dync1h1	2.33
O08917	Flotillin-1	Flot1	2.32
Q3V132	ADP/ATP translocase 4	Slc25a31	2.32
Q91WK2	Eukaryotic translation initiation factor 3 subunit H	Eif3h	2.26
Q9JIS5	Synaptic vesicle glycoprotein 2A	Sv2a	2.26
A2AQ25-2	Isoform 2 of Sickle tail protein	Skt	2.25

Q99MN1|	Lysine--tRNA ligase	Kars	2.24
O55143	Sarcoplasmic/endoplasmic reticulum calcium ATPase 2	Atp2a2	2.22
tr|E9Q6P5	Protein Ttc7b	Ttc7b	2.21
P97390	Vacuolar protein sorting-associated protein 45	Vps45	2.20
Q9DB05	Alpha-soluble NSF attachment protein	Napa	2.20
P04919-2	Isoform Kidney of Band 3 anion transport protein	Slc4a1	2.19
P46097	Synaptotagmin-2	Syt2	2.19
Q9DCX2	ATP synthase subunit d, mitochondrial	Atp5h	2.19
Q8CCT4	Transcription elongation factor A protein-like 5	Tceal5	2.18
Q6PGE7	Sodium-dependent proline transporter	Slc6a7	2.17
Q8CBY8-2	Isoform 2 of Dynactin subunit 4	Dctn4	2.16
Q9CZW5	Mitochondrial import receptor subunit TOM70	Tomm70a	2.15
Q8BFZ9	Erlin-2	Erlin2	2.11
Q8CGU1	Calcium-binding and coiled-coil domain-containing protein 1	Calcoco1	2.10
E9Q5J9	Tropomyosin alpha-3 chain	Tpm3	2.08
P31324	cAMP-dependent protein kinase type II-beta regulatory subunit	Prkar2b	2.07
P62715	Serine/threonine-protein phosphatase 2A catalytic subunit beta isoform	Ppp2cb	2.06
B1AWC8	Protein Pde4b	Pde4b	2.05
E9PUL5	Proline-rich transmembrane protein 2	Prrt2	2.04
Q9R1L5	Microtubule-associated serine/threonine-protein kinase 1	Mast1	2.04
Q9D0M3-2	Isoform 2 of Cytochrome c1, heme protein, mitochondrial	Cyc1	2.03
P60229	Eukaryotic translation initiation factor 3 subunit E	Eif3e	2.03
Q3TXX4	Vesicular glutamate transporter 1	Slc17a7	2.03
Q8VEK0	Cell cycle control protein 50A	Tmem30a	2.02
P62196	26S protease regulatory subunit 8	Psmc5	2.00

[1] *KI: knock in; WT: wild type; KI only: only found in knock in; FI: Fold increase compared to wildtype*

Table 2: Functional protein-interaction partners of $Na_v1.7$ (single purification)

MGI symbol	Protein name	Function (GO-family/ PHANTER protein class)	UniProt Acc	SPECTRAL INDEX MIC SIn		
				S1	S2	S3
Channels/receptor/transporters						
Adrm1	Proteasomal ubiquitin receptor ADRM1	Proteasomal ubiquitin receptor	Q9JKV1		1.37 E-07	1.52 E-07
Aqp1	Aquaporin-1	Transporter Transfer/carrier protein	Q02013		1.31 E-06	1.03 E-06
Atp2a2	Sarcoplasmic/endoplasmic reticulum calcium ATPase	Cation transporter; Ion channel	O55143	1.82 E-06	8.86 E-07	8.71 E-07
Atp6v1g2	V-type proton ATPase subunit G 2	ATP synthase	Q9WTT4	1.95 E-06		1.81 E-07
Bcap31	B-cell receptor-associated protein 31	Transporter Membrane traffic protein	Q61335	1.07 E-06	8.57 E-07	4.92 E-07
Cd47	Leukocyte surface antigen CD47	Immunoglobulin receptor superfamily	Q61735	2.99 E-07	3.29 E-07	5.09 E-07
Fxyd7	FXYD domain-containing ion transport regulator 7	Anion channel; Enzyme modulator	P59648		1.27 E-05	1.57 E-05
Gabra1	Gamma-aminobutyric acid receptor subunit alpha-1	GABAreceptor; Acetylcholine receptor	P62812	1.27 E-06	2.64 E-07	3.65 E-07
Kcnj10	ATP-sensitive inward rectifier potassium channel 10	Voltage-gated ion channel	Q9JM63		1.23 E-06	4.59 E-07
Lpar1	Lysophosphatidic acid receptor 1	G-protein coupled receptor	P61793		4.23 E-08	4.58 E-08
Lphn3	Latrophilin-3	G-protein coupled receptor	Q80TS3	1.16 E-06	3.05 E-08	
Scn3b	Sodium channel subunit beta-3	Voltage-gated ion channel	Q8BHK2	3.48 E-06	5.27 E-06	2.68 E-06
Scn4b	Sodium channel subunit beta-4	Voltage-gated ion channel Cell adhesion molecule	Q7M729	1.58 E-06		2.39 E-06
Scn9a	Sodium channel protein type 9 subunit alpha	Voltage-gated ion channel	Q62205	2.84 E-06	5.08 E-06	2.67 E-06
Sema7a	Semaphorin-7A	Membrane-bound signaling molecule	Q9QUR8	3.38 E-07		3.13 E-08
Slc12a2	Solute carrier family 12 member 2	Cation transporter	E9QM38	9.85 E-07	1.17 E-06	1.26 E-06

Slc2a3	Solute carrier family 2, facilitated glucose transporter member 3	Carbohydrate transporter	P32037	2.12 E-07		1.75 E-06
Slc30a9	Zinc transporter 9	Transporter	Q5IRJ6		1.48 E-07	1.06 E-07
Slc4a1	Band 3 anion transport protein	Transporter	P04919	1.47 E-06	2.92 E-07	3.16 E-07
Slc4a8	Electroneutral sodium bicarbonate exchanger 1	Cation transporter	Q8JZR6	1.62 E-07		5.42 E-08
Slc6a5	Sodium- And Chloride-Dependent Glycine Transporter 2	Cation transporter	B2RQX9		3.02 E-08	1.29 E-07
Slc7a5	Large neutral amino acids transporter small subunit 1	Amino acid transporter	Q9Z127	4.43 E-08	3.88 E-07	4.47 E-07
Slc8a1	Sodium/calcium exchanger 1	Cation transporter	G3X9J1	3.51 E-07	1.92 E-07	4.70 E-07
Tf	Serotransferrin	Type I/II cytokine receptor	P20352	1.30 E-07	5.38 E-07	
Vdac3	Voltage-dependent anion-selective channel protein 3	Anion channel; Voltage-gated ion channel	Q60931	3.08 E-06	1.37 E-06	1.19 E-06
Enzymes						
Kinases						
Csnk2a1	Casein kinase II subunit alpha	Serine/threonine protein kinase	Q60737	3.66 E-07	4.73 E-07	1.02 E-06
Mapk8ip3	C-Jun-amino-terminal kinase-interacting protein 3	Kinase modulator	Q9ESN9	9.47 E-09	2.02 E-07	5.11 E-07
Mpp2	MAGUK p55 subfamily member 2	Nucleotide kinase	Q9WV34-2		1.27 E-07	2.38 E-07
Mtor	Serine/threonine-protein kinase mTOR	Serine/threonine protein kinase	Q9JLN9		4.82 E-09	2.42 E-08
Ndufa10	NADH dehydrogenase [ubiquinone] 1 alpha subcomplex subunit 10,mitochondrial	Nucleotide kinase	Q99LC3	8.82 E-07	1.77 E-06	8.84 E-07
Pi4ka	Phosphatidylinositol 4-Kinase Alpha	Kinase	E9Q3L2		4.92 E-07	4.18 E-07
RP2	Protein retinitis pigmentosa 2, XRP2	Nucleotide kinase	Q9EPK2-2	3.89 E-06	1.21 E-06	2.98 E-07
Sgk223	Tyrosine-protein kinase SgK223	Protein kinase	Q571I4		2.02 E-08	1.87 E-08
Tab1	TGF-beta-activated kinase 1 and MAP3K7-binding protein 1	Kinase inhibitor Protein phosphatase	Q8CF89		1.94 E-06	2.16 E-07
Tek	Angiopoietin-1 receptor	Transmembrane tyrosine kinase protein	Q02858		1.35 E-06	1.21 E-06
Phosphatase						
Enpp6	*Ectonucleotide*	*Nucleotide*	*Q8BGN3*	9.66		1.16

	pyrophosphatase/phosphodiesterase family member 6	*phosphatase*		E-07		E-07
Lppr3	Lipid phosphate phosphatase-related protein type 3	*Phosphatase*	Q7TPB0	1.09 E-07	2.48 E-07	1.89 E-07
Ppp1r9a	Neurabin-1, Protein protein phosphatase 1, regulatory subunit 9A	*Phosphatase*	H3BJD0		2.65 E-07	1.06 E-07
Ligase						
Carns1	Carnosine synthase 1, Isoform 2	Other	Q6ZPS2-2		1.47 E-06	1.02 E-06
Kars	*Lysine--tRNA ligase*	RNA binding protein;aminoacyl-tRNA synthetase	Q99MN1		1.85 E-07	2.95 E-07
Mccc1	Methylcrotonoyl-CoA carboxylase subunit alpha; Mitochondrial	Ligase	Q99MR8		1.31 E-07	9.25 E-07
Mccc2	Methylcrotonoyl-CoA carboxylase beta chain; Mitochondrial	Ligase	Q3ULD5		1.98 E-07	3.80 E-08
Mthfd1l	Monofunctional C1 tetrahydrofolate synthase; Mitochondrial	Ligase	Q3V3R1		1.79 E-07	5.02 E-08
Neurl4	*Neuralized-like protein 4*	Ubiquitin-protein ligase	Q5NCX5		2.02 E-08	1.23 E-08
Isomerase/lhydrolase/protease						
Ahcyl1	Putative adenosylhomocysteinase 2	Hydrolase	Q80SW1		3.13 E-07	8.18 E-07
Cox5a	Cytochrome c oxidase subunit 5A, mitochondrial	Oxidase	P12787	2.95 E-05		4.09 E-07
Hmox2	Heme oxygenase 2	Oxygenase	O70252	5.10 E-07		3.62 E-07
Ndufa8	NADH dehydrogenase [ubiquinone] 1 alpha subcomplex subunit 8	Dehydrogenase	Q9DCJ5	1.52 E-05		1.50 E-07
Ndufa9	NADH dehydrogenase [ubiquinone] 1 alpha subcomplex subunit 9, mitochondrial	Dehydrogenase Reductase	Q9DC69	9.46 E-06	1.03 E-06	8.71 E-07
Ndufv2	NADH dehydrogenase [ubiquinone] flavoprotein 2, mitochondrial	Dehydrogenase; Reductase	Q9D6J6	3.83 E-06	9.37 E-07	
Ndufa3	NADH dehydrogenase [ubiquinone] 1 alpha subcomplex subunit 3	Oxidoreductase	Q9CQ91	4.92 E-06		1.28 E-06
Ndufa7	NADH dehydrogenase [ubiquinone] 1 alpha subcomplex subunit 7	Oxidoreductase	Q9Z1P6	1.37 E-06	1.83 E-06	1.64 E-06
Ndufs8	ADH dehydrogenase [ubiquinone] iron-sulfur protein 8, mitochondria	Oxidoreductase	Q8K3J1	2.66 E-06	9.24 E-07	7.46 E-07

Ndufv3	NADH dehydrogenase [ubiquinone] flavoprotein 3, mitochondrial	Oxidoreductase	Q8BK30	4.32 E-06	1.57 E-06	
Pde4b	Camp-Specific 3',5'-Cyclic Phosphodiesterase 4b	Phosphodiesterase	B1AWC9		3.29 E-07	1.96 E-07
Psmc1	26S protease regulatory subunit 4	Hydrolase	P62192		2.64 E-07	4.02 E-07
Psmc5	26S protease regulatory subunit 8	Hydrolase	P62196		4.77 E-07	2.90 E-07
Psmc6	26S protease regulatory subunit 10B	Hydrolase	P62334		1.25 E-06	8.12 E-07
Uqcrc2	Cytochrome b-c1 complex subunit 2, mitochondrial	Metalloprotease Reductase	Q9DB77	1.20 E-05	1.76 E-06	2.63 E-06
Transferase						
Agpat3	1-acyl-sn-glycerol-3-phosphate acyltransferase gamma	Acyltransferase	Q9D517		1.27 E-07	3.66 E-07
Maob	Amine oxidase [flavin-containing] A	Methyltransferase	Q64133	2.00 E-07	1.61 E-07	
Mat2a	S-adenosylmethionine synthase isoform type-2	Nucleotidyltransferase	Q3THS6		1.17 E-07	4.80 E-08
Ogt	Isoform 2 of UDP-N-Acetyl glucosamine-peptide Nacetylglucosaminy-ltransferase	Glycosyltransferase	Q8CGY8-2		1.19 E-07	1.65 E-07
Ttc7b	Tetratricopeptide Repeat Protein 7b	Glycosyltransferase	E9Q6P5		2.61 E-07	1.16 E-07
Modulators/ Regulators/Signalling						
Kctd16	BTB/POZ domain-containing protein KCTD16	Enzyme modulator	Q5DTY9	2.61 E-07		3.71 E-08
Psmd12	26S proteasome non-ATPase regulatory subunit 12	Enzyme modulator	Q9D8W5		1.32 E-07	7.89 E-07
Psmd3	***26S proteasome non-ATPase regulatory subunit 3***	Enzyme modulator	P14685	5.47 E-08	1.06 E-06	7.76 E-07
Ccar2	Cell cycle and apoptosis regulator protein 2	Enzyme inhibitor	Q8VDP4		1.45 E-07	5.97 E-08
Vesicular/trafficking/transport						
Ap3b2	AP-3 complex subunit beta-2	Membrane traffic protein	Q9JME5	1.47 E-06	1.14 E-06	2.01 E-07
Apba1	Amyloid beta A4 precursor protein-binding family A member 1	Membrane trafficking regulatory protein	B2RUJ5		8.35 E-08	3.29 E-07
Cope	Coatomer subunit epsilon	Vesicle coat protein	Q9D1D4		2.49	2.42

					E-07	E-07
Cpne7	Copine-7	Membrane traffic protein	Q0VE82		1.81 E-07	7.79 E-07
Flot1	Flotillin-1	Membrane traffic protein	O08917	3.18 E-07	3.15 E-07	4.73 E-07
Llgl1	Lethal(2) giant larvae protein homolog 1	Membrane trafficking regulatory protein	Q80Y17		2.83 E-07	1.45 E-07
Napa	Alpha-soluble NSF attachment protein	Membrane traffic protein	Q9DB05	8.07 E-07	6.77 E-07	1.39 E-06
Osbpl6	Oxysterol-binding protein-related protein 6	Transfer/carrier protein	Q8BXR9		2.71 E-08	1.46 E-08
Sec22b	Vesicle-trafficking protein SEC22b	SNARE protein	O08547	1.21 E-06	5.26 E-07	2.35 E-07
Stx12	Syntaxin-12	SNARE protein	Q9ER00	1.20 E-07	6.97 E-07	5.05 E-07
Stx1a	Syntaxin-1A	SNARE protein	O35526	1.70 E-05		2.10 E-06
Stx7	Syntaxin 7	SNARE protein	Q8BH40	4.01 E-06		1.62 E-07
Stxbp5	Syntaxin-binding protein 5	Membrane trafficking regulatory protein	Q8K400	2.12 E-06		3.37 E-09
Sv2a	Synaptic vesicle glycoprotein 2A	Transfer/carrier protein	Q9JIS5	7.41 E-06	2.76 E-06	5.56 E-06
Syt2	Synaptotagmin-2	Membrane trafficking regulatory protein	P46097	2.25 E-05	1.86 E-06	1.64 E-06
Tmed10	Transmembrane emp24 domain-containing protein 10	Transfer/carrier protein Vesicle coat protein	Q9D1D4	1.08 E-06		9.98 E-08
Vapb	Vesicle-associated membrane protein, associated protein B and C	Membrane trafficking regulatory protein	Q8BH80	4.55 E-06		1.33 E-07
Cytoskeletal/structural/cell adhesion						
Actr1b	Beta-centractin	Actin and actin related protein	Q8R5C5		1.05 E-06	4.41 E-07
Ank3	Ankyrin-3	Cytoskeletal protein	G5E8K5	1.44 E-06	4.38 E-07	1.30 E-07
Arhgap32	RhoGTPase-activating protein 32	Cytoskeletal regulator protein	Q811P8		4.69 E-08	1.81 E-08
Cdh13	Cadherin-13	Cell junction protein	Q9WTR5	1.39 E-07	7.25 E-08	2.54 E-07
Chaperones						
Ckap5	Cytoskeleton-associated protein 5	Non-motor microtubule binding protein	A2AGT5	6.00 E-07	1.18 E-06	
Cttn	Src substrate cortactin	Non-motor actin binding protein	Q60598		1.91 E-07	1.57 E-06

Dnajb6	DnaJ homolog subfamily B member 6	Chaperonin	O54946		8.15 E-07	9.65 E-07
Dst	Dystonin	Non-motor actin binding protein	E9Q9X1	1.45 E-08	9.94 E-09	6.52 E-08
Dync1h1	Cytoplasmic dynein 1 heavy chain 1	Microtubule family cytoskeletal protein	Q9JHU4		5.70 E-07	1.19 E-06
Dync1li2	Cytoplasmic dynein 1 light intermediate chain 2	Microtubule family cytoskeletal protein	Q6PDL0		3.32 E-07	3.63 E-07
Flii	Protein flightless-1 homolog	Non-motor actin binding protein	Q9JJ28		2.63 E-08	4.03 E-08
Fry	Protein furry homolog, Isoform 2	Structural/scaffold	E9Q8I9-2		5.41 E-09	7.10 E-09
Gdap1	Ganglioside-induced differentiation-associated protein	Cytoskeletal protein	O88741		2.29 E-06	1.78 E-06
Hepacam	Hepatocyte cell adhesion molecule	Cell-adhesion molecule	Q640R3		2.89 E-07	3.19 E-07
Hspb1	Heat shock protein beta-1	Structural protein Chaperone	P14602		5.96 E-07	4.94 E-07
Kif5b	Kinesin-1 heavy chain	Microtubule binding motor protein	Q61768	1.30 E-07	2.81 E-07	1.04 E-06
Kif5c	Kinesin heavy chain isoform 5C	Microtubule binding motor protein	P28738	2.64 E-08		3.89 E-08
Klc1	Kinesin light chain 1	Microtubule family cytoskeletal protein	E9Q7C9		4.38 E-07	1.40 E-06
Limch1	LIM and calponin homology domains-containing protein 1	Actin family cytoskeletal protein	Q3UH68	5.36 E-07		1.27 E-07
Mlst8	Target of rapamycin complex subunit LST8	Actin cytoskeleton and mTor regulator	Q9DCJ1		1.50 E-06	6.75 E-07
Myo6	Unconventional myosin-VI	G-protein modulator; actin binding motor protein	E9Q174		1.47 E-06	6.20 E-07
Ntm	Neurotrimin	Cell adhesion molecule	Q99PJ0	4.27 E-07		7.61 E-08
Tmod2	Tropomodulin-2	Non-motor actin binding protein	Q9JKK7	7.03 E-08	8.19 E-07	1.13 E-05
Tomm70a	Mitochondrial import receptor subunit TOM70	Chaperone	Q9CZW		5.32 E-07	3.93 E-07
Tubg1	Tubulin gamma-1 chain	Tubulin	P83887		1.82 E-07	1.87 E-07
Ca2+/ Calmodulin binding						
Camsap3	Calmodulin-regulated spectrin-associated protein 3	Microtubule dynamics Calmodulin-regulated	Q80VC9-2		2.63 E-07	6.61 E-08
Creld1	Cysteine-rich with EGF-like domain protein 1	Calcium binding	Q91XD7		2.21 E-07	7.58 E-07

Epb41	Protein 4.1	Calmodulin binding Actin cytoskeleton organization	P48193	4.62 E-07		1.21 E-07
Ppp1cc	Serine/threonine-protein phosphatase PP1-gamma catalytic subunit	Protein phosphatase; Calcium-binding protein	P63087	6.62 E-07	1.16 E-06	8.77 E-07
Ppp2cb	Serine/threonine-protein phosphatase 2A catalytic subunit beta isoform	Protein phosphatase; Calcium-binding protein	P62715		5.66 E-07	9.02 E-07
Slc9a1	Sodium/hydrogen exchanger 1	Calmodulin binding Antiporter	Q6116	3.00 E-07		2.84 E-07
Strn	Striatin	Calmodulin binding	O55106		2.23 E-07	1.42 E-07
Strn3	Striatin-3	Calmodulin binding	Q9ERG2		3.36 E-07	1.13 E-07
Strn4	Striatin-4	Calmodulin binding	P58404		2.11 E-07	1.01 E-07
Nuclei acid binding protein/Transcription factor						
Agap3	Arf-GAP with GTPase, ANK repeat, PH domain-containing protein 3	Nucleic acid binding; G-protein modulator	F8VQE9		1.02 E-06	1.09 E-07
Atxn2l	Ataxin-2-like protein;	RNA binding protein	Q7TQH0-2		8.76 E-08	5.64 E-08
Calcoco1	Calcium-binding and coiled-coil domain-containing protein 1	DNA binding	Q8CGU1		2.13 E-07	3.09 E-07
Ddb1	DNA damage-binding protein 1	mRNA polyadenylation factor	*Q3U1J4*		1.82 E-07	2.01 E-07
Eif3a	Eukaryotic translation initiation factor 3 subunit A	Translation initiation factor	P23116		1.25 E-06	3.40 E-06
Eif3b	Eukaryotic translation initiation factor 3 subunit B	Translation initiation factor	Q8JZQ9		2.17 E-06	2.54 E-06
Eif3c	Eukaryotic translation initiation factor 3 subunit C	Translation initiation factor	Q8R1B4		8.12 E-07	1.47 E-06
Eif3d	Eukaryotic translation initiation factor 3 subunit D	Translation initiation factor	O70194		1.44 E-06	1.85 E-06
Eif3e	Eukaryotic translation initiation factor 3 subunit E	Translation initiation factor	P60229		2.94 E-06	3.83 E-06
Eif3h	Eukaryotic translation initiation factor 3 subunit H	Transcription factor	Q91WK2		2.02 E-07	1.17 E-06
Eif3k	Eukaryotic translation initiation factor 3 subunit K	Translation initiation factor	Q9DBZ5		1.08 E-06	1.33 E-06

Eif3l	Eukaryotic translation initiation factor 3 subunit L	Translation initiation factor	Q8QZY1		4.25 E-07	2.18 E-06
Eif4b	Eukaryotic translation initiation factor 4B;	Translation initiation factor	Q8BGD9	5.03 E-07	2.53 E-05	1.10 E-05
Igf2bp2	Insulin-like growth factor 2 mRNA-binding protein 2	mRNA splicing factor; Ribonucleoprotein;	Q5SF07	2.60 E-06	7.96 E-07	1.76 E-06
Prrc2c	Protein PRRC2C	Transcription factor; Nuclease	Q3TLH4		5.81 E-08	3.46 E-08
Rpl19	60S ribosomal protein L19	Ribosomal protein	P84099		1.77 E-06	8.94 E-07
Sart3	Squamous cell carcinoma antigen recognized by T-cells 3	Nuclease	Q9JLI8		2.22 E-07	2.38 E-07
Tardbp	TAR DNA-binding protein 43	DNA binding protein;	Q921F2		1.46 E-06	4.75 E-07
Zranb2	Zinc finger Ran-binding domain-containing protein 2	RNA binding	Q9R020		2.61 E-07	2.50 E-07
Unclassified						
Apoo	Apolipoprotein O; protein FAM121B	Uncharacterised	Q9DCZ4		1.33 E-06	1.06 E-06
Atp5h	ATP synthase subunit d, mitochondrial	Transmembrane transporter	Q9DCX2	1.30 E-05	3.55 E-06	2.63 E-06
Atp5j	ATP synthase-coupling factor 6, mitochondrial	Transmembrane transporter	P97450	1.70 E-05		3.14 E-06
BC068157	Protein BC068157	Uncharacterised	E9PV26		3.35 E-08	2.18 E-08
Chchd6	Coiled-coil-helix-coiled-coil-helix domain-containing protein 6, mitochondrial	Unclassified/ function unknown	Q91VN4	2.42 E-06	3.67 E-07	6.08 E-07
Cyc1	Cytochrome c1, heme protein, mitochondrial		Q9D0M3	5.74 E-06	7.47 E-07	8.62 E-07
Dctn4	Dynactin subunit	Putative uncharacterised Protein	Q8CBY8		3.56 E-06	3.37 E-06
Endod1	Endonuclease domain-containing 1 protein	Putative uncharacterised Protein	Q8C522	8.30 E-06	5.00 E-08	2.02 E-07
Erlin2	Erlin-2	Protein binding / function unknown	Q8BFZ9	7.46 E-07	1.60 E-07	9.27 E-08
1Ig heavy chain V region AC38 205.12	Ig heavy chain V region AC38 205.12	Uncharacterised	P06330	2.78 E-05	7.71 E-06	2.50 E-06
Ig kappa chain C region	Ig kappa chain C region	Uncharacterised	P01837	6.72 E-05	8.17 E-05	8.27 E-05

Ig kappa chain V-II region 26-10	Ig kappa chain V-II region 26-10	Uncharacterised	P01631	6.19 E-04	7.58 E-05	5.59 E-05
Igsf8	Immunoglobulin superfamily member 8	Function unknown	Q8R366	5.32 E-06	2.17 E-06	1.16 E-06
Immt	Mitochondrial inner membrane protein	Function unknown	Q8CAQ8	8.80 E-06	7.09 E-07	9.05 E-07
Kctd12	BTB/POZ domain-containing protein KCTD12	Auxiliary subunit of GABA-B receptors	Q6WVG	1.82 E-06	3.56 E-07	6.69 E-07
Kctd16	BTB/POZ domain-containing protein KCTD16	Auxiliary subunit of GABA-B receptors	Q5DTY9	2.61 E-07		3.71 E-08
Lnp	Protein lunapark	Uncharacterised	Q7TQ95	1.07 E-07	8.69 E-08	4.28 E-07
Phb2	Prohibitin-2	Protein binding	O35129	3.58 E-06	4.19 E-06	1.74 E-06
Plp2	Plp2	Function unknown	Q9R1Q7	7.88 E-07		7.70 E-07
Ppfia3	Liprin-alpha 3	Function unknown	B8QI35	4.14 E-07	5.76 E-07	2.63 E-07
Prrt2	Proline-rich transmembrane protein 2	Function unknown	E9PUL5	7.51 E-07	6.43 E-07	1.03 E-06
Psmd11	26S proteasome non-ATPase regulatory subunit 11	Function unknown	Q8BG32		2.88 E-06	2.75 E-06
Psmd7	26S proteasome non-ATPase regulatory subunit 7	Proteosome complex	P26516		1.11 E-06	4.89 E-07
Samm50	Sorting and assembly machinery component 50 homolog	Possibly mitochondrial protein binding	Q8BGH2	2.58 E-07	2.74 E-07	2.00 E-07
Smpd3	Sphingomyelin phosphodiesterase 3	Uncharacterised	Q9JJY3	1.04 E-07		1.29 E-07
Spef2	Sperm flagellar protein 2	Uncharacterised	Q8C9J3		1.05 E-07	1.05 E-07
Wfs1	Wolframin	Uncharacterised	P56695		1.03 E-07	1.26 E-07

Table 3: Protein-interaction[1] partners of $Na_v1.7$ by subcellular location

MGI symbol	Protein Name	Subcelluar localisation (GO Component[2])
Plasma membrane		
Aqp1	Aquaporin-1	Plasma membrane
Kcnj10	ATP-sensitive inward rectifier potassium channel 10	Plasma membrane
Lppr3	Lipid phosphate phosphatase-related protein type 3	Membrane
Mpp2	MAGUK p55 subfamily member 2	Plasma membrane
Ntm	Neurotrimin	Plasma membrane
Osbpl6	Oxysterol-binding protein-related protein 6	Plasma membrane
Plp2	Plp2	Plasma membrane
Ppp1r9a	Neurabin-1, Protein protein phosphatase 1, regulatory subunit 9A	Plasma membrane
Scn3b	Sodium channel subunit beta-3	Plasma membrane
Scn4b	Sodium channel subunit beta-4	Plasma membrane
Scn9a	Sodium channel protein type 9 subunit alpha	Plasma membrane
Slc30a9	Zinc transporter 9	Plasma membrane
Slc6a5	Sodium-and Chloride-Dependent Glycine Transporter 2	Plasma membrane
Slc9a1	Sodium/hydrogen exchanger 1	Plasma membrane
Stx7	Syntaxin 7	Plasma membrane SNARE complex
Nucleus		
Ddb1	DNA damage-binding protein 1	Nucleus
Eif3k	Eukaryotic translation initiation factor 3 subunit K	Nucleus, Cytoplasm
Flii	Protein flightless-1 homolog	Nucleus
Mtor	Serine/threonine-protein kinase mTOR	Nucleus; TORC1 complex; TORC2 complex
Psmc1	26S protease regulatory subunit 4	Nucleus Proteasome complex
Sart3	Squamous cell carcinoma antigen recognized by T-cells 3	Nucleus
Zranb2	Zinc finger Ran-binding domain-containing protein 2	Nucleus
Cytoplasm		
Agpat3	1-acyl-sn-glycerol-3-phosphate acyltransferase gamma	Cytoplasm
Arhgap32	RhoGTPase-activating protein 32	Cytoplasm
Atp5j	ATP synthase-coupling factor 6, mitochondrial	Cytoplasm Mitochondrial membrane
Atp6v1g2	V-type proton ATPase subunit G2	Cytoplasm Integral component of synaptic vesicle membrane
Camsap3	Calmodulin-regulated spectrin-associated protein 3	Cytoplasm

Cope	Coatomer subunit epsilon	Cytoplasm Vesicle coat protein
Llgl1	Lethal(2) giant larvae protein homolog 1	Cytoplasm
Mat2a	S-adenosylmethionine synthase isoform type-2	Cytoplasm
Mccc1	Methylcrotonoyl-CoA carboxylase subunit alpha; Mitochondrial	Cytoplasm Mitochondrial membrane
Mccc2	Methylcrotonoyl-CoA carboxylase beta chain; Mitochondrial	Cytoplasm Mitochondrial membrane
Mlst8	Target of rapamycin complex subunit LST8	Cytoplasm TORC1 complex; TORC2 complex
Mthfd1l	Monofunctional C1 tetrahydrofolate synthase; Mitochondrial	Cytoplasm Mitochondrial membrane
Ndufa3	NADH dehydrogenase [ubiquinone] 1 alpha subcomplex subunit 3	Cytoplasm Mitochondrial membrane
Ndufv3	NADH dehydrogenase [ubiquinone] flavoprotein 3, mitochondrial	Cytoplasm Mitochondrial membrane
Neurl4	*Neuralized-like protein 4*	Cytoplasm
Ogt	Isoform 2 of UDP-N-Acetyl glucosamine--peptide Nacetylglucosaminyltransferase	Cytoplasm
Pde4b	Camp-Specific 3',5'-Cyclic Phosphodiesterase 4b	Cytoplasm Voltage-gated calcium channel complex; Z- disc, cell pheriphery
Psmd12	26S proteasome non-ATPase regulatory subunit 12	Cytoplasm Proteasome complex
Psmd7	26S proteasome non-ATPase regulatory subunit 7	Cytoplasm Proteasome complex
RP2	Protein retinitis pigmentosa 2, XRP2	Cytoplasm; cytoplasmatic vesicle
Samm50	Sorting and assembly machinery component 50 homolog	Cytoplasm Mitochondrial membrane
Strn4	Striatin-4	Cytoplasm
Tab1	TGF-beta-activated kinase 1 and MAP3K7-binding protein 1	Cytoplasm
Tmed10	Transmembrane emp24 domain-containing protein 10	Cytoplasm Copi-coated Vesicle
Tubg1	Tubulin gamma-1 chain	Cytoplasm; Cytoskeleton
Other		
Ap3b2	AP-3 complex subunit beta-2	Other
Apoo	Apolipoprotein O; protein FAM121B	Extracellular Space
Carns1	Carnosine synthase 1, Isoform 2	Other
Sgk223	Tyrosine-protein kinase SgK223	Other
Tf	Serotransferrin, F3	Extracellular Space

[1] *all proteins specific for $Na_v1.7^{TAP/TAP}$ and/or had more than 8-fold increase*
[2] *UniProt and IPA analysis*

LS-MS/MS of tandem affinity purified TAP-tagged $Na_v1.7^{TAP/TAP}$

Tandem affinity purification is a consecutive four-step purification protocol. In the first steps, $Na_v1.7^{TAP/TAP}$ tag is captured with anti-FLAG coupled Dynabeads and released by the addition of TEV protease, completing the single-step purification. The third and fourth steps of the tandem affinity purification exploit the specificity of the HAT domain, $Na_v1.7^{TAP/TAP}$ is captured by Ni^{2+} beads and released by boiling in SDS and DTT. However, my tandem affinity purification (TAP) of $Na_v1.7^{TAP/TAP}$ was not successful. LC-MS runs were not enriched in $Na_v1.7^{TAP/TAP}$ and beta subunits, although immunoblotting with anti-HAT showed a strong band at 260-280kDa after tandem affinity purification (Figure 3-5,b). This suggests that $Na_v1.7^{TAP/TAP}$ was present and enriched through the tandem purification protocol. However, it is unclear why $Na_v1.7$ was detectable on a western blot but not through mass spectrometry, particularly given the high sensitivity of this technique. One possible explanation might be that the protein storage before the mass spectrometry was not sufficient to stabilize and prevent protein degradation.

Verification of a $Na_v1.7^{TAP/TAP}$ interaction partner *Scn3b*

Scn3B

Next the obtained mass spectrometry data was verified. One of the interaction partners found on the list is $Na_v\beta3$ subunit, a small (~ 40 kDa) transmembrane protein that is non-covalently linked to Na_v alpha subunits and regulates its functional activity. In contrast to $Na_v\beta4$, $Na_v\beta3$ forms trimers in the plasma membrane and is believed to act as a scaffold to cluster and facilitate interaction with various signaling molecules and other ion channels (Namdurai et al. 2014). Recent studies discovered the role of *Scn3b* in the intracellular trafficking of Na_v alpha subunits. Laedermann *et al.* (2013) showed that β1 and β3, but not β2 or β4 associate with $Na_v1.7$ in the ER/Golgi and mediate from there the channels' glycosylation state and membrane expression (Laedermann, Syam et al. 2013). Furthermore, a recent study by Ishikawa *et al.* (2013) showed that certain mutations in *SCN3B* lead to dysregulated trafficking of $Na_v1.5$, which is linked to Brugada syndrome. Alex Kanellopoulos performed

a reverse Co-IP of $Na_v1.7^{TAP/TAP}$ and β3-subunit from DRG/olfactory bulb with anti-FLAG antibodies and immunoblotting with anti-*SCN3B* antibody to verify the interaction of $Na_v1.7$ with the β3-subunit (see Methods 6.5.5) and showed that $Na_v1.7$ and β3-subunit are interacting.

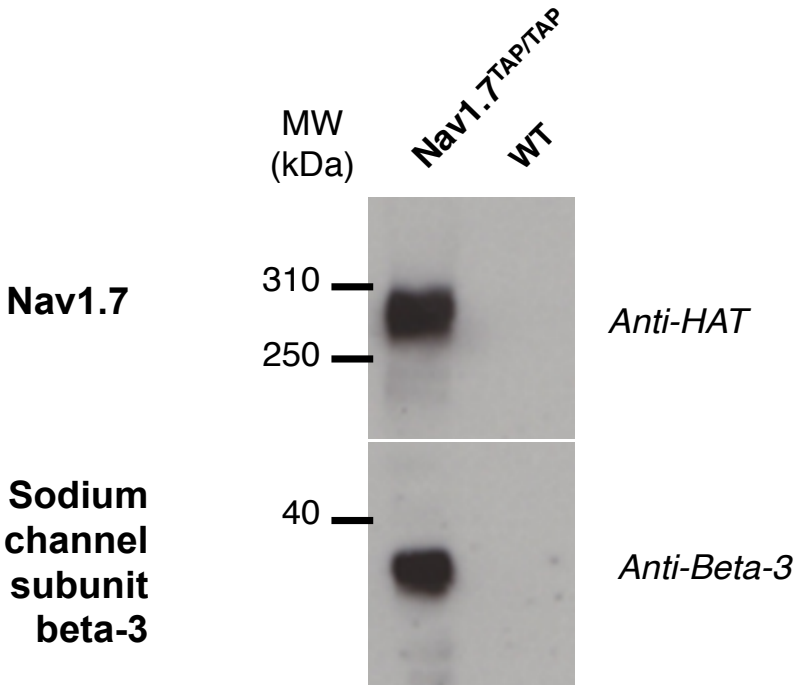

Figure 3-7: Validation of $Na_v1.7$ interaction partner *Scn3b*.

Upper panel: Co-immunoprecipitation of $Na_v1.7^{TAP/TAP}$ from DRG and olfactory bulb with anti-FLAG and immunoblotting with anti-HAT. Lower panel: Co-immunoprecipitation of $Na_v1.7$-TAP from DRG and olfactory bulb with anti-FLAG and immunoblotting with anti-*SCN3B* (performed by Alex Kanellopoulos).

Other interaction partners

mTOR

The serine/thereonine kinase, mammalian target of rapamycin (mTOR), is an important regulator of cell growth, maintenance and synaptic plasticity. There are two known mTOR complexes (mTORC1 and mTORC2) that differ in activation stimuli, protein composition, sensitivity to rapamycin and subcellular localization (Ma and Blenis 2009). Functionally mTOR controls local protein

synthesis and translation in neuronal and non-neuronal cells via intracellular signaling and phosphorylation (activation) of transcription initiation factors and ribosomal protein kinases (Li, Kim et al. 2014). Chronic pain states are characterized by increased excitability of primary afferents and by short and long-term changes in protein expression leading to peripheral and central sensitization. TTXs voltage-gated sodium channel $Na_v1.7$ expression is upregulated during acute and chronic pain states (Matzner and Devor 1994, Omana-Zapata, Khabbaz et al. 1997). Wada *et al.* (2004) found that inhibition of mTOR in chromaffin cells increases the number of plasma membrane localized voltage-gated sodium channels via increased trafficking of Na^+ channels from the trans-Golgi (Wada, Yanagita et al. 2004). Inhibition of mTOR through intracethecal injection or direct application of rapamycin in inflammatory and neuropathic animal pain models attenuates mechanical hypersensitivity (Asante, Wallace et al. 2009, Liang, Tao et al. 2013). Given the contradicting effects of mTOR inhibition, this might indicate a tissue specific regulation of the protein. However, it also shows that mTOR plays a role in mediating inflammatory (Norsted Gregory, Codeluppi et al. 2010) and neuropathic pain states (Zhang, Sun et al. 2013, Lisi, Aceto et al. 2015). In my $Na_v1.7^{TAP/TAP}$ single step purification, mTOR was significantly enriched in $Na_v1.7^{TAP/TAP}$ but not in the wildtype samples.

Aquaporin-1 (AQP-1)

Aquaporins are small (24-30 kDa) pore-forming membrane proteins ubiquitously expressed in most tissues and fundamental in selective transport of water and solute molecules across membranes. Aquaporins are members of a large major intrinsic protein family. Structurally aquaporins are homotetrameric complexes, comprised of 6 transmembrane and one pseudo-transmembrane segment. In mammals at least 13 isoforms are known that differ in expression pattern and water/solute transport selectivity. *AQP1, AQP2, AQP3, AQP4, AQP5, AQP8* and *AQP9* are expressed in the peripheral or central nervous system (Agre, King et al. 2002, Zhang and Verkman 2010). Furthermore some isoforms, *AQP1, AQP2* and AQP4 have been implicated in pain processing. Aquaporin-1 (*AQP1*) is robustly expressed in the somata and in peripheral and central

branches of small diameter nociceptive DRG neurons. Aquaporin-1 (*AQP1)* was also found in small diameter sensory neurons in the trigeminal and nodose ganglia (Oshio, Watanabe et al. 2006, Shields, Mazario et al. 2007). This expression coincides with the expression pattern of peripherally located Na+ channels. Indeed Aquaporin-$1^{-/-}$mice exhibit a decreased response in thermal and cold inflammatory pain tests and Aqp1 was shown to directly interact with $Na_v1.8$. The decrease in inflammatory pain response in Aqp1 knockouts was due to impaired $Na_v1.8$ activity in DRG neurons (Zhang and Verkman 2010).

Tmed 10 (or TMP21or p23)

The intracellular secretory pathway consists of a number of consecutive steps to ensure the correct synthesis/folding, transport and secretion of proteins. This transport is achieved through selective packing of newly synthesized, correctly folded proteins into COP-II coated vesicles in the ER that bud off and transport the cargo to the Golgi. Escaped ER resident proteins are transported back from the Golgi in COP-I-coated vesicles. In the Golgi, proteins are subject to extensive post-translational modification and when matured, exit the Golgi through the TGN (*trans* Golgi exit). However, from the TGN, there are two routes for a protein 1) the consecutive secretory pathway and 2) the regulated secretory pathway. The regulated secretory pathway is common in highly specialized cell types, like neurons, where the protein cargo is only released upon strong extracellular stimulation (Strating and Martens 2009). Transmembrane emp24 domain (TMED) or p24 protein family of trafficking proteins are important regulators of protein-cargo selection and bidirectional vesicular transport from the ER to the Golgi apparatus (Nickel, Sohn et al. 1997, Dominguez, Dejgaard et al. 1998). TMED family members are small (24kDa) type I transmembrane proteins primarily found in COP-I and COP-II coated vesicles in ER and Golgi that consist of four functional domains: an ER membrane targeting sequence, a N-terminal GOLD domain (Golgi dynamics) that is important in cargo selectivity and C-terminal COPI and COPII vesicle-binding domains. Structurally TMED proteins can form monomers, dimers, oligomers or hetero-oligomer complexes (Gommel, Orci et al. 1999, Strating and Martens 2009).

Tmed 10 also known as *Tmp21* or *p23* is predominately found in COP-I and COP-II coated vesicles in the ER and Golgi apparatus but also the plasma membrane of secretory granules in the pancreatic beta cells (Hosaka, Watanabe et al. 2007, Strating and Martens 2009). Additionally *Tmed10* is associated with presenilin/γ-secretase complex in the plasma membrane and shown to be an important regulator of the γ-secretase. Chen *et al.* (2006) showed that *Tmed10* specifically modulates γ-secretase activity and not the complex assembly or stability (Chen, Hasegawa et al. 2006). It is believed that *Tmed10* luminal domain is responsible for its efficient trafficking to the cell surface (Blum and Lepier 2008). Recently, it was also reported that *Tmed10* interacts with PKC isoforms via their C1 domain. The C1 domain in PKC is highly conserved and present in all isoforms and is important in plasma membrane targeting of PKC (Wang and Kazanietz 2010, Wang, Xiao et al. 2011).

3.4 Discussion

Voltage-gated sodium channels (VGSC) are large glycoprotein complexes that reside in the plasma membrane and consist of a pore-forming Na_v α-subunit and an associated β-subunit(s). Similar to other proteins, voltage-gated sodium channels are subject to transcriptional and translational regulations and intracellular trafficking that controls the electrophysiological properties and functional expression of Na^+ channels. However very little is known about which proteins are involved in the trafficking of Na_v channels to the plasma membrane and through which mechanisms the transport is achieved with regards to specific isoforms.

Here, I focused on the voltage-gated sodium channel $Na_v1.7$, which is important in initiation and propagation of action potentials in excitable cells and has emerged as key player in human pain pathways. Therefore investigating $Na_v1.7$ protein-protein interaction partners and channel trafficking can provide insights into the nature of pain signaling. Therefore, I analyzed a newly synthesized $Na_v1.7^{TAP}$ tagged mouse. The clear advantages of using a knock-in TAP-tagged mice over methods like Yeast-2-Hybrid is that background noise is reduced and sensitivity is increased as the endogenous expression of RNA and protein is mimicked *in vivo*, which limits the possibility of artefactual interactions. Also, the use of a small terminally located TAP-tag allows the detection of the tagged protein and interaction partners without further consideration of post-translation modifications or protein interactions. Additionally, through the use of the TAP-tag method instead of Yeast 2-hybrid assays, all interaction partners can be detected in one experiment (Puig, Caspary et al. 2001, Fernandez, Collins et al. 2009).

In the case of voltage-gated sodium channels, where family members share a high degree of sequence homology, the TAP method allows isoform specific isolation of $Na_v1.7$. Targeted insertion of a TAP-tag into $Na_v1.7$ enables us to breed homozygous mice ($Na_v1.7^{TAP/TAP}$). Here, $Na_v1.7^{TAP/TAP}$ mice have a normal phenotype and I found no evidence that TAP-tag insertion into $Na_v1.7$

alters RNA, protein expression or the electrophysiological properties of the channel. I examined the expression of the $Na_v1.7^{TAP/TAP}$ in various tissues, and found it to be highly expressed in DRG, olfactory bulb and to a lower extent in spinal cord, sciatic nerve and testis. However, I also found $Na_v1.7$ to be expressed in the hypothalamus/thalamus. This is consistent with recent findings from Black *et al.* (2013) that $Na_v1.7$ is present in supraoptic nuclei in the hypothalamus and is upregulated in response to osmotic stress (Black, Hoeijmakers et al. 2013). I also looked at the expression of TAP-tagged $Na_v1.7$ in the pancreas and could not detect any expression. This is in contradiction with findings from previous studies (Zhang, Chibalina et al. 2014), however as the pancreas is loaded with digestive enzyme, I cannot preclude that $Na_v1.7$ was not degraded prior to the analysis.

Until now, only a few protein-interaction partners of $Na_v1.7$ are known and it is unclear how the channel is trafficked to the plasma membrane. Through the use of a knock-in TAP-tag fused to $Na_v1.7$, I was able to isolate multiprotein complexes from primary DRG and olfactory neurons of $Na_v1.7^{TAP/TAP}$ mice. I identified a total of 164 proteins that were more than two-fold increased in $Na_v1.7^{TAP/TAP}$ samples compared to wild-type, 42 of which were specific in the $Na_v1.7^{TAP/TAP}$ group. I grouped the proteins according to their functional classes and cellular localization. $Na_v1.7^{TAP/TAP}$ samples were enriched in plasma membrane located ion channels, receptors and transporters as well as cytoplasmic resident enzymes but also uncharacterized proteins. In particular, *Scn3b, mTOR, Tmed10* and Aquaporin-1 that were highly enriched in $Na_v1.7^{TAP/TAP}$ sparked my interest. These genes have previously been reported to play a crucial role in protein synthesis, intracellular trafficking and pain processing.

β1-and β3-subunits are believed to associate with $Na_v1.7$ in the ER/Golgi and can mediate different glycosylation states and plasma membrane expression (Laedermann, Syam et al. 2013). The data revealed that $Na_v1.7$ is in complex with β3 and β4 but not β1 or β2 and through Co-IP, β3 (*Scn3b*) was verified as direct interaction partner of $Na_v1.7$. This is consistent with findings from Ho *et*

al. (2012) that in small diameter DRG neurons $Na_v1.7$ primarily interacts and co-localizes with β3 subunits in the periphery. As for *Scn4b* (β4), mRNA expression is low in both small and large diameter DRG neurons and does not correlate with expression of *Scn9a* in DRG (Ho, Zhao et al. 2012). However, as the samples contained pooled DRG and olfactory bulb extracts it is possible that $Na_v1.7$ in the olfactory bulb is associated with β3 and β4.
Strikingly, the mass spectrometry data obtained did not indicate an interaction between $Na_v1.7$ and Nedd-4 as reported by Laedermann *et al.,* (2013). I can only speculate that the lysis buffer (CHAPS) might have disrupted the interaction. Interestingly, mass spectrometry identified an E3 ubiquitin ligase, namely Neurl4, to be in complex with $Na_v1.7$.

In summary, I achieved the first purification of the $Na_v1.7$ protein-protein interaction complexes *in vivo* under native conditions and obtained a list of 164 enriched proteins, 42 of which were only found in $Na_v1.7$-TAP knock-in samples. Among those interaction partners, I identify and verified a previously described interaction partner of $Na_v1.7$. Additionally, I identified proteins in complex with $Na_v1.7$ that are implicated in pain processing but have not been described as interaction partners of $Na_v1.7$ before. For instance, I identified Aquaporin-1, a plasma membrane localized pore-forming protein that is found in the somata and in the peripheral and central branches of damage sensing neurons and has recently been implicated in nociception. *Aqp1*$^{-/-}$ mice exhibit decreased inflammatory and noxious cold responses as $Na_v1.8$ is a direct interaction partner of the channel. While $Na_v1.8$ mRNA and protein is significantly upregulated, Zhang and Verkman *et al.* (2010) did not find changes in *Scn9A* expression. They concluded that the impaired electrophysiological properties of $Na_v1.8$ but not $Na_v1.7$ are responsible for the *Aqp1*$^{-/-}$ phenotype in mice (Zhang and Verkman 2010). However, as seen in chapter 2, mRNA expression levels of *Scn9a* are unaltered in pain models of inflammatory and neuropathic pain (Koenig, Werdehausen et al. 2015) although it is reported that $Na_v1.7$ levels are increased. This may indicate that *Scn9a* is not newly transcribed but mRNA is stored intracellularly and released and translated

locally upon external stimulation, possibly through mTOR, another protein highly enriched in my TAP experiment.

Mass spectrometry also revealed uncharacterized proteins that interact with $Na_v1.7$. In the future, it will be interesting to further study the functionally known and uncharacterized interaction partners to gain a comprehensive picture of their significance in the $Na_v1.7$ interactome. Additionally it will be interesting to purify $Na_v1.7$ complexes from different tissues and under normal and pathological conditions, which may shed light on why seemingly genetically similar mutations have different phenotypes i.e. PE and PEPD and may help to understand if during chronic pain states different signal transduction complexes are recruited. Furthermore, a comprehensive understanding of which proteins normally interact with $Na_v1.7$ may help in the development of a new class of analgesic drugs.

4 A mouse model of inherited Primary Erythromelalgia

4.1 Summary

Inherited Primary Erythromelalgia (PE) is a rare autosomal dominant disease that is characterized by recurring episodes of excruciating pain, redness and swelling in the lower extremities that are induced by moderate exercise, warmth and humidity (Finley, Lindsey et al. 1992). PE is caused by *SCN9A* ($Na_v1.7$) gain-of-function mutations that alter the channel's electrophysiological properties and render the dorsal root ganglia neurons hyperexcitable. The line of treatment for congenital PE patients is very limited and to date the most effective strategy to alleviate pain is cooling of the affected areas. One of most common and best-studied PE mutations is L858F in $Na_v1.7$, which was first identified in a Chinese (Han, Rush et al. 2006) and Canadian family (Drenth, te Morsche et al. 2005). To further understand and investigate possible drug treatments for PE and chronic pain disorders that map to the *SCN9A* locus, I analyzed a newly developed transgenic mouse carrying the human $Na_v1.7$ L858F mutation (together with a C-terminal TAP-tag) that recapitulates the human primary erythromelalgia phenotype.

4.2 Introduction

Inherited primary erythromelalgia is a rare autosomal dominant neuropathy characterized by an early onset phenotype with painful reddened feet and hands. Painful episodes are induced by moderate physical exercise, long periods of standing and exposure to warm temperatures. In the later stages of inherited PE, affected individuals experience reoccurring episodes of persistent pain, redness and elevated temperatures of lower extremities, upper legs, feet, and also the hands (Cohen and Samorodin 1982, Finley, Lindsey et al. 1992, van Genderen, Michiels et al. 1993). Genome-wide linkage analysis in a three-generation Chinese family (Yang, Wang et al. 2004) first identified mutations in *SCN9A* to cause Primary Erythromelalgia. To date, all known PE mutations are gain-of-function mutations that lead to increased $Na_v1.7$ activity (Dib-Hajj, Rush et al. 2005, Harty, Dib-Hajj et al. 2006, Cheng, Dib-Hajj et al. 2008). The $Na_v1.7$

L858F mutation was first identified in a Chinese (Han, Rush et al. 2006) and Canadian family (Drenth, te Morsche et al. 2005) and is so far the most reported PE mutation. Here, a leucine residue at position 858 that encodes for a segment in the DII/S4-S5 pore region of $Na_v1.7$, is substituted for phenylalanine. Leucine in this position is highly conserved in all VGSCs and related sub-mammalian sodium channels (Han, Rush et al. 2006, Cregg, Cox et al. 2014). For instance, a mutation in $Na_v1.4$ in this region has been linked to cold-sensitive paramyotonia congenita (Plassart, Eymard et al. 1996). Voltage-clamp recordings show that functionally the $Na_v1.7$ L858F mutation lowers the channel's activation threshold. This in turns makes it easier to activate $Na_v1.7$. Simultaneously, L858F slows $Na_v1.7$ deactivation kinetics and increases the channel's response to slow ramp stimuli, thereby allowing more channels to be open for longer at a given time (Cummins, Dib-Hajj et al. 2004). Additionally, various reported mutations including L858F boost $Na_v1.7$'s recovery from inactivation (Han, Rush et al. 2006, Harty, Dib-Hajj et al. 2006, Cheng, Dib-Hajj et al. 2008). This renders DRG neurons hyperexcitable with activation thresholds shifting towards hyperpolarized potentials, increased frequency of repetitive firing and prolonged opening of the channel (Dib-Hajj, Rush et al. 2005). A correlation of clinical severity, age of PE onset and mutation has been reported with the greater the hyperpolarization shift due to the mutation, the earlier the PE age of onset (Han, Dib-Hajj et al. 2009, Cregg, Cox et al. 2014). Patients carrying a PE mutation, including L858F, report that cooling of the affected areas alleviates pain. Han *et al.* (2007) found that cooler temperatures (16°C) shift the activation threshold of $Na_v1.7$ L858F to more depolarized potentials. Most likely this effect is responsible for the cold mediated pain relief in PE (Han, Lampert et al. 2007).

Here, I ran a duplex Taqman assay for *TAP* and *GAPDH* to determine the transgenic $hNa_v1.7$ L858F copy number of founders and offspring. I found that the transgene was present in all founders with the highest number of integration in founder A. Immunoblotting showed that $hNa_v1.7$ L858F is only present in the transgenic animals and it is highly expressed in olfactory bulb, dorsal root ganglia and in lower levels in spinal cord. Behavioural tests on $hNa_v1.7$ L858F

mice show that motor function and levels of behavioural responses to acute noxious pain tests are normal. However, hNa$_v$1.7 L858F mice show increased nociceptive and inflammatory behavioural responses to the formalin test and elevated temperatures of the affected areas. Taken together, the human Na$_v$1.7-L858F mice mimic aspects of the human Primary Erythromelalgia phenotype.

4.3 Results

Generation of TAP-tagged Na$_v$1.7 L858F mouse

Transgenic mice carrying human Na$_v$1.7 with a L858F mutation (hNa$_v$1.7-L858F) were generated by Yury Bogdanov (Post-doctoral fellow, Molecular Nociception Group) using a recombineering protocol (Copeland, Jenkins et al. 2001). The backbone for the shuttle vector was constructed using a pCreERT2 plasmid (a kind gift from P. Chambon, Collège de France) (Metzger and Chambon 2001). The pCreERT2 plasmid was modified using PCR to insert mouse Na$_v$1.7 5'-and 3'-homology arms that span from exon 2 to intron 2-3. The CreERT2 sequence was then excised while preserving a FRT-flanked Kanamycin selection cassette. The L858F mutation was induced in human Na$_v$1.7 cDNA using PCR with primers carrying the point mutation, before being inserted into the shuttle vector (Figure 4-1,a) The resulting shuttle vector contained a cassette expressing hNa$_v$1.7-L858F cDNA and a *kanamycin* resistance gene in place of mouse Na$_v$1.7 exon 2. The complete shuttle vector was fully sequenced before being incorporated into BAC clone RP23-304D3, which contains exons 1 to 7 of the mouse Na$_v$1.7 gene as well as regulatory sequence 5'-upstream of the gene. The integrity and the absence of recombination within the BAC clone was confirmed by PCR, restriction analysis and pulse-field gel electrophoresis (Figure 4-1, b-c). The BAC vector containing hNa$_v$1.7-L858F was purified and sent to Cyagen Biosciences for microinjection into mouse oocytes. A total of 4 founders were identified using PCR screening, with the progeny of founder 'A' being used for subsequent experiments.

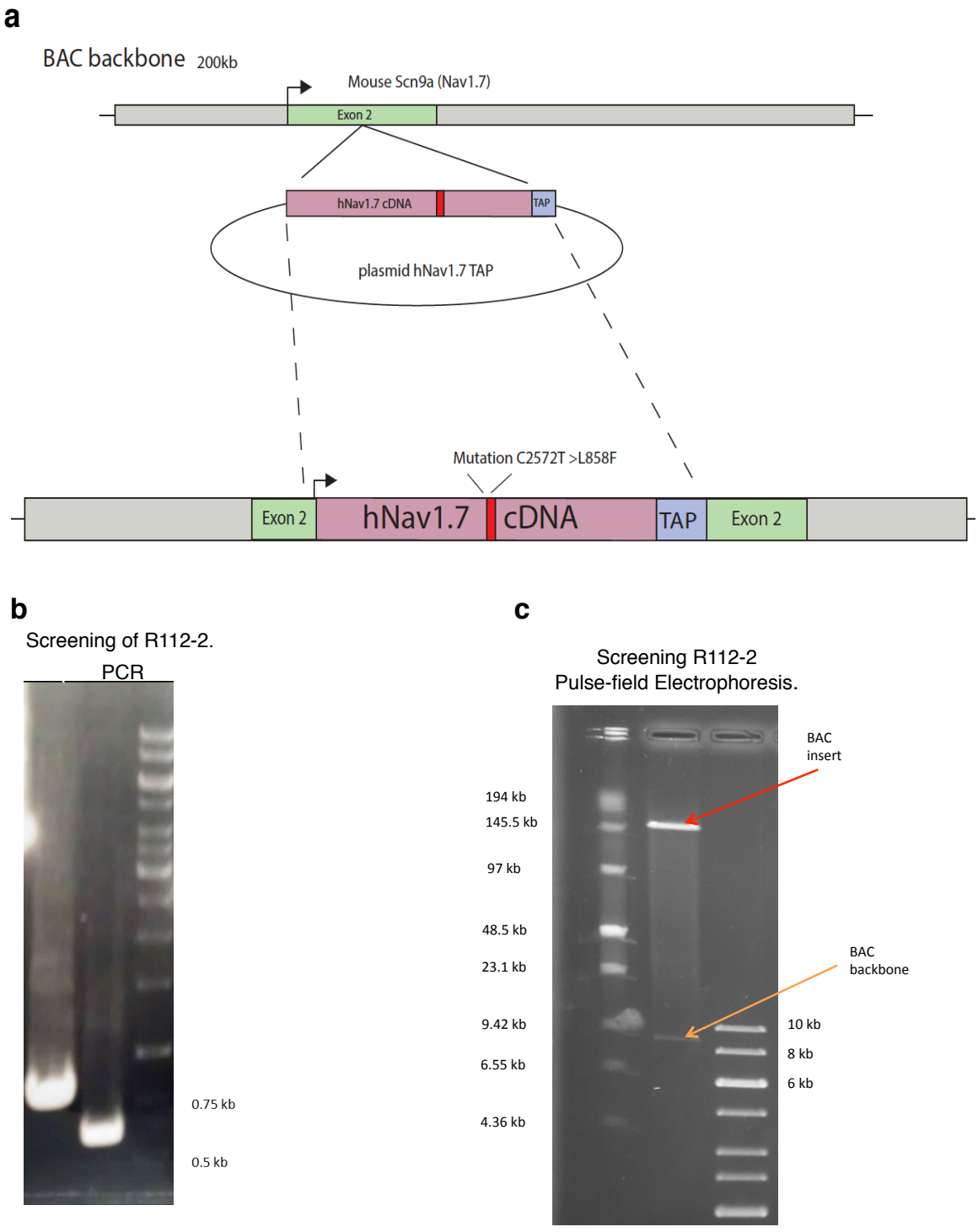

Figure 4-1: Generation of TAP-tagged $Na_v1.7$ L858F mouse.

(a) Shuttle vector containing a cassette expressing $hNa_v1.7$-L858F cDNA and *kanamycin* resistance gene was inserted in mouse $Na_v1.7$ exon 2. The integrity and the absence of recombination within the BAC clone was confirmed by **(b)** PCR **(c)** restriction analysis and pulse-field gel electrophoresis. Performed by Dr. Yury Bogdanov.

Transgenic copy number estimation using real-time qPCR

Traditionally, Southern blotting is used to estimate DNA copy numbers in transgenic animals. However this method strongly depends on a variety of parameters and optimization of these parameters can be a time consuming and costly procedure. Real-time PCR based estimation of transgenic copy numbers provides a fast, inexpensive and high throughput tool to assess copy numbers in transgenic animals and plants (Ingham, Beer et al. 2001, Alexander, Erwin et al. 2004, Chandler, Chandler et al. 2007, Yuan, Burris et al. 2007). Here, I used the quantitative ΔΔCt method (Livak and Schmittgen 2001) to determine the transgenic copy number of human $Na_v1.7$ L858F-TAP in mice by comparing the genomic TAP integration to a calibrator with a known TAP copy number. The ΔΔCt method requires a similar amplification efficacy of transgene (*TAP*) and internal reference gene (*Gapdh*), and a calibrator with known copy number (*TAP*) (Ballester, Castello et al. 2004, Yuan, Burris et al. 2007). I determined the efficiency of the customized TaqMan primers for *TAP* tag (FAM, labeled) and TaqMan assay *Gapdh* (VIC/MGB labeled, limited) by setting up a standard curve of genomic DNA (see Methods 6.1.3.3). The efficiencies were calculated from the standard curve with E_{TAP} (2.15) and E_{Gapdh} (1.97) (Figure 4-2, Top). As calibrator I used a Southern blot verified heterozygous one copy TAP tagged $Na_v1.7$ knock-in mouse. Copy number was calculated by comparing ΔCt values of *TAP* in PE mice to the ΔCt value of *TAP* calibrator (see Method 6.1.3.2), resulting in a specific ΔΔCT value. The final copy number was calculated as 2X RQ ($RQ = 2^{-\Delta\Delta CT}$)

In total four founders (A, C, D, E) and 34 transgenic mice from breeding lines A2, A3 and F1 were tested by multiplex qPCR for *TAP* and *Gapdh* expression. ΔCt values for each transgenic mouse and the calibrator were determined by normalization of TAP Ct (threshold cycle) to the reference gene Gapdh Ct:

$$\Delta Ct\ (TAP) = Ct\ (TAP, FAM) - Ct\ (Gapdh, VIC/MGB)$$

ΔΔCt was calculated by subtraction of the calibrator ΔCt from the average ΔCt for each sample (from duplicates):

$$\Delta\Delta Ct\ (TAP) = \Delta Ct\ (TAP, unknown) - \Delta Ct\ (TAP, calibrator)$$

The fold-change in copy number for the transgenic samples was evaluated using relative quantification (RQ) = $2^{-\Delta\Delta Ct}$ and final copy number is 2X RQ (Livak and Schmittgen 2001) (Figure 4-2, bottom).

Based on the ΔΔCt method I estimated the copy numbers of founder A to be 7 copies (± 0.42SD), founder C 3 copies (±0.34SD), founder D 1 copy (± 0.01SD) and founder E 3 copies (± 0.18SD) (Figure 4-2,bottom). 34 transgenic $Na_v1.7$ L858F mice were tested from line A2, A3 and F1 and around 20 per cent (n=6) had no detectable copies of $Na_v1.7$ L858F TAP, more than 30 per cent (n=12) had 1-2 copies, 20 per cent (n=7) had 3-4 copies of the transgene and around 30 per cent of the mice had > 5 copies of the transgene (n=9) (Figure 4-3,A). Furthermore, I verified the expression of TAP-tagged *SCN9A* by PCR genotyping (Figure 4-3, B).

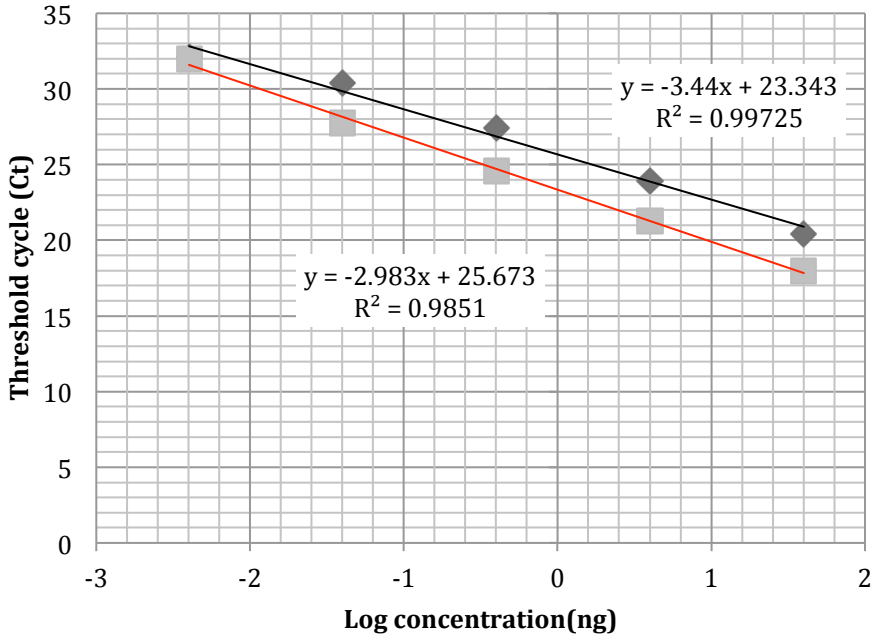

Founder	Avg. ΔΔCt ΔCt (*TAP*) - ΔCt (*calibrator*)	Avg. $2^{-\Delta\Delta Ct}$ (RQ)	Estimated Copy number 2 X (RQ) ± SD
A	-1.84	3.584	**7 ± 0.42**
C	-0.56	1.479	**3 ± 0.34**
D	1.71	0.306	**1 ± 0.01**
E	-0.61	1.52	**3 ± 0.18**

Figure 4-2: Standard curve and transgenic copy number estimation

Top I Standard curve *TAP* (red) and *Gapdh* (black) TaqMan primers. Delta Ct plotted against the log (concentration/ng). **Bottom I** Copy number estimation of $Na_v1.7$ L858F founders using relative quantification ΔΔCt method. Copy number is determined by a series of calculations. ΔCt is calculated by subtracting the *Gapdh* Ct from the *TAP* Ct for each replicate. The average ΔCt from the 3 replicates was then calculated. $Na_v1.7$ TAP-tag knock-in mouse with a single copy was used as calibrator for the $Na_v1.7$ L858F TAP-tag copy number estimation. ΔCt from each unknown DNA sample was normalized to the calibrator to determine the ΔΔCt. Relative quantity (RQ) is $2^{-\Delta\Delta Ct}$, and finally copy number was obtained by 2 X RQ and ± 2 X SD (Livak and Schmittgen 2001).

Co-Immunoprecipitation of hNa$_v$1.7 L858F

Next, I examined the protein expression in the newly developed hNa$_v$1.7 L858F TAP-tagged mouse line through the use of the integrated TAP-tag. The TAP-tag construct consists of a 3XFLAG tag, a TEV protease cleavage site and a HAT-domain (Puig, Caspary et al. 2001) that was inserted C-terminally before the stop coding of exon 28 in human Na$_v$1.7. Up to now it has been very challenging to examine the distribution of specific subtypes of voltage-gated sodium channels due to the high degree of homology among family members. Hence, this Na$_v$1.7 L858F TAP-tagged mouse allows the isoform specific isolation of Na$_v$1.7.

First, I compared the DRG protein expression of a transgenic TAP-tagged hNa$_v$1.7 mouse to a littermate control. I found that TAP-tagged Na$_v$1.7 is only expressed in the transgenic animal and can be detected with antibodies (Figure 4-3, c).

Next, I examined the channel's expression in different tissues. It was previously reported that in rodents and humans, Na$_v$1.7 is mainly expressed in small diameter nociceptive DRG neurons (Toledo-Aral, Moss et al. 1997) and olfactory neurons (Weiss, Pyrski et al. 2011) but was also found in lower expression levels in other peripheral tissues**.** Therefore I collected six tissues including DRG and olfactory bulb from a hNa$_v$1.7 L858F TAP-tagged mouse, co-immunoprecipitated the samples with anti-FLAG and immunoblotted them with an anti-HAT antibody (see Methods 6.5.4, 6.5.5 and 6.5.7). I found that Na$_v$1.7 is highly expressed in olfactory bulb and to a lower extent in DRG and spinal cord but besides these three tissues, expression of Na$_v$1.7 was absent in tissues such as heart, liver and cerebellum (Figure 4-3,d). Interestingly, immunoblotting of Na$_v$1.7 in dorsal root ganglia showed two band sizes (at 260 and 280 kDa) that are believed to be the result of glycosylation states (Laedermann, Syam et al. 2013).

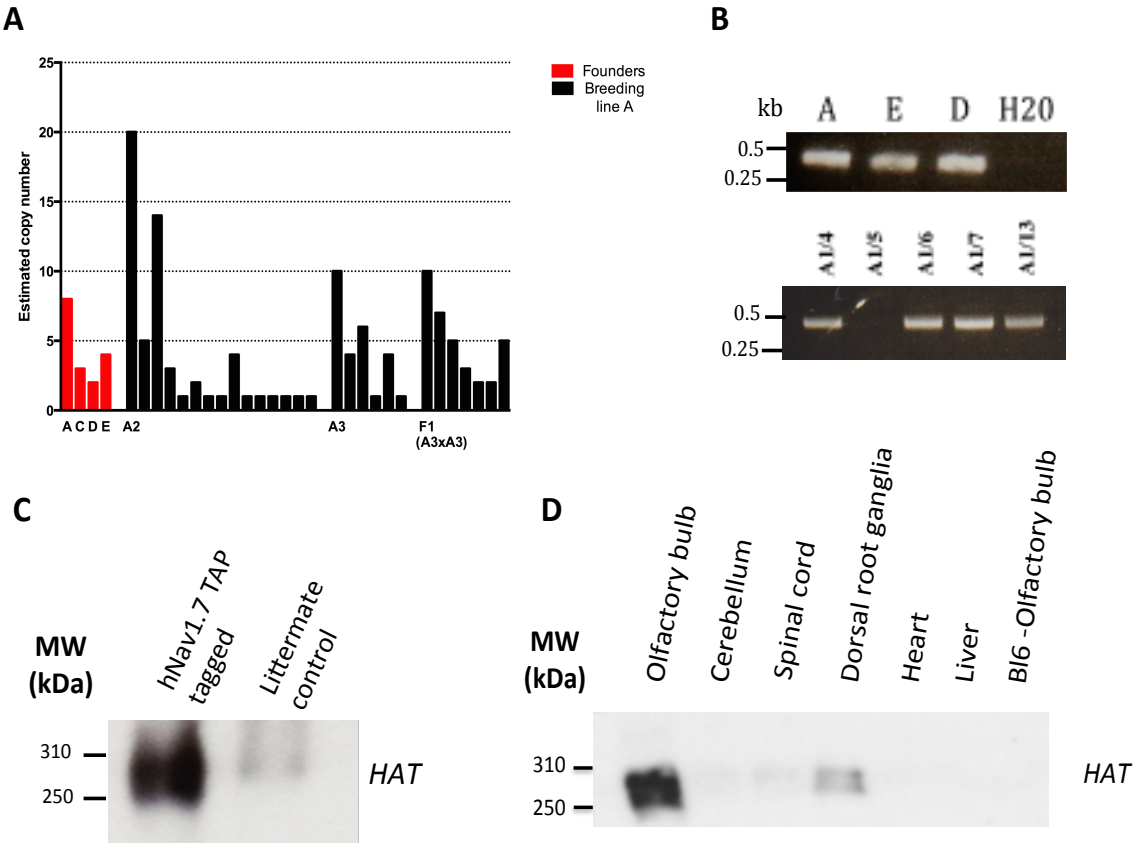

Figure 4-3: hNa$_v$1.7L858F TAP mice show normal expression of RNA and protein

(A) Transgenic copy number estimation for offspring of Founder A. In total 4 founders and 34 animals were tested for the expression of hNa$_v$1.7 L858F TAP-tag. 20 per cent were negative for the transgene, more than a third had the transgene integrated in 1-2 copies, 20 per cent had 3-4 copies and more than 30 per cent of all tested animals had >5 copies **(B)** Genotyping of hNa$_v$1.7 L858F TAP founders and offspring **(C)** Co-Immunoprecipitation of hNa$_v$1.7 TAP-tagged protein from DRGs of transgenic and littermate control mice **(D)** Co-Immunoprecipitation of human Na$_v$1.7 L858F TAP-tag with anti-FLAG and immunoblotting with anti-HAT shows that Na$_v$1.7L858F TAP-tagged protein is only expressed in transgenic hNa$_v$1.7 L858F TAP-tag mice with an estimated size of 260-280 kDa. Na$_v$1.7 is expressed in olfactory bulb, dorsal root ganglia and spinal cord, besides these three tissues expression of Na$_v$1.7 was not detected in tissues such as heart, liver and cerebellum.

Behavioural tests of hNa$_v$1.7 L858F mice

Behavioural tests were performed by Mike Minett, Post-doctoral fellow, Molecular Nociception group (see Methods 6.4.3) to determine whether the pain phenotype seen in the transgenic mice recapitulates primary erythromelalgia. The Rotarod test showed that hNa$_v$1.7 L858F mice have normal motor function when compared to wildtype littermate mice (Figure 4-4,A). Behavioural responses of hNa$_v$1.7 L858F (red columns, n=8) and littermate (white columns, n=11) mice to the: von Frey test – hindpaw and abdomen (Figure 4-4,B), Randall-Selitto test applied to the tail and hindpaw (Figure 4-4,C), Hargreaves' test – 0.6°C.s^{-1} and 2.0°C.s^{-1} heat ramps (Figure 4-4,D), Hotplate test – 50°C and 55°C (Figure 4-4,E) and Acetone test (Figure 4-4,F) all showed no significant difference between transgenic and littermate control mice. Furthermore the body weight of hNa$_v$1.7 L858F mice and core body temperature were also not significantly different from littermate controls (Figure 4-4,G-H). However, hNa$_v$1.7 L858F mice showed a significant avoidance of stimuli approaching the noxious heat threshold in comparison to littermate controls in the thermal place preference test (Figure 4.4,I). The hNa$_v$1.7 L858F mice also showed significantly more nociceptive behaviours following intraplantar injection of formalin in both the first and second phase (Figure 4-5,A-B)(see Methods 6.4.1). Also, hNa$_v$1.7 L858F mice showed an increase in hind paw temperatures (Figure 4-4,H and 4-5,C).

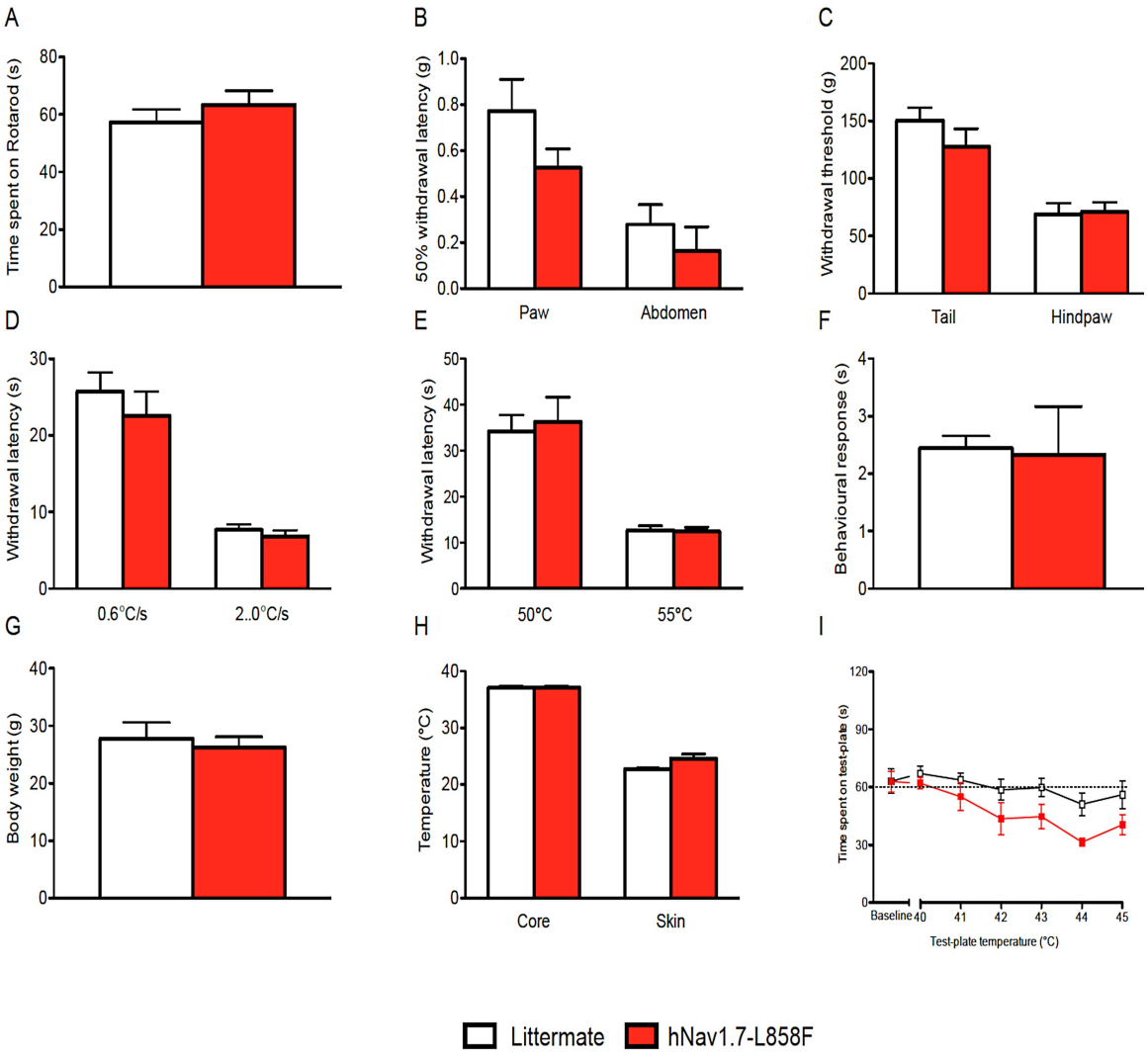

Figure 4-4: hNa$_v$1.7 L858F mice show normal behavioural responses to acute noxious pain tests.

Behavioural responses of hNav1.7 L858F (red columns, n=8) and littermate (white columns, n=11) mice to the: **(A)** Rotarod test, **(B)** von Frey test – hindpaw and abdomen, **(C)** Randall-Selitto test – tail and hindpaw, **(D)** Hargreaves' test – 0.6°C.s^{-1} and 2.0°C.s^{-1} heat ramps, **(E)** Hotplate test – 50°C and 55°C, **(F)** Acetone test, **(G)** body weight. **(H)** hNa$_v$1.7 L858F mice (red columns, n=6) show an increased hindpaw skin temperature but not core body temperature in comparison to littermate mice (white columns, n=6). **(I)** hNa$_v$1.7 L858F mice (red squares, n=7) significantly avoid pre-noxious heat temperature in the thermal place preference test in comparison to littermate mice (white squares, n=9). Data analysed by t-test, except (i) analysed by two-way analysis of variance followed by a Bonferroni post-hoc test. Results are presented as mean ± S.E.M.

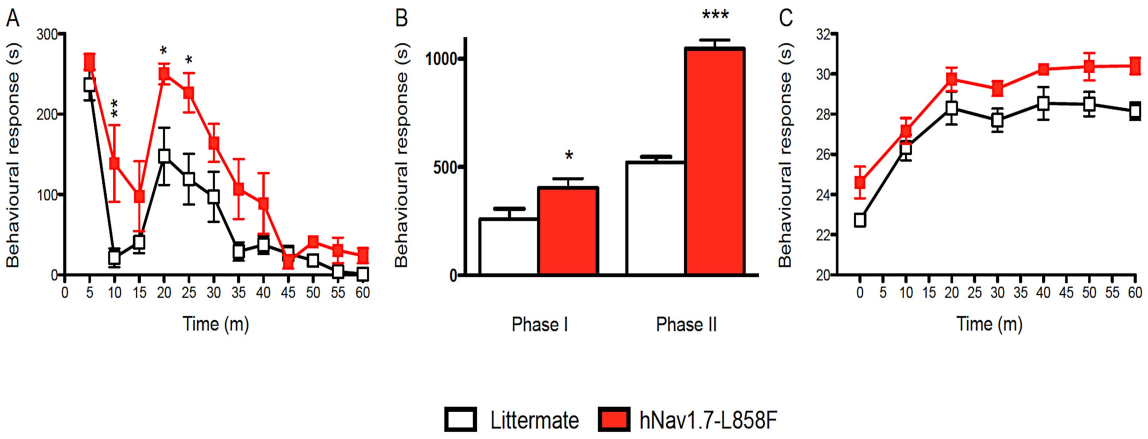

Figure 4-5: hNa$_v$1.7 L858F mice show increased nociceptive behaviours in response to the formalin test.

(A) hNa$_v$1.7 L858F mice (red columns, n=6) show increased nociceptive behaviours in comparison to littermate mice (white columns, n=6) following intraplantar injection of formalin. **(B)** hNa$_v$1.7 L858F mice (red columns, n=6) show increased nociceptive behaviours during both phase I & II in comparison to littermate mice (white columns, n=6). **(C)** hNa$_v$1.7 L858F mice (red columns, n=6) show increased hindpaw skin temperature at baseline and throughout the formalin test in comparison to littermate mice (white columns, n=6). Data analysed by two-way analysis of variance followed by a Bonferroni post-hoc test. Results are presented as mean ± S.E.M. * $P < 0.05$, *** $P < 0.001$

Next, I was interested if the number of integrated transgenic Na$_v$1.7L858F copies impacts the pain thresholds of hNa$_v$1.7L858F mice. Na$_v$1.7L858F is an autosomal dominant mutation and individuals who carry one copy of the mutated gene suffer from painful episodes. I hypothesized that a high number of transgenic hNa$_v$1.7 L858F copies might translate into an increased number of mutant Na$_v$1.7 channels expressed. This in turn could potentially increase the pain-related behaviour in transgenic animals. Therefore the behavioural responses of hNa$_v$1.7 L858F mice with high (more than 5 copies) and low (1-2 copies) transgenic copy numbers were compared to littermate controls.

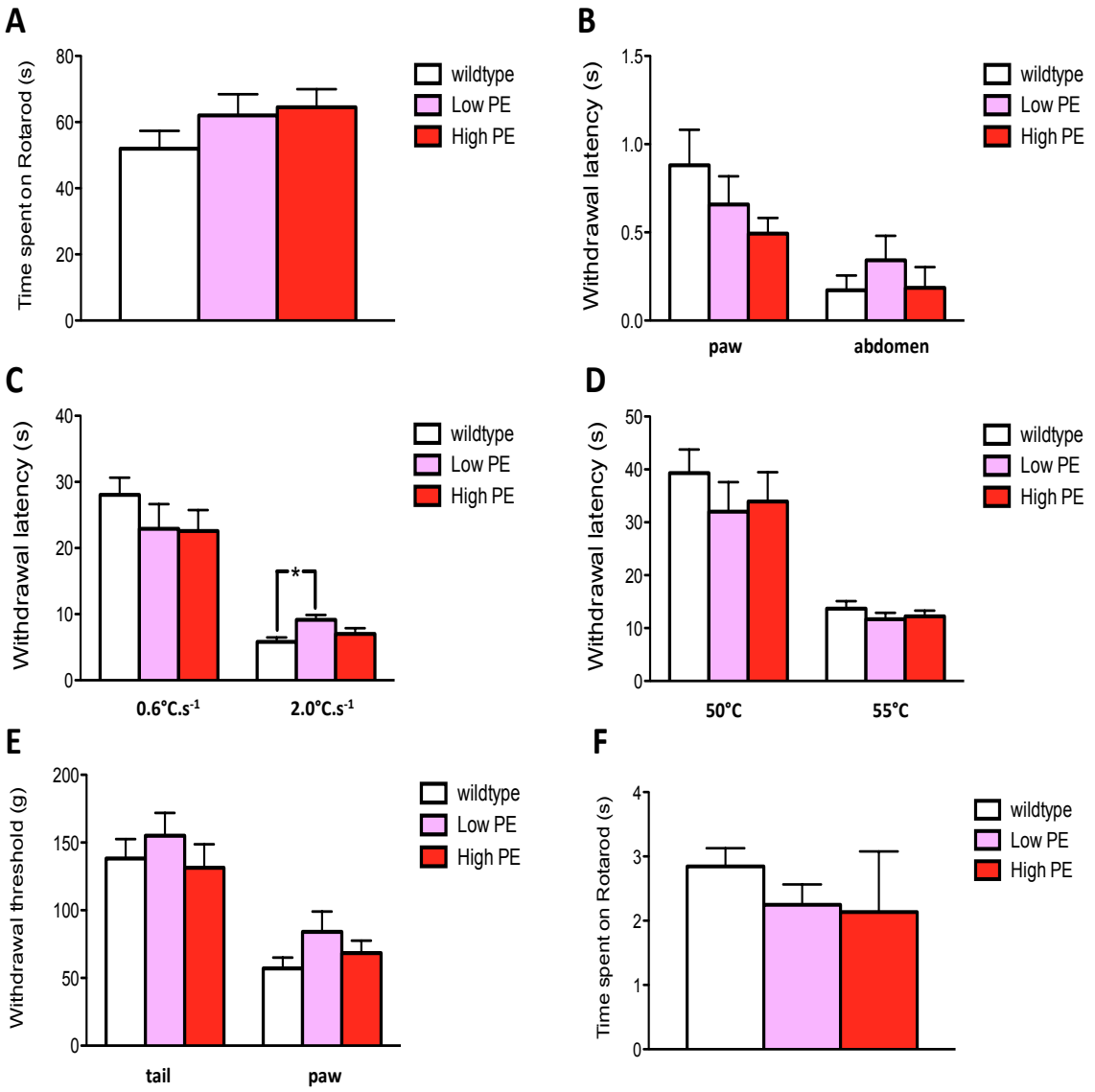

Figure 4-6: hNa$_v$1.7 L858F mice show normal behavioural responses to acute noxious pain tests independently of transgenic copy number

Behavioural responses of hNav1.7 L858F mice with high copy number (red columns, more than 5 copies, n=5), low copy number (pink column, 1-2 copies, n=5) and littermate control (white columns, n=5) mice to the **(A)** Rotarod test, **(B)** von Frey test – hindpaw and abdomen, **(C)** Hargreaves' test – 0.6°C.s^{-1} and 2.0°C.s^{-1} heat ramps, **(D)** Hotplate test – 50°C and 55°C, **(E)** Randall-Selitto test – tail and hindpaw, **(F)** Acetone test. Data were analysed by t-test and results are shown as mean ± S.E.M. (Experiments were performed by Michael Minett.)

In the Rotarod test $hNa_v1.7$ L858F mice, independently of the transgenic copy number, showed normal motor function when compared to wildtype littermate mice (Figure 4-6,A). Furthermore, the behavioural responses of $hNa_v1.7$ L858F with a high number of transgene copies (red columns, n=5), low number of copies (pink columns, n=5) and littermate (white columns, n=5) mice to the von Frey test – hindpaw and abdomen (Figure 4-6,B), Hargreaves' test – $0.6°C.s^{-1}$ (Figure 4-6,D) Randall-Selitto test applied to the tail and hindpaw (Figure 4-6,E), Hotplate test – 50°C and 55°C (Figure 4-6,D) and Acetone test (Figure 4-6,F) all showed no significant difference between transgenic, and littermate control mice independently of the transgenic copy number. However, in the Hargreaves' test at $2.0°C.s^{-1}$, heat ramps (Figure 4-6,C) $hNa_v1.7$L858F mice with a low but not a high number of copies showed an increase in behavioural response when compared to the littermate control.

Humans with PE suffer from on-going and/or episodic pain that is triggered by heat and moderate exercise, while Quantitative Sensory Testing shows that sensory detection and pain thresholds are within two standard deviations of unaffected individuals (Segerdahl, Xie et al. 2012). The data suggest that TAP tagged $hNa_v1.7$ L858F mice have a phenotype that resembles aspects of the human PE phenotype. Akin to human PE patients with L858F, as well as other gain-of-function mutations, report that pain is exacerbated by warmth, exercise and local exposure to heat (Yang, Wang et al. 2004, Segerdahl, Xie et al. 2012) and skin temperature of the affected area during painful episodes is measurably increased (Samuels, te Morsche et al. 2008).

4.4 Discussion

Inherited Primary Erythromelalgia (PE or IEM) is a rare autosomal dominant disease caused by mutations in *SCN9A*. To date, all known *SCN9A*-related PE mutations are gain-of-function mutations that shift the $Na_v1.7$ threshold of activation and increase neuronal excitability. The best-studied and most commonly reported mutation in $hNa_v1.7$ is L858F (Cummins, Dib-Hajj et al. 2004, Drenth, te Morsche et al. 2005, Han, Rush et al. 2006). Here, a conserved leucine residue at position 858 within exon 15 of *SCN9A* (segment in the DII/S4-S5 pore region) is substituted for phenylalanine (Han, Rush et al. 2006, Cregg, Cox et al. 2014). Functionally the L858F mutation in $Na_v1.7$ lowers the channel's activation threshold, slows its deactivation kinetics while simultaneously boosts recovery from inactivation and increases the channel's response to slow ramp stimuli, thereby allowing more channels to be activated easier and to be open for longer (Cummins, Dib-Hajj et al. 2004, Han, Rush et al. 2006, Harty, Dib-Hajj et al. 2006, Cheng, Dib-Hajj et al. 2008). This in turn leads to hyperexcitability of DRG neurons. A correlation of clinical severity, age of PE onset and mutation has been reported and the greater the hyperpolarization shift induced by the mutation, the earlier the PE age of onset and severity (Han, Dib-Hajj et al. 2009, Cregg, Cox et al. 2014).

Clinical symptoms and treatment of inherited primary erythromelalgia

Clinically, inherited primary erythromelalgia (PE) is characterized by recurring episodes of painful reddened feet, lower legs and in some cases the upper extremities. Painful episodes are accompanied by elevated skin temperature and swelling of the affected areas. Other symptoms may include dry mouth, eyes and gastro-intestinal problems (Drenth and Waxman 2007). Generally, episodes are provoked by moderate exercise, warmth, eating hot, spicy food, wearing tight shoes or drinking alcohol (Samuels, te Morsche et al. 2008). Typically the first symptoms appear in early childhood or adolescence (Mandell, Folkman et al. 1977, Michiels, te Morsche et al. 2005) but there are rare cases of late onset PE (Gaur and Koroscil 2009). Over the course of PE, the symptoms, length and intensity of episodes steadily increase (Finley, Lindsey et

al. 1992, van Genderen, Michiels et al. 1993). hNa_v1.7 L858F is a temperature sensitive mutation and reportedly patients cool the affected areas (i.e. ice buckets or fan) to alleviate pain. Han *et al.* (2007) showed that cooler temperatures (below 16°C) shift the activation threshold of Na_v1.7 L858F to more depolarized potentials (Han, Lampert et al. 2007). Although cooling is a very effective analgesic, possible secondary complications include skin infections and in severe cases gangrene (Gaur and Koroscil 2009). Besides the severe pain, PE patients exhibit no neurological deficiency and quantitative sensory testing (QST) is within 2SD of unaffected individuals. However Segerdahl *et al.* (2012) found that affected individuals exhibit decreased sensitivity to deep pressure and vibration in the feet. It was concluded that these altered thresholds were caused by thickened skin, a phenomena which is commonly observed in PE patients (Segerdahl, Xie et al. 2012).

In common with human PE individuals, the newly generated hNa_v1.7 L858F TAP tagged mice exhibit normal weight and no obvious neurological deficiency. Furthermore, there was no altered response to acute pain tests or any evidence of motor coordination deficiencies. However, hNa_v1.7 L858F TAP mice show avoidance of pre-noxious temperatures, which is consistent with previous reports of human PE patients, as warm temperatures are a known trigger of painful episodes. Strikingly, withdrawal latency in hotplate testing (50-55^{o}C) for noxious heat was unchanged between littermate controls and hNa_v1.7 L858F mice. One possible explanation is that at noxious temperatures of around 50-55 degrees, a distinct molecular mechanism is in place that is independent of Na_v1.7. This is contradictory to prior findings in $Na_v1.7^{Nav1.8}$ mice (Nassar, Stirling et al. 2004, Minett, Nassar et al. 2012). However, I cannot be sure that this randomly inserted human gene will be regulated and processed in the same way as the endogenous gene (e.g. the *SCN9A NAT* is not included in the transgenic design). Although I showed that the transgene exhibits a normal transmission pattern, and *SCN9A* mRNA and Na_v1.7L858F protein are normally expressed, the question remains whether the human protein was sufficiently trafficked and correctly inserted into the membrane. Strikingly, I also did not find

a correlation between copy number and severity of pain related behaviour (Figure 4-6). PE is an autosomal dominant disease, therefore one copy of the gene should be sufficient to see a pain related phenotype.

However, hNa_v1.7 L858F mice show significantly increased pain related behavior and increased hindpaw temperatures compared to littermate controls in the first and second phase of formalin, which supports the idea that the human Na_v1.7 L858F transgene produces a functional membrane localized protein. Therefore an initial trigger might be required to see the full spectrum of behaviour responses in Na_v1.7 L858F mice.

In summary, I analyzed a transgenic hNa_v1.7 L858F TAP-tag mouse that resembles aspects of the human inherited Primary Erythromelalgia phenotype. This mouse model (hNa_v1.7 L858F-TAP) will allow us to further study the effects of drug treatments. Current medical treatment of inherited primary erythromelalgia is challenging and no single effective drug treatment is available. Generally individuals suffering from painful episodes often receive individualized treatment and medication depending on their medical history (Davis, Sandroni et al. 2003). Drugs that are most commonly used and proven effective in some PE patients are: Aspirin, SNRIs (serotonin-norepinephrine reuptake inhibitors) and SSRI (selective serotonin reuptake inhibitors) and other anti-depressants, sodium channel blockers, carbamazepine and others (Hisama, Dib-Hajj et al. 1993). This mouse model of human primary erythromelalgia will allow us to further our understanding of the molecular mechanisms underlying pain processing. The TAP tag inserted in the final exon of the transgene will allow the tissue specific purification of Na_v1.7 L858F and protein interaction partners and might shed light on why PE and PEPD, two inherited pain disorders linked to gain of function *SCN9A* mutations, affect different areas and why clinical symptoms vary significantly between PE and PEPD.

5 Conclusions and Future work

The work in this thesis has aimed to provide a more detailed understanding of the functional regulation and expression of *SCN9A*/$Na_v1.7$. Firstly, in Chapter 2, I showed that *SCN9A*/$Na_v1.7$ expression is specifically controlled by a naturally occurring, long non-coding RNA (or *NAT),* which might be physiologically relevant in human pain disorders that map to the *SCN9A* locus. I demonstrated that *in vitro* the *NAT* regulates *SCN9A*/$Na_v1.7$ expression and electrophysiological properties in an isoform specific manner. Therefore, *in vivo* study of the *NAT* i.e. through injection of a viral construct containing the mouse natural antisense transcript, will be necessary to determine if overexpression of the transcript potentially reduces pain related behaviour. Studies in humans and mice have shown that $Na_v1.7$ is crucial for initiation and propagation of action potentials. The channel functions as a threshold and amplifier of initial membrane depolarisations and is required for the activation of $Na_v1.8$ which is non-redundant in the uprising phase of the action potential. A 30 percent decrease in $Na_v1.7$ expression, as shown in chapter 2*,* could prove sufficient to prevent the activation of $Na_v1.8$ and in this way inhibit the action potential from firing off. Additionally, through the use of CRISPR/Cas9 technolgy a *NAT* knockout mouse line will be generated where exon 1 in *NAT* is deleted. This deletion will disrupt the *NAT* transcription and enables us to study the impact on *NAT* ablation on *Scn9a* RNA and protein distribution *in vivo*. Based on my findings highlighted in Chapter 2, I speculate that ablation of *NAT in vivo* will result in a painful phenotype in the *NAT* knockout mice.

Another aspect that merits further investigation is *NAT* splice variants and their individual role in *Scn9A* expression. *Scn9a* is alternatively spliced in two mutually exclusive sites in exon 11 and exon 5 (Raymond, Castle et al 2009). For instance, the alternative splice variants 5N and 5A from exon 5, are significantly different in their electrophysiological properties and expression patterns i.e. 5N is a neonatal splice variant. The exact purpose of a neonatal 5N splicing variant is not yet fully understood. Although splicing patterns of *NAT* and *Scn9a* do not appear to be coupled as reported for other *NATs* i.e. *Kcna2* antisense RNA and *Kcn2a* (Zhao, Tang et al 2013). There is the possibility that

the alternative splicing of *NAT* potentially shifts the splicing events in *SCN9A*. The proposed mechanism is that the expression of a particular antisense transcript variant could either stabilize the neonatal or adult sense transcript in a tissue specific manner, or binding may mask the splicing site of the sense mRNA and therefore represses the neonatal splicing variant in favor of the adult one.

Strikingly, my in vivo studies showed no change in total expression of *NAT* or *Scn9a* in neuropathic and inflammatory models. This is interesting given the fact that the protein levels of $Na_v1.7$ are reportedly increased in carrageenan induced inflammatory pain (Black, Liu et al. 2004). Zhao, Tang *et al* (2013) found that *Kcna2* antisense transcript is expressed in medium sized DRG neurons. However, nerve injury not only upregulated the expression of the *Kcna2 NAT in vivo* but also shifted the *NAT* distribution in DRG subpopulations from mostly medium, to medium and large sized damage sensing neurons. Hence this shift in subpopulation distribution could potentially be the case for Scn9a *NAT* and would explain the unchanged mRNA levels in the pain induced mouse models. Therefore, using RNA-seq could be most helpful to study the distribution patterns of the *NATs* and *Scn9a* with the aim of understanding the dynamic expression of *NAT* and *Scn9a* within subpopulations of damage-sensing neurons in pathological pain states.

Finally, how is the expression of the *NAT* induced *in vivo*? In this thesis I examined the regulatory effects of *NAT* expression on *SCN9A*/$Na_v1.7$. However, in the future it will be important to understand what induces the transcription of the *NAT* itself. To answer this question, further structural investigation is required to identify transcription start sites and promoter regions in the transcripts. In-silico analysis of *NAT* sequences through online search tools such as TFsearch could give clues on possible transcriptional activators that bind to these regions.

In Chapter 3, I describe a newly developed TAP-tagged $Na_v1.7$ knock-in line that enabled me to purify $Na_v1.7$ and its protein-interaction partners under physiological conditions. This study provides the first comprehensive large-

scale analysis of $Na_v1.7$ protein complexes. This is particularly exciting as until now very little was known about the $Na_v1.7$ protein interactome and the role these interaction partners play in the trafficking and regulation of the channel. As shown in chapter 3, some protein interaction partners found through my TAP experiment have previously been shown to be implicated in nociception and pain processing i.e. mTor and Aquaporin-1, but have not been associated with $Na_v1.7$. However, as tandem affinity purification isolates all direct and indirect interaction partners of the TAP-tagged protein, the isolated proteins need to be verified as direct interaction partners of $Na_v1.7$. There are various ways to test for the direct interaction of proteins. One possible approach, as shown in chapter 3, is Co-IP of $Na_v1.7$ and immunostaining against the protein of interest. This allowed for the confirmation of the direct interaction between $Na_v1.7$ and *Scn3b* and also validated our TAP-tagged approach as *Scn3b* has previously been shown to directly interact with the channel to influence trafficking and glycosylation of $Na_v1.7$ (Laedermann, Syam et al. 2013). Other approaches to verify and study direct interaction between two proteins are Yeast 2-hybrid and fluorescence resonance energy transfer (FRET). Notably, my mass spectrometry data also revealed various mitochondrial proteins in complex with $Na_v1.7$. There are no reports of $Na_v1.7$ being expressed in the mitochondrial membrane or $Na_v1.7$ interactions with mitochondrial proteins. I speculate that these proteins are possibly indirect interaction partners of the channel. However, as some mitochondrial proteins are encoded by nuclear genes and also translated and folded in the ER/Golgi, they could potentially directly assemble with $Na_v1.7$ in the ER/Golgi and in this way influence the channels' trafficking and function. Further investigation into the direct interaction of $Na_v1.7$ with these proteins will shed light on a possible mechanism.

Taken together, studying these interaction partners will help to gain insights into how $Na_v1.7$ is trafficked to the plasma membrane under normal and pathological conditions and may lead to the discovery of a potential new analgesic drug target.

Finally, Chapter 4 of this thesis described the characterization of a newly developed transgenic mouse model of human primary erythromelalgia (PE), a rare pain disorder. In this chapter I investigated the transgenic integration of hNav1.7L858F and corresponding behavioral response to acute, neurogenic and inflammatory pain and found that the PE mouse model resembles in some aspects the human PE phenotype. Akin to human PE patients, in transgenic PE mice an initial trigger is required to induce painful episodes. For instance, injection of formalin increases the pain-mediated behavioral response in transgenic PE mice. However, it is still unclear why the transgenic mice did not respond to the hotplate test. In human PE sufferers, warm temperatures are the most common trigger for a painful episode. Another finding was that the number of transgenic $hNa_v1.7L858F$ copies had not impact the response to acute pain. The question remains if the transgene is processed and integrated in a similar manner to the endogenous $Na_v1.7$. Further investigation into the expression and function of $hNa_v1.7L858F$ via immunohistochemistry and electrophysiological recordings will be necessary to answer these questions.

In the past, transgenic animal studies have provided pivotal insights into the molecular and cellular mechanisms underlying nociception. This in turn has opened up exciting prospects in the design of new analgesic drugs. Therefore, a transgenic PE model offers the advantage of an in-depth analysis of the molecular mechanisms underlying nociception and pain sensation in PE, as well as the opportunity to test newly developed analgesic drugs *in vivo*.

6 Material and Methods

6.1 Molecular biology

6.1.1 Reagents, cloning and kits

Gels, LB and plates

- **Agarose gel** 1%, 1.8 g agarose (Sigma) in 180ml 1x TAE Buffer
- **LB** 10 g LB broth (Sigma) in 500ml ddH_2O and autoclaved for 20 min at 121 degrees
- **LB Agar** 10 g LB (Sigma) and 7.5 g Agar (Sigma) broth in 500 ml ddH_2O autoclaved for 20 min at 121 degrees; **Antibiotics (**Ampicillin, 100µg/ml or Kanamycin, 25µg/ml) **added to LB or LB+Agar**

DNA and protein ladders

- Spectra™ Multicolor High Range Protein Ladder (Fermentas, SM1859)
- Thermo Scientific PageRuler Plus Prestained Protein Ladder (Invitrogen, 26619)
- 1 kb Plus DNA Ladder (Invitrogen, 10787-018)
- 100 bp DNA Ladder (Invitrogen, 15628-050)

Competent cells

- OneShot© Top10 chemically competent cells (Invitrogen C4040-10)
- XL10-Gold ultracompetent Cells (Stratagene C-200314)

Purification kits

- Miniprep (Spin Miniprep kit, Qiagen)
- Maxiprep (High speed Maxiprep kit, Qiagen)
- Gel purification (Gel purification kit, Qiagen)
- PCR Purification (Qiagen)
- DreamTaq Green DNA polymerase kit (Invitrogen)

Restriction digests

- Single Digest*:* 15 µL of H_2O, 2 µL of appropriate restriction enzymebuffer, 2 µL of DNA (200ng), 1 µL of restriction enzyme. Leave 3 hours at 37 or 65 °C

- Double Digest for 2 restriction enzymes: 1 µL of each enzyme with 2 µL of buffer, 2 µL of DNA (200 ng) and 14 µL of H_2O. *Enzymes used EcoRI, BamHI, BstBI, BsaAI, KpnI, HindIII (New England Biolabs)*

Cloning the human and mouse NATs

Human dorsal root ganglia total RNA was purchased from Clontech; Mouse total RNA was isolated from DRGs dissected from wild-type black6 mice using the RNeasy MinElute Kit (Qiagen). Total RNA was reverse transcribed into cDNA using Superscript III (Life Technologies) and oligo d(T), according to the manufacturer's instructions. The human *SCN9A NAT* was PCR-amplified from DRG cDNA using KAPA HiFi DNA polymerase (Kapa Biosystems) or LA Taq (TaKaRa) in three overlapping fragments using the following primers: Fragment 1, 5' GAA TGA AAT TTA GTG TTT CCC ATC C, 5' AGC AAT GTT TCA CCT CCA GAG ATC; Fragment 2, 5' GGA ATT CAG GCA AAG TTG GA, 5' CAC CAA CAT TCA GCC ATT TG; Fragment 3, 5' CTG ATT ATT GGG AGA CTT TTG GAG, 5' GCT CCT ATT TCT GAG TTT ATA CTG TG. The mouse *Scn9a* NAT was PCR-amplified using the primers 5' AGC AAG AGT AAG AAG TAT TGG c, 5' CAT TAT ATT TCA TTT TAA TG. PCR products were cloned using the Zero Blunt TOPO PCR Cloning Kit (Life Technologies). Individual colonies were Sanger sequenced and submitted to GenBank under the accession numbers KM096550 (clone LA5), KM096551 (clone LA8), KM096552 (clone 3.2) and KM096553 (clone 3.1).

6.1.2 DNA and RNA isolation

Genomic DNA isolation and genotyping

Ear tissue was collected and genomic DNA extracted according to the manufacturer's protocol using the Pure Link Genomic DNA Purification Kit (Invitrogen). Primers for genotyping were designed using the Primer3 Plus software. The PCR reaction consisted of 95 °C for 5 min followed by 35 cycles of 1 min at 95 °C, 30 sec at 57 °C and 2 min at 72 °C (Thermocycler PeqStar). The products were separated on a 1.5% agarose gel to verify that the reaction products yielded the expected fragment size.

Table 6-1 Genotyping primers

Primer Name	Sequence (5'-3')	Description
Nav1.7L858F	TTCATCCACCACCTCTCCAC	RefSeq, NM_002977.3
TAP-L858F	ATCTTGTTGTGGGCATGAGCGT	L858F-TAP-tag
5aR4	CCGAGGCCAGGGAACAAATTCC	$Na_v1.7$ 5' UTR
3aR4	AACACGAGTGAGTCACCTTCGC	$Na_v1.7$ 3'UTR
TAP-R1	ATCTTGTTGTGGGCATGAGCGT	TAP-tag

RNA isolation in primary cells

Mice were deeply anaesthetized with CO_2 and terminated through neck breaking, DRGs were taken out and brought into RNAlater (Ambion) for storage up to one week at 4°C. DRGs were transferred into Precellys ceramic kit 4.1 (Peqlab) with TriZol (Ambion). Homogenized samples were transferred into QIAshredder mini column (Qiagen). Supernatant from QIAshredder was separated in PLG tubes (VWR) by addition of chloroform isopropanol alcohol 24:1 (Sigma) via centrifugation for 15 min,16000g at 4°C. The upper colourless aqueous layer was removed and mixed with 70% EtOH and spun down in an RNeasy MinElute spin column (Qiagen). The spin column was washed with RPE Buffer (Qiagen). DNaseI/Buffer RDD (Qiagen) was added onto the membrane and left for 15min at RT. The spin column was washed with RPE Buffer and 80% EtOH. RNA was eluted in RNAse free water (Ambion).

RNA isolation HEK293 and SH-SY5Y

HEK293 cells were pelleted and washed in 1XPBS (Gibco) and resuspended in TriZol (Ambion). Chloroform (VMR) was added and the sample was centrifuged at 11,000 g, 15 minutes at 4°C. Top phase supernatant containing RNA was mixed with isopropyl alcohol (Sigma), shortly incubated and centrifuged at 11,000 g for 10 min at 4°C. The pellet was washed in 75% EtOH and centrifuged at 7,500 g, 5 min at 4°C. After a short incubation, the pellet was resuspended in ultra-pure water.

Reverse transcription

- SuperScript III RT First Strand (Invitrogen) performed according to manufacturer's protocol.

6.1.3 qPCR

6.1.3.1 qPCR for mouse tissue panel and cell lines

One ug of total RNA derived from a range of tissues (Clontech) or prepared in-house (DRG) were reverse-transcribed into cDNA using Superscript III (Life Technologies) and oligo d(T). SYBR Green assay (Bio-Rad) was performed according to the manufacturer's protocol using primers to *Scn9a*, the *NAT* and β-actin.

Relative expression of the target gene was calculated using the comparative ΔΔCT method (Livak and Schmittgen et al. 2001,Pfaffel et al, 2001). Expression of the test gene was compared with that of β-actin measured on the same sample, giving a CT difference (ΔCT) for β-actin minus the test gene. The relative expression of *Scn9A* and *NAT* in specific tissues was calculated in relation to the expression levels in DRG using the comparative ΔΔCT method (Livak and Schmittgen et al. 2001). ΔCT values of individual tissues were compared to ΔCT of DRG, giving ΔΔCT values of a specific tissue and relative expression was calculated as $2^{-\Delta\Delta CT}$. Mean, S.E.M. and statistics were calculated from the ΔΔCT method. Data were analyzed using Microsoft Excel, and statistics were performed using GraphPad Prism 5.01 software (GraphPad Software, San Diego, CA).

qPCR analysis of animal models

Total RNA was isolated from dissected L2-L6 ipsilateral DRGs from Carrageenan, CFA and CCI treated mice and L5-L6 DRG from SNT treated mice using the RNeasy MinElute Kit (Qiagen). Real-time qPCR was performed using SYBR Green (Applied Biosystems) and the following primers: *Scn9a* (efficiency 1.91), *NAT* (efficiency 1.96) and *Gapdh* (efficiency 1.76). Relative expression levels of mRNA were calculated using the comparative ΔΔCt (Ct) method and statistical significance was determined using an unpaired t-test.

6.1.3.2 Taqman Assays

SCN1A, SCN2A and *SCN3A* expression in *NAT*-SH-SY5Y stable cell line

NAT-SH-SY5Y stable and untreated SH-SY5Y cell line samples were tested for the expression of *SCN1A*, *SCN2A* and *SCN3A* using TaqMan assays for hm *SCN1A* (Hs00374696_m1), hm *SCN2A* (Hs01109877_m1) and hm *SCN3A* (Hs00366902_m1) and hm *GAPDH* (Hs02758991_g1). TaqMan assays were performed according to manufacturer's protocol in an Eppendorf Realplex under the following thermal cycling conditions: 50°C for 2 minutes, 95°C for 10 minutes, and 40 cycles of 95°C for 15 seconds and 60°C for 1 minute. All reactions were performed on biological and technical triplicates. Relative expression was calculated using the comparative ΔΔCT Method (Livak and Schmittgen et al. 2001,Pfaffel et al. 2001). ΔCT was obtained by subtraction of *GAPDH* Ct values from Ct values of the target gene. Next, ΔCT values of the target gene were compared between groups, giving ΔΔCT. Relative expression was calculated using $2^{-\Delta\Delta CT}$ indicating the fold change in expression of the target gene in the *NAT*-stable cell line compared to untreated SH-SY5Y. Mean, SEM and statistics were calculated from the ΔΔCT method. Data were analyzed using Microsoft Excel, and statistics were performed using GraphPad Prism 5.01 software (GraphPad Software, San Diego, CA).

TaqMan Mulitplex Assays

$Na_v1.7$ L858F TAP-tag copy number was determined using TaqMan copy number assays (Life Technologies) according to the manufacturer's instructions. Isolated genomic DNA (40 ng) was mixed with 2×TaqMan Expression Master Mix and 20XTaqMan probes in a 96 well plate (Bio-Rad). Custom Taqman Assays-by-Design tool (Invitrogen) was used to a generate a primer and probe set for the TAP tag (inserted in $Na_v1.7$ L858F gene**,** Assay Id: AJPADNX) and TaqMan Mouse *GAPDH* (GAPDH, NM_008084.2) as endogenous control (VIC/MGB) in a 20*μ*l reaction volume. The TaqMan multiplex assay was performed using the Eppendorf Realplex and the following thermal cycling conditions: 50°C for 2 minutes, 95°C for 10 minutes, and 40 cycles of 95°C for 15 seconds and 60°C for 1 minute. All reactions were performed in duplicate or

triplicate. Copy numbers were estimated by relative quantification. *TAP* Ct values for PE mice were normalized to endogenous *GAPDH* Ct values and compared to a calibrator TAP sample known to have 1 copy of the target sequence using the comparative Ct (ΔΔCt) method. Data were analyzed and statistics performed using Microsoft Excel.

Table 6-1.2: Overview SYBR Green and TaqMan PCR primers

Primer name	Sequence (5'-3') / Assay ID	Description
Scn9a F	GAGGGGCAAACTGACTACA	Mouse tissue panel, animal models
Scn9a R	AGAAACATTCCTACAATGGAG	Mouse tissue panel, animal models
NAT F	TGCTGTCAACTCCTGAACCA	Mouse tissue panel, animal models
NAT R	TCCAACTTTGCCACAATGAG	Mouse tissue panel animal models
β-actin *F*	TTCTTTGCAGCTCCTTCGTT	Mouse tissue panel, animal models
β-actin *R*	ATGGAGGGGAATACAGCCC	Mouse tissue panel, animal models
Gapdh F	TGC GAC TTC AAC AGC AAC TC	Mouse tissue panel, animal models
Gapdh R	CTT GCT CAG TGT CCT TGC TG	Mouse tissue panel, animal models
SCN9A F	AGA GGG GTA CAC CTG TGT GAA	SH-5YSY
SCN9A R	CCC AGG AAA ATC ACT ACG ACA AA	SH-5YSY
hNAT F	GGA GTC ACT GGG ATT AAA GGC AT	SH-5YSY
hNAT R	TTC TTT GTC GCT GGT GGC TAG AG	SH-5YSY
b-ACT F	CGC CGC CAG CTC ACC ATG	SH-5YSY
b-ACT R	CAC GAT GGA GGG GAA GAC GG	SH-5YSY
TAP	AJPADNX	L858F-TAP
GAPDH	GAPD	NM_008084.2
SCN1A	Hs00374696_m1	NM_001165963.1 NM_001165964.1 NM_001202435.1 NM_006920.4
SCN2A	Hs01109877_m1	NM_001040142.1 NM_001040143.1

		NM_021007.2
SCN3A	Hs00366902_m1	NM_001081676.1 NM_001081677.1 NM_006922.3
GAPDH	Hs02758991_g1	NM_001256799.1 NM_002046.4

6.1.3.3.Standard curve -Transgenic Nav1.7 L858F mice copy number estimation

A dilution series of purified gDNA (neat, 1/10,1/100,1/1000,1/10000) was prepared and 4 µl of each sample was set up in a 96-well plate (Bio-Rad) for a Taqman assay according to the manufacturer's protocol. Obtained threshold cycles (Ct) were plotted against Log10 concentration (ng/ul) for each sample. Efficiency was calculated as followed: E = 10 [–1/slope] (Pfaffle *et al.* 2001). Efficiencies for *TAP* and *GAPDH* are 1.97 and 2.15 respectively. Data were analyzed and statistics performed using Microsoft Excel.

6.1.4 Expression vectors

Human and mouse antisense expression vector

Human full length, BC051759, was amplified from a cDNA clone: IMAGE human cDNA clone, BC051759 Clone ID 5582690. Mouse full length transcript AK138532 was amplified from Fantom FLS clone A330052F22. DNA was isolated using Miniprep protocol (Qiagen) and used as template in Phusion PCR (NEB) using the primers: hm AS HINDIII FWD 5'CCCAAGCTTGTCTTAGTCCTCTGAATATTTT-3', hm AS KpnI REV5'-CGG GGTACC CCA ATTGATGGAGAATTTTAT-3' and ms HindIII FWD 5'-CCCAAGCTT GAGCAAGAGT AAGAAGTA-3', ms AS KpnI REV 5'- CGG GGTACC GCCATTATATTTCAT-3'. Amplified DNA was further gel purified (Qiagen). pcDNA3 (Invitrogen) mammalian expression vector and purified full length human/mouse *SCN9A* and *Scn9a NAT* were double digested overnight at 37^{o}C with *Kpn*I and *Hind*III (NEB), linearized pcDNA3 vector was also treated with SAP (NEB) before ligation. Ligation of full length *Scn9a/SCN9A NAT* to pcDNA3 vector was carried out with T4 DNA Ligase (Fermentas). Ligation reactions were transformed into XL10 Gold ultracompetent cells (Agilent).

Single positive colonies were picked and inoculated in LB+Ampicillin and grown overnight at 220 rpm at 37^{o}C. The bacterial cells were then pelleted by centrifugation at 5000 rpm for 10 min. DNA was isolated using Miniprep and Maxiprep kits (Qiagen). The expression vectors were then sequenced (Source Bioscience) and sequences were compared against reference sequence databases using the Genome UCSC (http://genome.ucsc.edu/) and NCBI BLAST (http://blast.ncbi.nlm.nih.gov/Blast.cgi) web tools. Nucleotide *blast* (Data base: Reference genomic sequences (refseq_genome), organism: mus musculus taxid: 10090 or Homo sapiens taxid: 9606) identified the sequenced inserts as full length human BC051759 and mouse AK138532 full length *SCN9A NAT.* Herein these are referred to as human and mouse *NAT* in pcDNA3.

6.2 Cell culture

6.2.1 Cell culture maintenance

Table 6.2: Cell culture medium

Cell line	Medium
HEK293	DMEM (GIBCO), 10% FBS, 1%Pen/Strep
HEK293 hm Nav1.7 TAP tag stable cell line	DMEM (GIBCO), 10% FBS, 1% Pen/Strep, 0.5% G418 (Sigma)
Nav1.7/Nav1.6 stable cell line	MEM (Sigma), 2mM L- Glutamine (Sigma), 10% FBS (Invitrogen), 2µg/ml Blastocydin (calbiochem), 0.6mg/ml Geneticin (Invitrogen), 10ml/L Penicillin – streptomycin (Sigma)
SH-SY5Y	Ham's F12: EMEM (1:1) 2 mM glutamine (Life technologies) 1% non essential amino acids and 10% FBS (Life technologies)
SH-SY5Y-NAT stable cell line	Ham's F12: EMEM (1:1) 2 mM glutamine (Life technologies) 1% non essential amino acids (Life technologies) and 10% FBS (Life technologies) selection antibiotic G418 (500 µg/ml)(Sigma)

Cell splitting

Cell culture medium was removed and trypsin added (GIBCO, Life Technologies) for 2-3 minutes. Trypsin was aspirated and cells resuspended in 10 ml of culture media. The cell suspension was transferred into 15ml tubes and

centrifuged 5 min at 800rpm. The supernatant was aspirated and the cell pellets were resuspended in 10 ml stable cell media. Cells were split into 2ml dishes or a flask. Best transfection results were obtained with cells at around 90 per cent confluence on the day of transfection.

6.2.2 Transfection of cell lines

HEK293 $Na_v1.7$ and $Na_v1.6$ stable cell line

HEK293 cells stably expressing human $Na_v1.7$ plus *SCN1B* (L11) or $Na_v1.6$ plus *SCN1B* (L40) (Scottish Biomedical) were grown according to the manufacturer's instructions and passaged four times before transfections begun. Cells were split into 3.5 cm^2 dishes and grown to 95% confluency. On the day of transfection, cells were transfected with 250 ng of pEGFP-N1 (Clontech) plus 1000 ng of human *NAT* in pcDNA3 or empty pcDNA3 using a ratio of 1 μg DNA:2.5 μl Lipofectamine 2000 (Life Technologies). After 6 hours, the transfected cells were re-seeded at a low density and left for 48 hours prior to patch clamp analysis or RNA extraction.

HEK293 cell line transfection

HEK293 were grown according to the manufacturer's instructions and passaged four times before transfections begun. Cells were split into 5 cm^2 dishes and grown to 95% confluency. On the day of transfection, cells were transfected with 5000 ng of human $Na_v1.7^{TAP}$ in pcDNA3 or empty pcDNA3 using a ratio of 1 μg DNA:2.5 μl Lipofectamine 2000 (Life Technologies). After 6 hours, the transfected cells were re-seeded at a low density and left for 48 hours prior to patch clamp analysis or RNA extraction.

6.2.3 Stable cell lines

NAT-SH-SY5Y stable cell line

The human neuroblastoma cell line, SH-SY5Y (Public Health England) was cultured at 37^{o}C/5% CO2 in Ham's F12:EMEM (1:1) supplemented with 2 mM glutamine, 1% non essential amino acids and 10% foetal bovine serum (Life Technologies). The human *NAT* in pcDNA3 was linearised with PvuI and following gel purification (Qiagen), 10 ug was transfected into a 10 cm 80%

confluent dish of SH-SY5Y cells using Lipofectamine 2000 (Life Technologies). Six hours later, the medium was replaced with the selection antibiotic G418 (500 µg/ml). Cells were monitored on a daily basis until twenty-four discrete colonies could be selected for expansion and screening by RT-PCR. Real-time qPCR was performed using SYBR Green (Applied Biosystems) and the following primers: Human *SCN9A* (efficiency 1.9); Human *NAT* (efficiency 2); Human (efficiency 1.85). Relative expression levels of mRNA were calculated using the comparative ΔΔCt (Ct) method and statistical significance was determined using an unpaired t-test.

$Na_v1.7$ TAP-tag stable HEK293A cell line

The human *SCN9A* mammalian expression construct, FLB (full-length SCN9A without the downstream IRES-DsRED2 sequence) was modified by cloning in a sequence encoding a TAP-tag (peptide: SRK DHL IHN VHK EEH AHA HNK IEN LYF QGE LPT AAD YKD HDG DYK DHD IDY KDD DDK) prior to the stop codon. The TAP tag at the extreme C-terminus of $Na_v1.7$ is comprised of a HAT-domain and 3XFLAG tags, enabling immunodetection with either anti-HAT or anti-FLAG antibodies. The $Na_v1.7$-TAP stable HEK293A cell line was generated using the same methods as described for the *NAT*-SH-SY5Y stable cell line. For the immunoprecipitation experiments, the $Na_v1.7$-TAP stable HEK293A cell line was firstly transiently transfected with the human *NAT* expression construct or an empty pcDNA3 control (as described above) and cells collected 48 hrs later. Protein was isolated using RIPA buffer (50 mM Tris-HCl pH 7.4, 150 mM NaCl, 1% Nonidet P40, 0.5% of Sodium deoxycholic acid, 0.1 % SDS, 1 tablet complete EDTA-free protease inhibitor cocktail) and equal amounts loaded onto 100 ul anti-FLAG (Sigma, F1804) coupled Dynabeads (Life Technologies), according to the manufacturer's instructions. Samples were then boiled in Laemmli buffer (4% SDS, 20% glycerol, 10% 2-mercaptoethanol, 0.004% bromphenol blue, 125 mM Tris HCl, pH 6.8) and equal volumes loaded onto 4-12% polyacrylamide gels. Immunopurified $Na_v1.7$-TAP was detected on immunoblots using an anti-HAT antibody (LSBio, LS-C51508). In addition, equal amounts of crude lysate protein were run on a western blot and detected using anti-FLAG and anti-alpha tubulin (Abcam, ab7291) antibodies. Densitometry

readings were performed using ImageJ software whereby the ROI reading for alpha-tubulin was compared to the region of interest (ROI) reading for the HAT or FLAG bands and subsequently normalized to the sham control.

6.3 Electrophysiology recordings

Patch clamp analysis of $Na_v1.7$-HEK293, $Na_v1.6$-HEK293 and NAT-SH-SY5Y stable cell lines

Whole cell patch clamp recordings were made from $Na_v1.7$-HEK293, $Na_v1.6$-HEK293 and *NAT*-SH-SY5Y stable cell lines at room temperature. In the case of the transient $Na_v1.7$ *NAT* transfections, whole-cell membrane current recordings were performed 46 to 78 hrs after transfection. Micropipettes were pulled from borosilicate glass capillaries (GC150F-10; Harvard Apparatus, Kent, UK) using a Brown-Flaming P-97 horizontal micropipette puller (Sutter Instruments, Novato, CA, USA) and then fire polished on a microforge (MF-830 Narishige Group, Tokyo, Japan). Voltage errors were minimised with correction and prediction mode of series resistance compensation both set to 50%. Extracellular solution contained (in mmol/L): 140 NaCl, 4 KCl, 2 $CaCl_2$, 1 $MgCl_2$, 10 HEPES, adjusted to pH 7.4 with NaOH, osmolarity 320-325 mOsm/L with glucose. Pipettes were filled with an intracellular solution containing (in mmol/L): 140 CsCl, 5 NaCl, 5 EGTA, 2 $MgCl_2$, 10 HEPES adjusted to pH 7.3 with CsOH, osmolarity 305-310 mOsm/L with glucose. Once filled with the appropriate intracellular solution, recording electrodes had a resistance between 2.0 and 3.0 MΩ. A silver chloride coated silver wire served as a reference electrode with one end connected to the ground input of the amplifier and the tip placed directly into the bath solution. Cells having a leak current after establishing whole-cell configuration of more than 10% of the peak sodium current were discarded and those which had developed leak of this magnitude during the experiment were not used in the final analysis. The liquid junction potential between the bath and the pipette solutions was not corrected. Whole-cell membrane currents were filtered at 5 kHz and sampled at 20 kHz using either an Axopatch 200B patch clamp amplifier or Axon Multiclamp 700B (Molecular Devices, Foster City, CA) and Digidata 1200B A/D converter (Molecular

Devices, Foster City, CA). Data were acquired on a Windows-based PC using Clampex (Molecular Devices, Foster City, CA) software and analysed by pCLAMP (Clampfit) 9.2 software (Molecular Devices, Foster City, CA).To characterize the voltage dependency of steady-state channel activation, currents were evoked by voltage increments of 5 mV from -80 to +40 mV for 10 ms from a holding potential of -120 mV with 5 s between pulses. Peak whole cell currents (pA) were measured in response to a 10 ms voltage step from a holding potential of -120 mV to 0 mV and normalized to cell capacitance (pF).

6.4 Animal models

6.4.1 Murine models of inflammatory pain

Carrageenan

Lambda Carrageenan (Sigma) was prepared as 2% W/V solution in 0.9% sodium chloride and 25µl was injected into the left hind paw of C57BL/6, 6-8 weeks, males. Control animals Black6, 6-8 weeks, males were injected with 25µl of 0.9% sodium chloride solution. Behaviour was assessed with Hot Hargreaves (AI=12, RL 20sec); withdrawal latency (control around 8-10sec) was measured for left and right hind paws independently (Morris 2003, Minett, Quick et al. 2011).

Complete Freund's adjuvant (CFA)

6-8 week old male C57BL/6 mice were intraplantar injected into the left hind paw with complete Freund's adjuvant (or 0.9% sodium chloride solution for the sham controls), as described in Minett and Quick *et al.* (2011).

Formalin test

Mice received a 20µL intraplantar injection of 5% formalin into the left hindpaw. Spontaneous nocifensive behavioural responses were recorded for 60 minutes post-injection. Additionally, hindpaw skin temperatures were measured pre-injection and for 60 minutes post-injection.

6.4.2 Murine models of neuropathic pain

Chronic constriction injury (CCI)

Surgery was performed on 6-8 week old male C57BL/6 mice. Mice were deeply

anaesthetized and though an incision in the skin the sciatic nerve was loosely ligated various times (Minett and Quick et al. 2011).

Sciatic nerve transection (SNT)

Surgery was performed on 6-8 week old male C57BL/6 mice. Mice were deeply anaesthetized and though an incision in the skin the sciatic nerve at the height of L5 was completely transected (Minett and Quick et al. 2011).

6.4.3 Behaviour phenotyping

Motor coordination

Rotarod test described in (Jones and Roberts 1968) was used to asses motor coordination in transgenic $Na_v1.7$ L858F mice and wildtype controls.

Mechanical thresholds

A modified version of the Randall-Selitto test was used to measure mechanical nociceptive thresholds in transgenic and wildtype mice. Pressure was applied to the tail via a $3mm^2$ blunt conical probe with a 500-gram cut-off or to the dorsal surface of the hindpaws with a 250-gram cut-off (Randall and Selitto 1957, Takesue, Schaefer et al. 1969, Andersson, Gentry et al. 2012). Touch perception was assed using von Frey hairs to either the plantar surface of the hindpaw or the inferior half of the abdomen on hairy and non-hairy skin, respectively (Chaplan, Bach et al. 1994).

Thermal thresholds

Thermal nociceptive thresholds were measured by hindpaw-withdrawal latencies using the Hargreaves apparatus (Hargreaves, Dubner et al. 1988) and the hotplate test (50 & 55°C) (Eddy and Leimbach 1953). Additionally a thermal place preference (BioSeb) was performed to assess cold and pre-noxious heat avoidance as described in Minett, Nassar *et al.* (2012).

6.5 Biochemistry and proteomics

6.5.1 Immunocytochemistry on HEK293 cells

Cells were seeded on EtOH sterilized, BD matrix gel (BD Biosciences) coated glass coverslips and grown to confluence. Cell culture medium was aspirated and cells were put on ice. Coverslips were washed three times with cold 1XPBS (GIBCO) and blocked for 30 min in 5% goat serum (Sigma) in 1X PBS. Incubation with primary antibody in blocking buffer for 1hr on ice was followed by secondary antibody goat anti-mouse IgG conjugated Alexa Fluor-488 (1:200) in blocking buffer. Coverslips were washed in 1XPBS and fixed in 4%PFA at RT for 15min. Cells on coverslips were washed and mounted in VECTASHIELD HardSet Mounting Medium with DAPI.

6.5.2 Immunohistochemistry on tissue sections

Perfusion of mice and preparation of mouse DRG, spinal cord and olfactory tissues for immunohistochemistry used previously described methods Zhao *et al.* (2006). Cryosections (12 - 20μm) of mouse DRG, spinal cord and olfactory tissues were postfixed using 4% PFA in PBS, before blocking and antibody administration. Primary antibodies were: mouse anti-FLAG (1:500, Sigma, F1804), Rabbit anti-FLAG (1:500, Sigma F7425). Secondary antibodies and conjugated compounds were: Alexa-Fluor 594 goat-anti-mouse (1:1000; Invitrogen), Alexa-Fluor 488 goat-anti-rabbit (1:1000; Invitrogen).

6.5.3 Total protein extractions from cell lines

Cells were grown to confluence in culture medium, washed 1X PBS (Gibco) and cells scraped from dishes and pelleted by centrifugation for 5 min at 800 rpm. Pellets were re-suspended in an appropriate volume of RIPA buffer or modified RIPA buffer (50 mM Tris-HCl pH 7.4, 150 mM NaCl, 1% Nonidet P40, 0.5% of Sodium deoxycholic acid, 1 tablet complete EDTA-free protease inhibitor cocktail). Extracts were clarified after incubated on ice by 5000 rpm for 10 mins at 4^{o}C.

6.5.4 Total protein extracts from tissue

Tissues were dissected on dry ice and homogenized (Precellys ceromic kit 4.1, Peqlab) in RIPA or modified RIPA buffer. Cell lysates were incubated for 1hr shaking on ice and clarified by centrifugation at 14 000g for 8 min at 4^{o}C. Lysate short-term storage at -80^{o}C.

6.5.5 Co-Immunoprecipitation

Proteins were isolated from homogenized tissue (Precellys) in RIPA buffer and concentrations measured using BCA Protein assay kit (Pierce). A total starting amount of 1mg of protein was incubated with 100ul magnetic M-270 Epoxy Dynabeads (14311D, Invitrogen) covalently coupled to mouse Anti-Flag M2 (Sigma, F-1804). The coupling was carried out for 2hrs at 4°C with constant agitation. Captured proteins were boiled off the beads by addition of equal amounts of SDS sample buffer (4% SDS, 10% 2-mercaptoethanol, 20% glycerol, 0.004% bromophenol blue 125 mM Tris HCl; pH 6.8). Mini-PROTEAN TGX Stain-Free precast gels (4-12% Gradient, Bio-Rad) were loaded with equal amounts of volume per lane. 1D-SDS-PAGE separations was followed by detection of immunopurified $Na_v1.7$-TAP using an anti-HAT antibody or *SCN3B* antibody.

6.5.6 Single and Tandem Affinity purification

In each round of sample preparation for single and tandem affinity purification, DRG olfactory bulbs and spinal cord samples were separately homogenized (Precellys ceramic kit 4.1, Peqlab) in 1% CHAPS (30mM Tris HCL pH 7.5; 150mM NaCl, 1% CHAPS, 1 complete EDTA free Protease inhibitor cocktail (Roche)) and further homogenized using an insulin syringe. The lysates were incubated shaking horizontally on ice and clarified by centrifugation at 14 000 g for 8 min at 4°C. Protein concentrations were measured using the BCA Protein assay kit (Pierce) and a total starting amount of 8 -10 mg of protein containing supernatant was incubated with magnetic M-270 Epoxy Dynabeads (14311D, Invitrogen) covalently coupled to mouse Anti-Flag M2 (F-1804, Sigma). The coupling was carried out for 2hrs at 4°C using an end-over-end shaker. Magnetic Dynabeads were collected on a DynaMAG rack (Invitrogen) and

washed three times in 1% CHAPS Buffer and 1X AcTEV protease cleavage buffer (50 mM Tris-HCl pH 8.0, 0.5 mM EDTA, 1 mM DTT, Invitrogen). Dynabead-captured $Na_v1.7$ TAP-tag complex was released from the beads by incubation with AcTEV protease (Invitrogen) for 3 hours at 30^oC, finalizing the single step purification. For the tandem affinity purification, protein elutes were collected after AcTEV cleavage and 15 X diluted in protein binding buffer (50 mM Sodium phosphate, 300mM NaCL, 10 mM imidazole, 0.01% Tween; pH 8). $Na_v1.7$ TAP tag was captured using Ni-NTA beads (Qiagen). Ni-NTA beads were washed three times in protein binding buffer and overnight incubated at 4^oC on an end-over-end shaker. TAP-tagged protein complexes were released from the Ni^{2+}beads by boiling with SDS and DTT.

6.5.7 Western Blotting

Cell lysate samples were prepared for Western blotting by addition of 2X SDS sample buffer (4% SDS, 10% 2-mercaptoehtanol 20% glycerol, 0.004% bromophenol blue 125 mM Tris HCl; pH 6.8) and denatured for 5 min at 95^oC. Mini-PROTEAN TGX Stain-Free precast gels (4-12% Gradient, Bio-Rad) were loaded with 20-30ug per lane and Spectra Multicolor High Range Protein Ladder (Thermo scientific). 1D SDS-PAGE separations were performed in 1X Western blot Running buffer (10X stock; 25mM Tris, 190mM glycine, 0.1% SDS pH 8.3) for 1h 30 min at 120 V. Proteins were then wet transferred to Immobilin-P membranes (Millipore) activated with Methanol (Sigma) in 1X ice cold transfer buffer (10X Stock Transfer Buffer, 25 mM Tris, 192 mM glycine, 20% (v/v) methanol) for 1hrs at 100V followed by incubation in blocking solution (1 x PBS for 10X stock Gibco pH7.5, 0.1% Tween 20,Sigma; 5% Marvel) and overnight incubation at 4°C with primary antibody (dilution 1:500-1:1000) in blocking solution. Membranes were washed 4 times in 1X PBST (1X PBS, 0.1% Tween 20) and incubated with anti-rabbit or anti-mouse secondary antibody 1:5000 (GE healthcare) in blocking buffer for 1-2 hours at room temperature with constant agitation. PVDF Membranes were washed 4 times 1X PBST (1X PBS, 0.1% Tween 20). Protein was visualized with SuperSignal West Dura Extended Duration Substrate (Thermo Scientific) on X-ray films (GE healthcare) using an X-ray film developer.

6.5.8 Silver staining

Samples were run on Mini-PROTEAN TGX Stain-Free precast (4-12% Gradient, Bio-Rad) 8+1 or 12 gels respectively. Silver staining was carried out according to the manufacturer's protocol (LifeTechnology, SilverQuest™ Silver Staining).

6.5.9 Antibodies

Table 6.5: Antibodies

Antibody	Description	Dilution	Application
HAT	LSBio, LS-C51508, rabbit	1:500	Western Blot (WB)
FLAG	Sigma, F1804, mouse	1:1000	Purification, WB, IHC
Alpha tubulin	AB cam ab7291-100	1:1000	WB
Pan-sodium	Sigma, S8809	1:1000	WB
β-actin	AB cam	1:1000	WB
Anti-$Na_v1.7$	NeuroMab	1:250	WB

Secondary Antibody	Description	Dilution/ Application
ECL mouse NA931	Amersham ECL Mouse IgG, HRP-linked whole Ab (from sheep)	1:5000/WB
ECL rabbit NA934	Amersham ECL Rabbit IgG, HRP-linked whole Ab (from donkey)	1:5000/WB
Alexa-488	Life Technology, A-20181	1:200 and 1:1000 IHC
Alexa-594	Life Technology, A-11014	1:200 and 1:1000 IHC

6.6 Mass spectrometry

Filter-aided sample preparation (FASP) for tryptic digestion

Proteins either TEV-protease cleaved or eluted from NI^{2+} beads from WT and $Na_v1.7^{TAP/TAP}$ mice were loaded to 30 KDa filters (Millipore), then filter units were centrifuged at 14 000g for 15 min to remove other detergents. Two hundred µl of urea buffer (10 mM DTT 8M urea (Sigma) in 0.1 M Tris/HCl pH 8.5) were

added to the filters and incubated at room temperature for 1 hour to reduce proteins. The filters were centrifuged at 14000 g for 15 min to remove DTT. 200 µl of 50 mM Iodoacetamide (IAA) in urea buffer was added to filters and incubated for 30 min in the dark. The filters were centrifuged as before to remove IAA. The samples were then buffer exchanged twice to remove detergents using 200µl of urea buffer, and one more time using 200 µl of 50 mM NH_4HCO_3 in water. 40µl of 50 ng/ul trypsin in 50 mM NH_4HCO_3 was added to the filters. Filters were then vortexed briefly and proteins digested at 37 °C overnight. After tryptic digestion, the filters were transferred to new collection tubes, and all the peptides were collected by placing the filter upside down and centrifuging. The filters were washed with 200 µl of 500 mM NaCl, and collected all of the washing solution by placing the filter upside down and centrifuging. The filters were washed with 100 µl of water and spun at 14 000 g for 15 min in the same collection tube. The samples were then acidified with CF_3COOH and desalted with C18 cartridges (Waters). The pure peptides were dried by Spedvac (Millipore) and resuspended with 20 ul of 2% ACN, 0.1% FA. 5ul of samples were injected into a Orbitrap velos mass spectrometer (Thermo) coupled to a UPLC (Waters).

Mass spectrometry analysis

LC-MS/MS analysis of the digested material was carried out by nano-ultra performance liquid chromatography tandem MS (nano-UPLC-MS/MS) using a 75 μm-inner diameter x 25 cm C18 nanoAcquityTM UPLCTM column (1.7-μm particle size, Waters) with a 180 min gradient of 3–40% solvent B (solvent A: 99.9% H2O, 0.1% formic acid; solvent B: 99.9% ACN, 0.1% Formic acid). The Waters nanoAcquity UPLC system (final flow rate, 250 nl/min) was coupled to a LTQ Orbitrao Velos (Thermo Scientific, USA) and run in positive ion mode. The MS survey scan was performed in the FT cell recoding a window between 300 and 2000 m/z. The resolution was set to 30,000, the automatic gain control target was set to 1,000,000 ions with a maximal acquisition time of 100 ms. Minimum MS signal for triggering MS/MS was set to 500 m/z values triggering MS/MS were put on a dynamic exclusion list (500 entries), exclusion duration as

30. Maximum of 20 MS/MS scans were triggered per MS scan. The lock mass option was enabled and Polysiloxane (m/z 371.10124) was used for internal recalibration of the mass spectra. CID was done with a target value of 30,000 in the linear ion trap, maximal acquisition time 500ms, collision energy of 35% and an activation time of 10 ms. All samples were measured in triplicate with the MS setting charge state rejection enabled and only more than 1 charges procures ions selected for fragmentation.

7 References

Abrahamsen, B., J. Zhao, C. O. Asante, C. M. Cendan, S. Marsh, J. P. Martinez-Barbera, M. A. Nassar, A. H. Dickenson and J. N. Wood (2008). "The Cell and Molecular Basis of Mechanical, Cold, and Inflammatory Pain." Science **321**(5889): 702-705.

Abriel, H. and O. Staub (2005). "Ubiquitylation of ion channels." Physiology (Bethesda) **20**: 398-407.

Adams, P. J., M. Ben-Johny, I. E. Dick, T. Inoue and D. T. Yue (2014). "Apocalmodulin itself promotes ion channel opening and Ca(2+) regulation." Cell **159**(3): 608-622.

Agre, P., L. S. King, M. Yasui, W. B. Guggino, O. P. Ottersen, Y. Fujiyoshi, A. Engel and S. Nielsen (2002). "Aquaporin water channels--from atomic structure to clinical medicine." J Physiol **542**(Pt 1): 3-16.

Ahlgren, S. C. and J. D. Levine (1994). "Protein kinase C inhibitors decrease hyperalgesia and C-fiber hyperexcitability in the streptozotocin-diabetic rat." J Neurophysiol **72**(2): 684-692.

Akopian, A. N., L. Sivilotti and J. N. Wood (1996). "A tetrodotoxin-resistant voltage-gated sodium channel expressed by sensory neurons." Nature **379**(6562): 257-262.

Alberts, B. (2010). "Cell Biology: The Endless Frontier." Molecular Biology of the Cell **21**(22): 3785.

Alberts, B., D. Bray, J. Lewis, M. Raff, K. Roberts, J. D. Watson and A. Grimstone (1995). "Molecular Biology of the Cell (3rd edn)." Trends in Biochemical Sciences **20**(5): 210-210.

Alexander, G. M., K. L. Erwin, N. Byers, J. S. Deitch, B. J. Augelli, E. P. Blankenhorn and T. D. Heiman-Patterson (2004). "Effect of transgene copy number on survival in the G93A SOD1 transgenic mouse model of ALS." Brain Res Mol Brain Res **130**(1-2): 7-15.

Aley, K. O., R. O. Messing, D. Mochly-Rosen and J. D. Levine (2000). "Chronic hypersensitivity for inflammatory nociceptor sensitization mediated by the epsilon isozyme of protein kinase C." J Neurosci **20**(12): 4680-4685.

Allouis, M., F. Le Bouffant, R. Wilders, D. Peroz, J. J. Schott, J. Noireaud, H. Le Marec, J. Merot, D. Escande and I. Baro (2006). "14-3-3 is a regulator of the cardiac voltage-gated sodium channel Nav1.5." Circ Res **98**(12): 1538-1546.

Alvarez de la Rosa, D., S. R. Krueger, A. Kolar, D. Shao, R. M. Fitzsimonds and C. M. Canessa (2003). "Distribution, subcellular localization and ontogeny of ASIC1 in the mammalian central nervous system." J Physiol **546**(Pt 1): 77-87.

Amaya, F., H. Wang, M. Costigan, A. J. Allchorne, J. P. Hatcher, J. Egerton, T. Stean, V. Morisset, D. Grose, M. J. Gunthorpe, I. P. Chessell, S. Tate, P. J. Green and C. J. Woolf (2006). "The voltage-gated sodium channel Na(v)1.9 is an effector of peripheral inflammatory pain hypersensitivity." J Neurosci **26**(50): 12852-12860.

Amerik, A. Y. and M. Hochstrasser (2004). "Mechanism and function of deubiquitinating enzymes." Biochim Biophys Acta **1695**(1-3): 189-207.

Andersson, D. A., C. Gentry and S. Bevan (2012). "TRPA1 has a key role in the somatic pro-nociceptive actions of hydrogen sulfide." PLoS One **7**(10): e46917.

Andrade, E. L., F. C. Meotti and J. B. Calixto (2012). "TRPA1 antagonists as potential analgesic drugs." Pharmacol Ther **133**(2): 189-204.

Angrand, P. O., I. Segura, P. Volkel, S. Ghidelli, R. Terry, M. Brajenovic, K. Vintersten, R. Klein, G. Superti-Furga, G. Drewes, B. Kuster, T. Bouwmeester and A. Acker-Palmer (2006). "Transgenic mouse proteomics identifies new 14-3-3-associated proteins involved in cytoskeletal rearrangements and cell signaling." Mol Cell Proteomics **5**(12): 2211-2227.

Asante, C. O., V. C. Wallace and A. H. Dickenson (2009). "Formalin-induced behavioural hypersensitivity and neuronal hyperexcitability are mediated by rapid protein synthesis at the spinal level." Mol Pain **5**: 27.

Ashpole, N. M., A. W. Herren, K. S. Ginsburg, J. D. Brogan, D. E. Johnson, T. R. Cummins, D. M. Bers and A. Hudmon (2012). "Ca2+/calmodulin-dependent protein kinase II (CaMKII) regulates cardiac sodium channel NaV1.5 gating by multiple phosphorylation sites." J Biol Chem **287**(24): 19856-19869.

Attal, N., C. Fermanian, J. Fermanian, M. Lanteri-Minet, H. Alchaar and D. Bouhassira (2008). "Neuropathic pain: are there distinct subtypes depending on the aetiology or anatomical lesion?" Pain **138**(2): 343-353.

Averill, S., J. D. Delcroix, G. J. Michael, D. R. Tomlinson, P. Fernyhough and J. V. Priestley (2001). "Nerve growth factor modulates the activation status and fast axonal transport of ERK 1/2 in adult nociceptive neurones." Mol Cell Neurosci **18**(2): 183-196.

Baker, M. D., S. Y. Chandra, Y. Ding, S. G. Waxman and J. N. Wood (2003). "GTP-induced tetrodotoxin-resistant Na+ current regulates excitability in mouse and rat small diameter sensory neurones." J Physiol **548**(Pt 2): 373-382.

Ballester, M., A. Castello, E. Ibanez, A. Sanchez and J. M. Folch (2004). "Real-time quantitative PCR-based system for determining transgene copy number in transgenic animals." Biotechniques **37**(4): 610-613.

Bautista, D. M., S. E. Jordt, T. Nikai, P. R. Tsuruda, A. J. Read, J. Poblete, E. N. Yamoah, A. I. Basbaum and D. Julius (2006). "TRPA1 mediates the inflammatory actions of environmental irritants and proalgesic agents." Cell **124**(6): 1269-1282.

Bautista, D. M., J. Siemens, J. M. Glazer, P. R. Tsuruda, A. I. Basbaum, C. L. Stucky, S. E. Jordt and D. Julius (2007). "The menthol receptor TRPM8 is the principal detector of environmental cold." Nature **448**(7150): 204-208.

Beckh, S., M. Noda, H. Lubbert and S. Numa (1989). "Differential regulation of three sodium channel messenger RNAs in the rat central nervous system during development." EMBO J **8**(12): 3611-3616.

Beiter, T., E. Reich, R. W. Williams and P. Simon (2009). "Antisense transcription: a critical look in both directions." Cell Mol Life Sci **66**(1): 94-112.

Bennett, D. L., G. J. Michael, N. Ramachandran, J. B. Munson, S. Averill, Q. Yan, S. B. McMahon and J. V. Priestley (1998). "A distinct subgroup of small DRG cells express GDNF receptor components and GDNF is protective for these neurons after nerve injury." J Neurosci **18**(8): 3059-3072.

Bennett, E., M. S. Urcan, S. S. Tinkle, A. G. Koszowski and S. R. Levinson (1997). "Contribution of sialic acid to the voltage dependence of sodium channel gating. A possible electrostatic mechanism." J Gen Physiol **109**(3): 327-343.

Berggard, T., G. Arrigoni, O. Olsson, M. Fex, S. Linse and P. James (2006). "140 mouse brain proteins identified by Ca2+-calmodulin affinity chromatography and tandem mass spectrometry." J Proteome Res **5**(3): 669-687.

Berggard, T., S. Linse and P. James (2007). "Methods for the detection and analysis of protein-protein interactions." Proteomics **7**(16): 2833-2842.

Bessou, P. and E. R. Perl (1969). "Response of cutaneous sensory units with unmyelinated fibers to noxious stimuli." J Neurophysiol **32**(6): 1025-1043.

Biswas, S., I. Deschenes, D. Disilvestre, Y. Tian, V. L. Halperin and G. F. Tomaselli (2008). "Calmodulin regulation of Nav1.4 current: role of binding to the carboxyl terminus." J Gen Physiol **131**(3): 197-209.

Black, J. A., N. Frezel, S. D. Dib-Hajj and S. G. Waxman (2012). "Expression of Nav1.7 in DRG neurons extends from peripheral terminals in the skin to central preterminal branches and terminals in the dorsal horn." Mol Pain **8**: 82.

Black, J. A., J. G. Hoeijmakers, C. G. Faber, I. S. Merkies and S. G. Waxman (2013). "NaV1.7: stress-induced changes in immunoreactivity within magnocellular neurosecretory neurons of the supraoptic nucleus." Mol Pain **9**: 39.

Black, J. A., S. Liu, M. Tanaka, T. R. Cummins and S. G. Waxman (2004). "Changes in the expression of tetrodotoxin-sensitive sodium channels within dorsal root ganglia neurons in inflammatory pain." Pain **108**(3): 237-247.

Blum, R. and A. Lepier (2008). "The luminal domain of p23 (Tmp21) plays a critical role in p23 cell surface trafficking." Traffic **9**(9): 1530-1550.

Bosmans, F., M. Milescu and K. J. Swartz (2011). "Palmitoylation influences the function and pharmacology of sodium channels." Proc Natl Acad Sci U S A **108**(50): 20213-20218.

Brackenbury, W. J., A. M. Chioni, J. K. Diss and M. B. Djamgoz (2007). "The neonatal splice variant of Nav1.5 potentiates in vitro invasive behaviour of MDA-MB-231 human breast cancer cells." Breast Cancer Res Treat **101**(2): 149-160.

Brederson, J. D., P. R. Kym and A. Szallasi (2013). "Targeting TRP channels for pain relief." Eur J Pharmacol **716**(1-3): 61-76.

Breivik, H., B. Collett, V. Ventafridda, R. Cohen and D. Gallacher (2006). "Survey of chronic pain in Europe: prevalence, impact on daily life, and treatment." Eur J Pain **10**(4): 287-333.

Brittain, J. M., A. D. Piekarz, Y. Wang, T. Kondo, T. R. Cummins and R. Khanna (2009). "An atypical role for collapsin response mediator protein 2 (CRMP-2) in neurotransmitter release via interaction with presynaptic voltage-gated calcium channels." J Biol Chem **284**(45): 31375-31390.

Burgess, P. R. and E. R. Perl (1967). "Myelinated afferent fibres responding specifically to noxious stimulation of the skin." J Physiol **190**(3): 541-562.

Cachemaille, M., C. J. Laedermann, M. Pertin, H. Abriel, R. D. Gosselin and I. Decosterd (2012). "Neuronal expression of the ubiquitin ligase Nedd4-2 in rat dorsal root ganglia: modulation in the spared nerve injury model of neuropathic pain." Neuroscience **227**: 370-380.

Cain, D. M., S. G. Khasabov and D. A. Simone (2001). "Response properties of mechanoreceptors and nociceptors in mouse glabrous skin: an in vivo study." J Neurophysiol **85**(4): 1561-1574.

Campbell, T. M., M. J. Main and E. M. Fitzgerald (2013). "Functional expression of the voltage-gated Na(+)-channel Nav1.7 is necessary for EGF-mediated invasion in human non-small cell lung cancer cells." J Cell Sci **126**(Pt 21): 4939-4949.

Cantrell, A. R., V. C. Tibbs, R. E. Westenbroek, T. Scheuer and W. A. Catterall (1999). "Dopaminergic modulation of voltage-gated Na+ current in rat hippocampal neurons requires anchoring of cAMP-dependent protein kinase." J Neurosci **19**(17): RC21.

Cantrell, A. R., V. C. Tibbs, F. H. Yu, B. J. Murphy, E. M. Sharp, Y. Qu, W. A. Catterall and T. Scheuer (2002). "Molecular mechanism of convergent regulation of brain Na(+) channels by protein kinase C and protein kinase A anchored to AKAP-15." Mol Cell Neurosci **21**(1): 63-80.

Caterina, M. J., A. Leffler, A. B. Malmberg, W. J. Martin, J. Trafton, K. R. Petersen-Zeitz, M. Koltzenburg, A. I. Basbaum and D. Julius (2000). "Impaired nociception and pain sensation in mice lacking the capsaicin receptor." Science **288**(5464): 306-313.

Caterina, M. J., M. A. Schumacher, M. Tominaga, T. A. Rosen, J. D. Levine and D. Julius (1997). "The capsaicin receptor: a heat-activated ion channel in the pain pathway." Nature **389**(6653): 816-824.

Catterall, W. A. (2000). "From ionic currents to molecular mechanisms: the structure and function of voltage-gated sodium channels." Neuron **26**(1): 13-25.

Catterall, W. A., A. L. Goldin and S. G. Waxman (2005). "International Union of Pharmacology. XLVII. Nomenclature and structure-function relationships of voltage-gated sodium channels." Pharmacol Rev **57**(4): 397-409.

Cavanaugh, D. J., H. Lee, L. Lo, S. D. Shields, M. J. Zylka, A. I. Basbaum and D. J. Anderson (2009). "Distinct subsets of unmyelinated primary sensory fibers mediate behavioral responses to noxious thermal and mechanical stimuli." Proc Natl Acad Sci U S A **106**(22): 9075-9080.

Centonze, D., S. Rossi, I. Napoli, V. Mercaldo, C. Lacoux, F. Ferrari, M. T. Ciotti, V. De Chiara, C. Prosperetti, M. Maccarrone, F. Fezza, P. Calabresi, G. Bernardi and C. Bagni (2007). "The brain cytoplasmic RNA BC1 regulates dopamine D2 receptor-mediated transmission in the striatum." J Neurosci **27**(33): 8885-8892.

Chaib, H., M. A. Rubin, N. R. Mucci, L. Li, J. M. G. Taylor, M. L. Day, J. S. Rhim and J. A. Macoska (2001). "Activated in prostate cancer: a PDZ domain-containing protein highly expressed in human primary prostate tumors." Cancer Res **61**(6): 2390-2394.

Chandler, K. J., R. L. Chandler, E. M. Broeckelmann, Y. Hou, E. M. Southard-Smith and D. P. Mortlock (2007). "Relevance of BAC transgene copy number in mice: transgene copy number variation across multiple transgenic lines and correlations with transgene integrity and expression." Mamm Genome **18**(10): 693-708.

Chaplan, S. R., F. W. Bach, J. W. Pogrel, J. M. Chung and T. L. Yaksh (1994). "Quantitative assessment of tactile allodynia in the rat paw." J Neurosci Methods **53**(1): 55-63.

Charalambous, K. and B. A. Wallace (2011). "NaChBac: the long lost sodium channel ancestor." Biochemistry **50**(32): 6742-6752.

Chatelier, A., L. Dahllund, A. Eriksson, J. Krupp and M. Chahine (2008). "Biophysical properties of human Na v1.7 splice variants and their regulation by protein kinase A." J Neurophysiol **99**(5): 2241-2250.

Chattopadhyay, M., M. Mata and D. J. Fink (2008). "Continuous delta-opioid receptor activation reduces neuronal voltage-gated sodium channel (NaV1.7) levels through activation of protein kinase C in painful diabetic neuropathy." J Neurosci **28**(26): 6652-6658.

Chen, C., V. Bharucha, Y. Chen, R. E. Westenbroek, A. Brown, J. D. Malhotra, D. Jones, C. Avery, P. J. Gillespie, 3rd, K. A. Kazen-Gillespie, K. Kazarinova-Noyes, P. Shrager, T. L. Saunders, R. L. Macdonald, B. R. Ransom, T. Scheuer, W. A. Catterall and L. L. Isom (2002). "Reduced sodium channel density, altered voltage dependence of inactivation, and increased susceptibility to seizures in mice lacking sodium channel beta 2-subunits." Proc Natl Acad Sci U S A **99**(26): 17072-17077.

Chen, C., J. D. Calhoun, Y. Zhang, L. Lopez-Santiago, N. Zhou, T. H. Davis, J. L. Salzer and L. L. Isom (2012). "Identification of the cysteine residue responsible for disulfide linkage of Na+ channel alpha and beta2 subunits." J Biol Chem **287**(46): 39061-39069.

Chen, C., R. E. Westenbroek, X. Xu, C. A. Edwards, D. R. Sorenson, Y. Chen, D. P. McEwen, H. A. O'Malley, V. Bharucha, L. S. Meadows, G. A. Knudsen, A. Vilaythong, J. L. Noebels, T. L. Saunders, T. Scheuer, P. Shrager, W. A. Catterall and L. L. Isom (2004). "Mice lacking sodium channel beta1 subunits display defects in neuronal excitability, sodium channel expression, and nodal architecture." J Neurosci **24**(16): 4030-4042.

Catterall and L. L. Isom (2004). "Mice lacking sodium channel beta1 subunits display defects in neuronal excitability, sodium channel expression, and nodal architecture." J Neurosci **24**(16): 4030-4042.

Chen, F., H. Hasegawa, G. Schmitt-Ulms, T. Kawarai, C. Bohm, T. Katayama, Y. Gu, N. Sanjo, M. Glista, E. Rogaeva, Y. Wakutani, R. Pardossi-Piquard, X. Ruan, A. Tandon, F. Checler, P. Marambaud, K. Hansen, D. Westaway, P. St George-Hyslop and P. Fraser (2006). "TMP21 is a presenilin complex component that modulates gamma-secretase but not epsilon-secretase activity." Nature **440**(7088): 1208-1212.

Chen, J., S. K. Joshi, S. DiDomenico, R. J. Perner, J. P. Mikusa, D. M. Gauvin, J. A. Segreti, P. Han, X. F. Zhang, W. Niforatos, B. R. Bianchi, S. J. Baker, C. Zhong, G. H. Simler, H. A. McDonald, R. G. Schmidt, S. P. McGaraughty, K. L. Chu, C. R. Faltynek, M. E. Kort, R. M. Reilly and P. R. Kym (2011). "Selective blockade of TRPA1 channel attenuates pathological pain without altering noxious cold sensation or body temperature regulation." Pain **152**(5): 1165-1172.

Cheng, W., C. Sun and J. Zheng (2010). "Heteromerization of TRP channel subunits: extending functional diversity." Protein Cell **1**(9): 802-810.

Cheng, X., S. D. Dib-Hajj, L. Tyrrell and S. G. Waxman (2008). "Mutation I136V alters electrophysiological properties of the Na(v)1.7 channel in a family with onset of erythromelalgia in the second decade." Mol Pain **4**: 1.

Chi, X. X., B. S. Schmutzler, J. M. Brittain, Y. Wang, C. M. Hingtgen, G. D. Nicol and R. Khanna (2009). "Regulation of N-type voltage-gated calcium channels (Cav2.2) and transmitter release by collapsin response mediator protein-2 (CRMP-2) in sensory neurons." J Cell Sci **122**(Pt 23): 4351-4362.

Cho, J. H. and C. C. Askwith (2008). "Presynaptic release probability is increased in hippocampal neurons from ASIC1 knockout mice." J Neurophysiol **99**(2): 426-441.

Choi, J. S., X. Cheng, E. Foster, A. Leffler, L. Tyrrell, R. H. Te Morsche, E. M. Eastman, H. J. Jansen, K. Huehne, C. Nau, S. D. Dib-Hajj, J. P. Drenth and S. G. Waxman (2010). "Alternative splicing may contribute to time-dependent manifestation of inherited erythromelalgia." Brain **133**(Pt 6): 1823-1835.

Choi, J. S., L. Zhang, S. D. Dib-Hajj, C. Han, L. Tyrrell, Z. Lin, X. Wang, Y. Yang and S. G. Waxman (2009). "Mexiletine-responsive erythromelalgia due to a new Na(v)1.7 mutation showing use-dependent current fall-off." Exp Neurol **216**(2): 383-389.

Chorna-Ornan, I., V. Tzarfaty, G. Ankri-Eliahoo, T. Joel-Almagor, N. E. Meyer, A. Huber, F. Payre and B. Minke (2005). "Light-regulated interaction of Dmoesin with TRP and TRPL channels is required for maintenance of photoreceptors." J Cell Biol **171**(1): 143-152.

Chung, D. W., D. D. Rudnicki, L. Yu and R. L. Margolis (2011). "A natural antisense transcript at the Huntington's disease repeat locus regulates HTT expression." Hum Mol Genet **20**(17): 3467-3477.

Cohen, I. J. and C. S. Samorodin (1982). "Familial erythromelalgia." Arch Dermatol **118**(11): 953-954.

Colburn, R. W., M. L. Lubin, D. J. Stone, Jr., Y. Wang, D. Lawrence, M. R. D'Andrea, M. R. Brandt, Y. Liu, C. M. Flores and N. Qin (2007). "Attenuated cold sensitivity in TRPM8 null mice." Neuron **54**(3): 379-386.

Copeland, N. G., N. A. Jenkins and D. L. Court (2001). "Recombineering: a powerful new tool for mouse functional genomics." Nat Rev Genet **2**(10): 769-779.

Cox, J. J., F. Reimann, A. K. Nicholas, G. Thornton, E. Roberts, K. Springell, G. Karbani, H. Jafri, J. Mannan, Y. Raashid, L. Al-Gazali, H. Hamamy, E. M. Valente, S. Gorman, R. Williams, D. P. McHale, J. N. Wood, F. M. Gribble and C. G. Woods (2006). "An SCN9A channelopathy causes congenital inability to experience pain." Nature **444**(7121): 894-898.

Cox, J. J., J. Sheynin, Z. Shorer, F. Reimann, A. K. Nicholas, L. Zubovic, M. Baralle, E. Wraige, E. Manor, J. Levy, C. G. Woods and R. Parvari (2010). "Congenital insensitivity to pain: novel SCN9A missense and in-frame deletion mutations." Hum Mutat **31**(9): E1670-1686.

Cregg, R., J. J. Cox, D. L. Bennett, J. N. Wood and R. Werdehausen (2014). "Mexiletine as a treatment for primary erythromelalgia: normalization of biophysical properties of mutant L858F NaV 1.7 sodium channels." Br J Pharmacol **171**(19): 4455-4463.

Cronin, N. B., A. O'Reilly, H. Duclohier and B. A. Wallace (2005). "Effects of deglycosylation of sodium channels on their structure and function." Biochemistry **44**(2): 441-449.

Cummins, T. R., S. D. Dib-Hajj, J. A. Black, A. N. Akopian, J. N. Wood and S. G. Waxman (1999). "A novel persistent tetrodotoxin-resistant sodium current in SNS-null and wild-type small primary sensory neurons." J Neurosci **19**(24): RC43.

Cummins, T. R., S. D. Dib-Hajj and S. G. Waxman (2004). "Electrophysiological properties of mutant Nav1.7 sodium channels in a painful inherited neuropathy." J Neurosci **24**(38): 8232-8236.

Cummins, T. R., J. R. Howe and S. G. Waxman (1998). "Slow closed-state inactivation: a novel mechanism underlying ramp currents in cells expressing the hNE/PN1 sodium channel." J Neurosci **18**(23): 9607-9619.

Dai, S., D. D. Hall and J. W. Hell (2009). "Supramolecular assemblies and localized regulation of voltage-gated ion channels." Physiol Rev **89**(2): 411-452.
Dar, R., D. Ariely and H. Frenk (1995). "The effect of past-injury on pain threshold and tolerance." Pain **60**(2): 189-193.

Davis, M. D., P. Sandroni, T. W. Rooke and P. A. Low (2003). "Erythromelalgia: vasculopathy, neuropathy, or both? A prospective study of vascular and

neurophysiologic studies in erythromelalgia." Arch Dermatol **139**(10): 1337-1343.

de Oliveira Rocha, R., M. J. Teixeira, L. T. Yeng, M. G. Cantara, V. G. Faria, V. Liggieri, A. Loduca, B. M. Muller, A. C. Souza and D. C. de Andrade (2014). "Thoracic sympathetic block for the treatment of complex regional pain syndrome type I: a double-blind randomized controlled study." Pain **155**(11): 2274-2281.

Decosterd, I. and C. J. Woolf (2000). "Spared nerve injury: an animal model of persistent peripheral neuropathic pain." Pain **87**(2): 149-158.

Deguchi, M., T. Iizuka, Y. Hata, W. Nishimura, K. Hirao, I. Yao, H. Kawabe and Y. Takai (2000). "PAPIN. A novel multiple PSD-95/Dlg-A/ZO-1 protein interacting with neural plakophilin-related armadillo repeat protein/delta-catenin and p0071." J Biol Chem **275**(38): 29875-29880.

del Camino, D., S. Murphy, M. Heiry, L. B. Barrett, T. J. Earley, C. A. Cook, M. J. Petrus, M. Zhao, M. D'Amours, N. Deering, G. J. Brenner, M. Costigan, N. J. Hayward, J. A. Chong, C. M. Fanger, C. J. Woolf, A. Patapoutian and M. M. Moran (2010). "TRPA1 contributes to cold hypersensitivity." J Neurosci **30**(45): 15165-15174.

Deschenes, I., N. Neyroud, D. DiSilvestre, E. Marban, D. T. Yue and G. F. Tomaselli (2002). "Isoform-specific modulation of voltage-gated Na(+) channels by calmodulin." Circ Res **90**(4): E49-57.

Deuis, J. R., K. Zimmermann, A. A. Romanovsky, L. D. Possani, P. J. Cabot, R. J. Lewis and I. Vetter (2013). "An animal model of oxaliplatin-induced cold allodynia reveals a crucial role for Nav1.6 in peripheral pain pathways." Pain **154**(9): 1749-1757.

Deval, E., J. Noel, N. Lay, A. Alloui, S. Diochot, V. Friend, M. Jodar, M. Lazdunski and E. Lingueglia (2008). "ASIC3, a sensor of acidic and primary inflammatory pain." EMBO J **27**(22): 3047-3055.

Dhaka, A., A. N. Murray, J. Mathur, T. J. Earley, M. J. Petrus and A. Patapoutian (2007). "TRPM8 is required for cold sensation in mice." Neuron **54**(3): 371-378.

Dib-Hajj, S., J. A. Black, T. R. Cummins and S. G. Waxman (2002). "NaN/Nav1.9: a sodium channel with unique properties." Trends Neurosci **25**(5): 253-259.

Dib-Hajj, S. D., M. Estacion, B. W. Jarecki, L. Tyrrell, T. Z. Fischer, M. Lawden, T. R. Cummins and S. G. Waxman (2008). "Paroxysmal extreme pain disorder M1627K mutation in human Nav1.7 renders DRG neurons hyperexcitable." Mol Pain **4**: 37.

Dib-Hajj, S. D., A. M. Rush, T. R. Cummins, F. M. Hisama, S. Novella, L. Tyrrell, L. Marshall and S. G. Waxman (2005). "Gain-of-function mutation in Nav1.7 in familial erythromelalgia induces bursting of sensory neurons." Brain **128**(Pt 8): 1847-1854.

Dib-Hajj, S. D., L. Tyrrell, J. A. Black and S. G. Waxman (1998). "NaN, a novel voltage-gated Na channel, is expressed preferentially in peripheral sensory neurons and down-regulated after axotomy." Proc Natl Acad Sci U S A **95**(15): 8963-8968.

Dib-Hajj, S. D., Y. Yang, J. A. Black and S. G. Waxman (2013). "The Na(V)1.7 sodium channel: from molecule to man." Nat Rev Neurosci **14**(1): 49-62.

Dichgans, M., T. Freilinger, G. Eckstein, E. Babini, B. Lorenz-Depiereux, S. Biskup, M. D. Ferrari, J. Herzog, A. M. van den Maagdenberg, M. Pusch and T. M. Strom (2005). "Mutation in the neuronal voltage-gated sodium channel SCN1A in familial hemiplegic migraine." Lancet **366**(9483): 371-377.

Diss, J. K., D. Stewart, F. Pani, C. S. Foster, M. M. Walker, A. Patel and M. B. Djamgoz (2005). "A potential novel marker for human prostate cancer: voltage-gated sodium channel expression in vivo." Prostate Cancer Prostatic Dis **8**(3): 266-273.

Djouhri, L., X. Fang, K. Okuse, J. N. Wood, C. M. Berry and S. N. Lawson (2003). "The TTX-resistant sodium channel Nav1.8 (SNS/PN3): expression and correlation with membrane properties in rat nociceptive primary afferent neurons." J Physiol **550**(Pt 3): 739-752.

Dominguez, M., K. Dejgaard, J. Fullekrug, S. Dahan, A. Fazel, J. P. Paccaud, D. Y. Thomas, J. J. Bergeron and T. Nilsson (1998). "gp25L/emp24/p24 protein family members of the cis-Golgi network bind both COP I and II coatomer." J Cell Biol **140**(4): 751-765.

Dong, X., S. Han, M. J. Zylka, M. I. Simon and D. J. Anderson (2001). "A diverse family of GPCRs expressed in specific subsets of nociceptive sensory neurons." Cell **106**(5): 619-632.

Donier, E., F. Rugiero, K. Okuse and J. N. Wood (2005). "Annexin II light chain p11 promotes functional expression of acid-sensing ion channel ASIC1a." J Biol Chem **280**(46): 38666-38672.

Drenth, J. P., R. H. te Morsche, G. Guillet, A. Taieb, R. L. Kirby and J. B. Jansen (2005). "SCN9A mutations define primary erythermalgia as a neuropathic disorder of voltage gated sodium channels." J Invest Dermatol **124**(6): 1333-1338.

Drenth, J. P., R. H. Te Morsche, S. Mansour and P. S. Mortimer (2008). "Primary erythermalgia as a sodium channelopathy: screening for SCN9A mutations: exclusion of a causal role of SCN10A and SCN11A." Arch Dermatol **144**(3): 320-324.

Drenth, J. P. and S. G. Waxman (2007). "Mutations in sodium-channel gene SCN9A cause a spectrum of human genetic pain disorders." J Clin Invest **117**(12): 3603-3609.

Dustrude, E. T., S. M. Wilson, W. Ju, Y. Xiao and R. Khanna (2013). "CRMP2 protein SUMOylation modulates NaV1.7 channel trafficking." J Biol Chem **288**(34): 24316-24331.

Eberhardt, M., J. Nakajima, A. B. Klinger, C. Neacsu, K. Huhne, A. O. O'Reilly, A. M. Kist, A. K. Lampe, K. Fischer, J. Gibson, C. Nau, A. Winterpacht and A. Lampert (2014). "Inherited pain: sodium channel Nav1.7 A1632T mutation causes erythromelalgia due to a shift of fast inactivation." J Biol Chem **289**(4): 1971-1980.

Echarri, A., O. Muriel and M. A. Del Pozo (2007). "Intracellular trafficking of raft/caveolae domains: insights from integrin signaling." Semin Cell Dev Biol **18**(5): 627-637.

Eddy, N. B. and D. Leimbach (1953). "Synthetic analgesics. II. Dithienylbutenyl- and dithienylbutylamines." J Pharmacol Exp Ther **107**(3): 385-393.

Einheber, S., G. Zanazzi, W. Ching, S. Scherer, T. A. Milner, E. Peles and J. L. Salzer (1997). "The axonal membrane protein Caspr, a homologue of neurexin IV, is a component of the septate-like paranodal junctions that assemble during myelination." J Cell Biol **139**(6): 1495-1506.

Ernst, S. J., L. Aguilar-Bryan and J. L. Noebels (2009). "Sodium channel beta1 regulatory subunit deficiency reduces pancreatic islet glucose-stimulated insulin and glucagon secretion." Endocrinology **150**(3): 1132-1139.

Errington, A. C., T. Stohr, C. Heers and G. Lees (2008). "The investigational anticonvulsant lacosamide selectively enhances slow inactivation of voltage-gated sodium channels." Mol Pharmacol **73**(1): 157-169.

Escayg, A., A. Heils, B. T. MacDonald, K. Haug, T. Sander and M. H. Meisler (2001). "A novel SCN1A mutation associated with generalized epilepsy with febrile seizures plus--and prevalence of variants in patients with epilepsy." Am J Hum Genet **68**(4): 866-873.

Estacion, M., S. D. Dib-Hajj, P. J. Benke, R. H. Te Morsche, E. M. Eastman, L. J. Macala, J. P. Drenth and S. G. Waxman (2008). "NaV1.7 gain-of-function mutations as a continuum: A1632E displays physiological changes associated

with erythromelalgia and paroxysmal extreme pain disorder mutations and produces symptoms of both disorders." J Neurosci **28**(43): 11079-11088.

Faber, C. G., G. Lauria, I. S. Merkies, X. Cheng, C. Han, H. S. Ahn, A. K. Persson, J. G. Hoeijmakers, M. M. Gerrits, T. Pierro, R. Lombardi, D. Kapetis, S. D. Dib-Hajj and S. G. Waxman (2012). "Gain-of-function Nav1.8 mutations in painful neuropathy." Proc Natl Acad Sci U S A **109**(47): 19444-19449.

Faghihi, M. A., F. Modarresi, A. M. Khalil, D. E. Wood, B. G. Sahagan, T. E. Morgan, C. E. Finch, G. St Laurent, 3rd, P. J. Kenny and C. Wahlestedt (2008). "Expression of a noncoding RNA is elevated in Alzheimer's disease and drives rapid feed-forward regulation of beta-secretase." Nat Med **14**(7): 723-730.

Faghihi, M. A. and C. Wahlestedt (2009). "Regulatory roles of natural antisense transcripts." Nat Rev Mol Cell Biol **10**(9): 637-643.

Fahmi, A. I., M. Patel, E. B. Stevens, A. L. Fowden, J. E. John, 3rd, K. Lee, R. Pinnock, K. Morgan, A. P. Jackson and J. I. Vandenberg (2001). "The sodium channel beta-subunit SCN3b modulates the kinetics of SCN5a and is expressed heterogeneously in sheep heart." J Physiol **537**(Pt 3): 693-700.

Fang, X., L. Djouhri, J. A. Black, S. D. Dib-Hajj, S. G. Waxman and S. N. Lawson (2002). "The presence and role of the tetrodotoxin-resistant sodium channel Na(v)1.9 (NaN) in nociceptive primary afferent neurons." J Neurosci **22**(17): 7425-7433.

Farmer, C., J. J. Cox, E. V. Fletcher, C. G. Woods, J. N. Wood and S. Schorge (2012). "Splice variants of Na(V)1.7 sodium channels have distinct beta subunit-dependent biophysical properties." PLoS One **7**(7): e41750.

Fernandez, E., M. O. Collins, R. T. Uren, M. V. Kopanitsa, N. H. Komiyama, M. D. Croning, L. Zografos, J. D. Armstrong, J. S. Choudhary and S. G. Grant (2009). "Targeted tandem affinity purification of PSD-95 recovers core postsynaptic complexes and schizophrenia susceptibility proteins." Mol Syst Biol **5**: 269.

Fertleman, C. R., M. D. Baker, K. A. Parker, S. Moffatt, F. V. Elmslie, B. Abrahamsen, J. Ostman, N. Klugbauer, J. N. Wood, R. M. Gardiner and M. Rees (2006). "SCN9A mutations in paroxysmal extreme pain disorder: allelic variants underlie distinct channel defects and phenotypes." Neuron **52**(5): 767-774.

Fertleman, C. R., C. D. Ferrie, J. Aicardi, N. A. Bednarek, O. Eeg-Olofsson, F. V. Elmslie, D. A. Griesemer, F. Goutieres, M. Kirkpatrick, I. N. Malmros, M. Pollitzer, M. Rossiter, E. Roulet-Perez, R. Schubert, V. V. Smith, H. Testard, V. Wong and J. B. Stephenson (2007). "Paroxysmal extreme pain disorder (previously familial rectal pain syndrome)." Neurology **69**(6): 586-595.

Few, W. P., T. Scheuer and W. A. Catterall (2007). "Dopamine modulation of neuronal Na(+) channels requires binding of A kinase-anchoring protein 15 and PKA by a modified leucine zipper motif." Proc Natl Acad Sci U S A **104**(12): 5187-5192.

Finley, W. H., J. R. Lindsey, Jr., J. D. Fine, G. A. Dixon and M. K. Burbank (1992). "Autosomal dominant erythromelalgia." Am J Med Genet **42**(3): 310-315.

Fotia, A. B., J. Ekberg, D. J. Adams, D. I. Cook, P. Poronnik and S. Kumar (2004). "Regulation of neuronal voltage-gated sodium channels by the ubiquitin-protein ligases Nedd4 and Nedd4-2." J Biol Chem **279**(28): 28930-28935.

Foulkes, T., M. A. Nassar, T. Lane, E. A. Matthews, M. D. Baker, V. Gerke, K. Okuse, A. H. Dickenson and J. N. Wood (2006). "Deletion of annexin 2 light chain p11 in nociceptors causes deficits in somatosensory coding and pain behavior." J Neurosci **26**(41): 10499-10507.

Frankland, P. W., C. O'Brien, M. Ohno, A. Kirkwood and A. J. Silva (2001). "Alpha-CaMKII-dependent plasticity in the cortex is required for permanent memory." Nature **411**(6835): 309-313.

Fraser, S. P., J. K. Diss, A. M. Chioni, M. E. Mycielska, H. Pan, R. F. Yamaci, F. Pani, Z. Siwy, M. Krasowska, Z. Grzywna, W. J. Brackenbury, D. Theodorou, M. Koyuturk, H. Kaya, E. Battaloglu, M. T. De Bella, M. J. Slade, R. Tolhurst, C. Palmieri, J. Jiang, D. S. Latchman, R. C. Coombes and M. B. Djamgoz (2005). "Voltage-gated sodium channel expression and potentiation of human breast cancer metastasis." Clin Cancer Res **11**(15): 5381-5389.

Fritz, G., C. Brachetti, F. Bahlmann, M. Schmidt and B. Kaina (2002). "Rho GTPases in human breast tumours: expression and mutation analyses and correlation with clinical parameters." Br J Cancer **87**(6): 635-644.

Garrido, J. J., F. Fernandes, A. Moussif, M. P. Fache, P. Giraud and B. Dargent (2003). "Dynamic compartmentalization of the voltage-gated sodium channels in axons." Biol Cell **95**(7): 437-445.

Gaur, S. and T. Koroscil (2009). "Late-onset erythromelalgia in a previously healthy young woman: a case report and review of the literature." J Med Case Rep **3**: 106.

Gavillet, B., J. S. Rougier, A. A. Domenighetti, R. Behar, C. Boixel, P. Ruchat, H. A. Lehr, T. Pedrazzini and H. Abriel (2006). "Cardiac sodium channel Nav1.5 is regulated by a multiprotein complex composed of syntrophins and dystrophin." Circ Res **99**(4): 407-414.

Gavin, A. C., M. Bosche, R. Krause, P. Grandi, M. Marzioch, A. Bauer, J. Schultz, J. M. Rick, A. M. Michon, C. M. Cruciat, M. Remor, C. Hofert, M.

Schelder, M. Brajenovic, H. Ruffner, A. Merino, K. Klein, M. Hudak, D. Dickson, T. Rudi, V. Gnau, A. Bauch, S. Bastuck, B. Huhse, C. Leutwein, M. A. Heurtier, R. R. Copley, A. Edelmann, E. Querfurth, V. Rybin, G. Drewes, M. Raida, T. Bouwmeester, P. Bork, B. Seraphin, B. Kuster, G. Neubauer and G. Superti-Furga (2002). "Functional organization of the yeast proteome by systematic analysis of protein complexes." Nature **415**(6868): 141-147.

Gebhart, G. F. (1996). "Visceral polymodal receptors." Prog Brain Res **113**: 101-112.

George, A. L., Jr., T. J. Knittle and M. M. Tamkun (1992). "Molecular cloning of an atypical voltage-gated sodium channel expressed in human heart and uterus: evidence for a distinct gene family." Proc Natl Acad Sci U S A **89**(11): 4893-4897.

Gilchrist, J., S. Das, F. Van Petegem and F. Bosmans (2013). "Crystallographic insights into sodium-channel modulation by the beta4 subunit." Proc Natl Acad Sci U S A **110**(51): E5016-5024.

Gingras, J., S. Smith, D. J. Matson, D. Johnson, K. Nye, L. Couture, E. Feric, R. Yin, B. D. Moyer, M. L. Peterson, J. B. Rottman, R. J. Beiler, A. B. Malmberg and S. I. McDonough (2014). "Global Nav1.7 knockout mice recapitulate the phenotype of human congenital indifference to pain." PLoS One **9**(9): e105895.

Goldstein, M. E., S. B. House and H. Gainer (1991). "NF-L and peripherin immunoreactivities define distinct classes of rat sensory ganglion cells." J Neurosci Res **30**(1): 92-104.

Gommel, D., L. Orci, E. M. Emig, M. J. Hannah, M. Ravazzola, W. Nickel, J. B. Helms, F. T. Wieland and K. Sohn (1999). "p24 and p23, the major transmembrane proteins of COPI-coated transport vesicles, form hetero-oligomeric complexes and cycle between the organelles of the early secretory pathway." FEBS Lett **447**(2-3): 179-185.

Gonzales, E. B., T. Kawate and E. Gouaux (2009). "Pore architecture and ion sites in acid-sensing ion channels and P2X receptors." Nature **460**(7255): 599-604.

Gould, H. J., 3rd, J. D. England, R. D. Soignier, P. Nolan, L. D. Minor, Z. P. Liu, S. R. Levinson and D. Paul (2004). "Ibuprofen blocks changes in Na v 1.7 and 1.8 sodium channels associated with complete Freund's adjuvant-induced inflammation in rat." J Pain **5**(5): 270-280.

Gowrishankar, K., S. Ghosh, S. Saha, R. C, S. Mayor and M. Rao (2012). "Active remodeling of cortical actin regulates spatiotemporal organization of cell surface molecules." Cell **149**(6): 1353-1367.

Grinchuk, O. V., P. Jenjaroenpun, Y. L. Orlov, J. Zhou and V. A. Kuznetsov (2010). "Integrative analysis of the human cis-antisense gene pairs, miRNAs and their transcription regulation patterns." Nucleic Acids Res **38**(2): 534-547.

Guy, H. R. and P. Seetharamulu (1986). "Molecular model of the action potential sodium channel." Proc Natl Acad Sci U S A **83**(2): 508-512.
Hains, B. C., C. Y. Saab, J. P. Klein, M. J. Craner and S. G. Waxman (2004). "Altered sodium channel expression in second-order spinal sensory neurons contributes to pain after peripheral nerve injury." J Neurosci **24**(20): 4832-4839.

Hains, B. C., C. Y. Saab and S. G. Waxman (2006). "Alterations in burst firing of thalamic VPL neurons and reversal by Na(v)1.3 antisense after spinal cord injury." J Neurophysiol **95**(6): 3343-3352.

Hakim, P., N. Brice, R. Thresher, J. Lawrence, Y. Zhang, A. P. Jackson, A. A. Grace and C. L. Huang (2010). "Scn3b knockout mice exhibit abnormal sino-atrial and cardiac conduction properties." Acta Physiol (Oxf) **198**(1): 47-59.

Hakim, P., I. S. Gurung, T. H. Pedersen, R. Thresher, N. Brice, J. Lawrence, A. A. Grace and C. L. Huang (2008). "Scn3b knockout mice exhibit abnormal ventricular electrophysiological properties." Prog Biophys Mol Biol **98**(2-3): 251-266.

Halon, A., P. Donizy, P. Surowiak and R. Matkowski (2013). "ERM/Rho protein expression in ductal breast cancer: a 15 year follow-up." Cell Oncol (Dordr) **36**(3): 181-190.

Han, C., S. D. Dib-Hajj, Z. Lin, Y. Li, E. M. Eastman, L. Tyrrell, X. Cao, Y. Yang and S. G. Waxman (2009). "Early- and late-onset inherited erythromelalgia: genotype-phenotype correlation." Brain **132**(Pt 7): 1711-1722.

Han, C., A. Lampert, A. M. Rush, S. D. Dib-Hajj, X. Wang, Y. Yang and S. G. Waxman (2007). "Temperature dependence of erythromelalgia mutation L858F in sodium channel Nav1.7." Mol Pain **3**: 3.

Han, C., A. M. Rush, S. D. Dib-Hajj, S. Li, Z. Xu, Y. Wang, L. Tyrrell, X. Wang, Y. Yang and S. G. Waxman (2006). "Sporadic onset of erythermalgia: a gain-of-function mutation in Nav1.7." Ann Neurol **59**(3): 553-558.

Hardie, R. C. and B. Minke (1992). "The trp gene is essential for a light-activated Ca2+ channel in Drosophila photoreceptors." Neuron **8**(4): 643-651.

Hargreaves, K., R. Dubner, F. Brown, C. Flores and J. Joris (1988). "A new and sensitive method for measuring thermal nociception in cutaneous hyperalgesia." Pain **32**(1): 77-88.

Hartshorne, R. P., D. J. Messner, J. C. Coppersmith and W. A. Catterall (1982). "The saxitoxin receptor of the sodium channel from rat brain. Evidence for two nonidentical beta subunits." J Biol Chem **257**(23): 13888-13891.

Harty, T. P., S. D. Dib-Hajj, L. Tyrrell, R. Blackman, F. M. Hisama, J. B. Rose and S. G. Waxman (2006). "Na(V)1.7 mutant A863P in erythromelalgia: effects of altered activation and steady-state inactivation on excitability of nociceptive dorsal root ganglion neurons." J Neurosci **26**(48): 12566-12575.

Hastings, M. L., C. Milcarek, K. Martincic, M. L. Peterson and S. H. Munroe (1997). "Expression of the thyroid hormone receptor gene, erbAalpha, in B lymphocytes: alternative mRNA processing is independent of differentiation but correlates with antisense RNA levels." Nucleic Acids Res **25**(21): 4296-4300.

Hayden, R. and M. Grossman (1959). "Rectal, ocular, and submaxillary pain; a familial autonomic disorder related to proctalgia fugaz: report of a family." AMA J Dis Child **97**(4): 479-482.

Head, B. P., Y. Hu, J. C. Finley, M. D. Saldana, J. A. Bonds, A. Miyanohara, I. R. Niesman, S. S. Ali, F. Murray, P. A. Insel, D. M. Roth, H. H. Patel and P. M. Patel (2011). "Neuron-targeted caveolin-1 protein enhances signaling and promotes arborization of primary neurons." J Biol Chem **286**(38): 33310-33321.

Hedstrom, K. L. and M. N. Rasband (2006). "Intrinsic and extrinsic determinants of ion channel localization in neurons." J Neurochem **98**(5): 1345-1352.

Heimann, D., J. Lotsch, T. Hummel, A. Doehring and B. G. Oertel (2013). "Linkage between increased nociception and olfaction via a SCN9A haplotype." PLoS One **8**(7): e68654.

Herren, A. W., D. M. Bers and E. Grandi (2013). "Post-translational modifications of the cardiac Na channel: contribution of CaMKII-dependent phosphorylation to acquired arrhythmias." Am J Physiol Heart Circ Physiol **305**(4): H431-445.

Herzog, R. I., T. R. Cummins, F. Ghassemi, S. D. Dib-Hajj and S. G. Waxman (2003). "Distinct repriming and closed-state inactivation kinetics of Nav1.6 and Nav1.7 sodium channels in mouse spinal sensory neurons." J Physiol **551**(Pt 3): 741-750.

Herzog, R. I., C. Liu, S. G. Waxman and T. R. Cummins (2003). "Calmodulin binds to the C terminus of sodium channels Nav1.4 and Nav1.6 and differentially modulates their functional properties." J Neurosci **23**(23): 8261-8270.

Hisama, F. M., S. D. Dib-Hajj and S. G. Waxman (1993). SCN9A-Related Inherited Erythromelalgia. GeneReviews(R). R. A. Pagon, M. P. Adam, H. H. Ardinger et al. Seattle WA, University of Washington, Seattle.

Ho, C., J. Zhao, S. Malinowski, M. Chahine and M. E. O'Leary (2012). "Differential expression of sodium channel beta subunits in dorsal root ganglion sensory neurons." J Biol Chem **287**(18): 15044-15053.

Hoffman, J. F., A. Dodson, A. Wickrema and S. D. Dib-Hajj (2004). "Tetrodotoxin-sensitive Na+ channels and muscarinic and purinergic receptors identified in human erythroid progenitor cells and red blood cell ghosts." Proc Natl Acad Sci U S A **101**(33): 12370-12374.

Holm, A. N., A. Rich, S. M. Miller, P. Strege, Y. Ou, S. Gibbons, M. G. Sarr, J. H. Szurszewski, J. L. Rae and G. Farrugia (2002). "Sodium current in human jejunal circular smooth muscle cells." Gastroenterology **122**(1): 178-187.

Hong, S., T. J. Morrow, P. E. Paulson, L. L. Isom and J. W. Wiley (2004). "Early painful diabetic neuropathy is associated with differential changes in tetrodotoxin-sensitive and -resistant sodium channels in dorsal root ganglion neurons in the rat." J Biol Chem **279**(28): 29341-29350.

Hosaka, M., T. Watanabe, Y. Yamauchi, Y. Sakai, M. Suda, S. Mizutani, T. Takeuchi, T. Isobe and T. Izumi (2007). "A subset of p23 localized on secretory granules in pancreatic beta-cells." J Histochem Cytochem **55**(3): 235-245.

Hu, D., H. Barajas-Martinez, E. Burashnikov, M. Springer, Y. Wu, A. Varro, R. Pfeiffer, T. T. Koopmann, J. M. Cordeiro, A. Guerchicoff, G. D. Pollevick and C. Antzelevitch (2009). "A mutation in the beta 3 subunit of the cardiac sodium channel associated with Brugada ECG phenotype." Circ Cardiovasc Genet **2**(3): 270-278.

Huang, J., X. Zhang and P. A. McNaughton (2006). "Inflammatory pain: the cellular basis of heat hyperalgesia." Curr Neuropharmacol **4**(3): 197-206.

Huang, K., M. H. Kang, C. Askew, R. Kang, S. S. Sanders, J. Wan, N. G. Davis and M. R. Hayden (2010). "Palmitoylation and function of glial glutamate transporter-1 is reduced in the YAC128 mouse model of Huntington disease." Neurobiol Dis **40**(1): 207-215.

Huang, L., E. Kinnucan, G. Wang, S. Beaudenon, P. M. Howley, J. M. Huibregtse and N. P. Pavletich (1999). "Structure of an E6AP-UbcH7 complex: insights into ubiquitination by the E2-E3 enzyme cascade." Science **286**(5443): 1321-1326.

Huang, S. J., W. S. Yang, Y. W. Lin, H. C. Wang and C. C. Chen (2008). "Increase of insulin sensitivity and reversal of age-dependent glucose intolerance with inhibition of ASIC3." Biochem Biophys Res Commun **371**(4): 729-734.

Huibregtse, J. M., M. Scheffner, S. Beaudenon and P. M. Howley (1995). "A family of proteins structurally and functionally related to the E6-AP ubiquitin-protein ligase." Proc Natl Acad Sci U S A **92**(11): 5249.

Hund, T. J., O. M. Koval, J. Li, P. J. Wright, L. Qian, J. S. Snyder, H. Gudmundsson, C. F. Kline, N. P. Davidson, N. Cardona, M. N. Rasband, M. E. Anderson and P. J. Mohler (2010). "A beta(IV)-spectrin/CaMKII signaling complex is essential for membrane excitability in mice." J Clin Invest **120**(10): 3508-3519.

Igwe, O. J. and B. M. Chronwall (2001). "Hyperalgesia induced by peripheral inflammation is mediated by protein kinase C betaII isozyme in the rat spinal cord." Neuroscience **104**(3): 875-890.

Inagaki, N., K. Chihara, N. Arimura, C. Menager, Y. Kawano, N. Matsuo, T. Nishimura, M. Amano and K. Kaibuchi (2001). "CRMP-2 induces axons in cultured hippocampal neurons." Nat Neurosci **4**(8): 781-782.

Ingham, D. J., S. Beer, S. Money and G. Hansen (2001). "Quantitative real-time PCR assay for determining transgene copy number in transformed plants." Biotechniques **31**(1): 132-134, 136-140.

Isensee, J., M. Diskar, S. Waldherr, R. Buschow, J. Hasenauer, A. Prinz, F. Allgower, F. W. Herberg and T. Hucho (2014). "Pain modulators regulate the dynamics of PKA-RII phosphorylation in subgroups of sensory neurons." J Cell Sci **127**(Pt 1): 216-229.

Ishikawa, T., N. Takahashi, S. Ohno, H. Sakurada, K. Nakamura, Y. K. On, J. E. Park, T. Makiyama, M. Horie, T. Arimura, N. Makita and A. Kimura (2013). "Novel SCN3B mutation associated with brugada syndrome affects intracellular trafficking and function of Nav1.5." Circ J **77**(4): 959-967.

Isom, L. L., K. S. De Jongh, D. E. Patton, B. F. Reber, J. Offord, H. Charbonneau, K. Walsh, A. L. Goldin and W. A. Catterall (1992). "Primary structure and functional expression of the beta 1 subunit of the rat brain sodium channel." Science **256**(5058): 839-842.

Isom, L. L., D. S. Ragsdale, K. S. De Jongh, R. E. Westenbroek, B. F. Reber, T. Scheuer and W. A. Catterall (1995). "Structure and function of the beta 2 subunit of brain sodium channels, a transmembrane glycoprotein with a CAM motif." Cell **83**(3): 433-442.

Isom, L. L., T. Scheuer, A. B. Brownstein, D. S. Ragsdale, B. J. Murphy and W. A. Catterall (1995). "Functional co-expression of the beta 1 and type IIA alpha subunits of sodium channels in a mammalian cell line." J Biol Chem **270**(7): 3306-3312.

Iwanaga, T., R. Tsutsumi, J. Noritake, Y. Fukata and M. Fukata (2009). "Dynamic protein palmitoylation in cellular signaling." Prog Lipid Res **48**(3-4): 117-127.

Jasti, J., H. Furukawa, E. B. Gonzales and E. Gouaux (2007). "Structure of acid-sensing ion channel 1 at 1.9 A resolution and low pH." Nature **449**(7160): 316-323.

Jenkins, S. M. and V. Bennett (2001). "Ankyrin-G coordinates assembly of the spectrin-based membrane skeleton, voltage-gated sodium channels, and L1 CAMs at Purkinje neuron initial segments." J Cell Biol **155**(5): 739-746.

Jensen, T. S., R. Baron, M. Haanpaa, E. Kalso, J. D. Loeser, A. S. Rice and R. D. Treede (2011). "A new definition of neuropathic pain." Pain **152**(10): 2204-2205.

Ji, R. R., H. Baba, G. J. Brenner and C. J. Woolf (1999). "Nociceptive-specific activation of ERK in spinal neurons contributes to pain hypersensitivity." Nat Neurosci **2**(12): 1114-1119.
Ji, R. R., T. A. Samad, S. X. Jin, R. Schmoll and C. J. Woolf (2002). "p38 MAPK activation by NGF in primary sensory neurons after inflammation increases TRPV1 levels and maintains heat hyperalgesia." Neuron **36**(1): 57-68.

Jin, X. and R. W. t. Gereau (2006). "Acute p38-mediated modulation of tetrodotoxin-resistant sodium channels in mouse sensory neurons by tumor necrosis factor-alpha." J Neurosci **26**(1): 246-255.

Jo, T., T. Nagata, H. Iida, H. Imuta, K. Iwasawa, J. Ma, K. Hara, M. Omata, R. Nagai, H. Takizawa, T. Nagase and T. Nakajima (2004). "Voltage-gated sodium channel expressed in cultured human smooth muscle cells: involvement of SCN9A." FEBS Lett **567**(2-3): 339-343.

Joazeiro, C. A. and A. M. Weissman (2000). "RING finger proteins: mediators of ubiquitin ligase activity." Cell **102**(5): 549-552.

Jones, B. J. and D. J. Roberts (1968). "A rotarod suitable for quantitative measurements of motor incoordination in naive mice." Naunyn Schmiedebergs Arch Exp Pathol Pharmakol **259**(2): 211.

Ju, W., Q. Li, S. M. Wilson, J. M. Brittain, L. Meroueh and R. Khanna (2013). "SUMOylation alters CRMP2 regulation of calcium influx in sensory neurons." Channels (Austin) **7**(3): 153-159.

Julius, D. and A. I. Basbaum (2001). "Molecular mechanisms of nociception." Nature **413**(6852): 203-210.

Kasama, S., M. Kawakubo, T. Suzuki, T. Nishizawa, A. Ishida and J. Nakayama (2007). "RNA interference-mediated knock-down of transient receptor potential

vanilloid 1 prevents forepaw inflammatory hyperalgesia in rat." Eur J Neurosci **25**(10): 2956-2963.

Katayama, S., Y. Tomaru, T. Kasukawa, K. Waki, M. Nakanishi, M. Nakamura, H. Nishida, C. C. Yap, M. Suzuki, J. Kawai, H. Suzuki, P. Carninci, Y. Hayashizaki, C. Wells, M. Frith, T. Ravasi, K. C. Pang, J. Hallinan, J. Mattick, D. A. Hume, L. Lipovich, S. Batalov, P. G. Engstrom, Y. Mizuno, M. A. Faghihi, A. Sandelin, A. M. Chalk, S. Mottagui-Tabar, Z. Liang, B. Lenhard and C. Wahlestedt (2005). "Antisense transcription in the mammalian transcriptome." Science **309**(5740): 1564-1566.

Kazen-Gillespie, K. A., D. S. Ragsdale, M. R. D'Andrea, L. N. Mattei, K. E. Rogers and L. L. Isom (2000). "Cloning, localization, and functional expression of sodium channel beta1A subunits." J Biol Chem **275**(2): 1079-1088.

Khaitovich, P., J. Kelso, H. Franz, J. Visagie, T. Giger, S. Joerchel, E. Petzold, R. E. Green, M. Lachmann and S. Paabo (2006). "Functionality of intergenic transcription: an evolutionary comparison." PLoS Genet **2**(10): e171.

Kim, H., T. Sasaki, K. Maeda, D. Koya, A. Kashiwagi and H. Yasuda (2003). "Protein kinase Cbeta selective inhibitor LY333531 attenuates diabetic hyperalgesia through ameliorating cGMP level of dorsal root ganglion neurons." Diabetes **52**(8): 2102-2109.

King, G. F. and I. Vetter (2014). "No gain, no pain: NaV1.7 as an analgesic target." ACS Chem Neurosci **5**(9): 749-751.

Kis-Toth, K., P. Hajdu, I. Bacskai, O. Szilagyi, F. Papp, A. Szanto, E. Posta, P. Gogolak, G. Panyi and E. Rajnavolgyi (2011). "Voltage-gated sodium channel Nav1.7 maintains the membrane potential and regulates the activation and chemokine-induced migration of a monocyte-derived dendritic cell subset." J Immunol **187**(3): 1273-1280.

Kiyosawa, H., I. Yamanaka, N. Osato, S. Kondo and Y. Hayashizaki (2003). "Antisense transcripts with FANTOM2 clone set and their implications for gene regulation." Genome Res **13**(6B): 1324-1334.

Klein, C. J., Y. Wu, D. H. Kilfoyle, P. Sandroni, M. D. Davis, R. H. Gavrilova, P. A. Low and P. J. Dyck (2013). "Infrequent SCN9A mutations in congenital insensitivity to pain and erythromelalgia." J Neurol Neurosurg Psychiatry **84**(4): 386-391.

Klugbauer, N., L. Lacinova, V. Flockerzi and F. Hofmann (1995). "Structure and functional expression of a new member of the tetrodotoxin-sensitive voltage-activated sodium channel family from human neuroendocrine cells." EMBO J **14**(6): 1084-1090.

Knowlton, W. M., A. Bifolck-Fisher, D. M. Bautista and D. D. McKemy (2010). "TRPM8, but not TRPA1, is required for neural and behavioral responses to acute noxious cold temperatures and cold-mimetics in vivo." Pain **150**(2): 340-350.

Kobayashi, K., T. Fukuoka, K. Obata, H. Yamanaka, Y. Dai, A. Tokunaga and K. Noguchi (2005). "Distinct expression of TRPM8, TRPA1, and TRPV1 mRNAs in rat primary afferent neurons with adelta/c-fibers and colocalization with trk receptors." J Comp Neurol **493**(4): 596-606.

Koenig, J., R. Werdehausen, J. E. Linley, A. M. Habib, J. Vernon, S. Lolignier, N. Eijkelkamp, J. Zhao, A. L. Okorokov, C. G. Woods, J. N. Wood and J. J. Cox (2015). "Regulation of Nav1.7: A Conserved SCN9A Natural Antisense Transcript Expressed in Dorsal Root Ganglia." PLoS One **10**(6): e0128830.

Komine, Y., K. Nakamura, M. Katsuki and T. Yamamori (2006). "Novel transcription factor zfh-5 is negatively regulated by its own antisense RNA in mouse brain." Mol Cell Neurosci **31**(2): 273-283.

Kremeyer, B., F. Lopera, J. J. Cox, A. Momin, F. Rugiero, S. Marsh, C. G. Woods, N. G. Jones, K. J. Paterson, F. R. Fricker, A. Villegas, N. Acosta, N. G. Pineda-Trujillo, J. D. Ramirez, J. Zea, M. W. Burley, G. Bedoya, D. L. Bennett, J. N. Wood and A. Ruiz-Linares (2010). "A gain-of-function mutation in TRPA1 causes familial episodic pain syndrome." Neuron **66**(5): 671-680.

Laedermann, C. J., M. Cachemaille, G. Kirschmann, M. Pertin, R. D. Gosselin, I. Chang, M. Albesa, C. Towne, B. L. Schneider, S. Kellenberger, H. Abriel and I. Decosterd (2013). "Dysregulation of voltage-gated sodium channels by ubiquitin ligase NEDD4-2 in neuropathic pain." J Clin Invest **123**(7): 3002-3013.

Laedermann, C. J., I. Decosterd and H. Abriel (2014). "Ubiquitylation of voltage-gated sodium channels." Handb Exp Pharmacol **221**: 231-250.

Laedermann, C. J., N. Syam, M. Pertin, I. Decosterd and H. Abriel (2013). "beta1- and beta3- voltage-gated sodium channel subunits modulate cell surface expression and glycosylation of Nav1.7 in HEK293 cells." Front Cell Neurosci **7**: 137.

Lapidot, M. and Y. Pilpel (2006). "Genome-wide natural antisense transcription: coupling its regulation to its different regulatory mechanisms." EMBO Rep **7**(12): 1216-1222.

Le Pichon, C. E. and A. T. Chesler (2014). "The functional and anatomical dissection of somatosensory subpopulations using mouse genetics." Front Neuroanat **8**: 21.

Lee, E. C., D. Yu, J. Martinez de Velasco, L. Tessarollo, D. A. Swing, D. L. Court, N. A. Jenkins and N. G. Copeland (2001). "A highly efficient Escherichia

coli-based chromosome engineering system adapted for recombinogenic targeting and subcloning of BAC DNA." Genomics **73**(1): 56-65.

Lee, J. T., L. S. Davidow and D. Warshawsky (1999). "Tsix, a gene antisense to Xist at the X-inactivation centre." Nat Genet **21**(4): 400-404.

Leffler, A., B. Monter and M. Koltzenburg (2006). "The role of the capsaicin receptor TRPV1 and acid-sensing ion channels (ASICS) in proton sensitivity of subpopulations of primary nociceptive neurons in rats and mice." Neuroscience **139**(2): 699-709.

Leipold, E., L. Liebmann, G. C. Korenke, T. Heinrich, S. Giesselmann, J. Baets, M. Ebbinghaus, R. O. Goral, T. Stodberg, J. C. Hennings, M. Bergmann, J. Altmuller, H. Thiele, A. Wetzel, P. Nurnberg, V. Timmerman, P. De Jonghe, R. Blum, H. G. Schaible, J. Weis, S. H. Heinemann, C. A. Hubner and I. Kurth (2013). "A de novo gain-of-function mutation in SCN11A causes loss of pain perception." Nat Genet **45**(11): 1399-1404.

Lemaillet, G., B. Walker and S. Lambert (2003). "Identification of a conserved ankyrin-binding motif in the family of sodium channel alpha subunits." J Biol Chem **278**(30): 27333-27339.

Leterrier, C., A. Brachet, B. Dargent and H. Vacher (2011). "Determinants of voltage-gated sodium channel clustering in neurons." Semin Cell Dev Biol **22**(2): 171-177.

Leterrier, C., A. Brachet, M. P. Fache and B. Dargent (2010). "Voltage-gated sodium channel organization in neurons: protein interactions and trafficking pathways." Neurosci Lett **486**(2): 92-100.

Li, J., S. G. Kim and J. Blenis (2014). "Rapamycin: one drug, many effects." Cell Metab **19**(3): 373-379.

Li, M., J. W. West, Y. Lai, T. Scheuer and W. A. Catterall (1992). "Functional modulation of brain sodium channels by cAMP-dependent phosphorylation." Neuron **8**(6): 1151-1159.

Li, Y. Y., L. Qin, Z. M. Guo, L. Liu, H. Xu, P. Hao, J. Su, Y. Shi, W. Z. He and Y. X. Li (2006). "In silico discovery of human natural antisense transcripts." BMC Bioinformatics **7**: 18.

Liang, L., B. Tao, L. Fan, M. Yaster, Y. Zhang and Y. X. Tao (2013). "mTOR and its downstream pathway are activated in the dorsal root ganglion and spinal cord after peripheral inflammation, but not after nerve injury." Brain Res **1513**: 17-25.

Lindia, J. A., M. G. Kohler, W. J. Martin and C. Abbadie (2005). "Relationship between sodium channel NaV1.3 expression and neuropathic pain behavior in rats." Pain **117**(1-2): 145-153.

Ling, M. H., Y. Ban, H. Wen, S. M. Wang and S. X. Ge (2013). "Conserved expression of natural antisense transcripts in mammals." BMC Genomics **14**: 243.

Lisi, L., P. Aceto, P. Navarra and C. Dello Russo (2015). "mTOR kinase: a possible pharmacological target in the management of chronic pain." Biomed Res Int **2015**: 394257.

Liu, X. D., J. J. Yang, D. Fang, J. Cai, Y. Wan and G. G. Xing (2014). "Functional upregulation of nav1.8 sodium channels on the membrane of dorsal root Ganglia neurons contributes to the development of cancer-induced bone pain." PLoS One **9**(12): e114623.

Livak, K. J. and T. D. Schmittgen (2001). "Analysis of relative gene expression data using real-time quantitative PCR and the 2(-Delta Delta C(T)) Method." Methods **25**(4): 402-408.

Lopez-Santiago, L. F., W. J. Brackenbury, C. Chen and L. L. Isom (2011). "Na+ channel Scn1b gene regulates dorsal root ganglion nociceptor excitability in vivo." J Biol Chem **286**(26): 22913-22923.

Lopez-Santiago, L. F., M. Pertin, X. Morisod, C. Chen, S. Hong, J. Wiley, I. Decosterd and L. L. Isom (2006). "Sodium channel beta2 subunits regulate tetrodotoxin-sensitive sodium channels in small dorsal root ganglion neurons and modulate the response to pain." J Neurosci **26**(30): 7984-7994.

Lowe, J. S., O. Palygin, N. Bhasin, T. J. Hund, P. A. Boyden, E. Shibata, M. E. Anderson and P. J. Mohler (2008). "Voltage-gated Nav channel targeting in the heart requires an ankyrin-G dependent cellular pathway." J Cell Biol **180**(1): 173-186.

Lu, Q., L. J. Dobbs, C. W. Gregory, G. W. Lanford, M. P. Revelo, S. Shappell and Y. H. Chen (2005). "Increased expression of delta-catenin/neural plakophilin-related armadillo protein is associated with the down-regulation and redistribution of E-cadherin and p120ctn in human prostate cancer." Hum Pathol **36**(10): 1037-1048.

Lynn, B. and S. E. Carpenter (1982). "Primary afferent units from the hairy skin of the rat hind limb." Brain Res **238**(1): 29-43.

Ma, X. M. and J. Blenis (2009). "Molecular mechanisms of mTOR-mediated translational control." Nat Rev Mol Cell Biol **10**(5): 307-318.

Macias, M. J., M. Hyvonen, E. Baraldi, J. Schultz, M. Sudol, M. Saraste and H. Oschkinat (1996). "Structure of the WW domain of a kinase-associated protein complexed with a proline-rich peptide." Nature **382**(6592): 646-649.

Mahmoudi, S., S. Henriksson, M. Corcoran, C. Mendez-Vidal, K. G. Wiman and M. Farnebo (2009). "Wrap53, a natural p53 antisense transcript required for p53 induction upon DNA damage." Mol Cell **33**(4): 462-471.

Maier, S. K., R. E. Westenbroek, T. T. Yamanushi, H. Dobrzynski, M. R. Boyett, W. A. Catterall and T. Scheuer (2003). "An unexpected requirement for brain-type sodium channels for control of heart rate in the mouse sinoatrial node." Proc Natl Acad Sci U S A **100**(6): 3507-3512.

Makara, M. A., J. Curran, S. C. Little, H. Musa, I. Polina, S. A. Smith, P. J. Wright, S. D. Unudurthi, J. Snyder, V. Bennett, T. J. Hund and P. J. Mohler (2014). "Ankyrin-G coordinates intercalated disc signaling platform to regulate cardiac excitability in vivo." Circ Res **115**(11): 929-938.

Malik-Hall, M., W. Y. Poon, M. D. Baker, J. N. Wood and K. Okuse (2003). "Sensory neuron proteins interact with the intracellular domains of sodium channel NaV1.8." Brain Res Mol Brain Res **110**(2): 298-304.

Malmberg, A. B., C. Chen, S. Tonegawa and A. I. Basbaum (1997). "Preserved acute pain and reduced neuropathic pain in mice lacking PKCgamma." Science **278**(5336): 279-283.

Mandell, F., J. Folkman and S. Matsumoto (1977). "Erythromelalgia." Pediatrics **59**(1): 45-48.

Mansouri, M., S. Chafai Elalaoui, B. Ouled Amar Bencheikh, M. El Alloussi, P. A. Dion, A. Sefiani and G. A. Rouleau (2014). "A novel nonsense mutation in SCN9A in a Moroccan child with congenital insensitivity to pain." Pediatr Neurol **51**(5): 741-744.

Matzner, O. and M. Devor (1994). "Hyperexcitability at sites of nerve injury depends on voltage-sensitive Na+ channels." J Neurophysiol **72**(1): 349-359.
McClatchey, A. I. (2014). "ERM proteins at a glance." J Cell Sci **127**(Pt 15): 3199-3204.

Meadows, L. S. and L. L. Isom (2005). "Sodium channels as macromolecular complexes: implications for inherited arrhythmia syndromes." Cardiovasc Res **67**(3): 448-458.

Meisler, M. H. and J. A. Kearney (2005). "Sodium channel mutations in epilepsy and other neurological disorders." J Clin Invest **115**(8): 2010-2017.

Messner, D. J. and W. A. Catterall (1985). "The sodium channel from rat brain. Separation and characterization of subunits." J Biol Chem **260**(19): 10597-10604.

Metzger, D. and P. Chambon (2001). "Site- and time-specific gene targeting in the mouse." Methods **24**(1): 71-80.

Meyer, R. A., K. D. Davis, R. H. Cohen, R. D. Treede and J. N. Campbell (1991). "Mechanically insensitive afferents (MIAs) in cutaneous nerves of monkey." Brain Res **561**(2): 252-261.

Mi, H., A. Muruganujan, J. T. Casagrande and P. D. Thomas (2013). "Large-scale gene function analysis with the PANTHER classification system." Nat Protoc **8**(8): 1551-1566.

Miao, X. R., X. F. Gao, J. X. Wu, Z. J. Lu, Z. X. Huang, X. Q. Li, C. He and W. F. Yu (2010). "Bilateral downregulation of Nav1.8 in dorsal root ganglia of rats with bone cancer pain induced by inoculation with Walker 256 breast tumor cells." BMC Cancer **10**: 216.

Michiels, J. J., R. H. te Morsche, J. B. Jansen and J. P. Drenth (2005). "Autosomal dominant erythermalgia associated with a novel mutation in the voltage-gated sodium channel alpha subunit Nav1.7." Arch Neurol **62**(10): 1587-1590.

Minett, M. S., S. Falk, S. Santana-Varela, Y. D. Bogdanov, M. A. Nassar, A. M. Heegaard and J. N. Wood (2014). "Pain without nociceptors? Nav1.7-independent pain mechanisms." Cell Rep **6**(2): 301-312.

Minett, M. S., M. A. Nassar, A. K. Clark, G. Passmore, A. H. Dickenson, F. Wang, M. Malcangio and J. N. Wood (2012). "Distinct Nav1.7-dependent pain sensations require different sets of sensory and sympathetic neurons." Nat Commun **3**: 791.

Minett, M. S., K. Quick and J. N. Wood (2011). Behavioral Measures of Pain Thresholds. Current Protocols in Mouse Biology, John Wiley & Sons, Inc.

Mohler, P. J., I. Rivolta, C. Napolitano, G. LeMaillet, S. Lambert, S. G. Priori and V. Bennett (2004). "Nav1.5 E1053K mutation causing Brugada syndrome blocks binding to ankyrin-G and expression of Nav1.5 on the surface of cardiomyocytes." Proc Natl Acad Sci U S A **101**(50): 17533-17538.

Moilanen, L. J., M. Laavola, M. Kukkonen, R. Korhonen, T. Leppanen, E. D. Hogestatt, P. M. Zygmunt, R. M. Nieminen and E. Moilanen (2012). "TRPA1 contributes to the acute inflammatory response and mediates carrageenan-induced paw edema in the mouse." Sci Rep **2**: 380.

Montell, C. (2005). "The TRP superfamily of cation channels." Sci STKE **2005**(272): re3.

Moremen, K. W., M. Tiemeyer and A. V. Nairn (2012). "Vertebrate protein glycosylation: diversity, synthesis and function." Nat Rev Mol Cell Biol **13**(7): 448-462.

Morgan, K., E. B. Stevens, B. Shah, P. J. Cox, A. K. Dixon, K. Lee, R. D. Pinnock, J. Hughes, P. J. Richardson, K. Mizuguchi and A. P. Jackson (2000). "beta 3: an additional auxiliary subunit of the voltage-sensitive sodium channel that modulates channel gating with distinct kinetics." Proc Natl Acad Sci U S A **97**(5): 2308-2313.

Mori, M., T. Konno, T. Ozawa, M. Murata, K. Imoto and K. Nagayama (2000). "Novel interaction of the voltage-dependent sodium channel (VDSC) with calmodulin: does VDSC acquire calmodulin-mediated Ca2+-sensitivity?" Biochemistry **39**(6): 1316-1323.

Morris, C. J. (2003). "Carrageenan-induced paw edema in the rat and mouse." Methods Mol Biol **225**: 115-121.

Morris, K. V. and J. S. Mattick (2014). "The rise of regulatory RNA." Nat Rev Genet **15**(6): 423-437.

Morris, K. V., S. Santoso, A. M. Turner, C. Pastori and P. G. Hawkins (2008). "Bidirectional transcription directs both transcriptional gene activation and suppression in human cells." PLoS Genet **4**(11): e1000258.

Muroi, Y., F. Ru, M. Kollarik, B. J. Canning, S. A. Hughes, S. Walsh, M. Sigg, M. J. Carr and B. J. Undem (2011). "Selective silencing of Na(V)1.7 decreases excitability and conduction in vagal sensory neurons." J Physiol **589**(Pt 23): 5663-5676.

Murphy, B. J., S. Rossie, K. S. De Jongh and W. A. Catterall (1993). "Identification of the sites of selective phosphorylation and dephosphorylation of the rat brain Na+ channel alpha subunit by cAMP-dependent protein kinase and phosphoprotein phosphatases." J Biol Chem **268**(36): 27355-27362.

Nabbout, R., E. Gennaro, B. Dalla Bernardina, O. Dulac, F. Madia, E. Bertini, G. Capovilla, C. Chiron, G. Cristofori, M. Elia, E. Fontana, R. Gaggero, T. Granata, R. Guerrini, M. Loi, L. La Selva, M. L. Lispi, A. Matricardi, A. Romeo, V. Tzolas, D. Valseriati, P. Veggiotti, F. Vigevano, L. Vallee, F. Dagna Bricarelli, A. Bianchi and F. Zara (2003). "Spectrum of SCN1A mutations in severe myoclonic epilepsy of infancy." Neurology **60**(12): 1961-1967.

Nagata, K., A. Duggan, G. Kumar and J. Garcia-Anoveros (2005). "Nociceptor and hair cell transducer properties of TRPA1, a channel for pain and hearing." J Neurosci **25**(16): 4052-4061.

Nalefski, E. A. and J. J. Falke (1996). "The C2 domain calcium-binding motif: structural and functional diversity." Protein Sci **5**(12): 2375-2390.

Namadurai, S., D. Balasuriya, R. Rajappa, M. Wiemhofer, K. Stott, J. Klingauf, J. M. Edwardson, D. Y. Chirgadze and A. P. Jackson (2014). "Crystal structure and molecular imaging of the Nav channel beta3 subunit indicates a trimeric assembly." J Biol Chem **289**(15): 10797-10811.

Namadurai, S., N. R. Yereddi, F. S. Cusdin, C. L. Huang, D. Y. Chirgadze and A. P. Jackson (2015). "A new look at sodium channel beta subunits." Open Biol **5**(1): 140192.

Nassar, M. A., M. D. Baker, A. Levato, R. Ingram, G. Mallucci, S. B. McMahon and J. N. Wood (2006). "Nerve injury induces robust allodynia and ectopic discharges in Nav1.3 null mutant mice." Mol Pain **2**: 33.

Nassar, M. A., A. Levato, L. C. Stirling and J. N. Wood (2005). "Neuropathic pain develops normally in mice lacking both Na(v)1.7 and Na(v)1.8." Mol Pain **1**: 24.

Nassar, M. A., L. C. Stirling, G. Forlani, M. D. Baker, E. A. Matthews, A. H. Dickenson and J. N. Wood (2004). "Nociceptor-specific gene deletion reveals a major role for Nav1.7 (PN1) in acute and inflammatory pain." Proc Natl Acad Sci U S A **101**(34): 12706-12711.

Nickel, W., K. Sohn, C. Bunning and F. T. Wieland (1997). "p23, a major COPI-vesicle membrane protein, constitutively cycles through the early secretory pathway." Proc Natl Acad Sci U S A **94**(21): 11393-11398.

Nilius, B. (2007). "TRP channels in disease." Biochim Biophys Acta **1772**(8): 805-812.

Noda, M., S. Shimizu, T. Tanabe, T. Takai, T. Kayano, T. Ikeda, H. Takahashi, H. Nakayama, Y. Kanaoka, N. Minamino and et al. (1984). "Primary structure of Electrophorus electricus sodium channel deduced from cDNA sequence." Nature **312**(5990): 121-127.

Norsted Gregory, E., S. Codeluppi, J. A. Gregory, J. Steinauer and C. I. Svensson (2010). "Mammalian target of rapamycin in spinal cord neurons mediates hypersensitivity induced by peripheral inflammation." Neuroscience **169**(3): 1392-1402.

Nozawa, K., E. Kawabata-Shoda, H. Doihara, R. Kojima, H. Okada, S. Mochizuki, Y. Sano, K. Inamura, H. Matsushime, T. Koizumi, T. Yokoyama and H. Ito (2009). "TRPA1 regulates gastrointestinal motility through serotonin release from enterochromaffin cells." Proc Natl Acad Sci U S A **106**(9): 3408-3413.

Numann, R., W. A. Catterall and T. Scheuer (1991). "Functional modulation of brain sodium channels by protein kinase C phosphorylation." Science **254**(5028): 115-118.

O'Malley, H. A. and L. L. Isom (2015). "Sodium channel beta subunits: emerging targets in channelopathies." Annu Rev Physiol **77**: 481-504.

Obata, K., H. Yamanaka, Y. Dai, T. Mizushima, T. Fukuoka, A. Tokunaga and K. Noguchi (2004). "Activation of extracellular signal-regulated protein kinase in the dorsal root ganglion following inflammation near the nerve cell body." Neuroscience **126**(4): 1011-1021.

Ohsawa, M. and J. Kamei (1997). "Pretreatment with the protein kinase C activator phorbol 12,13-dibutyrate attenuates the ethanol-induced loss of the righting reflex in mice: modification by diabetes." Brain Res **764**(1-2): 244-248.

Ohsawa, M. and J. Kamei (1999). "Possible involvement of spinal protein kinase C in thermal allodynia and hyperalgesia in diabetic mice." Eur J Pharmacol **372**(3): 221-228.

Okuse, K., M. Malik-Hall, M. D. Baker, W. Y. Poon, H. Kong, M. V. Chao and J. N. Wood (2002). "Annexin II light chain regulates sensory neuron-specific sodium channel expression." Nature **417**(6889): 653-656.

Omana-Zapata, I., M. A. Khabbaz, J. C. Hunter, D. E. Clarke and K. R. Bley (1997). "Tetrodotoxin inhibits neuropathic ectopic activity in neuromas, dorsal root ganglia and dorsal horn neurons." Pain **72**(1-2): 41-49.

Oshio, K., H. Watanabe, D. Yan, A. S. Verkman and G. T. Manley (2006). "Impaired pain sensation in mice lacking Aquaporin-1 water channels." Biochem Biophys Res Commun **341**(4): 1022-1028.

Ostman, J. A., M. A. Nassar, J. N. Wood and M. D. Baker (2008). "GTP up-regulated persistent Na+ current and enhanced nociceptor excitability require NaV1.9." J Physiol **586**(4): 1077-1087.

Patino, G. A., W. J. Brackenbury, Y. Bao, L. F. Lopez-Santiago, H. A. O'Malley, C. Chen, J. D. Calhoun, R. G. Lafreniere, P. Cossette, G. A. Rouleau and L. L. Isom (2011). "Voltage-gated Na+ channel beta1B: a secreted cell adhesion molecule involved in human epilepsy." J Neurosci **31**(41): 14577-14591.

Payandeh, J., T. M. Gamal El-Din, T. Scheuer, N. Zheng and W. A. Catterall (2012). "Crystal structure of a voltage-gated sodium channel in two potentially inactivated states." Nature **486**(7401): 135-139.

Payandeh, J., T. Scheuer, N. Zheng and W. A. Catterall (2011). "The crystal structure of a voltage-gated sodium channel." Nature **475**(7356): 353-358.

Plant, P. J., F. Lafont, S. Lecat, P. Verkade, K. Simons and D. Rotin (2000). "Apical membrane targeting of Nedd4 is mediated by an association of its C2 domain with annexin XIIIb." J Cell Biol **149**(7): 1473-1484.

Plassart, E., B. Eymard, L. Maurs, J. J. Hauw, O. Lyon-Caen, M. Fardeau and B. Fontaine (1996). "Paramyotonia congenita: genotype to phenotype correlations in two families and report of a new mutation in the sodium channel gene." J Neurol Sci **142**(1-2): 126-133.

Prescott, E. M. and N. J. Proudfoot (2002). "Transcriptional collision between convergent genes in budding yeast." Proc Natl Acad Sci U S A **99**(13): 8796-8801.

Price, M. P., S. L. McIlwrath, J. Xie, C. Cheng, J. Qiao, D. E. Tarr, K. A. Sluka, T. J. Brennan, G. R. Lewin and M. J. Welsh (2001). "The DRASIC cation channel contributes to the detection of cutaneous touch and acid stimuli in mice." Neuron **32**(6): 1071-1083.

Priest, B. T., B. A. Murphy, J. A. Lindia, C. Diaz, C. Abbadie, A. M. Ritter, P. Liberator, L. M. Iyer, S. F. Kash, M. G. Kohler, G. J. Kaczorowski, D. E. MacIntyre and W. J. Martin (2005). "Contribution of the tetrodotoxin-resistant voltage-gated sodium channel NaV1.9 to sensory transmission and nociceptive behavior." Proc Natl Acad Sci U S A **102**(26): 9382-9387.

Pristera, A., M. D. Baker and K. Okuse (2012). "Association between tetrodotoxin resistant channels and lipid rafts regulates sensory neuron excitability." PLoS One **7**(8): e40079.

Proudfoot, C. J., E. M. Garry, D. F. Cottrell, R. Rosie, H. Anderson, D. C. Robertson, S. M. Fleetwood-Walker and R. Mitchell (2006). "Analgesia mediated by the TRPM8 cold receptor in chronic neuropathic pain." Curr Biol **16**(16): 1591-1605.

Puig, O., F. Caspary, G. Rigaut, B. Rutz, E. Bouveret, E. Bragado-Nilsson, M. Wilm and B. Seraphin (2001). "The tandem affinity purification (TAP) method: a general procedure of protein complex purification." Methods **24**(3): 218-229.

Qin, N., M. R. D'Andrea, M. L. Lubin, N. Shafaee, E. E. Codd and A. M. Correa (2003). "Molecular cloning and functional expression of the human sodium channel beta1B subunit, a novel splicing variant of the beta1 subunit." Eur J Biochem **270**(23): 4762-4770.

Qiu, F., Y. Jiang, H. Zhang, Y. Liu and W. Mi (2012). "Increased expression of tetrodotoxin-resistant sodium channels Nav1.8 and Nav1.9 within dorsal root ganglia in a rat model of bone cancer pain." Neurosci Lett **512**(2): 61-66.
Ramsey, I. S., M. Delling and D. E. Clapham (2006). "An introduction to TRP channels." Annu Rev Physiol **68**: 619-647.

Randall, L. O. and J. J. Selitto (1957). "A method for measurement of analgesic activity on inflamed tissue." Arch Int Pharmacodyn Ther **111**(4): 409-419.
Raouf, R., K. Quick and J. N. Wood (2010). "Pain as a channelopathy." J Clin Invest **120**(11): 3745-3752.

Raymond, C. K., J. Castle, P. Garrett-Engele, C. D. Armour, Z. Kan, N. Tsinoremas and J. M. Johnson (2004). "Expression of alternatively spliced sodium channel alpha-subunit genes. Unique splicing patterns are observed in dorsal root ganglia." J Biol Chem **279**(44): 46234-46241.

Reeh, P. W. and K. H. Steen (1996). "Tissue acidosis in nociception and pain." Prog Brain Res **113**: 143-151.

Reimann, F., J. J. Cox, I. Belfer, L. Diatchenko, D. V. Zaykin, D. P. McHale, J. P. Drenth, F. Dai, J. Wheeler, F. Sanders, L. Wood, T. X. Wu, J. Karppinen, L. Nikolajsen, M. Mannikko, M. B. Max, C. Kiselycznyk, M. Poddar, R. H. Te Morsche, S. Smith, D. Gibson, A. Kelempisioti, W. Maixner, F. M. Gribble and C. G. Woods (2010). "Pain perception is altered by a nucleotide polymorphism in SCN9A." Proc Natl Acad Sci U S A **107**(11): 5148-5153.

Renganathan, M., T. R. Cummins and S. G. Waxman (2001). "Contribution of Na(v)1.8 sodium channels to action potential electrogenesis in DRG neurons." J Neurophysiol **86**(2): 629-640.

Rigaut, G., A. Shevchenko, B. Rutz, M. Wilm, M. Mann and B. Seraphin (1999). "A generic protein purification method for protein complex characterization and proteome exploration." Nat Biotechnol **17**(10): 1030-1032.

Rinn, J. L. and H. Y. Chang (2012). "Genome regulation by long noncoding RNAs." Annu Rev Biochem **81**: 145-166.

Rossie, S. and W. A. Catterall (1987). "Cyclic-AMP-dependent phosphorylation of voltage-sensitive sodium channels in primary cultures of rat brain neurons." J Biol Chem **262**(26): 12735-12744.

Rotin, D. and S. Kumar (2009). "Physiological functions of the HECT family of ubiquitin ligases." Nat Rev Mol Cell Biol **10**(6): 398-409.

Rotin, D., O. Staub and R. Haguenauer-Tsapis (2000). "Ubiquitination and endocytosis of plasma membrane proteins: role of Nedd4/Rsp5p family of ubiquitin-protein ligases." J Membr Biol **176**(1): 1-17.

Roger, S., J. Rollin, A. Barascu, P. Besson, P. I. Raynal, S. Iochmann, M. Lei, P. Bougnoux, Y. Gruel and J. Y. Le Guennec (2007). "Voltage-gated sodium channels potentiate the invasive capacities of human non-small-cell lung cancer cell lines." Int J Biochem Cell Biol **39**(4): 774-786.

Rougier, J. S., M. X. van Bemmelen, M. C. Bruce, T. Jespersen, B. Gavillet, F. Apotheloz, S. Cordonier, O. Staub, D. Rotin and H. Abriel (2005). "Molecular determinants of voltage-gated sodium channel regulation by the Nedd4/Nedd4-like proteins." Am J Physiol Cell Physiol **288**(3): C692-701.

Sage, D., P. Salin, G. Alcaraz, F. Castets, P. Giraud, M. Crest, B. Mazet and N. Clerc (2007). "Na(v)1.7 and Na(v)1.3 are the only tetrodotoxin-sensitive sodium channels expressed by the adult guinea pig enteric nervous system." J Comp Neurol **504**(4): 363-378.

Salzer, J. L. (2003). "Polarized domains of myelinated axons." Neuron **40**(2): 297-318.

Samad, O. A., A. M. Tan, X. Cheng, E. Foster, S. D. Dib-Hajj and S. G. Waxman (2013). "Virus-mediated shRNA knockdown of Na(v)1.3 in rat dorsal root ganglion attenuates nerve injury-induced neuropathic pain." Mol Ther **21**(1): 49-56.

Samuels, M. E., R. H. te Morsche, M. E. Lynch and J. P. Drenth (2008). "Compound heterozygosity in sodium channel Nav1.7 in a family with hereditary erythermalgia." Mol Pain **4**: 21.

Sangameswaran, L., L. M. Fish, B. D. Koch, D. K. Rabert, S. G. Delgado, M. Ilnicka, L. B. Jakeman, S. Novakovic, K. Wong, P. Sze, E. Tzoumaka, G. R.

Stewart, R. C. Herman, H. Chan, R. M. Eglen and J. C. Hunter (1997). "A novel tetrodotoxin-sensitive, voltage-gated sodium channel expressed in rat and human dorsal root ganglia." J Biol Chem **272**(23): 14805-14809.

Schmidt, J., S. Rossie and W. A. Catterall (1985). "A large intracellular pool of inactive Na channel alpha subunits in developing rat brain." Proc Natl Acad Sci U S A **82**(14): 4847-4851.

Schmidt, J. W. and W. A. Catterall (1987). "Palmitylation, sulfation, and glycosylation of the alpha subunit of the sodium channel. Role of post-translational modifications in channel assembly." J Biol Chem **262**(28): 13713-13723.

Schmidt, R., M. Schmelz, C. Forster, M. Ringkamp, E. Torebjork and H. Handwerker (1995). "Novel classes of responsive and unresponsive C nociceptors in human skin." J Neurosci **15**(1 Pt 1): 333-341.

Schultz, J., U. Hoffmuller, G. Krause, J. Ashurst, M. J. Macias, P. Schmieder, J. Schneider-Mergener and H. Oschkinat (1998). "Specific interactions between the syntrophin PDZ domain and voltage-gated sodium channels." Nat Struct Biol **5**(1): 19-24.

Segerdahl, A. R., J. Xie, K. Paterson, J. D. Ramirez, I. Tracey and D. L. Bennett (2012). "Imaging the neural correlates of neuropathic pain and pleasurable relief associated with inherited erythromelalgia in a single subject with quantitative arterial spin labelling." Pain **153**(5): 1122-1127.

Serra, J., H. Bostock, R. Sola, J. Aleu, E. Garcia, B. Cokic, X. Navarro and C. Quiles (2012). "Microneurographic identification of spontaneous activity in C-nociceptors in neuropathic pain states in humans and rats." Pain **153**(1): 42-55.

Shah, B. S., E. B. Stevens, R. D. Pinnock, A. K. Dixon and K. Lee (2001). "Developmental expression of the novel voltage-gated sodium channel auxiliary subunit beta3, in rat CNS." J Physiol **534**(Pt 3): 763-776.

Shah, V. N., T. L. Wingo, K. L. Weiss, C. K. Williams, J. R. Balser and W. J. Chazin (2006). "Calcium-dependent regulation of the voltage-gated sodium channel hH1: intrinsic and extrinsic sensors use a common molecular switch." Proc Natl Acad Sci U S A **103**(10): 3592-3597.

Shan, B., M. Dong, H. Tang, N. Wang, J. Zhang, C. Yan, X. Jiao, H. Zhang and C. Wang (2014). "Voltage-gated sodium channels were differentially expressed in human normal prostate, benign prostatic hyperplasia and prostate cancer cells." Oncol Lett **8**(1): 345-350.

Shao, D., M. D. Baker, B. Abrahamsen, F. Rugiero, M. Malik-Hall, W. Y. Poon, K. S. Cheah, K. M. Yao, J. N. Wood and K. Okuse (2009). "A multi PDZ-domain protein Pdzd2 contributes to functional expression of sensory neuron-specific sodium channel Na(V)1.8." Mol Cell Neurosci **42**(3): 219-225.

Shao, D., K. Okuse and M. B. Djamgoz (2009). "Protein-protein interactions involving voltage-gated sodium channels: Post-translational regulation, intracellular trafficking and functional expression." Int J Biochem Cell Biol **41**(7): 1471-1481.

Shields, S. D., J. Mazario, K. Skinner and A. I. Basbaum (2007). "Anatomical and functional analysis of aquaporin 1, a water channel in primary afferent neurons." Pain **131**(1-2): 8-20.

Shumilina, E. V., Y. A. Negulyaev, E. A. Morachevskaya, H. Hinssen and S. Y. Khaitlina (2003). "Regulation of sodium channel activity by capping of actin filaments." Mol Biol Cell **14**(4): 1709-1716.

Sittl, R., A. Lampert, T. Huth, E. T. Schuy, A. S. Link, J. Fleckenstein, C. Alzheimer, P. Grafe and R. W. Carr (2012). "Anticancer drug oxaliplatin induces acute cooling-aggravated neuropathy via sodium channel subtype Na(V)1.6-resurgent and persistent current." Proc Natl Acad Sci U S A **109**(17): 6704-6709.

Sivilotti, L., K. Okuse, A. N. Akopian, S. Moss and J. N. Wood (1997). "A single serine residue confers tetrodotoxin insensitivity on the rat sensory-neuron-specific sodium channel SNS." FEBS Lett **409**(1): 49-52.

Skeik, N., T. W. Rooke, M. D. Davis, D. M. Davis, H. Kalsi, I. Kurth and R. C. Richardson (2012). "Severe case and literature review of primary erythromelalgia: novel SCN9A gene mutation." Vasc Med **17**(1): 44-49.

Smith, R. D. and A. L. Goldin (1996). "Phosphorylation of brain sodium channels in the I--II linker modulates channel function in Xenopus oocytes." J Neurosci **16**(6): 1965-1974.

Smith, R. D. and A. L. Goldin (2000). "Potentiation of rat brain sodium channel currents by PKA in Xenopus oocytes involves the I-II linker." Am J Physiol Cell Physiol **278**(4): C638-645.

Snider, W. D. and S. B. McMahon (1998). "Tackling pain at the source: new ideas about nociceptors." Neuron **20**(4): 629-632.

Stadler, T., A. O. O'Reilly and A. Lampert (2015). "Erythromelalgia mutation Q875E Stabilizes the activated state of sodium channel Nav1.7." J Biol Chem **290**(10): 6316-6325.

Stamboulian, S., J. S. Choi, H. S. Ahn, Y. W. Chang, L. Tyrrell, J. A. Black, S. G. Waxman and S. D. Dib-Hajj (2010). "ERK1/2 mitogen-activated protein kinase phosphorylates sodium channel Na(v)1.7 and alters its gating properties." J Neurosci **30**(5): 1637-1647.

Staub, O., S. Dho, P. Henry, J. Correa, T. Ishikawa, J. McGlade and D. Rotin (1996). "WW domains of Nedd4 bind to the proline-rich PY motifs in the epithelial Na+ channel deleted in Liddle's syndrome." EMBO J **15**(10): 2371-2380.

Story, G. M., A. M. Peier, A. J. Reeve, S. R. Eid, J. Mosbacher, T. R. Hricik, T. J. Earley, A. C. Hergarden, D. A. Andersson, S. W. Hwang, P. McIntyre, T. Jegla, S. Bevan and A. Patapoutian (2003). "ANKTM1, a TRP-like channel expressed in nociceptive neurons, is activated by cold temperatures." Cell **112**(6): 819-829.

Strating, J. R. and G. J. Martens (2009). "The p24 family and selective transport processes at the ER-Golgi interface." Biol Cell **101**(9): 495-509.

Strickland, I. T., J. C. Martindale, P. L. Woodhams, A. J. Reeve, I. P. Chessell and D. S. McQueen (2008). "Changes in the expression of NaV1.7, NaV1.8 and NaV1.9 in a distinct population of dorsal root ganglia innervating the rat knee joint in a model of chronic inflammatory joint pain." Eur J Pain **12**(5): 564-572.

Suter, M. R., Z. A. Bhuiyan, C. J. Laedermann, T. Kuntzer, M. Schaller, M. W. Stauffacher, E. Roulet, H. Abriel, I. Decosterd and C. Wider (2015). "p.L1612P, a novel voltage-gated sodium channel Nav1.7 mutation inducing a cold sensitive paroxysmal extreme pain disorder." Anesthesiology **122**(2): 414-423.

Svenningsson, P., K. Chergui, I. Rachleff, M. Flajolet, X. Zhang, M. El Yacoubi, J. M. Vaugeois, G. G. Nomikos and P. Greengard (2006). "Alterations in 5-HT1B receptor function by p11 in depression-like states." Science **311**(5757): 77-80.

Takesue, E. I., W. Schaefer and E. Jukniewicz (1969). "Modification of the Randall-Selitto analgesic apparatus." J Pharm Pharmacol **21**(11): 788-789.

Tan, Z. Y., A. D. Piekarz, B. T. Priest, K. L. Knopp, J. L. Krajewski, J. S. McDermott, E. S. Nisenbaum and T. R. Cummins (2014). "Tetrodotoxin-resistant sodium channels in sensory neurons generate slow resurgent currents that are enhanced by inflammatory mediators." J Neurosci **34**(21): 7190-7197.

Thakur, M., M. Crow, N. Richards, G. I. Davey, E. Levine, J. H. Kelleher, C. C. Agley, F. Denk, S. D. Harridge and S. B. McMahon (2014). "Defining the nociceptor transcriptome." Front Mol Neurosci **7**: 87.

Toledo-Aral, J. J., B. L. Moss, Z. J. He, A. G. Koszowski, T. Whisenand, S. R. Levinson, J. J. Wolf, I. Silos-Santiago, S. Halegoua and G. Mandel (1997). "Identification of PN1, a predominant voltage-dependent sodium channel expressed principally in peripheral neurons." Proc Natl Acad Sci U S A **94**(4): 1527-1532.

Tominaga, M., M. J. Caterina, A. B. Malmberg, T. A. Rosen, H. Gilbert, K. Skinner, B. E. Raumann, A. I. Basbaum and D. Julius (1998). "The cloned capsaicin receptor integrates multiple pain-producing stimuli." Neuron **21**(3): 531-543.

Tyrrell, L., M. Renganathan, S. D. Dib-Hajj and S. G. Waxman (2001). "Glycosylation alters steady-state inactivation of sodium channel Nav1.9/NaN in dorsal root ganglion neurons and is developmentally regulated." J Neurosci **21**(24): 9629-9637.

Uemoto, Y., S. Suzuki, N. Terada, N. Ohno, S. Ohno, S. Yamanaka and M. Komada (2007). "Specific role of the truncated betaIV-spectrin Sigma6 in sodium channel clustering at axon initial segments and nodes of ranvier." J Biol Chem **282**(9): 6548-6555.

Uchida, T., F. Rossignol, M. A. Matthay, R. Mounier, S. Couette, E. Clottes and C. Clerici (2004). "Prolonged hypoxia differentially regulates hypoxia-inducible factor (HIF)-1alpha and HIF-2alpha expression in lung epithelial cells: implication of natural antisense HIF-1alpha." J Biol Chem **279**(15): 14871-14878.

Usoskin, D., A. Furlan, S. Islam, H. Abdo, P. Lonnerberg, D. Lou, J. Hjerling-Leffler, J. Haeggstrom, O. Kharchenko, P. V. Kharchenko, S. Linnarsson and P. Ernfors (2015). "Unbiased classification of sensory neuron types by large-scale single-cell RNA sequencing." Nat Neurosci **18**(1): 145-153.

Uysal-Onganer, P. and M. B. Djamgoz (2007). "Epidermal growth factor potentiates in vitro metastatic behaviour of human prostate cancer PC-3M cells: involvement of voltage-gated sodium channel." Mol Cancer **6**: 76.

van Bemmelen, M. X., J. S. Rougier, B. Gavillet, F. Apotheloz, D. Daidie, M. Tateyama, I. Rivolta, M. A. Thomas, R. S. Kass, O. Staub and H. Abriel (2004). "Cardiac voltage-gated sodium channel Nav1.5 is regulated by Nedd4-2 mediated ubiquitination." Circ Res **95**(3): 284-291.

van Genderen, P. J., J. J. Michiels and J. P. Drenth (1993). "Hereditary erythermalgia and acquired erythromelalgia." Am J Med Genet **45**(4): 530-532.

Vasilets, L. A., G. Schmalzing, K. Madefessel, W. Haase and W. Schwarz (1990). "Activation of protein kinase C by phorbol ester induces downregulation of the Na+/K(+)-ATPase in oocytes of Xenopus laevis." J Membr Biol **118**(2): 131-142.

Veldkamp, M. W., P. C. Viswanathan, C. Bezzina, A. Baartscheer, A. A. Wilde and J. R. Balser (2000). "Two distinct congenital arrhythmias evoked by a multidysfunctional Na(+) channel." Circ Res **86**(9): E91-97.

Vetter, I., C. A. Mozar, T. Durek, J. S. Wingerd, P. F. Alewood, M. J. Christie and R. J. Lewis (2012). "Characterisation of Na(v) types endogenously expressed in human SH-SY5Y neuroblastoma cells." Biochem Pharmacol **83**(11): 1562-1571.

Vijayaragavan, K., M. Boutjdir and M. Chahine (2004). "Modulation of Nav1.7 and Nav1.8 peripheral nerve sodium channels by protein kinase A and protein kinase C." J Neurophysiol **91**(4): 1556-1569.

Wada, A., T. Yanagita, H. Yokoo and H. Kobayashi (2004). "Regulation of cell surface expression of voltage-dependent Nav1.7 sodium channels: mRNA stability and posttranscriptional control in adrenal chromaffin cells." Front Biosci **9**: 1954-1966.

Waechter, C. J., J. W. Schmidt and W. A. Catterall (1983). "Glycosylation is required for maintenance of functional sodium channels in neuroblastoma cells." J Biol Chem **258**(8): 5117-5123.

Wagner, S., N. Dybkova, E. C. Rasenack, C. Jacobshagen, L. Fabritz, P. Kirchhof, S. K. Maier, T. Zhang, G. Hasenfuss, J. H. Brown, D. M. Bers and L. S. Maier (2006). "Ca2+/calmodulin-dependent protein kinase II regulates cardiac Na+ channels." J Clin Invest **116**(12): 3127-3138.

Waldmann, R., G. Champigny, F. Bassilana, C. Heurteaux and M. Lazdunski (1997). "A proton-gated cation channel involved in acid-sensing." Nature **386**(6621): 173-177.

Wang, H. and M. G. Kazanietz (2010). "p23/Tmp21 differentially targets the Rac-GAP beta2-chimaerin and protein kinase C via their C1 domains." Mol Biol Cell **21**(8): 1398-1408.

Wang, H., L. Xiao and M. G. Kazanietz (2011). "p23/Tmp21 associates with protein kinase Cdelta (PKCdelta) and modulates its apoptotic function." J Biol Chem **286**(18): 15821-15831.

Wang, K. C., Y. W. Yang, B. Liu, A. Sanyal, R. Corces-Zimmerman, Y. Chen, B. R. Lajoie, A. Protacio, R. A. Flynn, R. A. Gupta, J. Wysocka, M. Lei, J. Dekker, J. A. Helms and H. Y. Chang (2011). "A long noncoding RNA maintains active chromatin to coordinate homeotic gene expression." Nature **472**(7341): 120-124.

Wang, Y., J. M. Brittain, B. W. Jarecki, K. D. Park, S. M. Wilson, B. Wang, R. Hale, S. O. Meroueh, T. R. Cummins and R. Khanna (2010). "In silico docking and electrophysiological characterization of lacosamide binding sites on collapsin response mediator protein-2 identifies a pocket important in modulating sodium channel slow inactivation." J Biol Chem **285**(33): 25296-25307.

Waxman, S. G., J. D. Kocsis and J. A. Black (1994). "Type III sodium channel mRNA is expressed in embryonic but not adult spinal sensory neurons, and is reexpressed following axotomy." J Neurophysiol **72**(1): 466-470.

Weiss, J., M. Pyrski, E. Jacobi, B. Bufe, V. Willnecker, B. Schick, P. Zizzari, S. J. Gossage, C. A. Greer, T. Leinders-Zufall, C. G. Woods, J. N. Wood and F. Zufall (2011). "Loss-of-function mutations in sodium channel Nav1.7 cause anosmia." Nature **472**(7342): 186-190.

Werner, A. and A. Berdal (2005). "Natural antisense transcripts: sound or silence?" Physiol Genomics **23**(2): 125-131.

Werner, A., M. Carlile and D. Swan (2009). "What do natural antisense transcripts regulate?" RNA Biol **6**(1): 43-48.
Werner, A. and J. A. Sayer (2009). "Naturally occurring antisense RNA: function and mechanisms of action." Curr Opin Nephrol Hypertens **18**(4): 343-349.

Westenbroek, R. E., D. K. Merrick and W. A. Catterall (1989). "Differential subcellular localization of the RI and RII Na+ channel subtypes in central neurons." Neuron **3**(6): 695-704.

Wild, S., G. Roglic, A. Green, R. Sicree and H. King (2004). "Global prevalence of diabetes: estimates for the year 2000 and projections for 2030." Diabetes Care **27**(5): 1047-1053.

Wilkinson, K. A. and J. M. Henley (2010). "Mechanisms, regulation and consequences of protein SUMOylation." Biochem J **428**(2): 133-145.

Woodall, A. J., M. A. Richards, D. J. Turner and E. M. Fitzgerald (2008). "Growth factors differentially regulate neuronal Cav channels via ERK-dependent signaling." Cell Calcium **43**(6): 562-575.

Woolf, C. J. and R. J. Mannion (1999). "Neuropathic pain: aetiology, symptoms, mechanisms, and management." Lancet **353**(9168): 1959-1964.

Wu, W. L., Y. W. Lin, M. Y. Min and C. C. Chen (2010). "Mice lacking Asic3 show reduced anxiety-like behavior on the elevated plus maze and reduced aggression." Genes Brain Behav **9**(6): 603-614.

Xu, P., D. M. Duong, N. T. Seyfried, D. Cheng, Y. Xie, J. Robert, J. Rush, M. Hochstrasser, D. Finley and J. Peng (2009). "Quantitative proteomics reveals the function of unconventional ubiquitin chains in proteasomal degradation." Cell **137**(1): 133-145.

Yanagita, T., H. Kobayashi, Y. Uezono, H. Yokoo, T. Sugano, T. Saitoh, S. Minami, S. Shiraishi and A. Wada (2003). "Destabilization of Na(v)1.7 sodium channel alpha-subunit mRNA by constitutive phosphorylation of extracellular signal-regulated kinase: negative regulation of steady-state level of cell surface functional sodium channels in adrenal chromaffin cells." Mol Pharmacol **63**(5): 1125-1136.

Yang, Q. Q. and Y. F. Deng (2014). "Genome-wide analysis of long non-coding RNA in primary nasopharyngeal carcinoma by microarray." Histopathology.

Yang, Y., Y. Wang, S. Li, Z. Xu, H. Li, L. Ma, J. Fan, D. Bu, B. Liu, Z. Fan, G. Wu, J. Jin, B. Ding, X. Zhu and Y. Shen (2004). "Mutations in SCN9A, encoding a sodium channel alpha subunit, in patients with primary erythermalgia." J Med Genet **41**(3): 171-174.

Yarbrough, T. L., T. Lu, H. C. Lee and E. F. Shibata (2002). "Localization of cardiac sodium channels in caveolin-rich membrane domains: regulation of sodium current amplitude." Circ Res **90**(4): 443-449.

Yelin, R., D. Dahary, R. Sorek, E. Y. Levanon, O. Goldstein, A. Shoshan, A. Diber, S. Biton, Y. Tamir, R. Khosravi, S. Nemzer, E. Pinner, S. Walach, J. Bernstein, K. Savitsky and G. Rotman (2003). "Widespread occurrence of antisense transcription in the human genome." Nat Biotechnol **21**(4): 379-386.

Yoo, H. S., F. S. Nahm, P. B. Lee and C. J. Lee (2011). "Early thoracic sympathetic block improves the treatment effect for upper extremity neuropathic pain." Anesth Analg **113**(3): 605-609.

Yu, F. H. and W. A. Catterall (2004). "The VGL-chanome: a protein superfamily specialized for electrical signaling and ionic homeostasis." Sci STKE **2004**(253): re15.

Yu, F. H., R. E. Westenbroek, I. Silos-Santiago, K. A. McCormick, D. Lawson, P. Ge, H. Ferriera, J. Lilly, P. S. DiStefano, W. A. Catterall, T. Scheuer and R. Curtis (2003). "Sodium channel beta4, a new disulfide-linked auxiliary subunit with similarity to beta2." J Neurosci **23**(20): 7577-7585.

Yuan, J. S., J. Burris, N. R. Stewart, A. Mentewab and C. N. Stewart, Jr. (2007). "Statistical tools for transgene copy number estimation based on real-time PCR." BMC Bioinformatics **8 Suppl 7**: S6.

Zha, X. M., J. A. Wemmie, S. H. Green and M. J. Welsh (2006). "Acid-sensing ion channel 1a is a postsynaptic proton receptor that affects the density of dendritic spines." Proc Natl Acad Sci U S A **103**(44): 16556-16561.

Zhang, H. and A. S. Verkman (2010). "Aquaporin-1 tunes pain perception by interaction with Na(v)1.8 Na+ channels in dorsal root ganglion neurons." J Biol Chem **285**(8): 5896-5906.

Zhang, Q., M. V. Chibalina, M. Bengtsson, L. N. Groschner, R. Ramracheya, N. J. Rorsman, V. Leiss, M. A. Nassar, A. Welling, F. M. Gribble, F. Reimann, F. Hofmann, J. N. Wood, F. M. Ashcroft and P. Rorsman (2014). "Na+ current properties in islet alpha- and beta-cells reflect cell-specific Scn3a and Scn9a expression." J Physiol **592**(Pt 21): 4677-4696.

Zhang, W., X. F. Sun, J. H. Bo, J. Zhang, X. J. Liu, L. P. Wu, Z. L. Ma and X. P. Gu (2013). "Activation of mTOR in the spinal cord is required for pain hypersensitivity induced by chronic constriction injury in mice." Pharmacol Biochem Behav **111**: 64-70.

Zhang, Y., H. A. Hartmann and J. Satin (1999). "Glycosylation influences voltage-dependent gating of cardiac and skeletal muscle sodium channels." J Membr Biol **171**(3): 195-207.

Zhang, Z. N., Q. Li, C. Liu, H. B. Wang, Q. Wang and L. Bao (2008). "The voltage-gated Na+ channel Nav1.8 contains an ER-retention/retrieval signal antagonized by the beta3 subunit." J Cell Sci **121**(Pt 19): 3243-3252.

Zhao, X., Z. Tang, H. Zhang, F. E. Atianjoh, J. Y. Zhao, L. Liang, W. Wang, X. Guan, S. C. Kao, V. Tiwari, Y. J. Gao, P. N. Hoffman, H. Cui, M. Li, X. Dong and Y. X. Tao (2013). "A long noncoding RNA contributes to neuropathic pain by silencing Kcna2 in primary afferent neurons." Nat Neurosci **16**(8): 1024-1031.

Zhou, J., H. G. Shin, J. Yi, W. Shen, C. P. Williams and K. T. Murray (2002). "Phosphorylation and putative ER retention signals are required for protein kinase A-mediated potentiation of cardiac sodium current." Circ Res **91**(6): 540-546.

Zimmer, T. and K. Benndorf (2002). "The human heart and rat brain IIA Na+ channels interact with different molecular regions of the beta1 subunit." J Gen Physiol **120**(6): 887-895.

Zimmer, T., C. Biskup, C. Bollensdorff and K. Benndorf (2002). "The beta1 subunit but not the beta2 subunit colocalizes with the human heart Na+ channel (hH1) already within the endoplasmic reticulum." J Membr Biol **186**(1): 13-21.

Zimmermann, K., A. Leffler, A. Babes, C. M. Cendan, R. W. Carr, J. Kobayashi, C. Nau, J. N. Wood and P. W. Reeh (2007). "Sensory neuron sodium channel Nav1.8 is essential for pain at low temperatures." Nature **447**(7146): 855-858.

Zylka, M. J., F. L. Rice and D. J. Anderson (2005). "Topographically distinct epidermal nociceptive circuits revealed by axonal tracers targeted to Mrgprd." Neuron **45**(1): 17-25.

8 Appendix: Paper

PLOS | ONE

RESEARCH ARTICLE

Regulation of $Na_v1.7$: A Conserved *SCN9A* Natural Antisense Transcript Expressed in Dorsal Root Ganglia

Jennifer Koenig[1], Robert Werdehausen[1,2], John E. Linley[1], Abdella M. Habib[1], Jeffrey Vernon[1], Stephane Lolignier[1], Niels Eijkelkamp[1,3], Jing Zhao[1], Andrei L. Okorokov[4], C. Geoffrey Woods[5], John N. Wood[1,6], James J. Cox[1]*

1 Molecular Nociception Group, Wolfson Institute for Biomedical Research, University College London, Gower Street, London, United Kingdom, **2** Department of Anesthesiology, Medical Faculty, Heinrich-Heine-University Düsseldorf, Moorenstr. 5, Düsseldorf, Germany, **3** Laboratory for Translational Immunology, UMC Utrecht, Utrecht, The Netherlands, **4** Wolfson Institute for Biomedical Research, University College London, Gower street, London, United Kingdom, **5** Cambridge Institute for Medical Research, University of Cambridge, Hills Road, Cambridge, United Kingdom, **6** Department of Molecular Medicine and Biopharmaceutical Sciences, Graduate School of Convergence Science and Technology, College of Medicine, Seoul National University, Seoul, South Korea

* j.j.cox@ucl.ac.uk

OPEN ACCESS

Citation: Koenig J, Werdehausen R, Linley JE, Habib AM, Vernon J, Lolignier S, et al. (2015) Regulation of $Na_v1.7$: A Conserved *SCN9A* Natural Antisense Transcript Expressed in Dorsal Root Ganglia. PLoS ONE 10(6): e0128830. doi:10.1371/journal.pone.0128830

Academic Editor: Alexander Binshtok, The Hebrew University Medical School, ISRAEL

Received: November 19, 2014

Accepted: April 30, 2015

Published: June 2, 2015

Data Availability Statement: Sequences are available from the Genbank database (accession numbers KM096550, KM096551, KM096552, KM096553).

Funding: JK is a UCL Grand Challenge PhD student; RW is supported by the German Research Foundation (DFG We 4860/1-1); JEL, AMH, JZ, JNW and JJC are supported by the Medical Research Council (http://www.mrc.ac.uk/); JV and SL are supported by Arthritis Research UK (http://www.arthritisresearchuk.org/); NE is supported by a Rubicon Fellowship of the Netherlands Organisation

Abstract

The $Na_v1.7$ voltage-gated sodium channel, encoded by *SCN9A*, is critical for human pain perception yet the transcriptional and post-transcriptional mechanisms that regulate this gene are still incompletely understood. Here, we describe a novel natural antisense transcript (NAT) for *SCN9A* that is conserved in humans and mice. The NAT has a similar tissue expression pattern to the sense gene and is alternatively spliced within dorsal root ganglia. The human and mouse NATs exist in cis with the sense gene in a tail-to-tail orientation and both share sequences that are complementary to the terminal exon of *SCN9A*/*Scn9a*. Overexpression analyses of the human NAT in human embryonic kidney (HEK293A) and human neuroblastoma (SH-SY5Y) cell lines show that it can function to downregulate $Na_v1.7$ mRNA, protein levels and currents. The NAT may play an important role in regulating human pain thresholds and is a potential candidate gene for individuals with chronic pain disorders that map to the *SCN9A* locus, such as Inherited Primary Erythromelalgia, Paroxysmal Extreme Pain Disorder and Painful Small Fibre Neuropathy, but who do not contain mutations in the sense gene. Our results strongly suggest the *SCN9A* NAT as a prime candidate for new therapies based upon augmentation of existing antisense RNAs in the treatment of chronic pain conditions in man.

Introduction

Following the cataloguing of the human genome and transcriptome it has become apparent that there are probably more genes in the human genome that encode regulatory RNAs than

for Scientific Research; CGW receives funding from the Cambridge NIHR BRC; JNW is supported by the Wellcome Trust (http://www.wellcome.ac.uk/index.htm) and the BK21 programme; JJC is a MRC Research Career Development fellow (G1100340). The funders had no role in study design, data collection and analysis, decision to publish, or preparation of the manuscript.

Competing Interests: The authors have declared that no competing interests exist.

those that encode proteins [1]. One major class of regulatory RNA genes contains the long non-coding RNAs (lncRNAs), of which natural antisense transcripts (NATs) are an important subset. NATs can be defined as processed transcripts that are complementary to the corresponding processed sense transcript in exonic regions [2]. NATs can exist in cis or trans to the target gene and are relatively common, with approximately 70% of all genomic loci showing evidence of transcription from both sense and antisense strands [3]. Prominent examples of NATs include *Tsix* (the NAT for *Xist*), *Wrap53* (the NAT for p53) and *BACE1-AS* (the NAT for beta-secretase-1) [4–6]. In the pain field, a NAT was recently reported for the voltage-dependent potassium channel Kcna2 [7]. This NAT is expressed in rat dorsal root ganglion (DRG) neurons and is upregulated in response to peripheral nerve injury. The increase in NAT levels downregulates Kcna2, attenuating total voltage-gated potassium currents, increasing excitability in DRG neurons and producing neuropathic pain symptoms.

We were interested to discover whether a NAT exists for *SCN9A*, another pain-related gene, which encodes the $Na_v1.7$ voltage-gated sodium channel. Previously we reported that recessive loss of function mutations in this channel result in a complete inability to perceive pain (CIP) [8]. In addition to being pain-free from birth, *SCN9A*-CIP patients also lack a sense of smell, but are otherwise normal [9]. Consequently, this channel has been identified as a promising target in the pharmaceutical industry for the development of new analgesic drugs [10]. In contrast to the pain-free phenotype, there are also debilitating painful Mendelian disorders resulting from gain of function of $Na_v1.7$, such as Inherited Primary Erythromelalgia (IEM), Paroxysmal Extreme Pain Disorder (PEPD) and painful small fibre neuropathy [11–13]. We considered that if a NAT did exist for *SCN9A*, then perhaps it played a role in regulating $Na_v1.7$ protein levels and hence altering responses to painful stimuli.

In this study, using an *in silico* approach to inform the design of RT-PCR reactions, we have cloned a NAT for *SCN9A* that is conserved in humans and mice. The tissue expression profile of the NAT is similar to the sense gene, indicating that it may play an important functional role. Overexpression analyses of the NAT have shown that it reduces $Na_v1.7$ mRNA, protein and currents. This NAT is therefore a potentially interesting candidate gene for IEM, PEPD and small fibre neuropathy patients that lack pathogenic mutations in *SCN9A* [14,15].

Results

Cloning the *SCN9A*/*Scn9a* natural antisense transcripts

In silico analyses of the human and mouse *SCN9A*/*Scn9a* gene footprints using the UCSC genome browser identified several expressed sequence tags (ESTs) that were partially complementary to exonic regions of the sense gene. Alignment of the longest human EST, BC051759, to the genomic sequence indicated a cDNA comprised of 12 exons; four of which were complementary to and partly or wholly overlapped exons from *SCN9A* (S1 Fig); and with five exons containing SINE and/or LINE repeat sequences. Exons were flanked with the canonical AG-GT splice acceptor and donor sites and the final exon contained an AAUAAA polyadenylation signal. In Genbank the assembly of ESTs has subsequently been annotated as LOC101929680 (NR_110260), which spans 220 kb on chromosome 2 and encodes an uncharacterized long non-coding RNA of 2305 bp (Fig 1A). Using human dorsal root ganglion cDNA as template we amplified two alternative splice variants, which were submitted to Genbank. Compared to NR_110260, the first splice variant (KM096550) excludes exon 2 and uses an alternative splice acceptor site within exon 7. The second splice variant (KM096551) excludes both exon 2 and exon 8 (Fig 1A). Interestingly, some *SCN9A* point mutations previously shown to cause the human monogenic pain disorders CIP, IEM and PEPD also change the sequence of the NAT (S1 Fig).

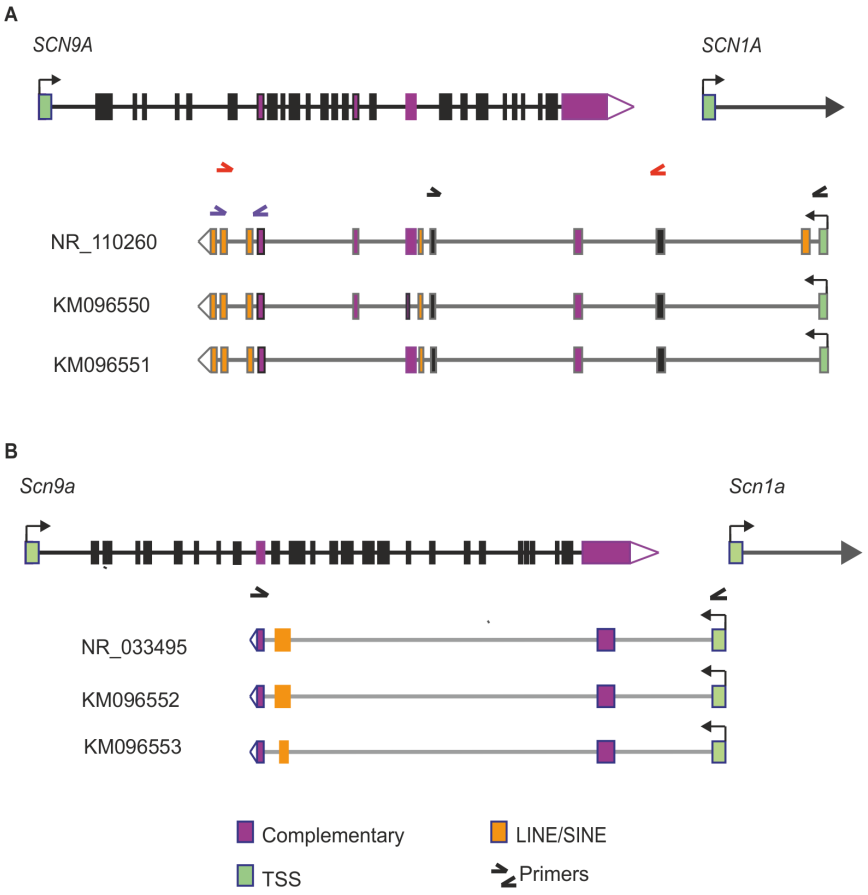

Fig 1. Genomic organization of the human (A) and mouse (B) *SCN9A/Scn9a* natural antisense transcripts (NATs). The sense genes are shown at the top of each panel with the NAT splice variants shown below. The sense genes and NATs are arranged in a tail-to-tail orientation (i.e. 3' ends overlapping). Transcriptional start sites (TSS) and direction of transcription are denoted by green exons and arrows respectively; overlapping regions between sense and NAT sequences are shown by purple exons; LINE and SINE repeat sequences are shown as orange exons; and the primer pairs used to amplify the respective NAT sequences are also highlighted.

doi:10.1371/journal.pone.0128830.g001

Analysis of the mouse genome also led to the identification of several ESTs that were antisense to *Scn9a*. For example, EST AK138532 indicated a cDNA comprised of four exons, one of which splices into a LINE repeat and two of which overlap *Scn9a* sense gene exons (NR_033495; Fig 1B). Similar to the human *SCN9A* NAT, exons were flanked with canonical AG-GT splice acceptor and donor sites and the final exon contained an AAUAAA polyadenylation signal. Both the human and mouse NATs contain sequences that overlap the final sense *SCN9A*/*Scn9a* exon, potentially indicating a conserved regulatory function of these NATs in man and mouse. Using mouse dorsal root ganglion cDNA as template we amplified the identical sequence to NR_033495 (KM096552, Fig 1B) as well as a splice variant (KM096553, Fig 1B), which uses an alternative splice donor site in exon 3.

In silico translation of the human and mouse NAT sequences shows that the longest potential open reading frames are 67 and 114 amino acids respectively (S2 Fig). The lack of a long

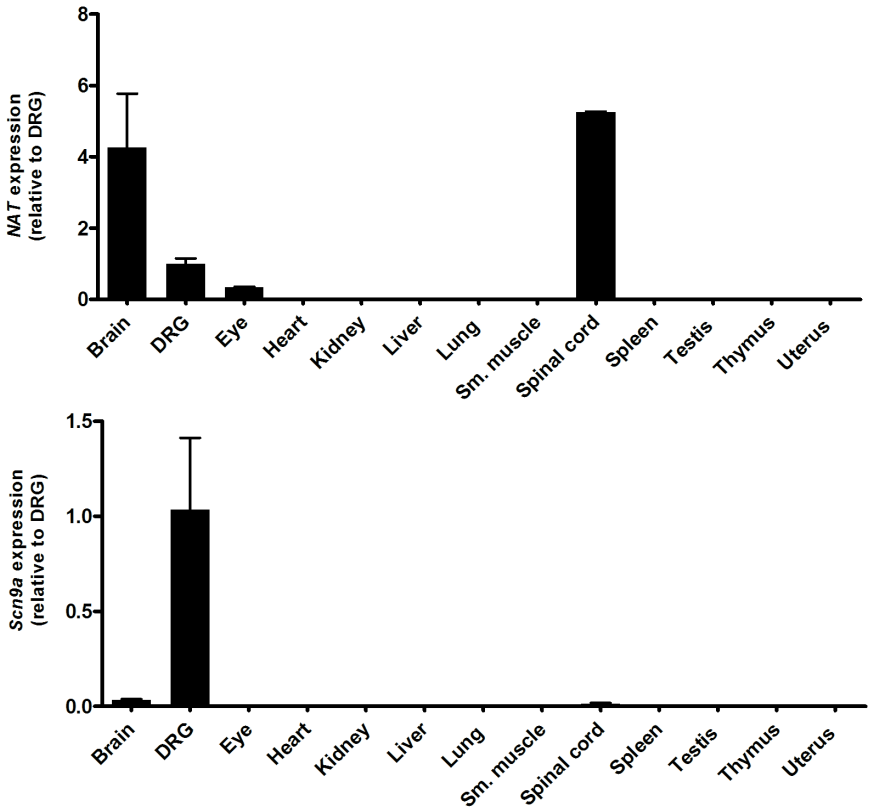

Fig 2. Real-time qPCR assays measuring the expression level of the NAT (A; upper panel) and *Scn9a* (B; lower panel) in specific mouse tissues (expression levels relative to DRG). Both the sense and NAT genes are expressed in similar tissues.

doi:10.1371/journal.pone.0128830.g002

open reading frame and the poor codon conservation is consistent with the definition of a long non-coding RNA [1].

Scn9a sense and NAT genes have a similar tissue expression profile

To investigate the tissue expression profile of the *Scn9a* NAT compared with the sense gene, we ran qPCR assays across a range of mouse tissue cDNA samples (Fig 2). The *Scn9a* sense and NAT genes have a relatively restricted expression pattern and are co-expressed in adult brain, DRG and spinal cord tissues. In addition, the NAT also shows expression within adult eye. The co-expression of the sense and NATs in similar tissues suggests that the NAT could have a direct regulatory effect on *Scn9a* gene functions. To further understand the relative expression of the NAT and *Scn9a* within DRG neurons, we analysed data from a recent paper in which DRG neurons have been categorized into 11 subtypes based on single-cell RNA-seq expression data (S3 Fig) [16]. This shows that the NAT is expressed in six of the eleven DRG neuronal subtypes. Interestingly, in the remaining five DRG subtypes with no NAT expression detected, there is robust *Scn9a* expression. Conversely, in the only neuronal subtype without *Scn9a* expression ('NF5'), there is relatively high expression of the NAT, indicating that within particular neuronal cell populations there are contrasting expression profiles of the NAT and *Scn9a*.

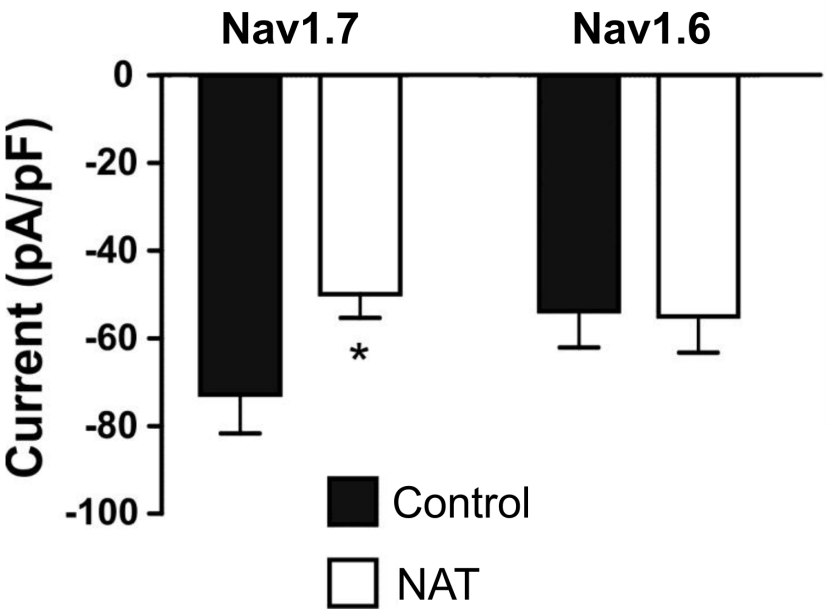

Fig 3. Overexpression of the human NAT inhibits $Na_v1.7$ but not $Na_v1.6$ currents. Whole cell voltage clamp recording from HEK cells stably expressing human $Na_v1.7$ or human $Na_v1.6$. Cells were transiently transfected with either pcDNA3 vector (black bars) or $Na_v1.7$ NAT (white bars) along with a GFP-expressing vector and recorded from 48 hrs later. Peak whole cell current (pA) was measured in response to a 10 ms voltage step from the holding potential of -120 mV to 0 mV and normalized to cell size (pF). n = 17–20; * indicates $p<0.05$ when compared to control (unpaired t-test).

doi:10.1371/journal.pone.0128830.g003

Overexpression of the human NAT specifically reduces $Na_v1.7$ peak sodium currents

To functionally test the effects of overexpressing the human NAT on sodium currents, HEK293 cells stably expressing either $Na_v1.7$ or $Na_v1.6$ were transfected with (1) NAT in pcDNA3 plus a GFP-expressing vector (pEGFP-N1) or (2) empty pcDNA3 plus pEGFP-N1. Two days after transfection the green fluorescing cells were patch clamped. Overexpression of the human *SCN9A* NAT in the $Na_v1.7$ stable cell line resulted in a statistically significant reduction in the peak sodium current (Fig 3). In $Na_v1.6$ stably expressing cells, overexpression of the NAT had no effect on the sodium current, indicating that the NAT specifically affects the activity of $Na_v1.7$.

Stable expression of the human NAT in SH-SY5Y neuroblastoma cells

The SH-SY5Y neuroblastoma cell line endogenously expresses the *SCN9A* gene [17] but does not co-express the NAT (Fig 4A). We generated a SH-SY5Y cell line that stably expresses the human NAT cDNA under the control of a CMV promoter to assess the effect of overexpression of the NAT on endogenously-expressed $Na_v1.7$. The *SCN9A* mRNA level in the NAT-stable cell line was significantly downregulated compared to wild-type SH-SY5Y cells (Fig 4B). Furthermore, patch clamping of this cell line showed a statistically significant reduction in the peak sodium current compared to a SH-SY5Y cell line that did not express the human NAT (Fig 4C and 4D). Voltage-current relationships were unaltered between the two cell lines.

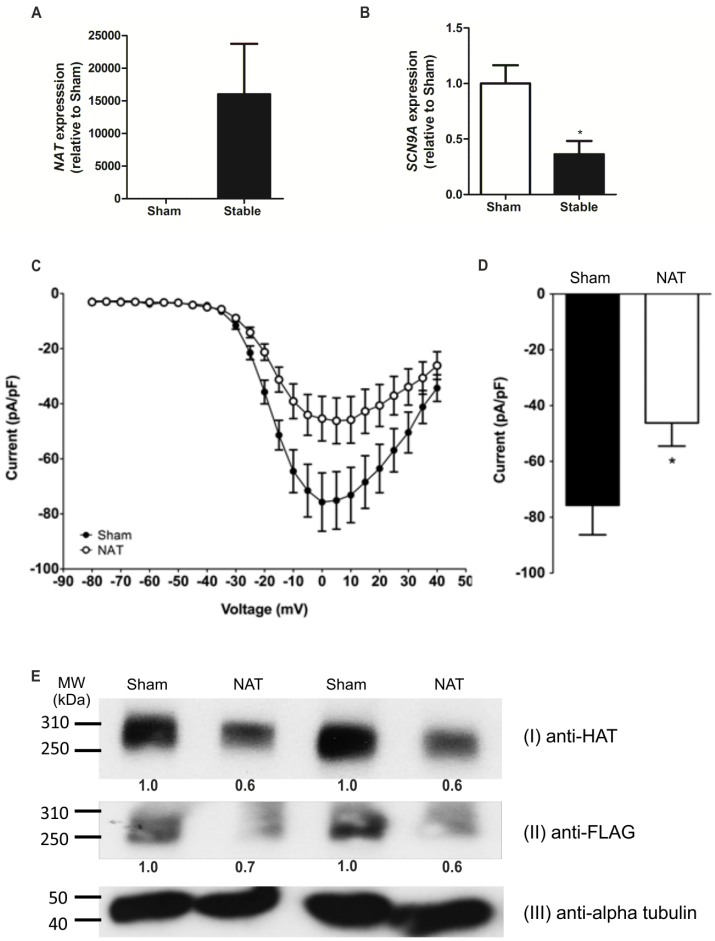

Fig 4. Overexpression of the NAT reduces $Na_v1.7$-mRNA, protein and currents. (A) Real-time qPCR showing that the NAT is not expressed in naïve SH-SY5Y cells (sham) but is expressed in the stable-*NAT* SH-SY5Y cell line (n = 3). (B) Real-time qPCR showing that the endogenous *SCN9A* mRNA level is significantly reduced in the stable-NAT SH-SY5Y cell line compared to in naïve SH-SY5Y cells (sham) (n = 3). (C-D) Whole cell voltage clamp recordings of naïve (sham) and stable-NAT SH-SYSY ($Na_v1.7$ NAT) cells showed a significant reduction of the peak sodium current (D), with voltage-current relationships unaltered (C) (n = 16–21). (E) Reduction in $Na_v1.7$-TAP tag protein levels due to overexpression of the NAT for 48 hrs in a $Na_v1.7$-TAP stable HEK293 cell line. Densitometry readings comparing alpha-tubulin to either HAT or FLAG bands were normalized to the sham controls and shown below each band. Transfection of the NAT results in a reduction in $Na_v1.7$ protein. (Ei) $Na_v1.7$-TAP protein detected by immunoblotting using an anti-HAT antibody following pull-down of $Na_v1.7$-TAP with an anti-FLAG antibody (sham corresponds to mock-transfected cells). (Eii) Immunoblot of crude lysate using an anti-FLAG antibody confirms a reduction in $Na_v1.7$ protein levels following NAT transfection. (Eiii) Immunoblot of crude lysate using an antibody to a house-keeping protein, confirming equal loading. * indicates $p<0.05$ when compared to control (unpaired t-test).

doi:10.1371/journal.pone.0128830.g004

In addition to sharing overlapping sequences with *SCN9A*, the NAT also contains sequences overlapping with two exons from each of *SCN1A*, *SCN2A* and *SCN3A* (S4 Fig). As the NAT shows high expression in the brain it is possible that the NAT may also regulate the

$Na_v1.1$-$Na_v1.3$ brain-expressed sodium channels encoded by *SCN1A*-*SCN3A*. We were therefore interested to determine whether overexpression of the NAT downregulated endogenously expressed $Na_v1.1$, $Na_v1.2$ or $Na_v1.3$ in the NAT-stable SH-SY5Y cell line. Real-time qPCR showed the expression level of *SCN2A* and *SCN3A* were not significantly different between the naïve SH-SY5Y cells (sham) and the stable-*NAT* SH-SY5Y cells (*SCN1A* expression could not be detected in the SH-SY5Y cell lines) (S5 Fig), further indicating that the functional effects of the NAT are *SCN9A*-specific.

Next, the effect of NAT overexpression on $Na_v1.7$ protein levels was investigated. A HEK293 cell line was generated which stably expressed an epitope-tagged (TAP) $Na_v1.7$ under the control of a CMV promoter. This cell line was transiently transfected with the human NAT, and anti-FLAG coupled Dynabeads were used to pull down TAP-tagged $Na_v1.7$, which was subsequently detected on a western blot using an anti-HAT antibody. Comparison of NAT transfected and sham transfected cells showed that the transient NAT transfection resulted in a reduction in TAP-tagged $Na_v1.7$ protein levels (Fig 4E). This reduction in protein level was further confirmed by immunoblotting using a pan sodium channel antibody (S6 Fig).

NAT and *Scn9a* mRNA levels are unchanged in inflammatory and neuropathic pain states

Given that the NAT specifically downregulates human $Na_v1.7$ protein levels and attenuates its currents, we investigated whether the NAT has a role *in vivo* to regulate mouse *Scn9a* mRNA levels in different pain states. Two different inflammatory pain mouse models (carrageenan and complete Freund's adjuvant (CFA)) and one neuropathic pain model (chronic constriction injury) were used. Injection of carrageenan into the hind paw induces an acute and highly reproducible inflammatory response resulting in oedema, hyperalgesia and erythema that can persist for 6 days [18]. Likewise, injection of CFA results in acute thermal and mechanical hyperalgesia that can persist for more than 2 weeks. In the chronic constriction injury model, sutures are tied around the sciatic nerve which leads to thermal and mechanical hyperalgesia presenting within the first week and persisting for several weeks. Real-time qPCR assays using RNA isolated from ipsilateral L4-L6 dorsal root ganglia dissected 3 days (CFA), 2 hrs and 24 hrs (carrageenan) and 2 weeks (CCI) following the start of each pain model showed that neither *Scn9a* sense nor NAT mRNA levels change significantly (Fig 5A–5C).

Discussion

We have identified, cloned and characterized a human and mouse natural antisense transcript for the *SCN9A* gene. Both human and mouse NATs are organised in a tail-to-tail configuration with the sense gene and both show evidence of alternative splicing, which is consistent with other reported NATs [1]. Although the mouse *Scn9a* NAT has fewer exons than the human NAT, both contain conserved sequences that overlap the final sense *SCN9A*/*Scn9a* exon. Given this conserved gene structure and the similar tissue expression profile of the sense and NAT genes, we hypothesized that the NAT regulates the function of *SCN9A*. We overexpressed the NAT in human cell lines that endogenously expressed $Na_v1.7$ and in cells that stably expressed from a CMV promoter either $Na_v1.7$ or epitope-tagged $Na_v1.7$. Real-time qPCR, immunoblotting and electrophysiological assays showed a significant reduction in $Na_v1.7$ mRNA, protein levels and currents.

How do NATs regulate the function of their sense gene counterparts? Characterization of other NATs has ascribed to them diverse cellular functions including transcriptional collision, RNA interference, regulation of alternative splicing, RNA editing, epigenetic regulation, RNA masking, translation inhibition and mRNA destabilisation [19]. In our experimental set-up we

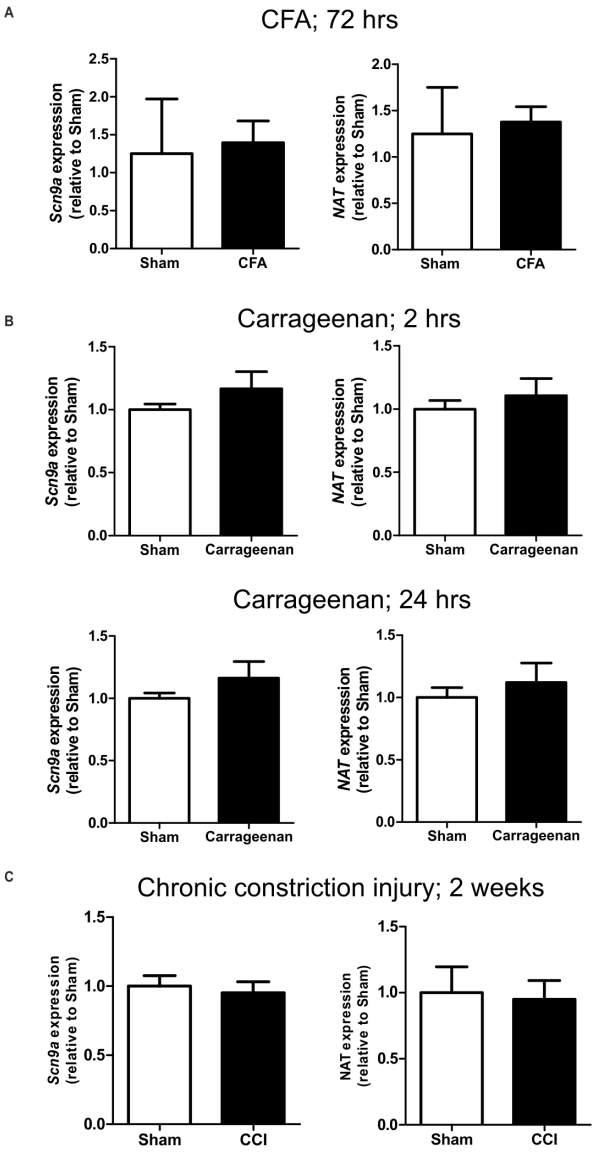

Fig 5. *Scn9a* and NAT expression levels in DRG do not change significantly in inflammatory and neuropathic pain models. Real-time qPCR assays for (A) CFA-induced pain (saline n = 3, CFA n = 4); (B) carrageenan-induced pain (saline n = 4, carrageenan n = 4); (C) chronic constriction injury (mock n = 6, CCI n = 6). Sham refers to saline injection (A, B) or mice undergoing a mock surgery (C).

doi:10.1371/journal.pone.0128830.g005

overexpressed the processed NAT from a CMV promoter in cell lines. This led to a reduction in sense mRNA and consequently a reduction in functional $Na_v1.7$ protein. The NAT might function by downregulating *SCN9A* transcription, for example by guiding chromatin-modifying enzymes to the *SCN9A* promoter region. Alternatively, overexpression of the NAT could

be leading to the generation of endogenous short RNAs (endo-siRNAs) thus leading to promotion of the RNA interference pathway [20]. A third mechanism could be that the NAT:sense mRNA duplexes are promoting destabilisation and degradation of the sense mRNA and/or inhibiting translation. A greater insight into the function of the NAT *in vivo* would be gleaned from the creation of a NAT knockout mouse. In a comparable experiment, Komine et al. generated a *Zfhx2-AS* knockout mouse through deletion of the transcriptional start site region for its corresponding NAT [21]. Normally, the *Zfhx2* expression pattern in the developing brain is complementary to the expression of its NAT. However in the *Zfhx2-AS* knockout mouse, the expression of the Zfhx2 homeobox-containing transcription factor becomes dysregulated. It would be interesting to determine whether the expression pattern of *Scn9a* is altered in a *Scn9a* NAT knockout mouse. Furthermore, the effects on transcription of other genes, which may also be potentially regulated by the NAT, could also be investigated in a NAT knockout, for example *Scn1a* and *Scn7a*, which reside in the same chromosomal region as *Scn9a*.

Detailed analyses of *Scn9a* knockout mice have shown that acute, inflammatory and some forms of neuropathic pain require the expression of $Na_v1.7$ [22–24]. We hypothesized that the NAT may be downregulated in pain states, hence leading to upregulation of *SCN9A*. To test this, we assessed mRNA levels of the sense and NAT genes in CFA and carrageenan-induced models of inflammatory pain and in the chronic constriction injury neuropathic pain model. This showed that the mRNA level of neither the sense nor the NAT gene was significantly altered. The lack of change in the sense gene mRNA was a surprising finding given that, for example, $Na_v1.7$ protein levels have previously been shown to increase following carrageenan injections [25]. Further work on epitope-tagged $Na_v1.7$ knockin mice using anti-FLAG/HAT antibodies should help to confirm whether protein levels change in different pain models. Furthermore, intrathecal NAT overexpression by viral delivery could help to determine whether the NAT is able to confer analgesia and reduce the pain experienced in different inflammatory and neuropathic pain states.

In summary, this DRG-expressed natural antisense transcript attenuates native sodium currents, is co-expressed with its corresponding gene, and consequently has the potential to regulate pain thresholds via transcriptional and post-transcriptional regulation of *SCN9A*. Given that the presence of the NAT reduces $Na_v1.7$ currents, then intuitively the lack of the NAT may increase sodium currents. This could lead to increased excitability of damage-sensing neurons, enabling a fine-control of responses to painful stimuli. Other regulatory mechanisms mediated by the NAT are also plausible, as discussed above. It will be interesting to determine whether loss of function mutations in the NAT are responsible for inherited painful disorders that map to human chromosome 2, and whether SNPs within the NAT alter pain thresholds in the general population.

Material and Methods

Cloning the human and mouse NATs

Human dorsal root ganglia total RNA was purchased from Clontech; mouse total RNA was isolated from DRGs dissected from wild-type C57BL/6 mice using the RNeasy MinElute Kit (Qiagen). Total RNA was reverse transcribed into cDNA using Superscript III (Life Technologies) and oligo d(T), according to the manufacturer's instructions. The human *SCN9A* NAT was PCR-amplified from DRG cDNA using KAPA HiFi DNA polymerase (Kapa Biosystems) or LA Taq (TaKaRa) in three overlapping fragments using the following primers: Fragment 1, 5' GAA TGA AAT TTA GTG TTT CCC ATC C, 5' AGC AAT GTT TCA CCT CCA GAG ATC; Fragment 2, 5' GGA ATT CAG GCA AAG TTG GA, 5' CAC CAA CAT TCA GCC ATT TG; Fragment 3, 5' CTG ATT ATT GGG AGA CTT TTG GAG, 5' GCT CCT ATT TCT GAG

TTT ATA CTG TG. The mouse *Scn9a* NAT was PCR-amplified using the primers 5' agc aag agt aag aag tat tgg c, 5' cat tat att tca ttt taa tg. PCR products were cloned using the Zero Blunt TOPO PCR Cloning Kit (Life Technologies). Individual colonies were Sanger sequenced and submitted to GenBank under the accession numbers KM096550 (clone LA5), KM096551 (clone LA8), KM096552 (clone 3.2) and KM096553 (clone 3.1).

Real-time qPCR assay for mouse tissue panel

One μg of total RNA derived from a range of tissues (Clontech) or prepared in-house from DRG was reverse-transcribed into cDNA using Superscript III (Life Technologies) and oligo d (T). Real-time qPCR using technical triplicates was performed using SYBR Green (Applied Biosystems) and the following primers: Mouse *Scn9a* 5' GAG GGG CAA ACT GAC TAC A and 5' AGA AAC ATT CCT ACA ATG GAG (efficiency 1.91); Mouse NAT 5' TGC TGT CAA CTC CTG AAC CA and 5' TCC AAC TTT GCC ACA ATG AG (efficiency 1.96); Mouse *Actb* 5' TTC TTT GCA GCT CCT TCG TT and 5' ATG GAG GGG AAT ACA GCC C (efficiency 1.83). Relative expression of the target gene was calculated using the comparative ΔΔCT method [26,27]. Briefly, expression of the test gene was compared with that of *Actb* measured on the same sample, giving a CT difference (ΔCT) for *Actb* minus the test gene. The relative expression of *Scn9a* and the NAT in specific tissues was calculated in relation to the expression levels in DRG using the comparative ΔΔCT method [26]. ΔCT values of individual tissues were compared to ΔCT of DRG, giving ΔΔCT values of a specific tissue and relative expression was calculated as $2^{-\Delta\Delta CT}$. Mean, standard error and statistics were calculated from the ΔΔCT data. Data were analysed using Microsoft Excel, and statistics were calculated using GraphPad Prism 5.01 software (GraphPad Software, San Diego, CA).

Cloning the human NAT into an expression vector

The human *SCN9A* NAT was PCR-amplified from IMAGE clone 5582960 (BC051759) using Phusion High-Fidelity DNA polymerase (NEB) and primers 5' CCC AAG CTT gtc tta gtc ctc tga ata ttt t and 5' CGG GGT ACC CCA ATT GAT GGA GAA TTT TAT. The PCR product was then cloned into the *Hind*III and *Kpn*I restriction sites of pcDNA3 (Life Technologies) and fully sequenced. The cloning was designed so that the NAT was inserted at the most 5' end of the multiple cloning site and near to the transcription start site of the vector, to minimise the additional nucleotides that were added to the 5' end of the transcribed long ncRNA.

Transfection of cell lines

HEK293 cells stably expressing human $Na_v1.7$ plus *SCN1B* (L11) or $Na_v1.6$ plus *SCN1B* (L40) (Scottish Biomedical) were grown according to the manufacturer's instructions and passaged four times before transfections began. Cells were split into 3.5 cm dishes and grown to 95% confluency. On the day of transfection, cells were transfected with 250 ng of pEGFP-N1 (Clontech) plus 1000 ng of human NAT in pcDNA3 or empty pcDNA3 using a ratio of 1 μg DNA:2.5 μl Lipofectamine 2000 (Life Technologies). After 6 hours, the transfected cells were re-seeded at a low density and incubated for 48 hours prior to patch clamp analysis. Two independent transfections were tested.

NAT-SH-SY5Y stable cell line

The human neuroblastoma cell line, SH-SY5Y (Public Health England) was cultured at 37°C/5% CO_2 in Ham's F12:EMEM (1:1) supplemented with 2 mM glutamine, 1% non essential amino acids and 10% foetal bovine serum (Life Technologies). The human NAT in pcDNA3

was linearised with *Pvu*I and following gel purification (Qiagen), 10 ug was transfected into a 10 cm 80% confluent dish of SH-SY5Y cells using Lipofectamine 2000 (Life Technologies). Six hours later, the medium was replaced with the selection antibiotic G418 (500 μg/ml). Cells were monitored on a daily basis until twenty-four discrete colonies could be selected for expansion and screening by RT-PCR. Real-time qPCR was performed using SYBR Green (Applied Biosystems) and the following primers: Human *SCN9A* 5' AGA GGG GTA CAC CTG TGT GAA and 5' CCC AGG AAA ATC ACT ACG ACA AA (efficiency 1.9); Human NAT 5' GGA GTC ACT GGG ATT AAA GGC AT and 5' TTC TTT GTC GCT GGT GGC TAG AG (efficiency 2); Human *ACTB* 5' CGC CGC CAG CTC ACC ATG and 5' CAC GAT GGA GGG GAA GAC GG (efficiency 1.85). The expression levels of *SCN1A*, *SCN2A* and *SCN3A* in the SH-SY5Y cells was determined using Taqman assays (Life Technologies) according to the manufacturer's instructions. The following probes were used *SCN1A* (Hs00374696_m1), *SCN2A* (Hs01109877_m1), *SCN3A* (Hs00366902_m1) and *GAPDH* (Hs02758991_g1). Relative expression levels of mRNA were calculated using the comparative ΔΔCt (Ct) method and statistical significance was determined using an unpaired t-test.

Patch clamp analysis of $Na_v1.7$-HEK293, $Na_v1.6$-HEK293 and NAT-SH-SY5Y stable cell lines

Whole cell patch clamp recordings were made from $Na_v1.7$-HEK293, $Na_v1.6$-HEK293 and NAT-SH-SY5Y stable cell lines at room temperature. In the case of the transient $Na_v1.7$ NAT transfections, whole-cell membrane current recordings were performed 46 to 78 hrs after transfection. Micropipettes were pulled from borosilicate glass capillaries (GC150F-10; Harvard Apparatus, Kent, UK) using a Brown-Flaming P-97 horizontal micropipette puller (Sutter Instruments, Novato, CA, USA) and then fire polished on a microforge (MF-830 Narishige Group, Tokyo, Japan). Voltage errors were minimised with correction and prediction mode of series resistance compensation both set to 50%. Extracellular solution contained (in mmol/L): 140 NaCl, 4 KCl, 2 $CaCl_2$, 1 $MgCl_2$, 10 HEPES, adjusted to pH 7.4 with NaOH, osmolarity 320–325 mOsm/L with glucose. Pipettes were filled with an intracellular solution containing (in mmol/L): 140 CsCl, 5 NaCl, 5 EGTA, 2 $MgCl_2$, 10 HEPES adjusted to pH 7.3 with CsOH, osmolarity 305–310 mOsm/L with glucose. Once filled with the appropriate intracellular solution, recording electrodes had a resistance between 2.0 and 3.0 MΩ. A silver chloride coated silver wire served as a reference electrode with one end connected to the ground input of the amplifier and the tip placed directly into the bath solution. Cells having a leak current after establishing whole-cell configuration of more than 10% of the peak sodium current were discarded and those which had developed leak of this magnitude during the experiment were not used in the final analysis. The liquid junction potential between the bath and the pipette solutions was not corrected. Whole-cell membrane currents were filtered at 5 kHz and sampled at 20 kHz using either an Axopatch 200B patch clamp amplifier or Axon Multiclamp 700B (Molecular Devices, Foster City, CA) and Digidata 1200B A/D converter (Molecular Devices, Foster City, CA). Data were acquired on a Windows-based PC using Clampex (Molecular Devices, Foster City, CA) software and analysed by pCLAMP (Clampfit) 9.2 software (Molecular Devices, Foster City, CA).

To characterize the voltage dependency of steady-state channel activation, currents were evoked by voltage increments of 5 mV from -80 to +40 mV for 10 ms from a holding potential of -120 mV with 5 s between pulses. Peak whole cell currents (pA) were measured in response to a 10 ms voltage step from a holding potential of -120 mV to 0 mV and normalized to cell capacitance (pF).

$Na_v1.7$-TAP tag stable HEK293A cell line

The human *SCN9A* mammalian expression construct, FLB [8] was modified by cloning in a sequence encoding a TAP tag (peptide: SRK DHL IHN VHK EEH AHA HNK IEN LYF QGE LPT AAD YKD HDG DYK DHD IDY KDD DDK) immediately prior to the stop codon. The TAP tag at the extreme C-terminus of $Na_v1.7$ is comprised of a HAT domain and 3 FLAG tags, enabling immunodetection with either anti-HAT or anti-FLAG antibodies. The $Na_v1.7$-TAP stable HEK293A cell line was generated using the same methods as described for the NAT-SH-SY5Y stable cell line. For the immunoprecipitation experiments, the $Na_v1.7$-TAP stable HEK293A cell line was firstly transiently transfected with the human NAT expression construct or an empty pcDNA3 control (as described above) and cells collected 48 hrs later. Protein was isolated using RIPA buffer and equal amounts loaded onto 100 ul anti-FLAG (Sigma, F1804) coupled Dynabeads (Life Technologies), according to the manufacturer's instructions. Samples were then boiled in Laemmli buffer and equal volumes loaded onto 4–12% polyacrylamide gels. Immunopurified $Na_v1.7$-TAP was detected on immunoblots using an anti-HAT antibody (LSBio, LS-C51508). In addition, equal amounts of crude lysate protein were subjected to immunoblotting and detected using anti-FLAG, anti-alpha tubulin (Abcam, ab7291), anti-pan sodium channel (SIGMA, S8809) and anti-beta actin (Santa Cruz) antibodies. Densitometry readings were performed using ImageJ software whereby the region of interest (ROI) reading for alpha-tubulin was compared to the ROI reading for the HAT or FLAG bands and subsequently normalized to the sham control.

Murine pain behaviour models

All experiments were performed in accordance with the UK Animals (Scientific Procedures) Act 1986 with prior approval under a Home Office project license (PPL 70/7382). Two different inflammatory pain models were used: intraplantar injection into the left hind paw of carrageenan or complete Freund's adjuvant (or 0.9% sodium chloride solution for the sham controls), as described in [18]. The chronic constriction injury (CCI) model of neuropathic pain was also used, in which sutures were tied around the sciatic nerve [18]. All experiments were performed using 6–8 week old male C57BL/6 mice. Total RNA was isolated from dissected L4-L6 ipsilateral DRGs using the RNeasy MinElute Kit (Qiagen). Real-time qPCR was performed using SYBR Green (Applied Biosystems) and the following primers: Mouse *Scn9a* 5' GAG GGG CAA ACT GAC TAC A and 5' AGA AAC ATT CCT ACA ATG GAG (efficiency 1.91); Mouse NAT 5' TGC TGT CAA CTC CTG AAC CA and 5' TCC AAC TTT GCC ACA ATG AG (efficiency 1.96); Mouse *Gapdh* 5' TGC GAC TTC AAC AGC AAC TC and 5' CTT GCT CAG TGT CCT TGC TG (efficiency 1.76); Mouse *Actb* 5' TTC TTT GCA GCT CCT TCG TT and 5' ATG GAG GGG AAT ACA GCC C (efficiency 1.83). Relative expression levels of mRNA were calculated using the comparative ΔΔCt (Ct) method and statistical significance was determined using an unpaired t-test.

Supporting Information

S1 Fig. Alignment of *SCN9A* coding exons (NM_002977) with complementary *SCN9A* NAT sequence (NR_110260). $Na_v1.7$ protein sequence (NP_002968) and location of human mutations associated with pain disorders highlighted.
(DOCX)

S2 Fig. Translation in three frames of the 2 human and 2 mouse NAT splice variants cloned from dorsal root ganglion cDNA. Potential open reading frames beginning with a methionine

residue are highlighted in red. Stop codons are denoted by a hyphen.
(DOCX)

S3 Fig. Expression profile (fraction of positive cells by thresholding method) for *Scn9a* and the NAT (*Gm13629*) across 11 genetically defined DRG neuronal subtypes. The population size and the fraction of the population that would correspond to one cell are shown at the top. Data taken from Usoskin et al., 2015.
(DOCX)

S4 Fig. Alignment of *SCN1A* exons (NM_001165963), *SCN2A* exons (NM_021007) and *SCN3A* exons (NM_006922) with complementary *SCN9A* NAT sequence (NR_110260). For *SCN4A* (NM_000334), *SCN5A* (NM_198056), *SCN7A* (NM_002976), *SCN8A* (NM_014191), *SCN10A* (NM_006514) and *SCN11A* (NM_014139) there was no significant similarity found with the *SCN9A* NAT (NR_110260).
(DOCX)

S5 Fig. Real-time qPCR showing that the endogenous *SCN2A* (A) and *SCN3A* (B) mRNA levels are not significantly different in the stable-NAT SH-SY5Y cell line compared to in naïve SH-SY5Y cells (sham) (n = 3). *SCN1A* is not expressed in these cell lines.
(DOCX)

S6 Fig. Reduction in $Na_v1.7$-TAP tag protein levels due to overexpression of the NAT for 48 hrs in a $Na_v1.7$-TAP stable HEK293 cell line. Upper: Immunoblot of crude lysate using an anti-pan sodium channel antibody confirms a reduction in $Na_v1.7$ protein levels following NAT transfection. Lower: Immunoblot of crude lysate using an antibody to the beta actin housekeeping protein, confirming equal loading.
(DOCX)

Acknowledgments

We thank Istvan Kovacs (WIBR, UCL) for technical help and Professor John Hardy (Institute of Neurology, UCL) for advice.

Author Contributions

Conceived and designed the experiments: JK RW JEL AMH JV SL NE JZ ALO CGW JNW JJC. Performed the experiments: JK RW JEL AMH JV NE JJC. Analyzed the data: JK RW JEL AMH JV SL NE JNW JJC. Contributed reagents/materials/analysis tools: JK RW JEL AMH SL CGW JNW JJC. Wrote the paper: JK RW JEL AMH JV SL NE JZ ALO CGW JNW JJC.

References

1. Morris KV, Mattick JS (2014) The rise of regulatory RNA. Nat Rev Genet 15: 423–437. doi: 10.1038/nrg3722 PMID: 24776770
2. Werner A, Carlile M, Swan D (2009) What do natural antisense transcripts regulate? RNA Biol 6: 43–48. PMID: 19098462
3. Katayama S, Tomaru Y, Kasukawa T, Waki K, Nakanishi M, Nakamura M, et al. (2005) Antisense transcription in the mammalian transcriptome. Science 309: 1564–1566. PMID: 16141073
4. Lee JT, Davidow LS, Warshawsky D (1999) Tsix, a gene antisense to Xist at the X-inactivation centre. Nat Genet 21: 400–404. PMID: 10192391
5. Mahmoudi S, Henriksson S, Corcoran M, Mendez-Vidal C, Wiman KG, Farnebo M (2009) Wrap53, a natural p53 antisense transcript required for p53 induction upon DNA damage. Mol Cell 33: 462–471. doi: 10.1016/j.molcel.2009.01.028 PMID: 19250907

6. Faghihi MA, Modarresi F, Khalil AM, Wood DE, Sahagan BG, Morgan TE, et al. (2008) Expression of a noncoding RNA is elevated in Alzheimer's disease and drives rapid feed-forward regulation of beta-secretase. Nat Med 14: 723–730. doi: 10.1038/nm1784 PMID: 18587408
7. Zhao X, Tang Z, Zhang H, Atianjoh FE, Zhao JY, Liang L, et al. (2013) A long noncoding RNA contributes to neuropathic pain by silencing Kcna2 in primary afferent neurons. Nat Neurosci 16: 1024–1031. doi: 10.1038/nn.3438 PMID: 23792947
8. Cox JJ, Reimann F, Nicholas AK, Thornton G, Roberts E, Springell K, et al. (2006) An SCN9A channelopathy causes congenital inability to experience pain. Nature 444: 894–898. PMID: 17167479
9. Weiss J, Pyrski M, Jacobi E, Bufe B, Willnecker V, Schick B, et al. (2011) Loss-of-function mutations in sodium channel Nav1.7 cause anosmia. Nature 472: 186–190. doi: 10.1038/nature09975 PMID: 21441906
10. King GF, Vetter I (2014) No Gain, No Pain: NaV1.7 as an Analgesic Target. ACS Chem Neurosci 5: 749–751. doi: 10.1021/cn500171p PMID: 25111714
11. Yang Y, Wang Y, Li S, Xu Z, Li H, Ma L, et al. (2004) Mutations in SCN9A, encoding a sodium channel alpha subunit, in patients with primary erythermalgia. J Med Genet 41: 171–174. PMID: 14985375
12. Fertleman CR, Baker MD, Parker KA, Moffatt S, Elmslie FV, Abrahamsen B, et al. (2006) SCN9A mutations in paroxysmal extreme pain disorder: allelic variants underlie distinct channel defects and phenotypes. Neuron 52: 767–774. PMID: 17145499
13. Faber CG, Hoeijmakers JG, Ahn HS, Cheng X, Han C, Choi JS, et al. (2012) Gain of function Nanu1.7 mutations in idiopathic small fiber neuropathy. Ann Neurol 71: 26–39. doi: 10.1002/ana.22485 PMID: 21698661
14. Klein CJ, Wu Y, Kilfoyle DH, Sandroni P, Davis MD, Gavrilova RH, et al. (2013) Infrequent SCN9A mutations in congenital insensitivity to pain and erythromelalgia. J Neurol Neurosurg Psychiatry 84: 386–391. doi: 10.1136/jnnp-2012-303719 PMID: 23129781
15. Drenth JP, Te Morsche RH, Mansour S, Mortimer PS (2008) Primary erythermalgia as a sodium channelopathy: screening for SCN9A mutations: exclusion of a causal role of SCN10A and SCN11A. Arch Dermatol 144: 320–324. doi: 10.1001/archderm.144.3.320 PMID: 18347287
16. Usoskin D, Furlan A, Islam S, Abdo H, Lonnerberg P, Lou D, et al. (2015) Unbiased classification of sensory neuron types by large-scale single-cell RNA sequencing. Nat Neurosci 18: 145–153. doi: 10.1038/nn.3881 PMID: 25420068
17. Vetter I, Mozar CA, Durek T, Wingerd JS, Alewood PF, Christie MJ, et al. (2012) Characterisation of Na (v) types endogenously expressed in human SH-SY5Y neuroblastoma cells. Biochem Pharmacol 83: 1562–1571. doi: 10.1016/j.bcp.2012.02.022 PMID: 22410003
18. Minett MS, Quick K, Wood JN (2011) Behavioral measures of pain thresholds. Current protocols in mouse biology: John Wiley & Sons, Inc., Hoboken, NJ, USA. PMID: 21743842
19. Lapidot M, Pilpel Y (2006) Genome-wide natural antisense transcription: coupling its regulation to its different regulatory mechanisms. EMBO Rep 7: 1216–1222. PMID: 17139297
20. Werner A, Cockell S, Falconer J, Carlile M, Alnumeir S, Robinson J (2014) Contribution of natural antisense transcription to an endogenous siRNA signature in human cells. BMC Genomics 15: 19. doi: 10.1186/1471-2164-15-19 PMID: 24410956
21. Komine Y, Nakamura K, Katsuki M, Yamamori T (2006) Novel transcription factor zfh-5 is negatively regulated by its own antisense RNA in mouse brain. Mol Cell Neurosci 31: 273–283. PMID: 16257534
22. Nassar MA, Stirling LC, Forlani G, Baker MD, Matthews EA, Dickenson AH, et al. (2004) Nociceptor-specific gene deletion reveals a major role for Nav1.7 (PN1) in acute and inflammatory pain. Proc Natl Acad Sci U S A 101: 12706–12711. PMID: 15314237
23. Minett MS, Nassar MA, Clark AK, Passmore G, Dickenson AH, Wang F, et al. (2012) Distinct Nav1.7-dependent pain sensations require different sets of sensory and sympathetic neurons. Nat Commun 3: 791. doi: 10.1038/ncomms1795 PMID: 22531176
24. Minett MS, Falk S, Santana-Varela S, Bogdanov YD, Nassar MA, Heegaard AM, et al. (2014) Pain without nociceptors? Nav1.7-independent pain mechanisms. Cell Rep 6: 301–312. doi: 10.1016/j.celrep.2013.12.033 PMID: 24440715
25. Black JA, Liu S, Tanaka M, Cummins TR, Waxman SG (2004) Changes in the expression of tetrodotoxin-sensitive sodium channels within dorsal root ganglia neurons in inflammatory pain. Pain 108: 237–247. PMID: 15030943
26. Livak KJ, Schmittgen TD (2001) Analysis of relative gene expression data using real-time quantitative PCR and the 2(-Delta Delta C(T)) Method. Methods 25: 402–408. PMID: 11846609
27. Pfaffl MW (2001) A new mathematical model for relative quantification in real-time RT-PCR. Nucleic Acids Res 29: e45. PMID: 11328886